Optimization of the biocrude nitrogen content during the hydrothermal fractionation of municipal sewage sludge including pre- and post-treatments

Zur Erlangung des akademischen Grades eines
DOKTORS DER NATURWISSENSCHAFTEN (DR. RER. NAT.)

von der KIT-Fakultät für Chemieingenieurwesen und Verfahrenstechnik des

Karlsruher Instituts für Technologie (KIT)

genehmigte

DISSERTATION

von
M. Sc. Joscha Victor Zimmermann
aus Berlin

Tag der mündlichen Prüfung: 11.04.2024

Erstgutachter Prof. Dr. rer. nat. Nicolaus Dahmen

Zweitgutachterin Prof. Dr. rer. nat. Andrea Kruse

Acknowledgements

I am deeply grateful to Prof. Dr. Nicolaus Dahmen, my primary supervisor, for his unwavering guidance and support throughout my doctoral studies. His extensive knowledge and passion for fostering a positive work ethic and enhancing my personal character and abilities have had a profound impact on my growth as a researcher.

I would also like to express my heartfelt thanks to Dr. Klaus Raffelt for his indispensable advice and invaluable feedback on my work. His tireless support and trust in my abilities have been instrumental in bringing this project to fruition.

My gratitude extends to my second reviewer, Professor Dr. Andrea Kruse, for her invaluable contribution. Her expertise in the fields of hydrothermal processes and the utilization of biogenic feedstocks has provided me with valuable insights and ideas that have greatly inspired me before and during my doctoral studies.

I am thankful to Birgit Rolli, Yannik Träutlein, Armin Lautenbach, Alexandra Böhm, Veronica Holderied, Jessica Heinrich, Thomas Zevaco, and Michael Zimmermann for their unwavering patience and thorough analysis of my often-difficult samples. I am especially grateful to Birgit Rolli for imparting valuable analytical skills and offering constant support. I would also like to express my thanks to Thomas Tietz and Matthias Pagel for their effective solutions to the technical issues encountered during my liquefaction experiments, which were crucial to their success. I would also like to acknowledge Monika Zimmer for engaging in conversations and for her organizational skills that were instrumental in navigating bureaucratic hurdles.

I am grateful to my colleagues and friends at the IKFT for the supportive and collaborative work environment. I would like to specifically acknowledge Maximilian Wörner, George Parku, Henri Steinweg, Eugen Aschenbrenner, Ankur Chowdhury, Marius Drexler, Frederico Fonseca, Yujie Fan, and Katharina Stoll for their contributions and for creating a welcoming atmosphere at the institute.

I am also thankful to my NextGenRoadFuels project colleagues, especially Irantzu Alegria Dallo, Stefano Chiaberge, Thomas Helmer Pedersen, Komeil Kohansal Sadetmahaleh, and Claus Uhrenhold Jensen for their collaborative efforts which led to productive outcomes and for their support during the project duration. I have gained valuable knowledge and insights through our interactions.

I would like to extend my gratitude to the BBW Forwerts, the Bioeconomy Graduate Program of Baden-Württemberg state, and especially to Prof. Dr. Thomas Rausch, Dr. Tanja Peskan-Berghoefer, and Hanni Truong for their commitment to providing soft skills courses, exciting excursions, and organisation of the Summer and Winter School in Trifels even in the complicated time of a pandemic. These opportunities have enriched my experience and provided me with invaluable knowledge and insights.

Lastly, I would like to express my gratitude to my family. My parents and brother have been my source of unconditional support and taught me the value of being curious. My partner, Anni, who has provided me with the strength and motivation to embark on this journey. She continues to challenge my knowledge and awaken my curiosity about science. And now, there is another special person in my life, my daughter Martha, who brings me endless joy and love. I am thankful to them for their unwavering support. Danke!

List of publications

Peer-reviewed original publications included in this thesis

Sequential Hydrothermal Processing of Sewage Sludge to Produce Low Nitrogen Biocrude
Joscha Zimmermann, Klaus Raffelt, Nicolaus Dahmen
Processes, 2021, 9, 3. DOI: 10.3390/pr9030491

Sequential Extraction and Characterization of Nitrogen Compounds after Hydrothermal Liquefaction of Sewage Sludge
Joscha Zimmermann, Stefano Chiaberge, Steen B. Iversen, Klaus Raffelt, Nicolaus Dahmen
Energy & Fuels, 2022, 36, 23. DOI: 10.1021/acs.energyfuels.2c02622

Submitted original manuscript included in this thesis

Suppressing the formation of N-heteroaromatics during hydrothermal liquefaction of proteinaceous model feedstock"
Joscha Zimmermann; Klaus Raffelt; Nicolaus Dahmen
Biomass Conversion and Biorefinery, 2023, submitted on March 31st, 2023

Peer-reviewed original publications not included in this thesis

Bio-Crude Production Improvement during Hydrothermal Liquefaction of Biopulp by Simultaneous Application of Alkali Catalysts and Aqueous Phase Recirculation
Komeil Kohansal, Kamaldeep Sharma, Saqib Sohail Toor, Eliana Lozano Sanchez, Joscha Zimmermann, Lasse Aistrup Rosendahl, Thomas Helmer Pedersen
Energies, 2021, 14, 15. DOI: 10.3390/ en14154492.

Hydrotreating of bio-crude obtained from hydrothermal liquefaction of biopulp: effects of aqueous phase recirculation on the hydrotreated oil
Komeil Kohansal, Kamaldeep Sharma, Muhammad Salman Haider, Saqib Sohail Toor, Daniele Castello, Lasse Aistrup Rosendahl, Joscha Zimmermann, Thomas Helmer Pedersen
Sustainable Energy & Fuels, 2022, 6. DOI: 10.1039/D2SE00399F

Treatment of Hydrothermal-Liquefaction Wastewater with Crossflow UF for Oil and Particle Removal
Ali Sayegh, Simon Merkert, Joscha Zimmermann, Harald Horn, Florencia Saravia
Membranes 2022, 12, 3. DOI: 10.3390/membranes12030255

Effect of transition metals and homogeneous hydrogen producers in the hydrothermal liquefaction of sewage sludge
Claudia Prestigiacomo, Joscha Zimmermann, Ursel Hornung, Klaus Raffelt, Nicolaus Dahmen, Onofrio Scialdone, Alessandro Galia
Fuel Processing Technology, 2022, 237. DOI: 10.1016/j.fuproc.2022.107452

Conference oral and poster presentations

Oral presentation:
Influence of Lipid, Protein, Cellulose interaction on the evolution of N-heteroatom compounds during hydrothermal liquefaction
European Biomass Conference & Exhibition 2022, Marseille, France

Oral presentation:
Fractional Extraction and Characterization of Nitrogen-Compounds from the Biocrude matrix
TCBiomass 2022, Denver, USA

Poster presentation:
Fractional Extraction and physiochemical Characterization of Biocrude from Hydrothermal Liquefaction of Sewage Sludge
4th Doctoral Colloquium BIOENERGY 2021, Eggenstein-Leopoldshafen

Poster Presentation:
Influence of thermochemical Pre-treatments on Hydrothermal Liquefaction (HTL) of Sewage Sludge
3th Doctoral Colloquium BIOENERGY 2020, Leipzig, Germany

Nomenclature

Names and definition

4Refinery	H2020 project – Development of new biofuels production technology
BIOTHELYS ®	Thermal sewage sludge hydrolysis process owned by Veolia
BL2F	H2020 project – Converting black liquor to fuel via HTL
CAMBI ®	Thermal sludge hydrolysis process owned by Cambi
H2020	Framework programme funding research, technological development, and innovation created by the European Union/European Commission
Heat-to-Fuel	H2020 project – Development of sustainable biofuel technologies
HyFlexFuel	H2020 project – Various biomass to fuels via hydrothermal liquefaction
NextGenRoadFuel	H2020 project – Urban waste feedstocks to fuels via hydrothermal liquefaction
Waste2Road	H2020 project – Utilization of biogenic residues as biofuels

Acronyms

AbfKlärV	Abfall Klärschlamm Verordnung	HHV	Higher Heating Value
AD	Anaerobic digestion	HPLC	High-Performance Liquid chromatography
ANOVA	Analysis of Variance	HTC	Hydrothermal Carbonization
BC	Biocrude	HTG	Hydrothermal Gasification
BSA	Bovine Serum Albumin	HTH	Hydrothermal Hydrolysis
CA	Citric Acid	HTL	Hydrothermal liquefaction
CI	Change Index	ICP-OES	Inductively coupled plasma optical emission spectrometry
CtoP	Cellulose-to-protein ratio	ISO	International Organization for Standardization
DCM	Dichloromethane	LtoP	Lipid-to-protein ratio
DIN	Deutsches Institut für Normung	MAS	Magic Angel Spinning
DKP	Diketopiperazine	MEK	Methyl Ethyl Ketone
DM	Dry Matter	MSS	Municipal Sewage Sludge
DW	De-ionized Water	NMR	Nuclear Magnetic Resonance Spectroscopy
EC	European Commission	PAH	Polycyclic aromatic hydrocarbons
ER	Elemental Recovery	PCB	Polychlorinated Biphenyls
EU	European Union	RED	Renewable Energy Directive
FAA	Fatty Acid Amides	RT	retention time
FAME	Fatty Acid Methyl Ester	SA	Sulphuric Acid
FBR	Fixed Bed Reactor	SIM	Selected Ion Monitoring
FC	Fixed Carbon	TCD	Thermal Conductivity Detector
FID	Flame Ionization Detector	TIC	Total Ion Current
FTICR MS	Fourier Transform Ion Cyclon Resonance Mass Spectrometry	TNb	Total Nitrogen Bound
GC	Gas Chromatography	TOC	Total Organic Carbon
GC-MS	Gas Chromatography-Mass Spectrometry	VDLUFA	Verband deutscher landwirtschaftlicher Untersuchungs- und Forschungsanstalten
HDA	Hydrodearomatization	VM	Volatile matter
HDM	Hydrodemetalization	wt.	Weight
HDN	Hydrodenitrogenation	WWTP	Waste Water Treatment Plant
HDO	Hydrodeoxygenation	Y	Yield
HDS	Hydrodesulfurization		

Summary

The present thesis work on “Hydrothermal Fractionation of Sewage Sludge” was designed to reduce the transfer of perturbing nitrogen from sewage sludge into the biocrude for fuel applications. In the context of this thesis, hydrothermal liquefaction (HTL) is the central process in producing biocrude, an energy-dense, tar-like organic liquid within the EU-Horizon2020 project “NextGenRoadFuels”. In addition, the study aims to investigate the underlying reaction mechanism of nitrogen during HTL and product fractionation processes and its impact on the final composition of biocrude on a molecular level, with the goal of developing innovative separation techniques to improve the quality of biocrude.

Sewage sludge is a biogenic waste with high moisture content that is generated in significant quantities during wastewater treatment. This waste material potentially contains pathogens, heavy metals, pharmaceutical residues, and microplastics, making it crucial to properly dispose of it. Hydrothermal liquefaction (HTL) technology offers a promising solution by converting the sewage sludge into a fuel precursor without the need for upstream dewatering. However, one major challenge in refining and subsequent using sewage sludge-derived biocrude as a transportation fuel is its elevated nitrogen content (4-8 wt.%) compared to conventional fossil heavy crude oil (<0.5 wt.%). Nitrogen-containing compounds in biocrude can cause issues such as inhibition and deactivation of acid catalysts, metal complexation and gum formation, as well as harmful NO_x emissions when burned. In general, the removal of nitrogen in high concentrations from oil is a challenge, and currently, catalytic hydrotreatment is the only feasible industrial process. However, nitrogen bound in heteroaromatic compounds such as pyrroles, pyridines, and pyrazines presents a particularly difficult challenge for catalytic processes, as these compounds require harsh reaction conditions, resulting in high hydrogen consumption rates.

Chapter 1 provides a comprehensive overview of the background on hydrothermal conversion of biomass to higher value products, various municipal sewage sludge generation systems, and their impact on the composition. The chapter also examines the chemistry of the major large molecule classes including lipids, carbohydrates, proteins, and their

mixtures. Furthermore, the chapter introduces the valorization chain of sewage sludge to a drop-in fuel and reviews their current state of research of nitrogen separation processes. Finally, research demand is concluded and the objectives of this thesis are presented.

Chapter 2 describes, how municipal sewage sludge samples from various wastewater treatment systems were analysed and transformed into HTL-biocrude at 35 0°C in 25 ml microautoclaves. The results showed that the sewage sludge from a biofilm waste water treatment plant exhibits the highest lipid content and performed best in terms of biocrude yield and quality. Interestingly, both mixed and digested sewage sludge produced similar amounts and qualities of biocrude. On the other hand, the activated, protein-rich sludge resulted in the lowest yield of biocrude with the highest nitrogen content. These findings demonstrate that the organic composition of the sewage sludge, which is heavily influenced by the upstream wastewater treatment process, greatly determines the quality of the biocrude produced.

These initial results indicate that the biogenic composition of the sewage sludge from named large molecules has a significant impact on the yield and quality of the HTL-biocrude produced. To further evaluate this relationship, **Chapter 3** examines the effect of different mixtures of lipids, carbohydrates, and proteins on the biocrude yield and nitrogen species. Model mixtures were created using lard oil (lipid), cellulose (polysaccarid), and bovine serum albumin (protein) to represent biogenic waste feedstocks. In each experiment, the protein content was kept constant, while the lipid and cellulose content was varied, as expressed by the lipid-to-protein (LtoP) or cellulose-to-protein ratio. The experiments were conducted at 350 °C with a residence time of 20 minutes in 25 mL micro autoclaves, and the carbon and nitrogen recovery into different product phases were analysed. Analysis of the chemical components was also performed to gain a comprehensive understanding of the biocrude composition. A high LtoP leads to increased biocrude yield and carbon recovery, while slightly lowering nitrogen recovery. The addition of lipids was found to suppress the formation of nitrogen-containing heteroaromatic species such as pyrazines and indoles, reducing the levels from 6.10% to 0.03% and 2.69% to 0.43%, respectively. Conversely, the formation and recovery of nitrogen-rich aliphatic amides increased from practically zero to

8.77%. Proposed reaction pathways suggest that by "trapping" reactive amines from protein degradation into stable amides, it prevents the formation of nitrogen heteroaromatics with oxygenated species from carbohydrates.

The findings from previous chapters were applied in **Chapter 4** by optimising the biogenic composition of sewage sludge feedstock through a mild hydrothermal pre-treatment. This approach led to a higher yield and improved quality of biocrude with a low nitrogen content. During the pre-treatment step (150 °C), deionized water, sulfuric acid (0.5 M), or citric acid (0.5 M) was used to solubilize nitrogen-containing compounds and separate them from the solid material. The residual solid material was then subjected to hydrothermal liquefaction (350 °C) with the addition of sodium carbonate, leading to increased yield and improved quality of the final biocrude product. The citric acid pre-treatment was found to be the most effective, transferring up to 66.7% of nitrogen into the aqueous supernatant and retaining 62.0% of carbon in the solid. In all pre-treatment lipids are retained in the sewage sludge solid, leading to an increased biocrude yield of up to 42.9% and a significant improvement in the quality evaluation value H/C_{eff} ratio to 1.48. Further characterization of the resulting biocrude samples using multiple methods revealed a decrease in the concentration of nitrogen-heterocycles and an increase in long-chain aliphatic derivates.

Chapter 5 deals with post-HTL treatments and aims to remove unwanted nitrogen contained in the biocrude of a continuous HTL process. To clarify the structure of the nitrogen compounds, three different aqueous solutions were used in sequential order for the extraction and recovery of polar nitrogen-containing compounds from the biocrude matrix. The solutions used were $NaHCO_3$ and NaOH (alkaline) and HCl (acidic). The extracted compounds were characterized using various analytical techniques such as gas chromatography-mass spectrometry (GC-MS), and Fourier transform ion cyclotron resonance mass spectrometry (FTICR-MS) coupled with atmospheric pressure chemical ionization in positive mode (APCI-MS). The results indicated that a significant portion of nitrogen compounds with a pyridinic structure were found in the acidic extracted fraction, with nitrogen content of 9.5 wt %. The aliphatic nitrogen-compounds were less affected by the separation and remained in the residual fraction. On the other hand, nitrogen-

compounds with multiple oxygen functionalizations were enriched in the alkaline extracted fractions. This showed that the presence of polar groups can strongly affect nitrogen-compounds with an aromatic structure and that they can potentially be extracted using appropriate solvents in downstream processes.

In **Chapter 6** conclusions on the main achievements are drawn and where to go from here. The main conclusion was that the transfer of nitrogen into biocrude during HTL of sewage sludge or, in general, of proteinaceous biomass cannot be prevented. Nevertheless, the information about the feedstock composition, made up of lipids, carbohydrates, and proteins, predicts how much nitrogen is recovered and which types of nitrogen species are formed. An in-depth evaluation of the entire valorization process, from feedstock to drop-in fuel, can lead to finding ways to lower nitrogen content and suppress the formation of undesirable heteroaromatics. This may involve improving the sewage sludge feedstock, pre-treatment, co-liquefaction with suitable large molecules, and integrating phase separation and recovery methods to create high-quality biocrude.

Zusammenfassung

Die vorliegende Arbeit "Hydrothermal Fractionation of Sewage Sludge“ zielt darauf ab, den Stickstofftverbleib bei der hydrothermalen Verflüssigung (HTL) vom Klärschlamm zu Biokraftstoffen zu klären und möglichst stark zu reduzieren. HTL ist der zentrale Prozess bei der Herstellung von "Biocrude", einem energiereichen, teerartigen Öl im EU-Horizon 2020 Projekt „NextGenRoadFuels“. Diese Arbeit untersucht zu diesem Zweck den zugrunde liegenden Reaktionsmechanismus von Stickstoff bei der HTL und seine Auswirkungen auf die molekulare Zusammensetzung von Biocrude einschließlich vor- und nachgelagerter Aufarbeitungsschritte mit dem Ziel, verbesserte Trennverfahren zur Steigerung der Qualität von Biocrude zu entwickeln.

Klärschlamm ist ein feuchter, biogener Abfall, der in großen Mengen bei der Abwasserbehandlung anfällt und oft Krankheitserreger, Schwermetalle, Arzneimittelrückstände und Mikroplastik enthält. Die HTL-Technologie bietet eine vielversprechende Lösung, indem sie den Klärschlamm in ein Kraftstoff-Vorprodukt umwandeln kann, ohne dass eine vorherige Entwässerung erforderlich ist. Eine große Herausforderung bei der Raffinierung und Verwendung von aus Klärschlamm gewonnenem Biocrude zu Kraftstoff ist jedoch dessen hoher Stickstoffgehalt (4-8%) im Vergleich zu herkömmlichem fossilem Schweröl (<0,5%). Diese stickstoffhaltigen Verbindungen im Biocrude können Probleme wie Hemmung und Deaktivierung von Säurekatalysatoren, Metallkomplexbildung, Bildung von hochviskosen Ablagerungen sowie schädliche NOx-Emissionen bei der Verbrennung verursachen. Die Entfernung von Stickstoff aus Öl in hohen Konzentrationen ist insgesamt eine Herausforderung; das einzige praktikable industrielle Verfahren dafür ist bislang die katalytische Hydrierung. Stickstoff in heteroaromatischen Verbindungen wie Pyrrolen, Pyridinen und Pyrazinen stellt jedoch eine besondere Herausforderung dar, da es drastische Reaktionsbedingungen erfordert, die einen hohen Wasserstoffverbrauch mit sich bringen.

In **Kapitel 1** wird ein Überblick über die hydrothermale Umwandlung von Biomasse zu höherwertigen Produkten gegeben. Zudem werden verschiedene Systeme der

Klärschlammerzeugung und ihre Auswirkungen auf desen Zusammensetzung erläutert. Außerdem wird die Reaktionschemie der wichtigsten Klassen großer, im Klärschlamm typischerweise enthaltenen Moleküle wie Lipide, Kohlenhydrate, Proteine und ihren Mischungen untersucht. Die Verwertungskette von Klärschlamm zu einem Drop-in-Kraftstoff wird ebenfalls beschrieben und der aktuelle Stand der Forschung zur Abtrennung von Stickstoff innerhalb dieser Kette wird erklärt.

Im **Kapitel 2** wird die Analyse von Klärschlammproben aus verschiedenen Kläranlagen beschrieben und die Umwandlung zu HTL-Biocrude in 25-ml-Mikroautoklaven bei 350 °C untersucht. Die Ergebnisse zeigen, dass der Klärschlamm aus einer Kläranlage mit Biofilm-Technologie einen hohen Lipidgehalt aufwies und im Hinblick auf Ertrag und Qualität des Biocrudes die besten Resultate lieferte. Überraschenderweise führten sowohl gemischter als auch ausgefaulter Klärschlamm zu ähnlichen Erträgen und Qualitäten an Biocrude. Der Klärschlamm mit hohem Proteingehalt und hoher Aktivität lieferte hingegen die geringste Ausbeute an Biocrude bei gleichzeitig hohen Stickstoffgehalt. Diese Befunde legen nahe, dass die organische Zusammensetzung des Klärschlamms, welche durch den Vorreinigungsprozess stark beeinflusst wird, einen bedeutenden Einfluss auf die Qualität des erzeugten Biocrudes hat.

Diese ersten Ergebnisse legen nahe, dass die biogene Zusammensetzung des Klärschlamms einen signifikanten Einfluss auf die Ausbeute und Qualität des erzeugten HTL-Biocrude hat. In **Kapitel 3** wurde daher untersucht, wie unterschiedliche Verhältnisse von Lipiden, Kohlenhydraten und Proteinen die Ausbeute und Stickstoffspezies des Biobruchs beeinflussen. Hierfür wurden Modellmischungen aus Schmalzöl (Lipid), Zellulose (Polysaccarid) und Rinderserumalbumin (Protein) hergestellt, um biogene Abfälle abzubilden. Dabei wurde der Proteingehalt konstant gehalten, während Lipid- und Zellulosegehalte variiert wurden. Dies kann durch das Verhältnis von Lipid-zu-Protein oder Zellulose-zu-Protein ausgedrückt werden. Die Versuche wurden bei 350 °C für 20 Minuten in 25-mL-Mikroautoklaven durchgeführt, und die Kohlenstoff- und Stickstoffrückgewinnung in den verschiedenen Produktphasen wurde analysiert. Eine chemische Analyse wurde ebenfalls durchgeführt, um ein umfassendes Verständnis der

Zusammensetzung zu gewinnen. Ein hoher Lipid-zu-Protein-Wert führte zu einer höheren Ausbeute an Biocrude und einer höheren Kohlenstoffrückgewinnung, während die Stickstoffrückgewinnung leicht sank. Es wurde festgestellt, dass die Zugabe von Lipiden die Bildung von stickstoffhaltigen heteroaromatischen Spezies wie Pyrazinen und Indolen unterdrückte. Deren Anteil am Stickstoff im Biocrude sank von 6,10% auf 0,03% bzw. von 2,69% auf 0,43%. Demgegenüber stieg die Bildung und Stickstoffbindungseffizienz von aliphatischen Amiden von praktisch Null auf 8,77%. Die vorgeschlagenen Reaktionsmechanismen deuten darauf hin, dass die Bildung von stickstoffhaltigen Heteroaromaten durch Carbonsäurealiphaten unterdrückt wird, indem reaktive Amine aus dem Proteinabbau in stabile Amide "eingeschlossen" werden.

In **Kapitel 4** wurden die Ergebnisse aus den vorherigen Kapiteln angewendet, indem die biogene Zusammensetzung des Klärschlamm-Einsatzmaterials durch milde hydrothermale Vorbehandlung optimiert wurde. Dies führte zu einer höheren Ausbeute und besseren Qualität des Biocrude mit niedrigem Stickstoffgehalt. Während des Vorbehandlungsschritts bei 150 °C wurden deionisiertes Wasser, Schwefelsäure (0,5 M) oder Zitronensäure (0,5 M) verwendet, um stickstoffhaltige Verbindungen zu lösen und vom Feststoff zu trennen. Der verbleibende Feststoff wurde dann durch Zugabe von Natriumcarbonat hydrothermal verflüssigt (350 °C). Die Vorbehandlung mit Zitronensäure erwies sich als am wirksamsten, da bis zu 66,7% des Stickstoffs in den wässrigen Überstand übertragen und 62,0% des Kohlenstoffs im Feststoff zurückgehalten werden konnten. Bei allen Vorbehandlungen wurden die Lipide im Klärschlammfeststoff zurückgehalten, was zu einer erhöhten Biocrude-Ausbeute von bis zu 42,9% und einem verbesserten H/C_{eff}-Verhältnis von 1,48 führte. Die Charakterisierung der resultierenden Biocrude-Proben mittels mehrerer analytischer Methoden ergab eine Abnahme der Konzentration an stickstoffhaltigen Heterozyklen und eine Zunahme an langkettigen aliphatischen Derivaten.

Kapitel 5 fokussiert sich auf die Entfernung unerwünschter Stickstoffstrukturen aus dem Biocrude, das in einem kontinuierlichen Pilot-HTL-Prozess hergestellt wurde. Um die Funktionalität der Stickstoffverbindungen besser zu verstehen, wurden drei wässrige Lösungen sequentiell zur Extraktion und Rückgewinnung polarer Stickstoffverbindungen

aus dem Biocrude eingesetzt. Die Lösungen waren $NaHCO_3$ und NaOH (beide alkalisch) sowie HCl (sauer). Die extrahierten Verbindungen wurden mithilfe von Analysemethoden wie Gaschromatographie-Massenspektrometrie (GC-MS), Fourier-Transform-Ionenzyklotron-resonanz-Massenspektrometrie (FTICR MS) in Verbindung mit Atmosphärendruck-Chemischer Ionisierung im positiven Modus (APCI-MS) charakterisiert. Die Ergebnisse zeigten, dass ein wesentlicher Anteil stickstoffhaltiger Verbindungen mit pyridin-basierter Struktur in der sauren Extraktion gefunden wurde, mit einem Stickstoffgehalt von 9,5 Gew.-%. Die aliphatischen Stickstoffverbindungen waren weniger von der Trennung betroffen und blieben in der Rückstandsfraktion. Außerdem waren Stickstoffverbindungen mit mehrfachen Sauerstoff-Funktionalitäten in den alkalisch extrahierten Fraktionen konzentriert. Dies legt nahe, dass das Vorhandensein polarer Gruppen die Stickstoffverbindungen mit aromatischer Struktur stark beeinflussen kann und dass diese in zukünftigen Prozessen durch geeignete Lösungsmittel extrahiert werden können.

In **Kapitel 6** werden Schlussfolgerungen aus den wichtigsten Erkentnissen gezogen und ein Überblick über die zukünftigen Schritte gegeben. Im Wesentlichen lässt sich schlussfolgern, dass die Übertragung von Stickstoff in die Biocrude-Phase bei der HTL von Klärschlamm oder proteinreicher Biomasse unvermeidbar ist. Die Informationen über die Zusammensetzung des Ausgangsmaterials, das aus Lipiden, Kohlenhydraten und Proteinen besteht, geben jedoch Aufschluss darüber, wie viel Stickstoff zurückgewonnen wird und welche Arten von Stickstoffarten gebildet werden. Eine gründliche Überprüfung des gesamten Valorisierungsprozesses, von der Rohstoffquelle bis zum Endprodukt Kraftstoff, kann mögliche Strategien zur Senkung des Stickstoffgehalts und zur Vermeidung unerwünschter Heteroaromaten aufzeigen. Hierbei kann es sich um die Optimierung des Klärschlamm-Ausgangsmaterials, die Vorbehandlung oder Ko-Verflüssigung mit passenden großen Molekülen verschiedener Biomassen und die Integration von Phasentrennungs- und Rückgewinnungsmethoden handeln, um hochwertiges Biocrude zu produzieren.

Table of contents

Chapter 1.

Introduction

1.1 Motivation

The exploration, extraction, utilisation, and processing of finite fossil petroleum cause significant interference with the natural environment and the emission of carbon gases that threaten environmental and climate conditions. Moreover, the current world situation shows once again that democratic industrial nations should make themselves more independent from the oil-producing states, particularly by diversification of resources and energy-saving measures. With the "Green Deal" and the actual Renewable Energy Directive III (REDIII) the European Commission (EC) sets targets to achieve a climate-neutral European Union (EU) [1,2]. RED III rose the aimed total share of renewable energies from 32.5% to 45% in 2030 and in the transport sector, the already binding target increases from 14% to 29%. Hereby, the heavy-road, aviation and marine transport sector are difficult to electrify completely and should be defossilized by introducing renewable fuels [3]. The previous REDII defines a share of only 7% of first-generation biofuels, as these are usually produced from energy crops [4]. As cultures of energy crops are primarily on valuable agricultural land they impact land grabs, and deforestation and rise the food versus fuel discussion [5]. Higher generation of biofuels should be one part of the solution to achieve at least an 80% reduction in greenhouse gas emissions below 1990 levels by 2050 [6]. Within the Annex IX Part A of the REDII a list of feedstocks for the production of higher generation- (called advanced biofuels) are given. Most of these feedstocks are agricultural or municipal organic waste material with a high moisture content.

At the same time, increasing waste streams from our society are challenging us to design sustainable, circular systems for the valorization of organic carbon and nitrogen, as well as inorganic components like metals or phosphorus. The Waste Framework Directive 2008/98 shows a priority pyramid in waste management, with prevention on top over preparing for reuse, recycling, energy recovery, and finally disposal [7]. With the amendment 2018/851, thermochemical conversion processes to recover crude chemicals are defined as a recycling process and therefore preferred over waste incineration for heat recovery [8]. One such waste

stream is municipal sewage sludge (MSS), a mixture of biological and inorganic matter. In Europe municipal wastewater is in general treated at the wastewater treatment plant (WWTP) to ensure environmental security by removing or reducing organic and inorganic pollutants. The worldwide and stringent directives for the treatment of wastewater have dramatically increased MSS generation. An amount of 10.14 million tons of dry solids of MSS was estimated for the year 2008 for Europe, which was expected to increase by 30% until 2020 [9]. The land application of MSS becomes nowadays more and more problematic as concerns rise about microplastic and pharmaceutical residuals and nutrient application rates are restricted by the EU [10]. The common subsequent anaerobic digestion cannot be accounted as a final disposal strategy, as it only reduces but does not avoid the sludge streams to incineration [11]. The amount of water in MSS takes a share of about 80 wt.%, which lowers the higher heating value (HHV) of incineration [12].

The current and most common best practice of MSS management considers the reliability of the treatment but needs to shift towards a recovery of the embedded energy and chemical value [13]. Thermochemical technologies like hydrothermal liquefaction (HTL) are able to valorise the organic content of MSS by converting it into value-added chemicals, fuel or at least energy, simultaneously reducing the residual volume and destroying potential pathogens. With the further valorization of by-products, HTL of MSS would fit into novel concepts of a biorefinery or the food-water-energy nexus [14,15].

1.2 Hydrothermal conversion of low-grade feedstocks

Hydrothermal processes valorize the organic content of wet wastes using water at elevated temperatures as reaction medium and reaction partner. Below the critical point of water, temperatures are kept at the corresponding vapour pressure to avoid evaporation of the water Therefore, these thermochemical conversions are orientated on the vapour pressure curve as shown in Figure 1 (A). These processes are named by their predominant product, hydrothermal hydrolysis (HTH), hydrothermal carbonization (HTC), hydrothermal liquefaction and

hydrothermal gasification (HTG). HTH of MSS takes place at temperatures between 100 and 180 °C, hydrolysing biopolymers like cellulose and proteins by into monomers, namely (poly)-carbohydrates, peptides or amino acids. Often these processes are supported by mild alkaline or acidic environments to improve and fasten downstream anaerobic digestion [16,17]. The HTC is reported to appear in a temperature range between 160 and 250 °C mainly by dehydration reactions [18]. By re-polymerization of carbohydrate and protein degradation products, a carbonaceous solid is yielded, which can be utilized as a solid fuel or as an advanced material for electricity generation and storage purposes after further treatment [19]. HTL aims to promote decarboxylation and cyclization reactions by increasing temperatures close to 400 °C [20]. HTL processes above the critical temperature of the water (374.12 °C, 22.1 MPa) would require high pressures beyond the vapor pressure saturation curve to suppress the usually predominant gasification of the biomass [21]. Ideally, the products after HTL separate spontaneously into the main product, the comparative non-polar tarry oil also referred as biocrude and the aqueous and solid, gaseous by-products. The HTG of biomass can be achieved near-critical with the addition of catalysts or at even higher temperatures in the super-critical state of water [19]. The desired products are small molecules like methane, carbon dioxide and hydrogen. It can be noted that the temperature ranges overlap since the product phases like gas, aqueous, oil and solid phases usually occur in different proportions in all mentioned processes.

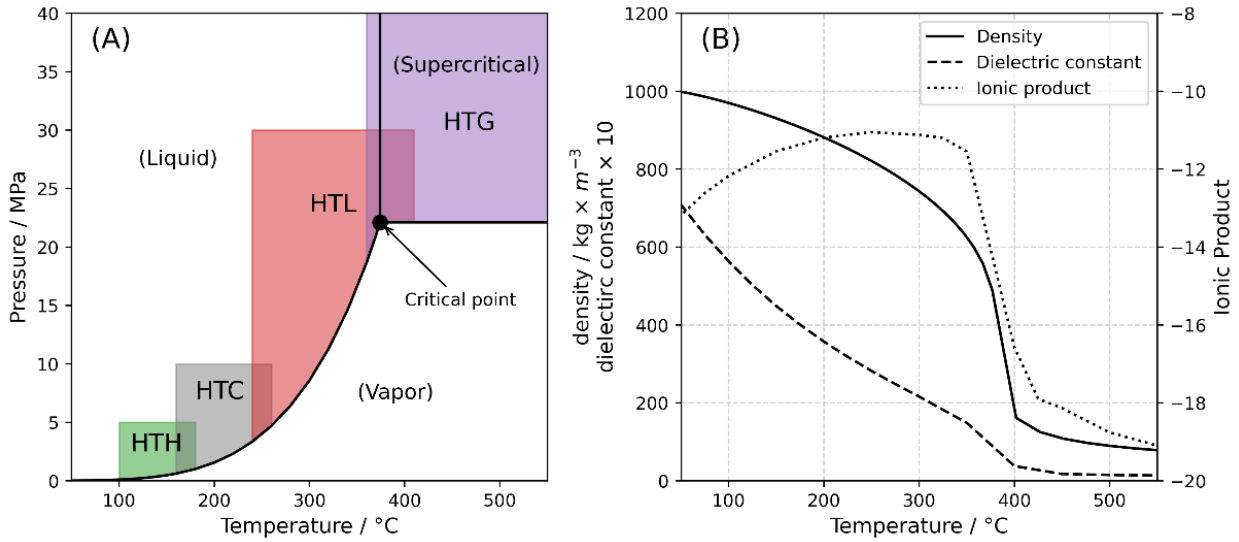

Figure 1. (A) Water phase diagram, including the orientation of hydrothermal processes and **(B)** properties of water at a pressure of 25 MPa. Data derived from [17–20] and [22–25].

The reaction medium water shows some advantageous properties at elevated temperatures and their corresponding vapour pressure. In Figure 1 (B) the density, dielectric constant and ionic product of water at a pressure of 25°MPa is plotted against the temperature. It can be noted that the density and the dielectric constant are continuously decreasing, while the ionic product is increasing at sub-critical temperatures. Approaching and going beyond the critical point the density, dielectric constant and ionic product are rapidly decreasing, as the water becomes a supercritical fluid with gas-like properties.

The constant decrease in the density of water is a consequence of the increased movement of water molecules with elevated temperatures. This correlates directly with the solvation power, a lower degree of hydrogen bonding, solvent polarity and viscosity, as well as increased diffusivity [26]. Specifically, the dielectric constant affects the miscibility of salts or non-polar hydrocarbons in water at ambient conditions and which at 300 °C becomes comparable with a solvent like acetone [27]. The higher ionic product at the HTC and HTL temperature range explains an increased self-dissociation of water into H_3O^+ and HO^- Ions, which accelerate acid- or base-catalysed reactions [28].

Within the hydrothermal processes described above, the primary goal is to split biogenic and other organic materials to derive energy carriers, chemical building blocks, or other materials. Also, a decrease of the heteroatom content of the biomass is intended to ease downstream processing and increase the heating value, if the product is applied as a fuel. The H-, and O- in relation to the C-content are here of special interest since it strongly define the heating value of a molecule. The effect of hydrothermal processes on different biomasses and organic wastes can be visualized within the so-called 'van Krevelen' diagram. In Figure 2 (A) the H-to-C ratio (H/C) is plotted against the O-to-C ratio (O/C). Within the diagram, different areas can be observed. Common biomasses are characterized by their relatively high H/C and O/C-ratio, shown here representatively by aspen wood, *chlorella vulgaris* and sewage sludge. These types of biomass usually consist of four different biogenic large molecules, namely lipids, proteins, cellulose and lignin, which are presented as well in the diagram. With a lower O/C-ratio other substance areas can be accessed. After an HTC process, the hydrochar product typically is located in the area of lignites and coals, whereas HTL results in biocrude comparable with fossil shale oils. By HTG the main product becomes gaseous with the H/C-ratio exceeding the diagram borders. Substances with an O/C-ratio close to zero are highly calcinated C, namely soot, carbon black or anthracites. Fossil petroleum substances and their refined products simultaneously have higher H/C-ratios. Lastly, it should be noted that the substances in the upper left quarter (high H/C-and low-O/C-ratio) are usually present in liquid or gaseous form. When it comes to organic wastes and low-rank biomasses like algae and sewage sludge also other elements play a role, such as the chlorine, sulphur, phosphorous and N-content. For the purpose of this work mainly dedicated to the fate of nitrogen compounds, the van Krevelen diagram was modified with a new x-axis, the N-to-C ratio (N/C), shown in Figure 2 (B). It can be noted that lignocellulosic materials are orientated on the left with an N/C-ratio of close to zero. Biogenic feedstocks such as algae and sewage sludge contain lipids and lignocellulosic polymers as well as proteins with a specific N-content. This increases the N/C ratio of such feedstocks.

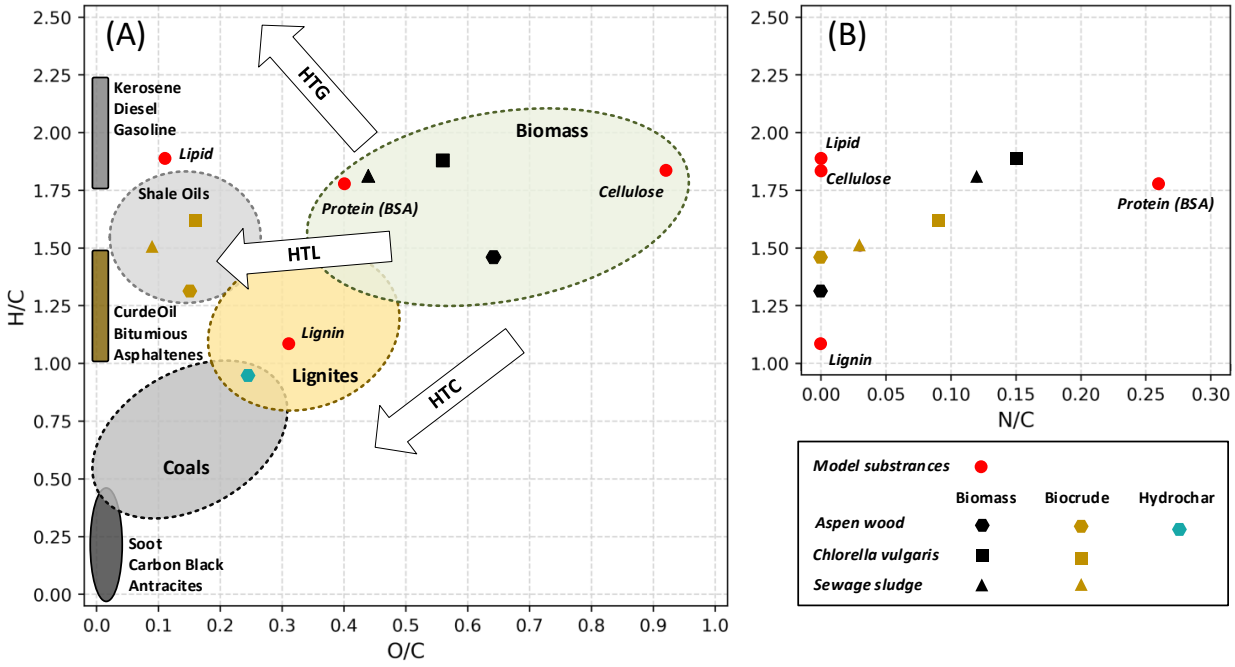

Figure 2. (A) van Krevelen diagram with x-axis O/C and (B) van Krevelen diagram with x-axis N/C. Representative areas of fossil fuels and specific biomass and organic waste as well as their hydrothermal-derived products are also included.

Likewise to the O-content, the application of HTL removes N-heteroatoms from the feedstock, resulting a in lower N/C-ratio of the biocrude product. The final chemical composition of the biocrude and consequently the chemical properties can vary substantially depending primarily on the type of feedstock and biomolecular composition, but also on the HTL reaction conditions applied (temperature, pressure, use of solvent, reaction time etc.) [29]. Due to these remaining heteroatoms, the biocrude shows usually a darker colour, higher viscosity, and is able to partially mix with water, resulting in a high moisture content, therefore needs to be considered as an unconventional oil [16]. Especially high levels of nitrogen in the biocrude of up to 10 wt.% have been reported from the valorization of municipal solid waste, manure, MSS, and algae due to the protein content of the feedstock, leading eventually to high NO_x emissions and soot formation tendencies during combustion [30,31]. Thus, the utilization of biocrude as a drop-in transportation fuel would require extensive upgrading of this intermediate product. The final product should then be orientated within the van Krevelen diagram between different distillation cut, the kerosene, diesel and gasoline and crude oil area [32].

1.3 De-nitrogenation issues

Biocrude derived from HTL of proteinaceous feedstock like sewage sludge is likely to contain a complex mixture of different N-compounds. These compounds impose limitations on the biocrude upgrading process development as they strongly affect the available selection of process operations and catalysts. The main issues regarding the processability of HTL-biocrude are listed in Table 3.

Table 1. Operational issues related to N-compounds during the refinement of HTL-derived biocrude.

Compound	Operational issue
Pyrrolic N-compounds	These compounds are prone to autooxidation and free radical reactions, thus they show poor storage and thermal stability, forming heavier compounds or gums [33,34].
Basic N-compounds	Pyridines or amines can neutralize the acid site of a catalyst. This largely depends on the acid site strength of the catalyst. E.g. acid site catalysts for low-temperature operations are poisoned by these N-compounds, while hydrocracking and fluid catalytic cracking catalysts 'only' inhibited, lowering the reaction rate [35,36].
Metals	N-compounds are likely to form metal complexes [37]. If transferred into the refinement process metals can deposit on the catalytic active site, which leads to catalyst fouling and reactor plugging [38,39].

Catalytic hydrotreating of biocrude is currently developed technology, aiming to remove the heteroatom content and was adapted from conventional petroleum treatment processes. In a H_2 environment at elevated pressures and temperatures and with help of metal or metal-supported hydrogenation catalysts the biocrude is deoxygenated (HDO) and -denitrogenated (HDN) [40]. The O-heteroatoms in this case are mainly removed in the form of water, undergoing dehydration or as CO_2 via decarboxylation , while N-heteroatoms undergo deamination, by removing amino groups (ammonia). These hydrotreating processes are not selective and run rather simultaneously besides hydrodemetalation (HDM), hydrodesulfurization (HDS) and hydrodearomatization (HDA).

For the denitrogenation of fossil fuels, HDN is the "base case" technology against which all other methods of N-removal are compared. However, for biocrude derived from proteinaceous high N-content is expected, where the functionalization of the N-heteroatom is loctated within an aromat, an heteroaromatic compounds. An example of possible reaction pathways of the HDN of Quinoline is shown in Figure 3. Simplified, two major reaction pathways can be detected. (1) hydrogenation of the aromatic nitrogen ring to covalent, aliphatic bonds, (2) a two-step hydrogenolysis of the covalent C-N bond. These reactions require more severe operation conditions, for example, higher reaction temperatures and high H_2 partial pressures [41]. This supports a simultaneously occurring rection, (3) the hydrogenation of the neighboring aromatic ring. This will increase the consumption of H_2, firstly due to the obvious N-denitrogenation and secondly due to the simultaneous running other hydrogenation reactions at such severe conditions and was shown for simple pyrrole and pyridine base structures as well as larger derivates with fused benzene rings [42]. The HDA which is likewise to the HDN strongly exothermic and can complicate heat management of the reaction system [43]. Furthermore, higher temperatures applied enhanced the parallel decarboxylation, and decarbonylation and increase the coking potential which lowered eventually the C-efficiency and lead to plugging and catalyst deactivation issues [44,45].

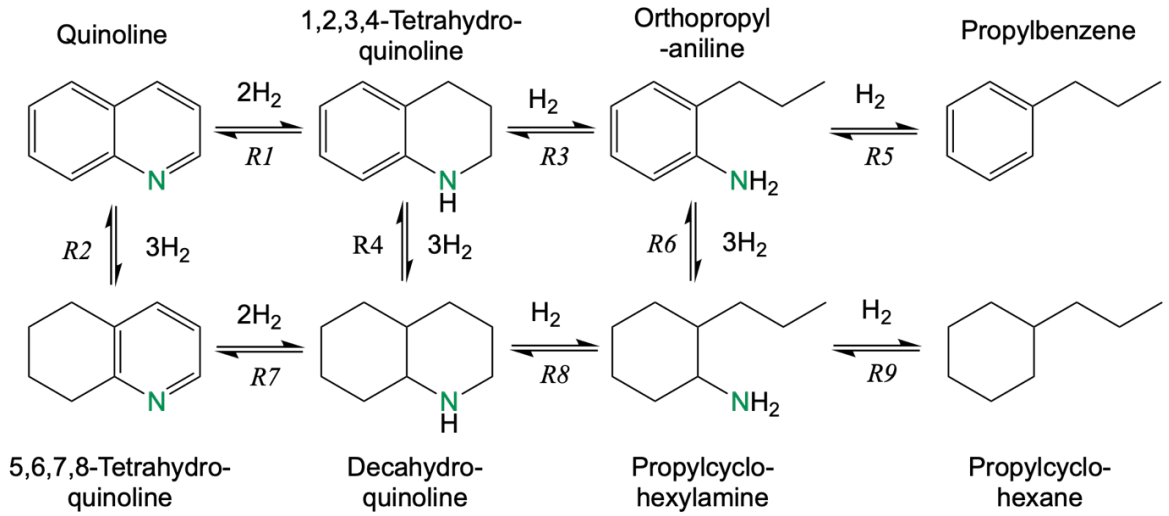

Figure 3. Pathway of the hydrodenitrogenation of quinoline (adapted from Wagner et al. [46])

1.4 Sewage sludge generation and characteristics

In this section, different wastewater treatment plant designs and the common sewage sludge treatment and disposal strategies are explained. Additionally, the influence on the final designation of sewage sludge and its composition are reviewed.

1.4.1 Wastewater treatment and sewage sludge disposal

Sewage originates from populated areas, including several emitters like domestic, industrial, commercial, hospital, road and agricultural sources. Depending on the emitting source the sewage consists of water polluted with human excreta, personal care products, detergents, disinfectants, pharmaceuticals and sediments, etc. [47]. With the sewage system, this waste water is channeled to the wastewater treatment plant (WWTP), where different purification steps are applied in series to remove impurities. To a certain level purified water is then released into the water bodies according to the regulations in place. At the WWTP, the sewage passes through different mechanical, biological and chemical treatment steps, depending on the process design. A general process layout is presented in Figure 4, including the sequential process steps and the occurring intermediates and residues, known as municipal sewage sludge (MSS).

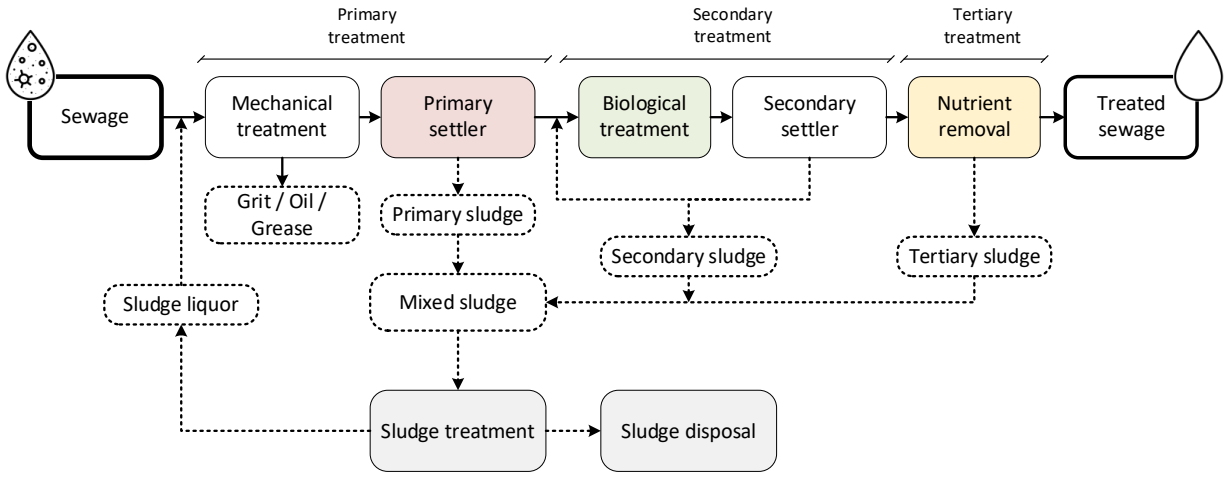

Figure 4. The layout of a conventional wastewater treatment process. Redrawn and modified from [47,48].

In the primary treatment, larger objects are removed mechanically by a strainer. In addition, other grit, consisting of non-biodegradable particles like sand and stones settles to the bottom and gets removed and oil and grease can be skimmed from the surface. In the primary settler, the sewage flows slowly trough large tanks where suspended organic material are able to sediment. This bottom phase is called 'primary sludge' and consists of 50-70 wt.% of the suspended solids of the incoming sewage [49]. The sedimentation can be chemically enhanced by simultaneous phosphate precipitation, using lime or chlorinated salts e.g. a $FeCl_3$ agent [50,51].

The secondary treatment consists of a combination of aerobic bioreactors and separation processes to remove non-colloidal particulated matter and decompose dissolved organic components. The activated sludge process is by far the most commonly applied, but various method designs are available, depending on the treated sewage composition and origin. Further examples are biofilm (percolation/tickling filters, membrane bioreactors, rotating contactors) based or granular sludge reactors systems [52]. This secondary treatment is combined with a subsequent solid-liquid separation stage, where active, non-stabilized sludge is removed by e.g. sedimentation in the activated sludge process or the biofilm is sheared off the support material. A certain amount of this 'secondary sludge' is returned to the process to maintain microbiological activity, while the excess is mixed with the primary sludge.

The tertiary treatment Is an optional, advanced stage, designed to remove high concentrations contaminations and unwanted, sensitive nutrients and compounds. There are different high-performance bacterial, chemical and physical processes available. The use of phosphorus-uptaking bacteria is a well-established process to remove phosphorus from wastewater and convert it to the sludge phase, accumulating intracellular polyphosphates [53]. Another novel biological nutrient uptaking process is called anammox, applied on wastewaters with high nitrogen content, utilizing anaerobic ammonium-oxidizing bacteria. The benefit of this process is the great reduction of carbon demand, which is usually required for the denitrification of wastewater [54]. An external biodegradable carbon-source needs to be added to sustain the

traditional denitrification process of high concentrations-nitrogen contaminated water. Likewise to the chemical phosphorus removal in the primary treatment stage, additional precipitation agents can be added to remove the remaining phosphorus and enhance the flocculation of sludge [55]. To prevent contamination of surface water with pharmaceutical residues and metabolites from urban wastewater, adsorption e.g. activated carbon is applied in certain WWTP [56]. The product of these treatment steps is called 'tertiary sludge' and occurs often in combination with secondary sludge. Most of the named 'tertiary' processes can be applied simultaneously or within the secondary treatment process line. The mixed stream of primary, secondary, and tertiary sludge is usually sent to a sludge treatment for thickening, stabilization, conditioning, and dewatering. Ultimately, the sludge amount should be reduced in weight and volume. At the same time, pathogens and unpleasant odours are eliminated which allows safe transport and disposal [57]. Novel granular sludge processes attempt to combine all three process steps in a sludge grain, a microbial conglomerate associated with extracellular polymers [58].

Sludge thicking is obtained by gravitation and increases the concentration of particulate-bound constituents to 3-6% [59]. The subsequent stabilization of the sludge can be achieved either by biological (anaerobic or aerobic), chemical (pH adjustment) or thermal treatment. The most common process applied in the EU for sludge stabilization is anaerobic digestion for larger WWTPs or aerobic digestion (composting) for smaller WWTPs, followed by the addition of chemicals like lime [60]. The commonly applied thermal methods like incineration and pyrolysis can be already accounted for in the disposal of MSS. Milder thermal hydrolysis at temperatures between 160 °C and 180 °C is often applied as pre-conditioning of the sludge prior to anaerobic digestion. This enhances biodegradability and subsequent dewaterability, degrading polysaccharides proteins and other extracellular polymers [61,62]. The concentration of volatile fatty acids (short carboxylic acids) and ammonia in the sludge liquor is hereby increased. As higher dewaterability and sludge digestion are achieved, costs for final disposal will eventually be reduced [63]. Other conditioning methods are the addition of

polymers or inorganic additives, improving the downstream mechanical dewatering. Here, mechanical tools like centrifuges, belt filter presses or even vacuum filtration are applied to increase particulate-bound constituents to 10-30%.

Stabilized MSS is usually disposed via landfilling or utilized in agriculture, landscaping or thermal treatment [64]. But nevertheless, in many developing countries, the sludge is also improperly dumped. According to the 2021 EurEau survey, approximately 8.7 million tons of MSS were generated in 2020 within the EU plus Switzerland and Norway (EU+) [65]. In Figure 5 the disposal destination within the EU+ and specifically Germany is given in percentages. It can be noted, that MSS is primarily applied in agriculture, followed by incineration. In countries like Portugal, Spain and the United Kingdom the MSS is commonly utilized in agricultural applications, whereas the Netherlands and Switzerland rely exclusively on incineration [60,65]. In Germany, the landfilling of MSS is banned since 2005 and a combination of incineration, agricultural utilization and landscaping is applied.

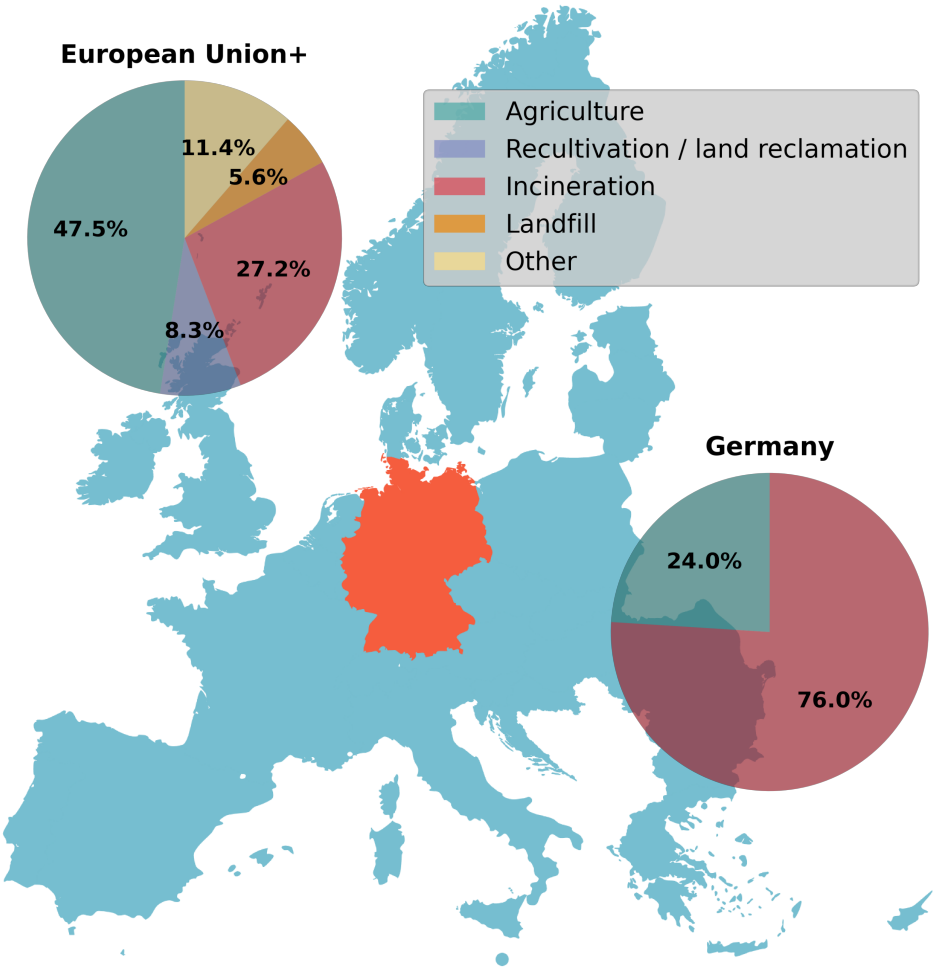

Figure 5. Sewage sludge disposal destinations in percentages within the EU+ and Germany. Data from the 2021 EurEau Survey [65].

1.4.2 Sludge classification and characteristics

In general, MSS is a complex mixture of microorganisms, undigested organics such as paper, plant residues, oils, or faecal material and inorganic materials, including high moisture content [66]. The organic material consists mainly of larger molecules and biogenic polymers like proteins (24-42 wt.%), lipids (1-14 wt.%), polysaccharides (7-18 wt.%) [67]. The inorganic phase consists primarily of inorganic salts of Si, Ca, Mg, Fe and Al [68,69]. Depending on the previously described process of water treatment and sludge generation, MSS is often referred by different names. A detailed classification of treated and untreated sludge is listed in Table 2.

Table 2. Types of treated and untreated sludge. Generated from the following references [60,70,71].

Type	Description
Primary sludge	Derived from the primary mechanical treatment and clarifier. The colour ranges from greyish black to greyish brown to yellow. The sludge contains easily recognizable debris like toilet paper. Untreated, unpleasant odours are emitted. May contain quantities of inorganics due to chemically enhanced precipitation (e.g. with FeCl3, AlCl3), see *tertiary sludge*. Easy to reduce water content by thickening or dewatering. Particle size is generally larger than in *secondary sludge*.
Secondary sludge	Generated in the secondary biological treatment stage by conventional activated sludge systems, also including separated sludge from biofilm or granular systems, such as trickling filters, biological aerated filters, membrane filters or up-flow anaerobic sludge blankets. The sludge shows a brownish colour and homogeneous distribution of particles.
Tertiary sludge	Generated in tertiary advanced nutrient removal step. Phosphorus removal in conjunction with the primary or secondary clarifier usually does not occur separately. Rather mixed with primary or secondary sludge. Usually stable and does not emit an unpleasant odour, as it consists of primarily inorganic phosphor salts.
Activated sludge	Unstabilized mixture of primary, secondary, and tertiary sludge.
Anaerobic digested sludge (fermented)	Produced in anaerobic digesters. Besides stabilization, the reduction of organic content and pathogens and the elimination of odours should be obtained. Anaerobic digestion can be run at mesophilic temperatures of around 37 °C or thermophilic temperatures of around 55 °C.
Aerobic digested sludge (composted)	Results from the decomposition of organic compounds by microorganisms under aerobic conditions.
Conditioned sludge	Sludge to which polymers or chemicals have been added or were exposed to the physical processes to improve subsequent processes.
Dewatered sludge	Sludge effluent of mechanical dewatering with centrifuges, filter belt presses or vacuum filtration with a dry matter content of 20-40%.
Other types of sludge	Obtained by different sludge treatment processes like: - Disinfection (aiming to reduce the pathogen concentration) - Pasteurization (aiming to eliminate most pathogens by heat) - Thermal hydrolysis (aiming to improve biodegradation of organics)

From here it can be already discussed, that the structural and chemical composition as well as the reaction behaviour, product distribution and composition after hydrothermal conversion of MSS is depending on the following factors: (i) the pollution load of sewage to be treated, and (ii) the technical and design features of the WWTP, as well as (iii) on the sludge treatment process (stabilization technology). In addition, the methodology of processes water- and downstream sludge-treatment applied in a WWTP are not standardized. Even sludge from the same WWTP can vary from one day to another. This results in a product with a much more variable composition than other organic waste streams and low-value biomasses [72]. These compositional differences are represented in Table 3 with MSS from different WWTP stages and MSS treatments and were compiled within a report of the EU [73]. The shown dry matter content (DM), proximate and ultimate analyses are important characteristics of solid fuels. The proximate analysis provides an estimation of the relative proportions of volatile matter (VM), against the residual (non-volatile) solids, fixed carbon (FC) and ash. The ultimate analysis provides information on the content of individual elements such as C, H, N, O, S. In addition, the composition of biogenic large molecules like lipids, proteins and fibres is given, which is from large interest for thermochemical conversion (e.g. HTC, HTL, pyrolysis) of biomass and organic waste into biofuels. It can be noted that different sludge origins strongly influence the DM, VM and elemental content and biogenic composition. The chemistry determining functionalization of the chemical structures within the organic fraction of sludge are aliphatic, carboxylic, amide, amine, aromatic, and methylene groups [74].

Besides the organic components, MSS shows a large share of inorganig material, also refereed to as ash content, being between 10-76 wt.% on a dry basis and mainly consisting of inorganic salts [72]. The main elements occurring within this fraction are Ca, Mg, Fe, Al, K, Si, P and Cl. Especially the phosphorus-rich MSS fractions are nowadays from large interest as resource scarcity and high fertilizer costs are increasing and recovery of phosphorus will be mandatory in Germany in 2029, according to the German Sewage Sludge Ordinance (AbfKlärV) [75,76].

Hydrothermal conversion processes like HTC or HTL offer here possibilities for effective phosphorus recovery [77,78]. However, MSS can contain different undesirable pollutants such as heavy metals e.g Zn, Pb, Cu, Cr, Ni, Cd, Hg and As. The concentrations can be varying from more than 1000 ppm to less than 1 ppm [79]. Organic pollutants can be of synthetic origin like polychlorinated biphenyls (PCBs), polycyclic aromatic hydrocarbons (PAHs), per- and polyflouroalkyl substances (PFAS), dioxins, pesticides, linear-alkyl-sulphonates, nonyl-phenols, polybrominated fire retardants, pharmaceutical residues and microplastics etc. or various pathogens produced by microorganisms [49,56,73,76,80].

Table 3. Examples for of MSS compositions after different treatment methods applied at the WWTP. Data obtained and modified from the EC report on disposal and recycling routes for sewage sludge [73].

	Unit	Primary sludge[b]	Secondary sludge 1[c]	Secondary sludge 2[d]	Mixed sludge[e]	Digested sludge[f]
Dry matter (DM)	wt. %	12	9	7	10	30
Proximate analysis (dry basis)						
Volatile matter (VM)	wt. %	65	67	77	72	50
Residual solid[a]	wt. %	35	33	23	28	50
Ultimate analysis (dry, volatile basis)						
C	wt. %	51.5	52.5	53.0	51.0	49.0
H	wt. %	7.0	6.0	6.7	7.4	7.7
O	wt. %	35.5	33.0	33.0	33.0	35.0
N	wt. %	4.5	7.5	6.3	7.1	6.2
S	wt. %	1.5	1.0	1.0	1.5	2.1
Biogenic composition (dry, volatile basis)						
Lipids	wt. %	27.7	11.9	13.0	19.4	20.0
Proteins	wt. %	36.9	53.7	44.2	41.7	36.0
Fibres	wt. %	24.6	25.4	13.0	18.1	20.0

[a]caluclated by difference (100-VM).
[b]primary sludge with physical/chemical treatment or high pollution load in sewage.
[c]biological sludge with low pollution load in sewage.
[d]biological sludge from clarified water with a low and middle pollution load.
[e]mix of primary sludge and biological sludge 2.
[f]stabilized, anerobic digested sludge.

1.5 Hydrothermal conversion chemistry of biogenic large molecules

In this section, the hydrothermal conversion chemistry of individual, large model molecules (lipids, carbohydrates and proteins), which were defined to represent the biogenic composition of MSS, are briefly reviewed. Subsequently, the reaction pathways during the conversion of mixtures of these large molecules are explained by the recent literature.

1.5.1 Lipids

Lipids are in general water-insoluble compounds, usually occurring as triglycerides. With elevated temperature, the dielectric constant of water is decreasing and miscibility with non-polar compounds like lipids is increased [81]. In hot compressed water, lipids hydrolyse into long-chain aliphatic carboxylic acids and glycerol. At temperatures around 240 °C, the ester bonds hydrolyse [82]. Especially the shorter chained and unsaturated fatty acids start to break off the glycerol backbone at already lower temperatures [83]. The released fatty acids show a relatively high stability against secondary decomposition reactions at sub-critical temperatures. Even unsaturated derivates like linoleic acid were reported to show low conversion at a temperature of 300 °C [84]. With increasing temperature, long-chain hydrocarbons are generated by decarboxylation, which can be accelerated under addition of KOH [85]. Here, it needs to be noted that in the presence of a caustic solution with NaOH or the precursor Na_2CO_3, saponification of the produced fatty acids was reported [84,86].

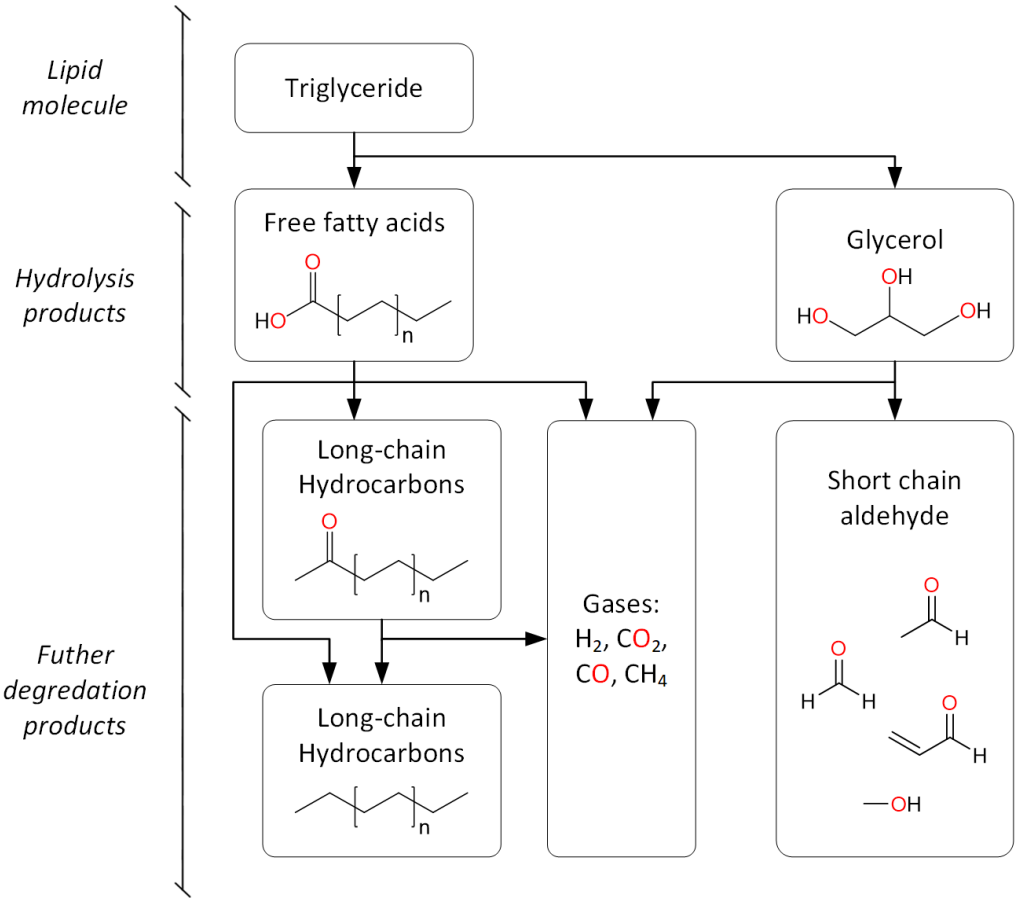

Figure 6. Simplified reaction for the hydrothermal lipid degradation [82,85,93].

As the long-chain fatty acids and hydrocarbons still show a non-polar character, these products are primarily found in the biocrude phase after the HTL. The other hydrolysation product, glycerol, is relatively unstable at near and supercritical temperatures. The main decomposition products are gases like CO_2, CO, CH_4, and some H_2, and water-soluble oxygenates (e.g. acetaldehyde, formaldehyde acrolein, methanol and allyl alcohol). Other lipid compounds like phospholipids often found in membranes of microorganisms hydrolyse rapidly under hydrothermal conditions to the fatty acid monomers, choline and phosphoric acid [87]. Sterols are lipid compounds present in all eucaryote cells and therefore also contained in MSS [88]. Several studies identified sterol derivates in the biocrude, but yet not much information is available about the hydrothermal degradation of sterols so far [89–91]. Hiatal et al. report that cholesterol undergoes dehydration reactions to form cholesta-3,5-diene at temperatures in the HTL range [92].

1.5.2 Carbohydrates

In biomass, carbohydrates primarily occur as polysaccharides. Common examples are cellulose, hemicellulose, starch, inulin, glycogen, pectin, chitin and callose. These polymers consist of different C_6- and C_5-carbonhydrate monomers connected to linear and branched structures with glycosidic bonds. Applying hydrothermal conditions, these carbohydrates rapidly hydrolyse into glucose and other monosaccharides, starting at temperatures around 130 °C [82]. Cellulose shows higher resistance, due to its crystallinity caused by hydrogen bonds. These monomers then undergo further degradation reactions at the HTL temperature range to form various products. The hydrothermal conversion of carbohydrates in sub and supercritical water has been reviewed in several publications [94–98]. A simplified degradation route was proposed by Kruse et al. in 2003 [99]. A modified scheme of this model is presented in Figure 7 with an additional proposed degradation of hemicellulose-originating pentoses proposed by Aida et al. [100]. The main hydrolysation product of starch and cellulose is glucose, which is able to isomerize reversibly into fructose via ketol enol tautomerism [101]. The latter is reported to degrade more rapidly than glucose [102]. Occurring degradations are dehydration, hydration, rearrangement and recombination reactions into a complex mixture of furfurals, phenols and different short-chain carboxylic acids and aldehydes. Furan derivates are formed by dehydration and can undergo secondary reactions to form phenols [103–105]. Hemicellulose, which is a non-uniform polysaccharide, consists primarily of pentoses like D-xylose and arabinose. These carbohydrates undergo comparable degradation and form furfural and different short-chain carboxylic acids as well [100]. Furanic compounds can polymerize to form a polyfuranic structure which can undergo further intramolecular condensation, dehydration and decarboxylation to form stable coke, often referred to as hydrochar [18]. Gases are formed via different reaction mechanisms. The CO_2 can be formed either via the already mentioned decarboxylation reactions or by the water gas shift reaction from CO. Other gases are primarily formed by free radical reactions [106].

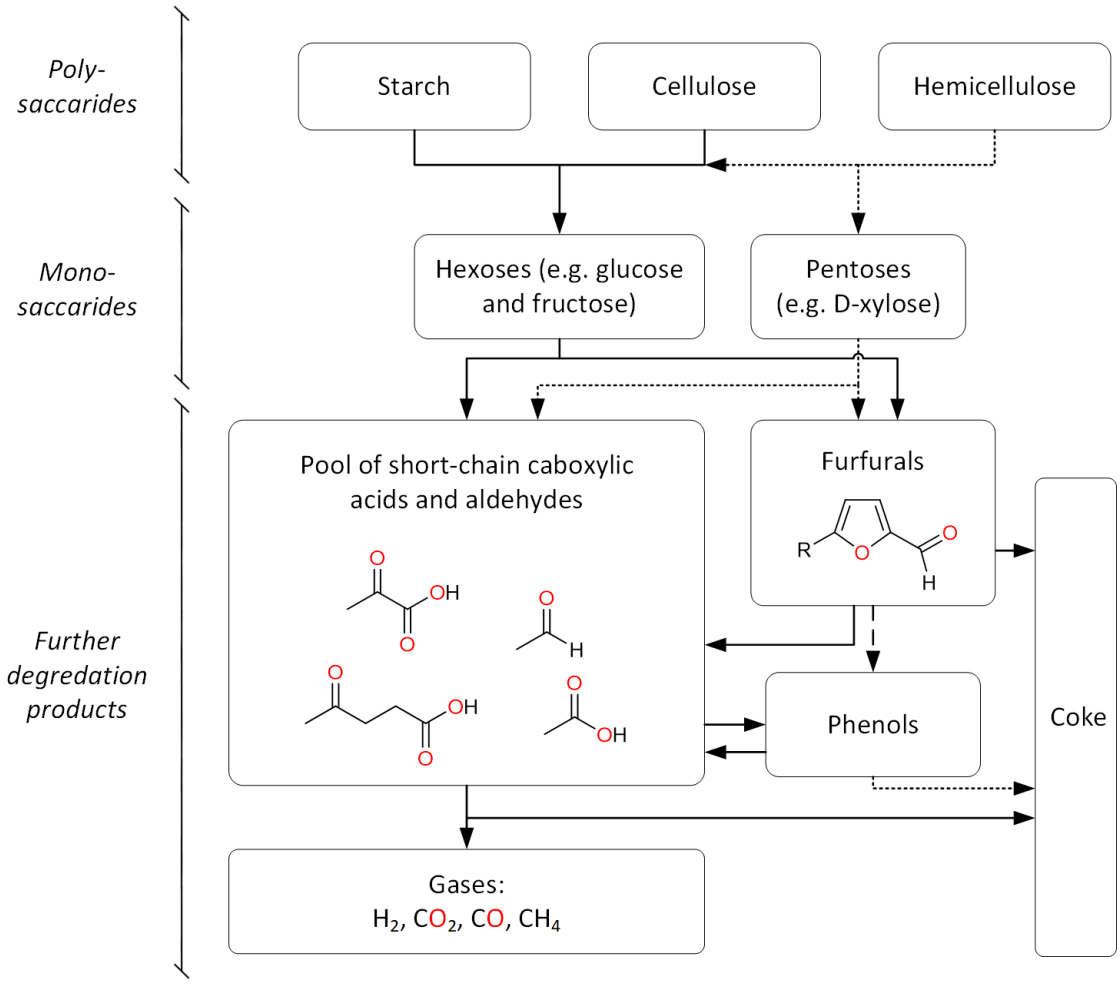

Figure 7. Simplified reaction scheme for hydrothermal carbohydrate degradation adapted and modified from [106].

1.5.3 Proteins

Proteins are omnipresent in biomass and biogenic waste containing cell material like MSS. Likewise to carbohydrates proteins are biogenic polymers, but consisting of polypeptide molecules, which in turn are composed of amino acids. The so-called peptide bond is an amide-type bond between the amine and the carboxyl group of an amino acid and is reported to be more resistant than the carbohydrate glycoside bond [107].

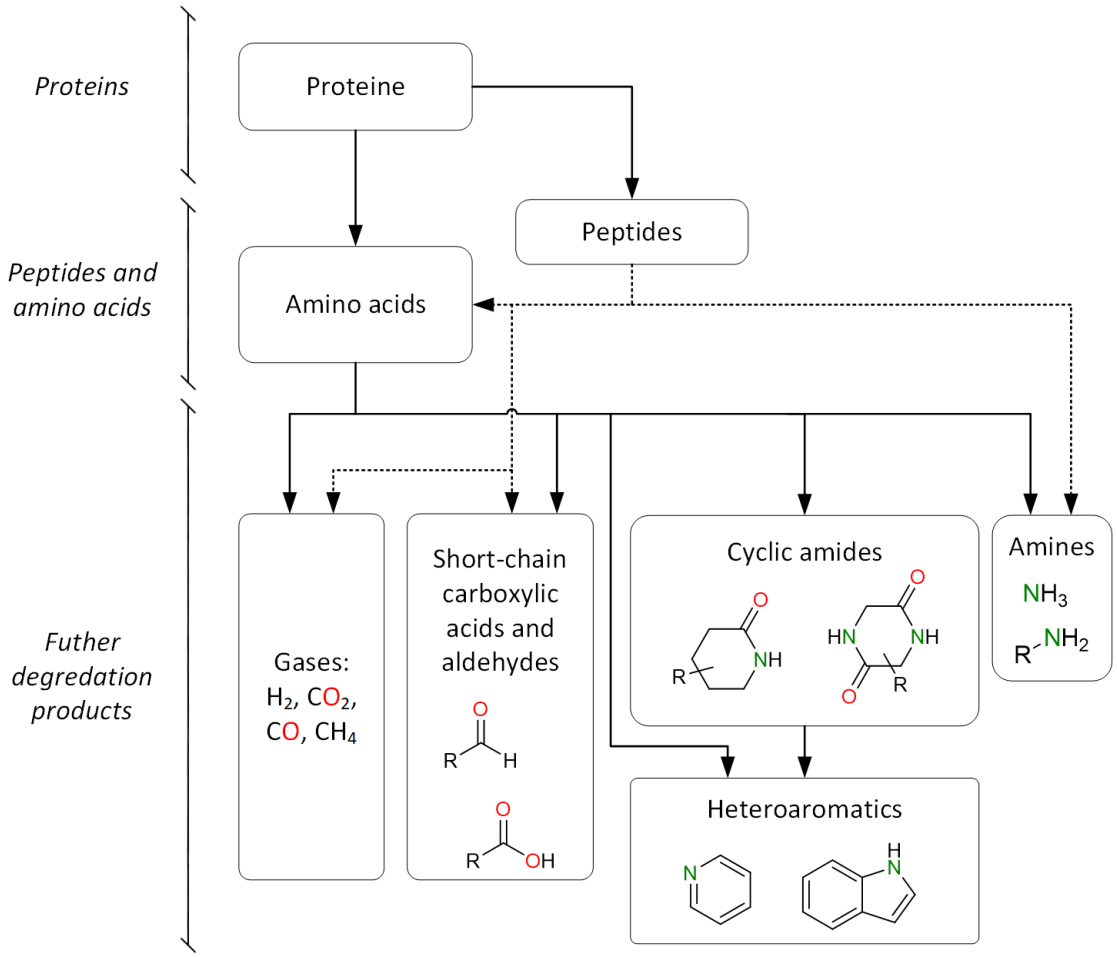

Figure 8. Simplified reaction scheme for hydrothermal protein degradation.

At around 65 °C proteins start to undergo denaturation (unfolding) and subsequent aggregation below 80 °C. The hydrothermal decomposition of proteins usually starts with the hydrolysis of the peptide bond, releasing peptide fragments and amino acids at a temperature of around 190 °C [82]. Peptides can undergo further hydrolysis and can't be decoupled off the simultaneous degradation of amino acids [107]. The decomposition rates of amino acids exceed the hydrolysis rate of peptides at 250 °C [108]. It is stated that even before hydrolysis of the protein backbone occurs, amino acids get oxidated and form pyroglutamate by releasing amines into the aqueous supernatant. According to Aida et al., a fast heating rate of the protein can yield larger peptide fragments, suppressing the secondary amino acid degradation [109].

With a view on amino acids, decomposition can be simplified down to two reactions. Either a decarboxylation, releasing CO_2 of the carboxylic group or deamination reactions, releasing NH_3

of the amine group, occur [110]. The splitting of the protein bond is reported to be catalysed by the addition of an acid or alkaline agent, where the latter leads to a higher amino acid yield [111]. Li et. al reported that a lower or higher pH-value increases the decarboxylation rate, depending on the amino acid [112]. With increasing temperature close to the critical point all amino acids are completely degraded into water-soluble compounds [108]. With regard to the hydrothermal liquefaction temperature range, Dote et al. investigated the elemental distribution in the product phases after hydrothermal conversion and revealed that only about 5 wt.% of nitrogen was retained in the non-polar biocrude [113]. Certain amino acids can also undergo internal ring closure via dehydration and deamination reactions, forming cyclic peptides, often referred to as lactams. Additionally, various heteroaromatic structures are formed in a certain HTL temperature range. Fan et al. report the formation of caprolactam, pyridine and cyclic dipeptide (2,5-diketopiperazine) of the hydrothermal conversion of lysine at a temperature of 300 °C [114,115]. The dipeptides were reported to be the most abundantly detectable components in the recovered non-polar phase of the hydrothermal conversion of bovine serum albumin (BSA) [116]. The amino acid tryptophan degrades to its indole base structure, which can react further to form alkylated pyrrole derivates [117].

1.5.4 Biogenic model molecule mixtures

The previously briefly discussed hydrothermal conversion of individual large model molecules shows a wide variety of reactions occurring. After the primary hydrolysis of the large molecule, different degradation pathways such as fragmentations, condensations, dehydrations and their combinations lead to a wide variety of products. Real feedstocks, especially biogenic waste material like sewage sludge, have a much more diverse and complex chemical composition. As different large molecules are mixed, interactions between either them or their degradation intermediates and products occur. As described previously in Section 1.2, depending on the temperature, the primary products are found in the biocrude, aqueous, gaseous or solid phase. In the following, the main interactions generating N-compounds are described employing a

lipid and protein, carbohydrate and protein, and a ternary model mixture of large molecules. In addition, the effect on the yield of resulting product phases is described.

When investigating the interactions between carbohydrates and proteins under hydrothermal conditions, the Maillard reaction is often discussed as the underlying mechanism, forming a variety of N-heterocyclic and heavy nitrogenous compounds. Within a lower temperature range (<200 °C) high molecular weight heterogeneous and nitrogen-containing polymers named melanoidins are formed from sugars and proteins. These compounds are occurring brownish and able to stabilize emulsions [118–120]. At higher temperatures around 250 °C, these melanoidins are likely to decompose via decarboxylation and deamination reactions, forming carbonyl, furan, pyrazine, pyridine and pyrrole derivates [119,121]. The reported N-species are often referred in the non-polar biocrude phase and can also be formed via the amination of a disaccharide to glucosylamine and amadori intermediates [114,122–124]. Various studies describe the hydrothermal conversion of a mixture of carbohydrates and proteins within the HTL-temperature range as beneficial regarding the biocrude yield [114,125,126]. Simultaneously, the N-recovery into this non-polar phase is significantly increased. Otherwise, Croce et al. found that after hydrothermal conversion at 300 °C of binary cellulose and BSA blend, the biocrude yield was lower compared to competing model stock blends [127].

The interactions between lipids and proteins were investigated under hydrothermal conditions, orientating in the HTL temperature range, as lipids start to hydrolyse above 240 °C. The free fatty acids react via condensation reactions with amines, which are formed by protein degradation [128,129]. Chiaberge et al. investigated the HTL-derived biocrude of organic municipal waste and could identify a variety of long-chain amide products, combinations of different fatty amides and branched amines [130]. Larger amines like phenylalanine-derived phenylethylamine can form amides with a free fatty acid [131]. This more complex compound seems not to be stable at higher temperatures and decomposes into styrene and a simpler, stable fatty acid amide [132]. Déniel reviews several studies and describes the positive effect of these

interactions on the biocrude yield, whereas Fan et al. identified the enhancing amidation reactions occurring only at higher temperatures of 350 °C [133,134]. Posmanik et al. even describes an antagonistic effect of this interaction at a lower temperature range. It is described that the hydrolysation of lipids is suppressed and reaction products are shifted into the gas and aqueous phase [126].

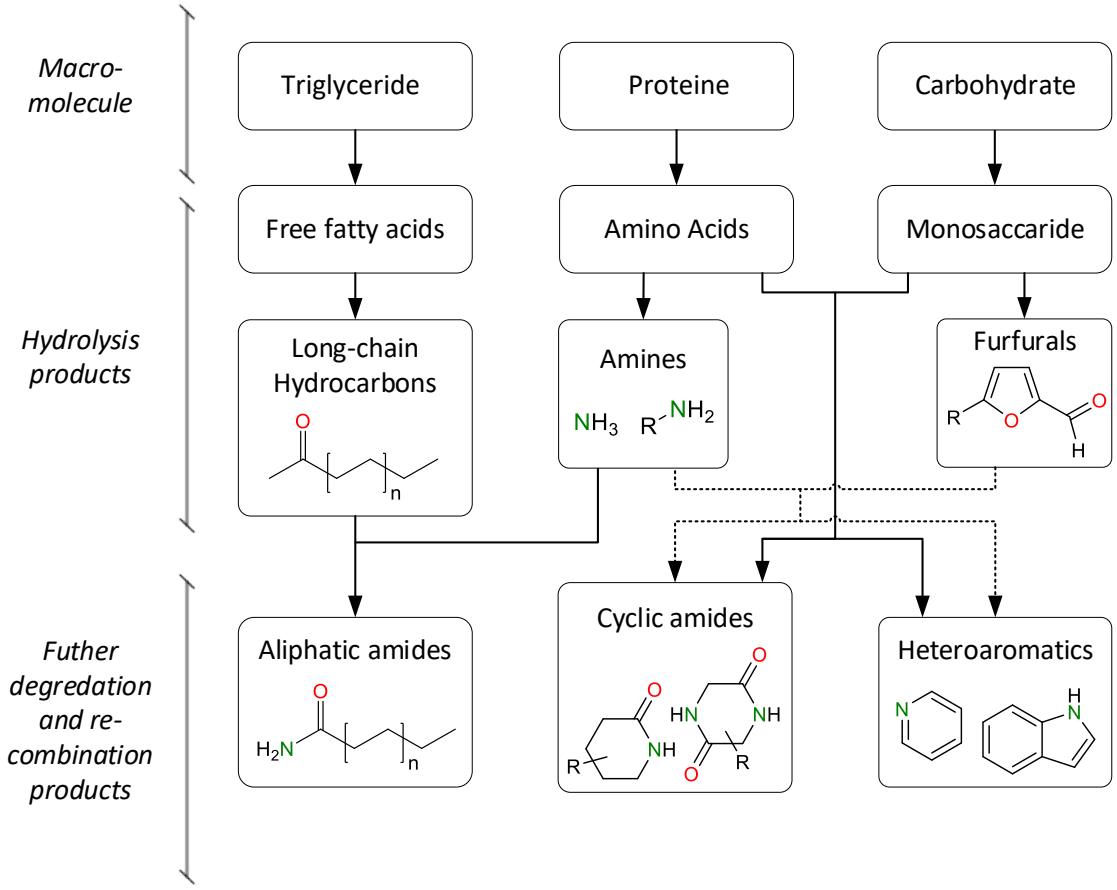

Figure 9. Simplified reaction scheme for the hydrothermal conversion large model molecule mixtures, adapted and modified from [134].

Within a ternary mixture proteins, lipids, and carbohydrates decompose and recombination reactions described in the binary mixtures occur simultaneously. Several reaction products of the previously explained binary mixtures were identified also in the ternary mixture derived biocrude [127] In a recent study, the importance of generated intermediates is described [135]. Depending on the reaction partner present, these further react to N-heterocyclic, -aromatic and carbonaceous material or form short and long-chain-aliphatic amides. Fan et al. stated that

the amidation of fatty acids competes with the proposed Maillard reaction of protein degradation products and sugars [134]. It was shown that this largely depended on the applied reaction temperature. A modified reaction scheme for the HTL of ternary mixtures is proposed in Figure 9. With a higher reaction severity, meaning longer reaction times and higher temperatures, the ternary mixture showed enhanced biocrude yields [126], which can be attributed to the beneficial reaction mechanism between free fatty acids and saccharides [126,136].

1.6 Hydrothermal liquefaction of biogenic waste to produce low nitrogen biocrude

Recent achievements in the conversion of biomass and biogenic waste have been made to produce drop-in transportation fuels. The EC supported six EU-H2020 projects within the last 5 years to explore HTL as a potential thermochemical conversion technology of biogenic waste feedstocks, namely 4REFINERY (2017), Heat-to-Fuel (2017), HYFLEXFUEL (2017), WASTE2ROAD (2018), NextGenRoadFuels (2018), BL2F (2020) [137–142]. All of these projects aim to cover the whole value chain from feedstock to drop-in-fuel, each with specific either feedstock generation, thermochemical conversion or upgrading. A generalized valorization chain is depicted in Figure 10. The following section reviews studies conducted in order to lower the N-content, in general, and molecular N-heteroaromatic content, in particular, along this proposed process chain.

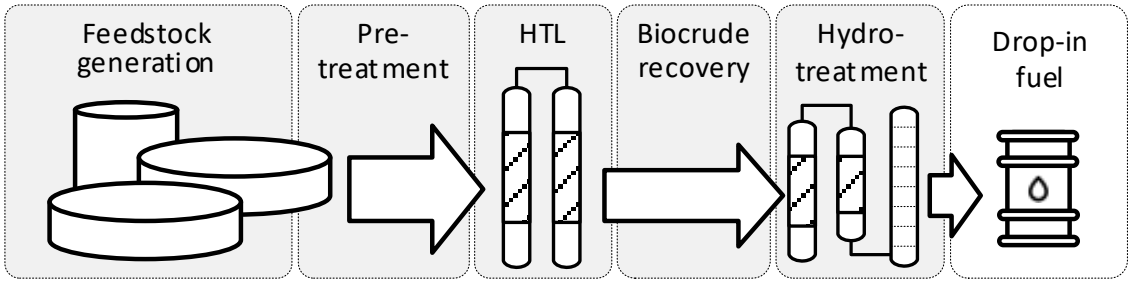

Figure 10. Hydrothermal conversion and fractionation value chain. Including feedstock generation, pre-treatment hydrothermal liquefaction, biocrude recovery and hydrotreatment to produce drop-in fuel.

1.6.1 Feedstock generation

Influence of feedstock composition

Strongly related to the pre-treatment is the influence of the biochemical composition of the HTL feedstock. Suzuki et al. converted MSS of different WWTPs and process steps via HTL into biocrude and showed that the yield strongly depends on the starting crude fat (lipids) content [143]. Lipid-rich raw primary and raw mixed sludge showed a significantly higher biocrude yield and lower N-contents than low lipid-containing activated and digested sludge. It was shown by Yoo et al., that high lipid-containing algae produce a better quality biocrude than low lipid-containing algae, which is also reflected in a higher energy return on investment [144]. The biocrude generated by algae with a low lipid content shows a greater amount of N-heterocyclic compounds and is rated as a less favourable feedstock for biocrude production [145]. Naturally less long-chain aliphatic derivates, generated from lipids are found.

Another option to influence the biochemical composition of the feedstock is the co-liquefaction, where different types of biomass or organic wastes are mixed prior to HTL. Ellersdorfer showed that co-liquefaction of MSS with *chlorella vulgaris* microalgae leads to higher biocrude yield and higher heating value of the HTL-derived biocrude [146]. Leng et al. found that the addition of rice straw to MSS shows a beneficial effect on the biocrude yield and properties as more esters and phenols are generated [147]. Mixing MSS with cellulose-rich brewery residues also increased the biocrude yield [148]. Bhatwadeker et al. investigated the co-liquefaction potential of MSS and wheat straw at slightly supercritical conditions and could not identify synergetic effects regarding the biocrude yield.

1.6.2 Hydrothermal conversion

Pre-treatment

Several pre-treatment technologies have been applied to change the HTL-feedstock composition. For example, various aqueous solutions, organic solvents and physical treatments

were used to improve the subsequent HTL process and lower the presence of problematic heteroatomic compounds. Liu et al. studied the effect of three inorganic and three organic acid pre-treatments on the HTL of MSS [149]. The highest biocrude yield was obtained after pre-treatment with HCl, while the lowest nitrogen content was achieved after an oxalic acid pre-treatment. If biogenic large molecules like proteins and lignocellulosic material should be degraded before the HTL conversion, milder hydrothermal hydrolysis (HTH) is an option and is already applied on MSS within commercialized processes like the CAMBI ® and BIOTHELYS ® processes [150]. In general, a degradation of carbohydrates and proteins should be achieved to produce short carboxylic acids (often referred to as volatile fatty acids). These are then easier digested by methane-producing microorganisms, while larger, long-chain carboxylic acids (fatty acids) remain more or less unaffected [63]. When proteins and related amino acids decompose, higher ammonia contents within the sludge liquor were identified [151]. In addition, Maillard reaction products like melanoidins were detected [152]. So far, only a few studies combined HTH of MSS with a subsequent HTL. Chen et al. applied a microwave pre-treatment with different intensities on MSS and achieved slightly lower N-contents in the resulting biocrude, while similar biocrude yields [153]. It needs to be noted that the pre-treated MSS was directly liquefied without the separation of an N-rich supernatant. For the HTH pre-treatment of algae various studies on the combination with a subsequent HTL are available. Constanzo et al. treated algae with water at temperatures between 125-225 C and separated the solids from the aqueous supernatant, removing about 45% of nitrogen before the HTL. The resulting biocrude showed a 26-28% lower N-content, but overall the biocrude yield was 35-71% lower [154]. Comparable results were obtained by studies with HTH pre-treatment on high protein and low lipid algae feedstock, respectively [155,156].

Another pre-treatment approach is the extraction of valuable lipids from the MSS, which can subsequently be converted into valuable fatty-acid-methyl-esters (FAME) or hydrotreated-vegetable-oils (HVO). In several studies lipid extraction via an organic solvent was performed [157,158]. Fan et al. extracted lipids with a hexane and methanol mixture and converted the

solid MSS residue by HTL [159]. With this integrated process, the biocrude yield was decreased, but in total, a higher energy recovery could be achieved.

Hydrothermal liquefaction and reaction-enhancing additives

The addition of reaction-enhancing materials, to the HTL process should increase the biocrude yield, e.g. by suppressing the formation of hydrochar or improve product quality by lowering e.g. the N-content. These materials are commonly referred as catalysts in the literature. However, in this work, they are designated as reaction-enhancing materials as it is uncertain whether the compounds were depleted or not after a reaction.

The most commonly applied additives are water-soluble sodium or potassium hydroxid or carbonate. In different studies, it was shown, that the reaction-enhancing effect is strongly dependent on the applied feedstock and, consequently, the biogenic composition. As previously discussed, carbohydrates are likely to form hydrochar, which can be suppressed by the addition of alkali metal ions. Their application was found to be very useful with lignocellulosic feedstocks, but which is relatively low in MSS [161]. An increased biocrude yield of MSS was found by Yokoyama et al. with the addition of Na_2CO_3 [162]. However, Suzuki et al. showed that for one of the MSS investigated, the carbonate additive increased the biocrude yield, while for the other only a negligible effect was observed [143]. Shah et al. identified only a minor, non-significant increase of the biocrude yield by the addition of K_2CO_3, whereas the N-content was significantly reduced [163]. In contrast, Qian et al. found lower biocrude yields when adding Na_2CO_3 or K_2CO_3 to the feedstock [164]. Within several studies, water-soluble organic acids were added to the HTL feedstock. Prestigiacomo et al. added formic acid as a hydrogen donor to MSS liquefaction experiments [165]. Under hydrothermal conditions formic acid decomposes into CO_2 and H_2, which is likely to hydrogenate the biocrude compounds, increasing the H/C-ratio and lowering the heteroatom content. On the one hand, it was found that acetic acid decreases the biocrude yield [164,166]. On the other hand Fan et al. showed a slightly positive effect of acetic acid at temperatures of 250 °C and 300 °C. Shah et al. added acetic acid in combination with K_2CO_3 to the HTL of MSS and could

increase the yield and simultaneously lower the N-content [167]. The addition of short-chain, water-soluble organics could be achieved with the recycling of the aqueous phase. Studies by Kohansal et al. showed that this could increase biocrude yield and carbon efficiency of the HTL process, simultaneously recovering the reaction improving additives and tackling the disposal issue of the highly polluted aqueous phase [168]. With the liquefaction of wet, protein-rich biomass, the concentration of nitrogen in this aqueous phase and separation of ammonia to suppress N-pollution of the biocrude must be considered.

Further studies investigated the addition of heterogeneous, catalytic active material to the MSS feedstock. Rahman et al. investigated the addition of red mud, a residual of the alumina production, to the HTL of MSS, but could only determine a negligible effect on the biocrude yield on N-content, while the content of acids within this phase was reduced [169]. Prestigiacomo added aluminum oxide supported NiMo, CoMo catalyst or an activated carbon felt to HTL experiment on MSS and achieved significantly lower N-contents in the biocrude obtained [170]. Similarly, Zhai et al. applied activated carbon of MSS within the HTL of MSS and could increase the biocrude yield [171]. Unfortunately, it is not clear from this study how this increase in yield is substantiated.

1.6.3 Downstream processing

Phase separation

Ideally, the HTL product phases separate spontaneously, allowing an effective recovery of biocrude. In practice, the phase separation of the biocrude from the aqueous and solid byproduct turns out to be problematic. The presence of surfactants stabilizes an emulsion of water with non-polar compounds, preventing the spontaneous separation [172]. It is assumed that this emulsification is even more increased by the effect of Pickering emulsion, a process, in which solid hydrochar particles are involved [173]. Additionally, MSS contains usually a high amount of inorganic material, which usually remains solid during the HTL-conversion

and contributes therefore to larger quantities of solid by-product. In continuous processing, two physical methods are commonly applied to separate the biocrude of the solid material by using either an in-line filtration system or subsequent distillation [174,175]. The in-line filtration makes use of the low viscosity of the dissolved biocrude at the HTL temperature range, whereas solid material remains mostly on the filter. However, this can only be effectively applied on the HTL of a feedstock with low inorganic contents like microalgae. The distillation procedure combines a flash separation and distillation to break the biocrude/solid/water emulsion in the first step before the solid char is removed from the biocrude by filtration. As the biocrude is rather composed of heavy compounds, only a low yield could be achieved (6 to 10.5 wt.%). Besides the low yield, it is questionable to break an emulsion by a distillation process. Another technique commonly applied in batch experiments, but also in continuously operated pilot plant scale, is the extraction with organic solvents to recover the biocrude and separate the other byproducts [176,177]. The solvent lowers the viscosity so that the highly viscous biocrude can be washed out of the solid deposits. Qian et al. and Jahromi et al. tested different organic solvents with different solvent polarities to recover biocrude from the HTL of MSS [164,178]. Dichloromethane (DCM), a solvent with a medium polarity, achieved the highest recovery of biocrude and energy in both studies. The influence of the solvent on the recovery was also tested in various studies on the HTL of algae feedstocks [179–181]. It was shown that the solvent polarity had a strong influence on the biocrude yield and heteroatom content, and consequently on the quality. Generally, it can be said that a solvent of lower polarity results in a low heteroatom content, whereas a solvent with higher polarity recovers more heteroatom compounds. Again, the feedstock composition influences the most suitable solvent [176]. The polarity can hereby be expressed, for example, by the empirical derived $E_t(30)$ value [182].

Demetallization

Despite the considerably increased quality due to the improved biocrude separation, the biocrude still contains significant amounts of inorganic contaminants, depending on the origin or the HTL and separation procedure [183–186]. It is believed that these compounds are incorporated in organometallic complexes, which can become problematic in further refining due to catalyst fouling, reactor plugging and product use [187]. Metals occur also in fossil-derived heavy oils, where various demetallization processes have been developed [188]. Within the field of HTL-derived biocrude, only a few research articles tackled this issue so far, coupling solvent extraction with a so-called metal washing step, including an acidic solution. Jensen applied citric acid coupled with a methyl-ethyl-ketone (MEK) extraction to remove alkali metals from the biocrude derived from lignocellulosic material, reducing the metal content from 11351 ppm down to 41 ppm [189]. Haider et al. used different organic and inorganic acids at a concentration of 0.1 mol·L^{-1} to wash *miscanthus*-derived biocrude, which had been mixed with acetone and achieved with sulphuric acid (H_2SO_4) a demineralization degree of 92.7% [190]. The procedure was again applied in a recent study on the biocrude of HTL of MSS and *spirulina* algae [186]. The MSS biocrude metal content could be reduced to 71 ppm, while it remained in the algae-derived biocrude at 380 ppm. It was also shown that metal-stabilizing species in the MSS biocrude were referred mainly to as oxygenated groups, whereas basic nitrogen groups are the stabilizing species within the algae biocrude. Cyanobacteria like *spirulina* are well known for containing porphyrin structures, which are stable within hydrothermal processing, also transferring metals like vanadium in fossil crude oil [184,191,192].

Specific separation of nitrogen-compounds

The addition of specific extractants to remove specific N-compounds from an oil matrix is widely applied within the research of fossil crude oil and petroleum products. Yet, the published research for biogenic, HTL-derived biocrude or pyrolysis-derived bio-oil is rather limited.

Besides disrupting the metal stabilizing complexes, acids affect the solubility of N-compounds and open the possibility to extract them from a non-polar matrix [193–196]. Dote et al. applied a liquid-liquid extraction methodology with aqueous polar solutions to isolate basic N-compounds from an HTL biocrude [197]. Das et al. applied a modified methodology, extracting primarily N-heterocyclic compounds from a pyrolysis bio-oil, derived from chicken manure [198]. Intending to extract valuable N-compounds from pyrolysis bio-oil from sewage sludge, Fonts et al. applied diluted HCl as one extraction agent, recovering amides [199].

A further liquid-liquid extraction methodology applies ionic liquid or deep eutectic solvents. These liquid salts can have different cation/anion combinations that provide unique properties and can be tailored to facilitate the specific extraction of N-containing compounds [200,201]. The application of both these extraction agents is relatively new and primality tested with model oil solutions. Laredo et al. achieved removal rates above 90% for pyrrolic-related indole and carbazole from a model solution with imidazolium-based ionic liquids [202]. Ali et al. applied choline chloride and phenyl-acetic acid deep eutectic solvents on a model oil and removed 99.2% of pyridine and 98.2% of carbazole [203]. Especially the separation of 'neutral' pyrrole-based compounds is in both cases (ionic liquid and deep eutectic solvent) from interest as acidic additives only achieve separation of basic N-compounds.

Another N-compounds-specific separation methodology is the application of solid sorption materials. Due to chemical (chemisorption) or physical (physisorption) interactions, the N-compounds retain within a solid. Laredo et al. reviewed different types of sorbent materials for the denitrogenation of oil, namely silica gel, activated alumina, activated carbon, metal-organic frameworks, ion exchange resins, modified polymers and zeolites [204]. All these have been tested only on model and fossil feedstock oils, but not on biogenic-derived matrices.

1.7 Identified knowledge gaps and the derived research proposal

In the previous review of the existing state-of-the-art, it became clear that wastewater pollution load, different wastewater treatment methodologies and downstream sludge treatment influence the biogenic composition of effluent MSS. Additionally, it was shown that biogenic large molecules and their mixtures generate different chemical species by hydrothermal conversion. The N-species are primarily generated from lipids via amidation and from carbohydrates via the Maillard reaction in the presence of proteins. Furthermore, it was found that several chemical and physical treatments are available to reduce the N-content along the valorization chain from feedstock to the final drop in fuel. The fractionation of the MSS or HTL biocrude into N-rich and N-poor phases is of special interest if the products are intended for fuel use. To further promote knowledge and technology development, the following three knowledge gaps are identified:

1) The effect of the origin of MSS on the HTL-derived biocrude yield and composition (quality) is not systematically investigated. Notably, the influence of different compositions of biogenic large molecules on the generation of problematic N-heteroaromatics is still barely discussed.
2) Related to the influence of the biogenic composition of the MSS the application of a pre-treatment to minimize the N-content in the obtained biocrude with only low losses has not been investigated.
3) Lastly, it was shown that the phase separation for biocrude recovery is still unsatisfactory and a strong, quality determining factor. With the addition of acids, N-compounds and metal could be separated from the biocrude matrix. A detailed description of the complex N-compounds within the biocrude matrix and their interaction and potential extraction with polar aqueous solutions have not been established.

Therefore this thesis aims to identify techniques along the value chain from MSS feedstock to drop-in fuel that can reduce the N-heteroatom content before the eventual hydrotreatment. This covers four research topics, considering the above identified knowledge gaps.

- The effect of the upstream wastewater treatment technology on the resulting biogenic MSS composition and subsequent HTL performance should be investigated. Therefore, MSS samples are converted via HTL and the derived biocrude yield and quality are examined. This work is reported in Chapter 2.
- The influence of the biogenic composition within the HTL feedstock on the generation of N-compounds should be investigated. Herby different ratios of model substances mixtures of lipids, proteins and cellulose are converted hydrothermally at HTL conditions and representative N-compounds of aliphatic and heteroaromatic nature are quantified in the resulting biocrude. Additionally, the potential suppression of N-heteroaromatics generation with carboxylic acids should be discussed (Chapter 3).
- The nitrogen and the presence of N-heteroaromatics should be reduced by intervening in the process chain. Therefore, a two-stage hydrothermal process involving a mild hydrothermal treatment to separate an N-rich phase and modify the MSS composition plus a subsequent HTL procedure should produce a high-quality biocrude (Chapter 4).
- Downstream the value chain and the HTL-reaction, the extraction of N-compounds from the biocrude should be investigated. With an advanced analytical approach structural and solubility characteristics of the extracted N-compounds should be explained (Chapter 5).
- Finally, Chapter 6 draws a conclusion and ventures an outlook on future related research topics and work.

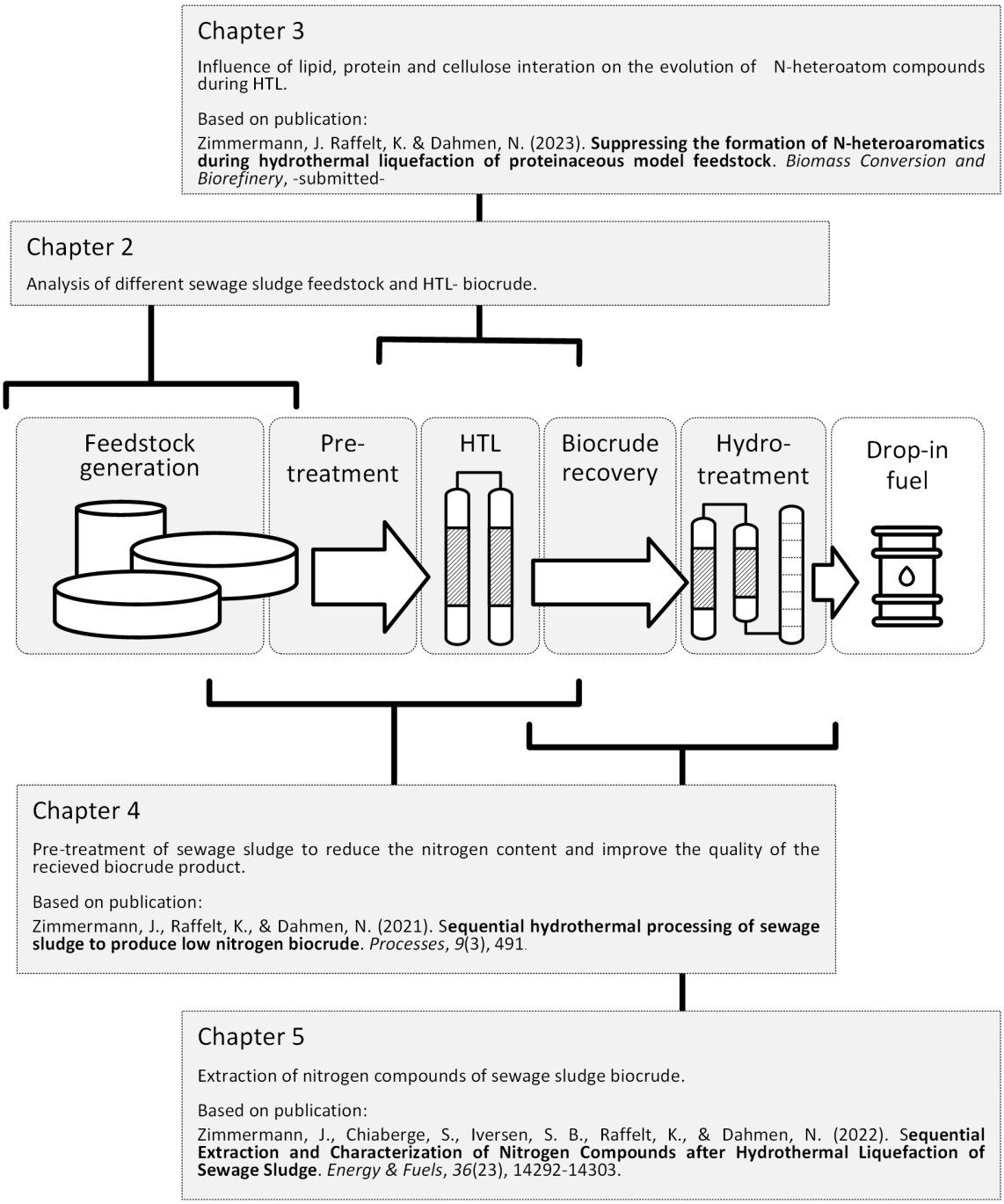

Figure 11. Alignment of chapters and associated publications along the proposed hydrothermal fractionation value chain..

Chapter 2.

Analysis of different sewage sludge feedstocks and hydrothermal liquefaction biocrude

2.1 Introduction

In Chapter 1 it was shown within the literature review, that different feedstocks influence the HTL process and the resulting yield and composition of the biocrude product

Within this Chapter, MSS samples from different regions within the EU and wastewater treatment technologies are extensively characterized and subsequently converted into biocrude via the HTL process. With the knowledge of the origin and analytical results of the MSS sample and the upstream wastewater process, the resulting composition and its influencing factors is discussed.

2.2 Materials and methods

2.2.1 Feedstock materials and chemicals

Sewage sludge samples were collected in early 2019 from wastewater treatment plants in different European cities (Karlsruhe, Thessaloniki, Tudela, Pamplona) by project partners within the NextGenRoadFuel-Horizon2020 project.

All other chemicals used in the following experiments were obtained in analytical grade quality from Merck (MilliporeSigma).

2.2.2 Experimental setup and hydrothermal liquefaction procedure

The HTL experiments were conducted in 25 mL micro-autoclaves (Stainless steel, EN 1.4571). These reactors were filled with 1.69 to 1.90 g of the specific MSS sample and deionized water. The final solution is occupying 60% of the available volume and has a dry-ash-free solid load of approximately 10 wt. %. Before closing the micro-autoclaves the headspace was purged with nitrogen three times and pressurized to 1 MPa, to identify potential leaking. A fluidized sand bath (SBL 2, Techne, Stone, UK [214]) at a temperature of 350 °C was used to rapidly heat the

reactor and start the conversion. The reaction pressure within the reactor was estimated to 20 MPa according to the gas saturation pressure of water [22]. The heating time to reach the final temperature was measured in previous experiments at 8.75 min. This time is not considered as reaction time, even though it's obvious that hydrothermal conversion reactions are occurring Once the temperature was reached the reaction time was set to 30 min. Afterward, the reactors were rapidly cooled down in a water bath for 10 min. The reactor was opened and the gaseous product discharged. The residuals in the reactor were mixed with 5 mL dichloromethane (DCM) and separated by a Büchner funnel (47 mm diameter, 0.45 µm pore size, Nylon, Whatman, GE Healthcare, Buckinghamshire, UK). Then, the reactor and filter residue were washed exhaustively with 45 mL DCM. After the spontaneous phase separation of water and DCM overnight, the aqueous top layer was separated with a syringe and stored below 5 °C for further analysis. DCM in the residual organic phase was removed overnight under a gentle nitrogen stream.

2.2.3 Analysis of starting materials and biocrude product

The water (moisture) content was determined by drying the sample at 105 °C for three hours, following the DIN 51718 standard. The amount of ash was determined following the standard, DIN 51719. The MSS samples were heated to 815 °C and held for 2 h in the oven, before cooling in an exicator. The content of volatile matter was determined according to the ISO 18123 standard, by. Heating the MSS samples rapidly to 900 °C and holding this temperature for 7 min. The HHV value of MSS samples was determined in a bomb calorimeter (IKA, Staufen, Germany), following DIN 51900.

The contents of crude fat, crude protein and crude fibre were determined following the methodologies explained in the VDLUFA MB III [215]. The crude fat was determined via a Soxhlet extraction. The crude protein content was determined by first measuring the organic nitrogen content via the Kjeldahl method and subsequently multiplying the result by the jones factor of 6.25 [216,217]. The crude fibre content as a sum of hemicellulose, cellulose and lignin

content was determined by measuring the aNDF (Neutral detergent fibre after amylase treatment), ADF (Acid detergent fibre) and ADL (acid detergent lignin) content.

The elemental composition of the starting materials and derived biocrude were determined by a CHNS-Analyser (Vario EL cube, Elementar Analysetechnik GmbH, Hanau, Germany.)

2.2.4 Calculations

The yield of biocrude was calculated by the following Equation (1).

$$\mathrm{Y}\ (dry, ash\ free) = \frac{m_{biocrude}}{m_{MSS} - m_{ash} - m_{moisture}} \quad (1)$$

where Y is the yield (wt. %) and m is the mass (g) of the biocrude, MSS or ash and moisture in the feedstock.

The carbon or nitrogen recovery of biocrude, solid, gas, and aqueous phases were calculated by Equation (2).

$$\mathrm{ER} = \frac{m_{biocrude} \cdot E_{biocrude}}{m_{MSS} \cdot E_{MSS}} \quad (2)$$

where ER is the element recovery of carbon or nitrogen in the biocrude, m is the mass (g) and E is the element content in wt. %.

2.3 Results and discussion

2.3.1 Sewage sludge characteristics

The feedstock materials were collected from four different WWTPs of European cities. The location and a brief description of the different MSS samples are presented in Figure 12. For all samples, the WWTP processes are differently designed, depending on the upstream sewer system. The samples from Karlsruhe, Thessaloniki and Tudela are considered activated sludge collected in different stages in the treatment process, while the sample from Pamplona is considered as a digestate after the anaerobic sludge stabilization. All characteristics of these MSS samples are listed in Table 4. The Karlsruhe MSS sample (KA-MSS) consists of a mixture of primary and secondary activated sludge, which was dewatered by centrifugation and would have been directly incinerated, resulting in a relatively low moisture content (69.6 wt. %). The

Thessaloniki MSS sample (TH-MSS) was collected after the activated sludge treatment and sedimentation stage and contains therefore the highest moisture content (89.3 wt. %).

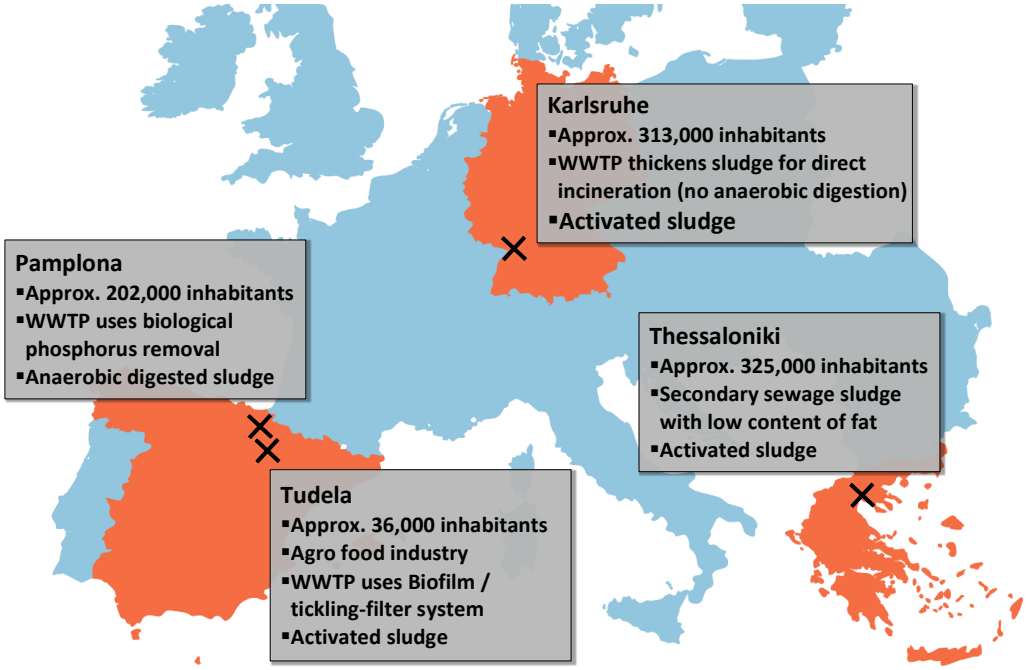

Figure 12. Brief description of different municipal sewage sludge (MSS) samples collected in various cities in three European states (Spain, Germany and Greece).

Another activated sludge sample was collected from the Tudela WWTP facility (TUD-MSS). This MSS sample has a very low ash content, the lowest of the samples compared (16.8 wt. %). It is assumed to be related to this specific biofilm wastewater treatment process in which no precipitating salts are added. The Pamplona MSS sample (PAM-MSS) shows the highest ash content (31.0 wt. %) as the upstream anaerobically digestion converted a certain amount of organic matter into methane/CO_2 biogas.

Concerning the higher heating value (HHV), based on dry basis, of the MSS samples the TUD-MSS shows the highest value with 26.3 $MJ \cdot kg^{-1}$, while TUD-MSS shows the lowest of the compared, with a value of 21.0 $MJ \cdot kg^{-1}$. This is reflected in the elemental composition where the HHV is highly dependent on, decisive factors are the C- and H-contents [218]. However, the elemental and organic composition of the water, ash-free, organic matter is largely dependent on the upstream wastewater treatment process [72,219]. The content of crude fats

and fibres was the highest in the TUD-MSS sample. As this sample origin was an activated biofilm, it can be assumed that a large portion of this sludge consists of extracellular polymeric substances, where lipids and carbohydrates (hemicellulose and cellulose) are found as building blocks [220,221]. The content of crude proteins was the highest in the raw activated TH-MSS, as this sample must mainly consist of microorganisms.

Table 4. Properties of the different feedstock MSS samples. The values in brackets indicate the standard deviation. All values are given on a dry and ash-free basis, except the moisture content.

	Karlsruhe	**Thessaloniki**	**Tudela**	**Pamplona**
Abbreviation	**KA-MSS**	**TH-MSS**	**TUD-MSS**	**PAM-MSS**
Proximate analysis				
Moisture content [wt. %]	69.6 (0.3)	89.3 (0.1)	77.8 (0.2)	79.2 (1.1)
Volatile content [wt. %]	73.0 (0.4)	70.1 (0.2)	76.7 (0.0)	64.1 (0.6)
Ash content [wt. %]	27.4 (1.8)	21.0 (0.2)	16.8 (0.1)	31.0 (0.1)
Higher heating value [MJ·kg^{-1}]	23.4 (0.1)	21.9 (0.0)	26.3 (0.1)	23.8 (0.1)
Elemental analysis				
Carbon [wt. %]	53.1 (0.1)	51.9 (0.1)	56.4 (0.2)	53.4 (0.3)
Hydrogen [wt. %]	7.6 (0.0)	7.5 (0.0)	8.3 (0.0)	8.1 (0.0)
Nitrogen [wt. %]	7.0 (0.1)	8.9 (0.1)	4.6 (0.0)	6.8 (0.0)
Sulfur [wt. %]	1.1 (0.0)	1.9 (0.0)	1.0 (0.0)	1.6 (0.0)
Oxygen [a] [wt. %]	31.2 (0.2)	29.9 (0.2)	29.8 (0.2)	30.0 (0.3)
Organic composition				
Crude fat [wt. %]	15.0 (1.1)	12.5 (1.0)	23.3 (0.8)	16.3 (0.3)
Crude protein [wt. %]	43.0 (0.2)	55.4 (0.3)	28.6 (0.4)	49.8 (0.4)
Crude fibres [b] [wt. %]	27.1 (0.6)	20.6 (0.3)	35.6 (0.6)	27.1 (0.2)
- Hemicellulose [wt. %]	8.0 (0.0)	3.9 (0.0)	5.1 (0.0)	3.8 (0.0)
- Cellulose [wt. %]	9.5 (0.2)	1.9 (0.0)	16.2 (0.3)	3.9 (0.0)
- Lignin [wt. %]	9.6 (0.4)	14.8 (0.3)	14.3 (0.3)	19.4 (0.2)

[a] Calculated by difference, [b] Sum of hemicellulose, cellulose and lignin content

2.3.2 Biocrude properties

The yield and elemental composition of biocrude obtained from the HTL of the different MSS samples are listed in Table 5. Since the lipid content should affect the biocrude yield, it was correlated against the crude fat content (solubles of petroleum ether soxhlet extraction) in the MSS feedstock samples, shown in Figure 13 (A). A linear relationship between the crude fat

content in the feedstock MSS and the amount of derived biocrude can be interpreted. The highest mean biocrude yield was obtained by the BC-TUD sample, which also had the highest crude fat content in the starting material. In contrast, the mean biocrude yield of the BC-TH sample was found to be the lowest compared, in line with the lowest crude fat content. The biocrude yields of BC-KA and BC-PAM show no significant difference. The crude fibre content of both of these feedstock MSS samples is more or less similar, though it needs to mention that the content of hydrolysable carbohydrates (hemicellulose and cellulose) is different in the samples examined.

Table 5. Properties of biocrude derived from different MSS samples. The values in brackets indicate the standard deviation. All values are given on a dry- and ash-free basis.

	Karlsruhe	**Thessaloniki**	**Tudela**	**Pamplona**
Sample abbreviation	**BC-KA**	**BC-TH**	**BC-TUD**	**BC-PAM**
Yield [wt. %]	36.3 (1.3)	30.3 (1.1)	45.3 (1.8)	35.7 (0.8)
Carbon [wt. %]	73.5 (0.2)	71.3 (0.2)	74.2 (0.3)	74.4 (0.1)
Hydrogen [wt. %]	9.6 (0.1)	8.7 (0.0)	10.2 (0.1)	9.6 (0.0)
Nitrogen [wt. %]	4.7 (0.1)	6.6 (0.1)	3.9 (0.1)	4.9 (0.1)
Sulfur [wt. %]	1.0 (0.0)	1.5 (0.1)	1.0 (0.0)	1.5 (0.0)
Oxygen [a] [wt. %]	11.2 (0.3)	11.9 (0.4)	10.7 (0.5)	9.6 (0.2)

[a] Calculated by difference

These carbohydrates are reported to contribute to the biocrude, especially in combination with proteins. Lignin, on the other hand, is relatively stable under hydrothermal conditions [126]. The biocrude yield is correlated against the hydrolysable carbohydrate content in the MSS samples in Figure 13 (B) and only a minor relationship can be identified, as the coefficient of determination, R squared (R2) shows a low value of 0.7144. Furthermore, the impact is much weaker as the straight shows a much lower slope value of 0.71. In Figure 13 (C), a correlation between the crude protein molecule class in the feedstock and the biocrude yield is observed. Practically, a linear relationship is depicted, demonstrating a decreasing influence on biocrude yield as crude protein content increases. However, it is noted that the impact of crude protein content on biocrude yield is comparatively weaker than that of crude fat content, with an absolute slope value of 0.6 of the straight.

In addition to the yield of biocrude, the content and type of nitrogen (N) containing substances in the biocrude is a quality-determining factor, as N-hetero compounds, especially N-heteroaromatics, are problematic for further refining processes and use as drop-in fuel [43]. The N-content is shown next to the N-recovery of the biocrude phase in Figure 14. It is noted that the N-content differs greatly between the biocrude samples. The BC-TH samples show the highest N-content, while the BC-TUD sample shows the lowest value. However, the depicted N-recoveries behave reversed.

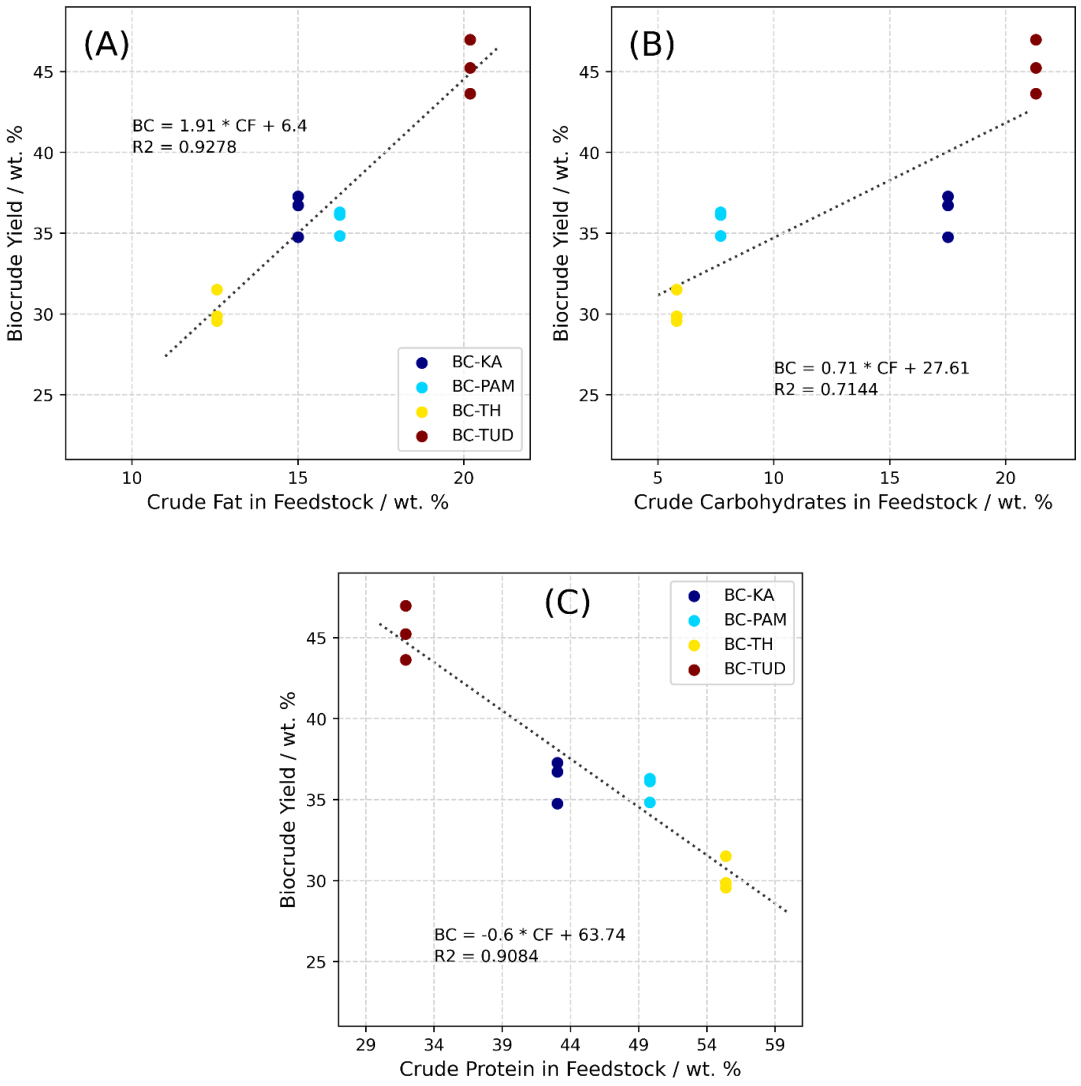

Figure 13. Correlation of biocrude yield over (A) crude fat content, (B) crude carbohydrates and (C) protein in MSS-Feedstock samples.

Fan et al. reported in a recent study that lipids increase the N-recovery in the biocrude, which in this study can be related to the high crude fat content of the MSS-TUD [134]. Comparing the BC-KA and BC-PAM no significant difference can be determined, but the slightly higher N-recovery into the BC-PAM can be related to similar phenomena. To better understand the relation between hydrogen and the problematic nitrogen within the biocrude samples a modified van Krevelen plot, showing the H/C-ratio against the N/C-ratio and the location of the different samples, is depicted in Figure 15.

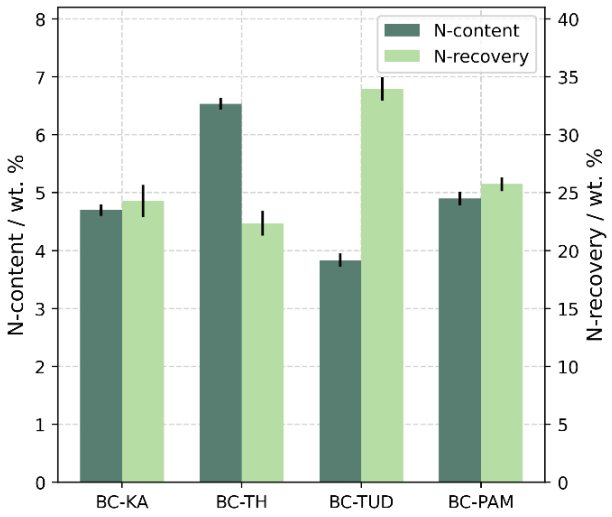

Figure 14. Nitrogen content in biocrude and the resulting nitrogen recovery.

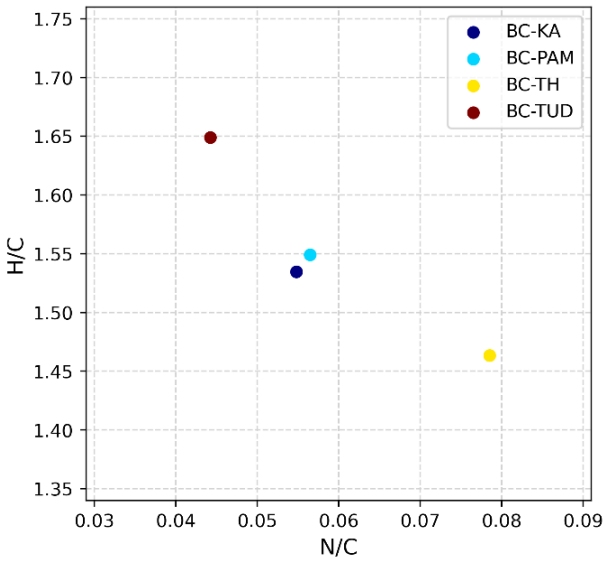

Figure 15. Location of the biocrude obtained from the different MSS in a modified van Krevelen diagram.

The derived elemental ratios are lumped values of all the different compounds in the biocrude. The long-chain aliphatic compounds like fatty acids and their amide products are located in the upper left region with a high H/C-ratio and low N/C-ratio. A common Amide in biocrude is hexadecane amide with a H/C value of 2.75 and an N/C value of 0.03. Aromatic compounds are located in the lower left and if a nitrogen atom is incorporated within the aromatic ring, the compounds are located in the lower right of the van Kreveln diagram [222]. For example, a common N-heteroaromatic compound is indole, with a H/C value of 0.875 and N/C value of 0.128. Therefore, the location of the BC-TUD suggests a matrix containing many aliphatic structures. On the other hand, the BC-TH samples should contain more N-heteroaromatic compounds. Again the samples BC-KA and BC-PAM show only minor differences. The higher H/C value of BC-PAM should be related to the presence of fatty acid amides, which agrees with the higher content of crude fat in the starting material MSS-PAM.

2.4 Conclusion

Municipal sewage sludge samples (MSS) from different wastewater treatment processes were extensively characterized and subsequently hydrothermally converted at HTL conditions. The

derived biocrude products were analysed again and compared, to conclude the influence of the composition of the feedstock material.

(1) The characterization of the MSS samples showed a significant influence of the upstream wastewater composition and subsequent treatment process on the bulk composition. Especially the elemental and organic composition consisting of crude fat, protein and fibres are strongly affected.

(2) In terms of biocrude yield the crude fat content in the MSS sample is the most influencing factor. A high crude fat content results in a high biocrude yield. Carbohydrates show only a low correlation. Furthermore carbohydrates and proteins show a minor effect on the biocrude yield, evaluated by the slope value of the straight.

(3) High crude fat contents result in more aliphatic biocrude, with low nitrogen content, even though the recovery of nitrogen is highly increased. A sludge with a low crude fat content results in a contrary biocrude with a high nitrogen content, presumably bound in aromatic strictures.

(4) The production of biocrude and its quality are subject to the influence of the upstream wastewater composition and the treatment process that follows. It is worth noting that despite this dependence, two distinct processes (KA-MSS after the activated process and PAM-MSS after anaerobic digestion) can generate a similar sewage sludge composition of organics like crude fat, protein and fibres. This is leading to the production of biocrude in comparable yields and of comparable quality.

Chapter 3.

Influence of lipid, protein and cellulose interaction on the evolution of N-heteroatom compounds during hydrothermal liquefaction

3.1 Introduction

Due to the rapid increase in global energy demand along with climate change issues, biomass gained interest as an alternative, carbon-neutral source for the production of chemical energy carriers. Bio-based residuals or waste feedstocks are of high interest as they need to be managed anyhow and are not included in the 'fuel vs food' discussion [223]. Sewage sludge, manure, or municipal organic waste are examples for kind of cheap waste biomass, often containing a high moisture content. Hydrothermal Liquefaction (HTL) is a promising technology which uses water as a heat carrier, solvent, and catalyst at the same time, avoiding pre-drying and making it suitable for a wide variety of feedstocks [30]. Elevated temperatures between 200 °C and 400 °C under the corresponding saturation pressure are applied to utilize the superior ionic product and a low dielectric permittivity of water, enhancing acid/base and ionic reactions [224]. With this higher reactivity, functional groups are attacked in the biogenic molecules in the organic waste. Usually, a mixture of natural polymers and other large molecules like polysaccharides, proteins and lipids are contained in the mixture, which needs to be depolymerized and converted into smaller molecules to utilize them in downstream refining processes. The intermediate product obtained by HTL for biofuel purposes consists of a mixture of different, compounds and is often referred to as biocrude [225]. This organic product contains less polar substances; therefore side products are carbon dioxide rich gas, and aqueous phase containing the more polar components with a low molecular weight [133,226]. Another side product occurs from re-polymerization as a solid, char-like material [227].

The usually high heteroatom content of Oxygen (O) in carbohydrates and lipids is transferred into the final product phases. Considering the utilization of protein-rich waste biomass, Nitrogen (N) is an additional concern if hydrocarbon fuels are the target product. Biocrude is therefore an intermediate along the process chain to fuel [45]. Extensive upgrading is needed to remove heteroatoms and to improve fuel properties to reach industrial standards in the aimed application. This refining consists usually of a catalytic hydrotreatment coupled with distillation for fractionation into the different fuel cuts [228]. Hydrodeoxygenation (HDO) and

hydrodenitrogenation (HDN) of the biocrude are conducted like in the processes developed for fossil crude oil, but are still under research, considering the huge concentrations of heteroatoms to deal with. Both HDO and HDN are occurring simultaneously and are competitive reactions [228]. Generally speaking, HDN is often referred to as the slower reaction mechanism, of course depending on the chemical feed composition [229,230]. Removing hetero-atoms from heterocyclic and -aromatic compounds is difficult as full hydrogenation and subsequent ring-opening are presumed [43]. Furthermore, Choudhary et al. showed an inhibiting effect on HDN in heavy crude fuel with high contents of polyaromatic compounds, as the latter are hydrogenated before [231]. N-heteroaromatics species are suspected to complex inorganic elements like iron, which are problematic for active catalyst sides, requiring an additional refinement for the biocrude [37,184]. Otherwise, aliphatic amides seemingly are easier to process during HDN, as shown experimentally by Kohansal et al. for the hydrotreatment of biocrude produced from food waste [232]. Therefore, the N-content in biocrude needs to be distinguished between N-heteroaromatic or N-aliphatic compounds.

Several studies showed the influence of the organic feedstock composition on the HTL process and the biocrude composition. Fan et al. demonstrated that Maillard reactions lead to increased biocrude yields for hydrothermal conversion of the model substances lactose and lysine as more non-polar reaction products are formed [114]. Accordingly, the N-content in the biocrude increased, eventually leading to a lower quality due to more N-heterocyclic compounds. Posmiak et al. used model substances as well in different combinations at different reaction temperatures and time, [126]. The beneficial effect of carbohydrates and proteins, regarding the yield, is highlighted, but also the ternary combination with lipids is introduced. The addition of lipids to the carbohydrate/protein mixture was found to improve the biocrude yield and quality. Yoo et al. tested HTL on two different microalgae strains with low or high lipid content [144]. When the focus lay on the production of transportation fuels, the high-lipid microalgae performed better in terms of biocrude yield, quality and energy efficiency. In a comparable experiment, Feng et al. used two algae strains with different lipid content, finding

a higher biocrude yield and more N-heterocyclic compounds in the biocrude derived from the low-lipid strain [145]. A pre-treatment, removing carbohydrates from the algae matrix was proposed, lowering the generation of N-heteroaromatics. In our previous work, we successfully pre-treated sewage sludge with water and different acidic solutions at (150°C), intending to solubilize proteins, eventually lowering the N-content in the feedstock and the resulting biocrude [233]. As lipids accumulated and proteins and carbohydrate were get washed out in the first step, the resulting biocrude showed higher yields and lower N-contents and fewer N-heterocycles. A study conducted by Croce et al., described in detail the chemical composition of biocrude obtained from different model substances and mixtures [127]. With high resolving mass spectroscopy, the composition of the biocrude derived from binary carbohydrate/protein and ternary mixtures including additional lipids was investigated. Among others, it could be shown that N-compounds differ between aliphatic amides and a large variety of heteroaromatics by the applied feedstock composition, proposing the more detailed examination of different feedstock combinations and changing ratios. In another recent study, the composition of lipid, protein and carbohydrate was varied by different preparations of artificial food waste slurries, to see an effect on the generation of N-species [135]. A strong influence of reactive N-intermediates on the generation of heteroaromatic species was observed and supported by the development of a thermodynamic model.

In this work, we aim to suppress the formation of N-heterocyclic compounds, especially in the aromatic form, in the biocrude obtained by HTL. Preceding research conducted by Fan and colleagues in our institute showed already a strong influence of lipids (long-chain carboxylic acids) on the formation of these problematic N-species [134]. It was demonstrated, that at elevated temperatures above 300 °C amidation reactions are promoted by Maillard reactions, which are dominating in lower temperature regimes. Therefore, a ternary model system of lipids (lard oil), carbohydrates (cellulose) and proteins (Bovine Serum Albumin) is introduced in this work and converted at hydrothermal conditions at 350 °C and 20 MPa. Within the model feedstock, the protein content is kept constant, while the amount of lipids and cellulose

is changed, resulting in different lipid to protein ratios. Subsequently, the distribution of nitrogen among various representative classes of species present in the biocrude is correlated with the lipid to protein ratio. The obtained results are utilized to identify the primary pathways responsible for the formation of N-heteroaromatic compounds and to propose potential strategies to mitigate their formation. In a subsequent experimental setup, de-ionized water is replaced with a 0.5 wt.% propionic acid solution to investigate the impact of this short-chain carboxylic acid on the aforementioned factors under investigation.

3.2 Material and methods

3.2.1 Material

The substances for the model feedstock mixture lard oil, cellulose, albumin serum bovine and propionic acid were purchased from Merck and were used without further treatment. Solvents like dichloromethane and tetrahydrofuran were obtained in chromatographic grade from Merck. Standards for GC-MS calibration like 2 piperdone, N-methylsuccinimde, 2-methylpyrazine, 2,6-dimethylpyrazine, indole, 2-methylindole, 2,3-dimethylindole quinoline, 2-methylquinoline, 2,6-dimethylquinoline were purchased from Alfa Aesar. The fatty acid amide derivates hexadecanamide and ocatadecanamide were obtained from cayman chemicals.

3.2.2 Hydrothermal liquefaction experiments and sample collection

Seven different feedstock mixtures were prepared; while the protein content was kept constant, the cellulose and lipid content was varied. The resulting mixtures were named according to their lipid to protein weight ratio (LtoP-ratio), which varied by $0.00 \leq \text{LtoP} \geq 2.00$. In a second series of experiments with LtoP-ratio between 0.00 and 1.00, the aqueous solvent contained 0.5 wt.% propionic. An overview of all experiments with the given concentrations of lipid, cellulose and protein are given in Table 6.

Table 6. Feedstock model mixtures experimental set-up.

Protein [g]	Lipid [g]	Cellulose [g]	**LtoP-ratio**	Experimental series and repetition	
				De-ionized water	0.5 wt.% Propionic acid
0.50	0.00	1.00	**0.00**	4	3
0.50	0.17	0.83	**0.34**	1	3
0.50	0.33	0.67	**0.66**	1	3
0.50	0.50	0.50	**1.00**	3	3
0.50	0.67	0.33	**1.34**	1	-
0.50	0.83	0.17	**1.66**	1	-
0.50	1.00	0.00	**2.00**	4	-

The HTL experiments were conducted in 25 ml autoclaves (Stainless steel, EN 1.4571). The vessels were loaded with the different organic feedstock mixtures and with 15 ml of de-ionized water to result in an organic weight fraction of 10 wt.%. Solid feedstock materials, namely cellulose and BSA, were introduced into the system using a spatula, while liquid lard oil was added using a pipette. Following this, a volume of 10 ml of de-ionized water was gradually incorporated into the mixture under continuous manual stirring with the spatula. Afterwards, the remaining 5 ml of water was used to rinse the spatula. In order to ensure uniform wetting of the solid materials, the sealed microreactors were subjected to ultrasonic treatment in a bath for a duration of 5 minutes.The complete mixture occupies about 60 % of the reactor volume. The headspace was purged with nitrogen three times and pressurised to 1 MPa before the autoclaves were sealed with a torque key. In one set-up, six autoclaves were placed into a fluidised sand bath at 350 °C (SBL 2; Techne). According to the gas saturation pressure of water and the available volume, this results in a pressure of 20 MPa during the reaction [22]. The heating rate inside the autoclave was measured previously and averaged at 40 °C·min^{-1}, resulting in a heating time of 8.75 min. After the reaction temperature was reached, the autoclaves remain in the sandbath for 20 min. To stop the reaction, the reactors were removed from the sandbath and rapidly cooled down in a water bath for 10 min. The pressurized autoclaves were opened in a gas-tight containment and the released reaction gas was discarded. The liquid content and the open vessel was rinsed with 5 ml of Dichloromethane (DCM) and

filtered by a Büchner funnel with filter paper of 0.45 µm pore size. The same procedure was repeated four times. Solids retained on the filter were dried at 105 °C overnight and stored for further analysis. The DCM extract was stored in a refrigerator, letting the heavier organic-rich biocrude phase separate from the lighter aqueous phase. The next day the two phases were separated by aspiration, an aqueous aliquot was collected for further analysis while the DCM of the biocrude phase was evaporated under a mild nitrogen stream overnight. This experimental procedure was repeated with 0.5 wt.% propionic acid instead of de-ionized water, between the lower LtoP range of 0.00 to 1.00.

3.2.3 Analysis

The HTL-feedstocks consisting of model substances and reaction products biocrude and residual solids were analysed for their elemental composition using a CHNS-Analyser (Vario EL cube, Elementar Analysetechnik GmbH, Hanau, Germany).

The aqueous phase including solubilized organics was tested by total organic carbon (TOC) and total nitrogen bound (TNb) analyser (DIMATOC 2100 and DIMA-N, Dimatec Analysetechnik GmbH, Essen, Germany).

To identify and quantitate representative N-heteroatomic compounds in the biocrude samples gas chromatography (GC) coupled with mass spectrometry (MS) using electron impact ionization (EI) was applied. As a stationary phase, a Rxi-5MS column with 30 m × 0.32 mmx0.25 µm (Restek Corporation, Bellefonte, PA, USA) was used. A quantity of 50 mg of samples was dissolved in 0.5 ml of tetrahydrofuran and, subsequently, prepared in a 1:100 dilution. 0.5 µL of this solution was injected at 280 °C in 1:20 split mode, using helium as carrier gas (1.5 $mL \cdot min^{-1}$). The temperature program of the oven started at 70 °C holding for 2 min and then heating to 180 °C with a heating rate of 8 $°C \cdot min^{-1}$, increasing again up to 280 °C with a rate of 4 $°C \cdot min^{-1}$ and holding there for 15 min. The temperature of the transfer line to the detector was kept at 280 °C, and the ion source to 230 °C. Qualitative analysis was

conducted with a scan of the total ion current (TIC) chromatogram. Scan rate was set at 3.9 scans·sec^{-1} over a mass charge to charge ratio range of 35-400 m/z. Agilents 'Unknown Analysis' software and NIST17 Database was used for identification with an applied match factor of 75%. The selected ion monitoring (SIM) mode was applied to acquire high-quality mass spectra for externally calibrated indole, quinolone, succinimide, piperidone and amide derivates. The compounds with their responding characteristic qualifier and quantifier ions, as well as calibration curves are listed in S 2.

The structural behaviour of the solid residues generated from model substances was additionally analysed by 13C-MAS NMR. The spectra were acquired by using a JEOL 400 MHz unit equipped with a 9.4T Oxford magnet for solid state (wide-bore) using 4 mm zirconia rotors spinning at a MAS frequency (nMAS) of 15 KHz.

3.2.4 Data evaluation and visualization

The yield (Y_i) of biocrude and solid residue was calculated by the following equation:

$$Y_i = \frac{m_i}{m_f} \cdot 100$$

Where m_i and m_f are the mass of the product and feedstock mixture, respectively.

The element recovery into a certain HTL-product phase were calculated by the following equation:

$$Element\ Recovery_i = \frac{m_i \cdot E_i}{m_f \cdot E_f} \cdot 100$$

The Element recovery means the recovery of carbon or nitrogen, the index i is indicating the biocrude, aqueous, or solid product phase, m_i and m_f are the masses of the feedstock mixture where as E_i and E_f are the elemental content of the feedstock mixture.

A change indicator (CI) was calculated to evaluate the effect of propionic acid on the nitrogen recovery in representative heteroatom species. The CI compares the N-recovery of a specific

species in the biocrude with and without the addition of propionic acid. If the CI value is negative, a lower N-recovery is obtained. A positive CI value indicates a higher N-recovery of such species when adding propionic acid to the feed mixture.

$$\mathrm{CI}_i = \frac{\mathrm{N.\,rec.}_{i,propionic\ acid} - \mathrm{N.\,rec.}_{i,deionized\ water}}{\mathrm{N.\,rec.}_{i,deionized\ water}}$$

where the index i denotes the N-heteroatom species; $\mathrm{N.\,rec.}_{i,deionized\ water}$ is the N-recovery of the species i in the biocrude derived in deionized water and $\mathrm{N.\,rec.}_{i,propionic\ acid}$ is the N-recovery of the species i in the biocrude derived in the aqueous propionic acid solution.

Evaluation of the fitted curves and their (ANOVA), was obtained in DesignExpert v8.0.6 (State-Ease, Minneapolis, MI, USA). The ANOVAs and plots of residuals are shown in the Supporting Information, S2. For data processing and plotting the Python libraries Numpy, Pandas and Matplotlib were used. Chemical structures were drawn in ChemDraw professional 16.0. Bovine Serum Albumin (BSA) and peptide structure were obtained from the SWISS-MODELL database [234].

3.3 Results & Discussion

3.3.1 Biocrude and solid yield

The yields of the biocrude and the solid products after hydrothermal treatment of the model mixtures with different lipid-to-protein ratio are shown in Figure 16. Additionally, the ratio of solid to biocrude product expressed in percentage is given. At the smallest LtoP-ratio, the biocrude yield shows its lowest value of 34.3 wt.%, while the highest solid yield was obtained at 5.99 wt.%. Correspondingly, the biocrude yield increases up to a value of 66.2 wt.% at a LtoP of 2.00. At the same time, the solid yield significantly decreases to 0.54 wt.%. This can also be expressed by the solid to biocrude ratio, illustrated by the fitted, dashed curve as a function over the LtoP-ratio in the figure. At a minimum ratio, the solid accounts in proportion to the biocrude 19.30 and decreased to almost half (10.90%), when the LtoP-ratio was 0.33. following

this exponential correlation, the lowest value of 0.82% can be reached. Overall, the sum of biocrude and solid yield was also significantly increased when lipids were added to the feedstock mixture. Due to the non-polar nature of the lipids, i.e. their resulting fatty acids, they contribute largely to the DCM extracted biocrude [134]. The formation of solids during HTL is often explained by re-polymerization of carbohydrate degradation products, like furfural and hydroxymethylfurfural into a carbonaceous material of high molecular weight [235]. Another reaction mechanism that is likely to contribute to the generation of solids are Maillard reactions, which can form larger N-polymers named melanoidins. Peterson et al. identified melanoidins after the hydrothermal conversion of a binary mixture of glucose and glycine as a brownish N-containing polymer [120]. Additionally, the Mannich reaction pathway is presumed to form solid material by utilizing carbohydrate degradation products and amino compounds [236,237]. Morpholicial and structural differences of the solid could not be identified. The ^{13}C-MAS NMR results show similar spectra of a solid obtained at an LtoP-ratio of 0.00 and 1.00, displayed in the Supporting Information, S 3. NMR analyses of solids obtained at larger LtoP-ratios could not be performed because not enough material could be generated by the process.

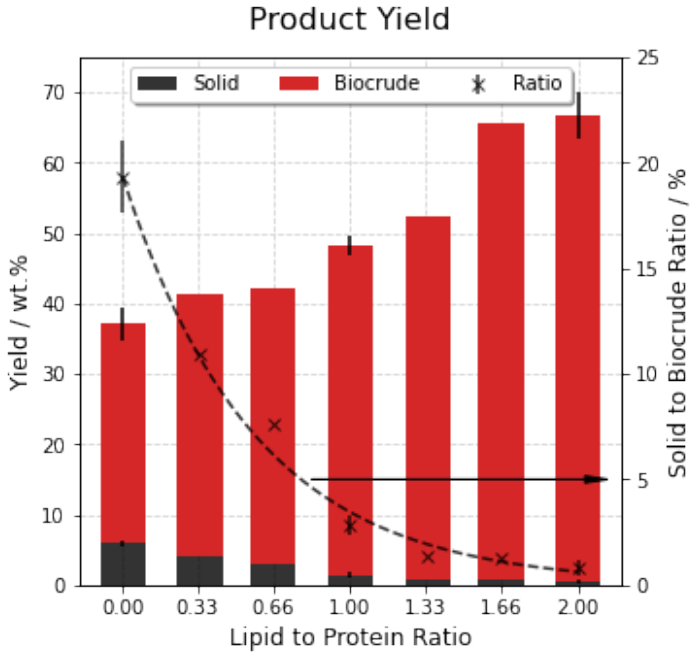

Figure 16. Yield of biocrude and solid residue over the lipid to protein ratio.

3.3.2 Carbon and nitrogen content of feedstock mixtures and recovery into the resulting HTL-products phases

The investigated feedstock mixtures contain different carbon-contents, as shown in Table 7. It can be noted that the C-, H- and O-content for the different model feedstock is changing gradually, as the applied cellulose and lipid contain a different elemental composition due to their different chemical structure. In addition, the elemental contents of the resulting biocrude samples are given in the table. Interestingly, the C- and O-content do not change much, while the H-content is increasing and that of N and S is decreasing with higher LtoP-ratios. Based on this data, the C- and N-recoveries in the different product phases are determined and displayed in Figure 2. For the HTL process, a best possible C-recovery in the biocrude phase is desired for an efficient carbon utilization and its transfer to downstream processes for potential biofuel production. Vice versa, the N-recovery should be small, affecting downstream hydrotreating for denitrogenation [233].

Table 7. Elemental content of model feedstocks and resulting biocrude samples. All values are given on a dry basis in wt. %.

LtoP-ratio	Feedstock mixture					Biocrude				
	C	H	N	S	O [a]	C	H	N	S	O [a]
0.00	44.60	6.80	5.00	0.57	43.03	73.28	8.08	6.40	1.00	11.25
0.34	48.50	7.43	5.00	0.57	38.50	74.70	9.30	5.10	0.70	10.20
0.66	52.17	8.03	5.00	0.57	34.23	75.10	9.90	4.50	0.50	10.00
1.00	56.07	8.67	5.00	0.57	29.70	74.37	10.53	3.90	0.57	10.63
1.34	59.97	9.30	5.00	0.57	25.17	74.60	11.20	3.20	0.40	10.60
1.66	63.63	9.90	5.00	0.57	20.90	74.50	11.70	2.70	0.40	10.70
2.00	67.53	10.53	5.00	0.57	16.37	74.93	12.18	2.43	0.33	10.15

[a] calculated by difference

In Figure 17 (A) the C-recovery and in (B) the N-recovery in the solid, biocrude and aqueous phases are shown. Likewise to the previously shown solid yield, the C- and N-recovery in the solid show a similar downward trend. The recoveries are significantly decrease from 9.75% to 0.58% for carbon and 6.85% to 0.46% nitrogen, respectively. Otherwise the element recoveries in the biocrude. The addition of lipid to the model mixtures significantly increases the C-

recovery of into the biocrude from 51.08% up to 73.64%, while the N-recovery is decreasing from 39.80% to 32.12%. In both figures, the ratio between these recoveries (N-recovery over C-recovery in the biocrude and aqueous) is plotted as a linear, dashed line. For the C-recovery it can be noted that at a low LtoP range up to 77.92% of the recovered carbon account as nitrogen recovery. With the addition of lipids this ratio can almost halved to a value of 43.60%. The element recoveries into the aqueous phase behave again differently. On the one hand, the C-recovery does not significant change for the applied different feedstock mixtures with an average value of 10.13%. On the other hand, the N-recovery in the aqueous phase increases with the LtoP-ratio starting at 41.92% for an LtoP-ratio of 0.00 and rising up to 52.36% by addition of lipids. This nicely corresponds to the decreasing N-recoveries in the biocrude. The N/C-ratio shows a positive slope ranging from 404% to 513%, indicating an extraordinary higher transfer of N into the aqueous phase compared to the carbon distribution, supported by the addition of lipids. Summing up the elemental recoveries of all samples, a certain loss (difference to a total of 100%) can be identified. The larger losses of carbon can be explained by predominant decarboxylation reactions to CO_2 from carbohydrates [238]. N-losses are likely to occur due to the vacuum assisted separation process and the stripping of ammonia and other volatile amines, as described in the experimental section and elsewhere [233].

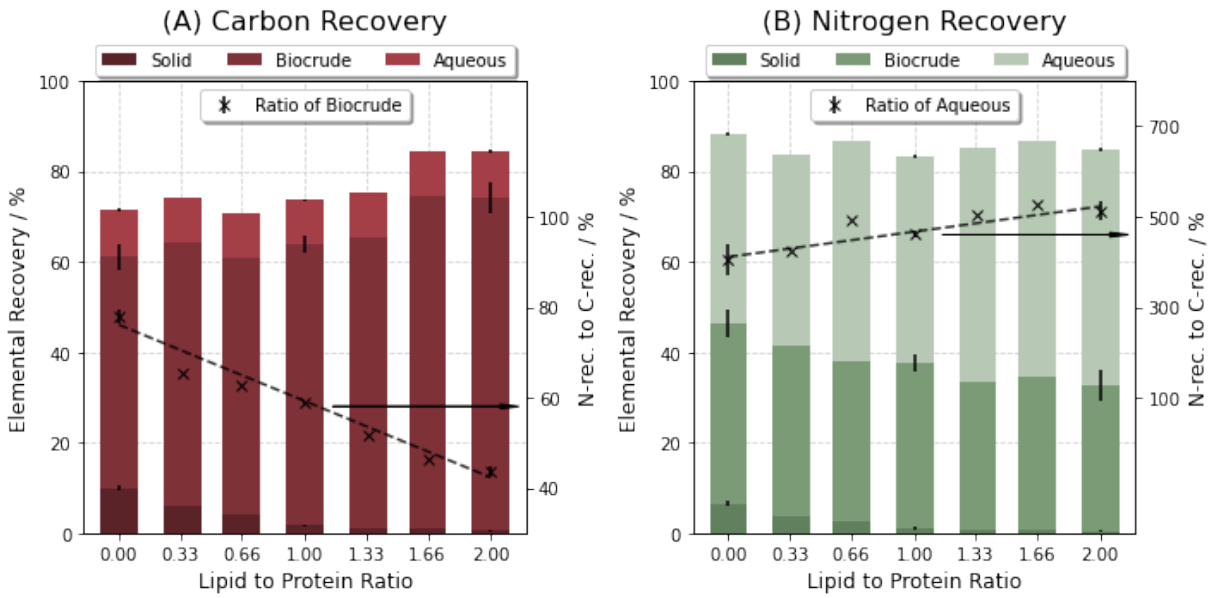

Figure 17. Element recoveries of carbon **(A)** and nitrogen **(B)** into HTL-product phases over the lipid to protein ratio. Additionally the ratio between N-rec. and C-rec. in the biocrude phase is plotted

The effects of feedstock composition on the C- and N-content in the biocrude product can be visualized by a Van Krevelen diagram, shown in Figure 18. The ratio of N/C is plotted against that of H/C. In this graph, the feedstock mixtures are and different biocrude products are depicted. By the colour code hand side the different LtoP-ratios are characterized. The typical removal of nitrogen from biogenic feedstocks via the hydrothermal conversion is likely to occur in form of

ammonia (NH_3), which is indicated by deamination parallels in the graph. The biocrude samples originating from a high LtoP-ratio are located in the upper left with high H/C- and low N/C-ratios. By reducing the LtoP-ratio in the feedstock mixture, the biocrude samples show lower H/C values in combination with increased N/C values. It can be observed that the resulting points of the biocrude samples can be arrange in a straight line, with a slope of around 13: When a biocrude contains 1 mol less N but 12 mol more hydrogen. This goes along in a lower degree of aromatization of the biocrude. The mean distance Δ, between the different product samples defined by the LtoP-ratio are determined and shown on the right hand side of Figure 18. The constant decrease of this mean distance over the LtoP-ratio range can be translated as a decrease in aromaticity and is reasonable, as cellulose is likely to form aromatic species under these hydrothermal conditions [239]. Notably is the drop of this mean distance between the ratios of 0.00 to 0.33 and 0.33 to 0.66, indicating a strong effect of the addition of lipids.

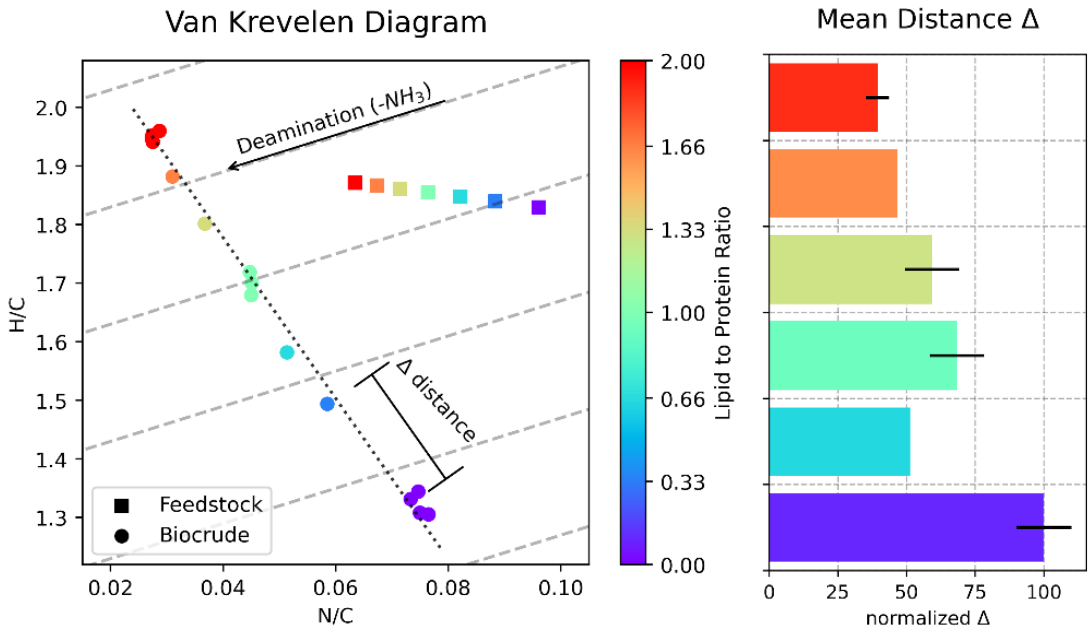

Figure 18. Orientation of feedstock mixtures and the resulting biocrude products in Van Krevelen diagram (N/C vs H/C) and mean distance between

3.3.3 Nitrogen recovery on a molecular level into different N-heteroatom species

Quantitative GC-MS analysis of the HTL-biocrude product obtained from the different feedstock mixtures was applied to explore the influence of the LtoP-ratio on the formation of N-heteroaromatics and other N-heterocomounds. Representative compounds were chosen, based on a qualitative result obtained from a GC-MS chromatogram in scan mode of a sample with an LtoP-ratio of 0.33, shown in S 4. Compounds with the highest abundances were selected and compared with GCMS analysis of several studies, applying comparable feedstock and HTL-procedure [116,127,133,134,172]. For these substance classes, the N-recoveries in the biocrude from the different initial LtoP-ratios and cellulose to protein (CtoP) ratios are shown in Figure 19 and Figure 20. The N-recoveries of representative N-heteroaromatics, pyrazines, indoles and quinolines derivates are shown in Figure 19. From the binary feedstock mixture of 2:1 cellulose and protein, a high quantity of pyrazine is identified, reflected in an N-recovery of 6.10%. With the addition of lipids and reduction of cellulose in the feed, the N-recoveries into pyrazines are drastically decreased to a seven-fold lower value of 0.87%. It seems that even

higher LtoP-ratios won't significantly affect the N-recovery in pyrazine structures. When no cellulose is present in the model feedstock almost no pyrazines are identified.

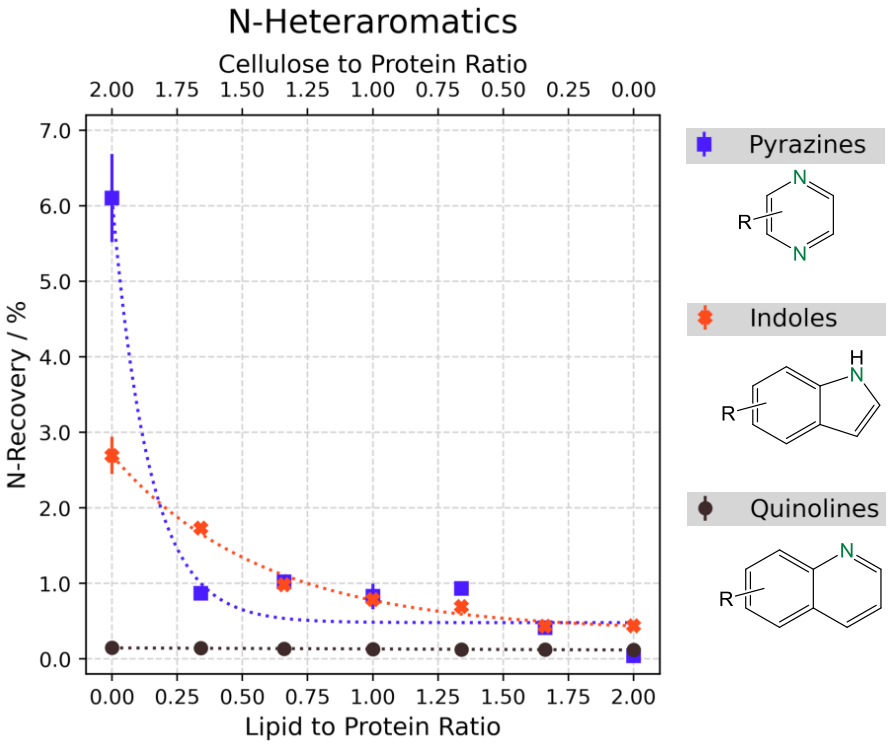

Figure 19. Correlation of nitrogen recovery in dependence of the LtoP- and CtoP-ratio with pyrazines, indoles, and quinolones as. representative N-heteroaromatics species in the biocrude products, obtained via HTL from different model feedstock mixtures.

The plot of the correlation of indole over the LtoP-ratio range also follows an exponential decay, though the effect of an increasing LtoP-ratio is weaker. The highest N-recovery in indoles is 2.69% at the LtoP-ratio of 0.00. From a ternary mixed feedstock of 1:1:1 cellulose, proteins, and lipids the N-recovery results in a value of 0.78%, which is further lowered to 0.44% in the binary mixture of 2:1 lipids and proteins. The exponential decrease of both pyrazines and indoles agrees with the observed changes of the distance between the points representing the product mixtures in the van Krevelen diagram. The drastic suppression of pyrazine formation could be an explanation on the leap of the mean distance between the LtoP-ratio 0.00 and 0.33.

Quinoline derivates with a low molecular size could not be identified in relevant quantities. However, it cannot be excluded that these may appear in larger structures [240]. As the correlation shows, the summed values of these substances do not exceed 0.1% of the recovered nitrogen in the biocrude fraction.

To represent the generation of long-chain N-heteroaliphatic species three palmitic (C16) and three stearic (C18) fatty acid amides (FAA) derivates were quantified, In addition, two non-aromatic N-heterocyclic species, 2-piperidon (5-ring lactam) and N-metylsuccinimide (4-ring imide), were analysed. Likewise to the N-heteroaromatics, the N-recoveries of these species are determined and displayed with a correlation over the LtoP- and inverted CtoP-ratio range in Figure 27. As no lipids were present in the binary feedstock mixture with a LtoP-ratio of 0.00, no nitrogen is recovered in the form of FAA, as the precursing fatty acids are missing. With a rising LtoP-ratio the N-recovery in FAA is significantly rising to 8.77%. Herby the correlation curve is again following an exponential fitting. In contrast to the FAA, the N-recovery in succinimide decreases over the LtoP-ratio range. With 8.09% the highest recovery value is achieved with a binary cellulose protein feedstock. When fitting a curve to this data, it is following an exponential decrease. The lowest N-recovery is found at an LtoP-ratio of 1.66 with a value of 1.90 %. The generation of piperidone seems not to be significantly affected by the changing feedstock mixture. The fitting is following a straight, almost horizontal line and the averaged N-recovery into this species is given at 7.36%.

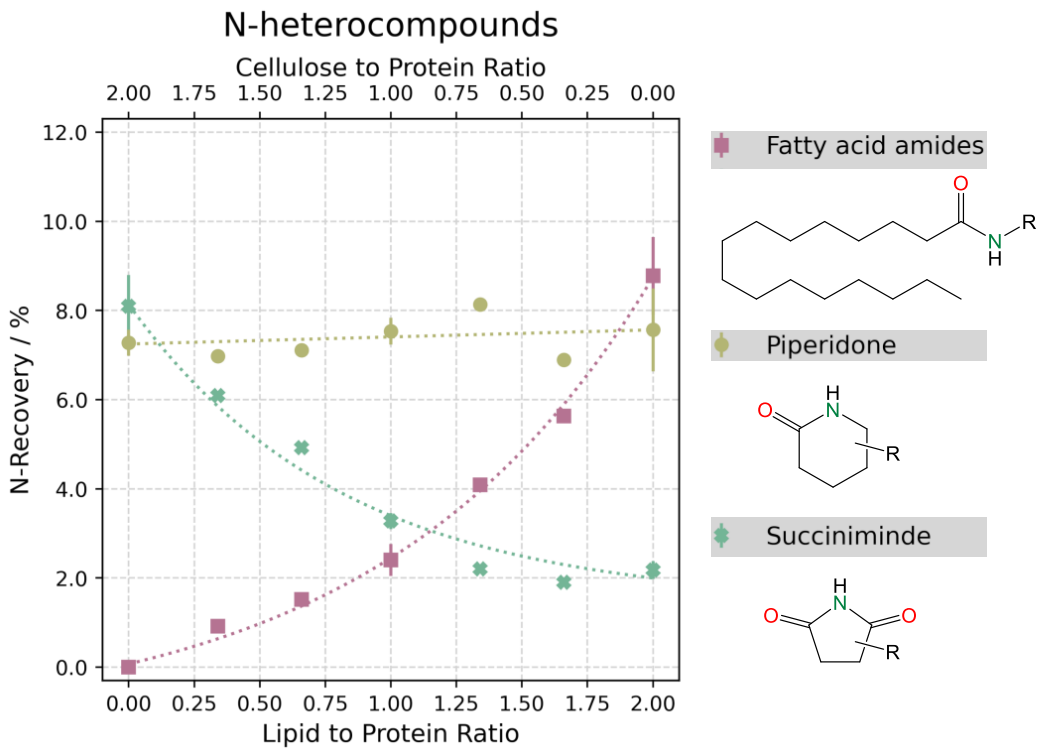

Figure 20. Correlation of nitrogen recovery in dependence of the LtoP- and CtoP-ratio. N-heteroaliphatic and two non-aromatic N-heterocyclic species are determined in biocrude products, obtained via HTL from different model feedstock mixtures.

3.3.4 Effect of propionic acid addition on N-recovery on a molecular level

The effect of the addition of propionic acid on the N-recovery in the biocrude and aqueous phase products and on the N-heterocompounds defined above is shown in Figure 21 by a change index graph. The change index is based on the corresponding experiment at the same LtoP-ratio but without the addition of propionic acid. It can be noted that the addition of propionic acid significantly lowers the N-recovery in the biocrude of model mixtures with an LtoP-ratio of 0.00 and 0.33. Accordingly, the N-recovery in the aqueous phase significantly increases for all experiments, especially for those in the low LtoP-ratio range, suggesting the formation of organic compounds like propanamide. Here it needs to be noted, that the addition of propionic acid eventually led to a lower pH of the aqueous products, which prevents the above described loss of ammonia by stripping during the separation procedure.

In the biocrude product, the change index describes in the following the N-recoveries on a molecular level. It can be observed that the formation of FAA increases when the model feedstock mixtures are liquefied in the presence of propionic acid. A proposed mechanism for the amidation reaction depends on a sequence of the protonation and deprotonation, which suggests the influence of the pH value. It needs to be noted that a strongly acidic or basic hydrothermal environment shows a contrary effect of the amide formation [241]. Formation of pyrazines is significantly increased at an LtoP-ratio of 0.00. This is in agreement with findings, where the formation of diketopiperazine (DKP), a suggested pyrazine precursor, was significantly increased at lower pH and at comparable temperature [242]. At higher LtoP-ratios, the formation of pyrazines is slightly reduced, as it was already strongly suppressed by the addition of lipids. In contrast, the formation of indoles is significantly reduced at lower LtoP-ratios of 0.00 and 0.33, while at higher ratios essentially no effect was observed. Likewise to indole, the succinimide formation is reduced at lower LtoP-ratios, while this effect becomes weaker with a ratio of 1.00. Both observations suggest that the addition of propionic acids can effectively intervene in the reaction pathway to these two compound classes. Due to a higher LtoP-ratio, more fatty acids are present in the reaction system, which are comparable to carboxylic acids with a long carbon chain, therefore weakening the effect of this propionic, short-chain organic acid. Piperidone formation is reduced, indicated by the negative index, but no significant difference over the LtoP-range can be determined, which reflects previous described behavious in the baseline model system without the addition of propionic acid.

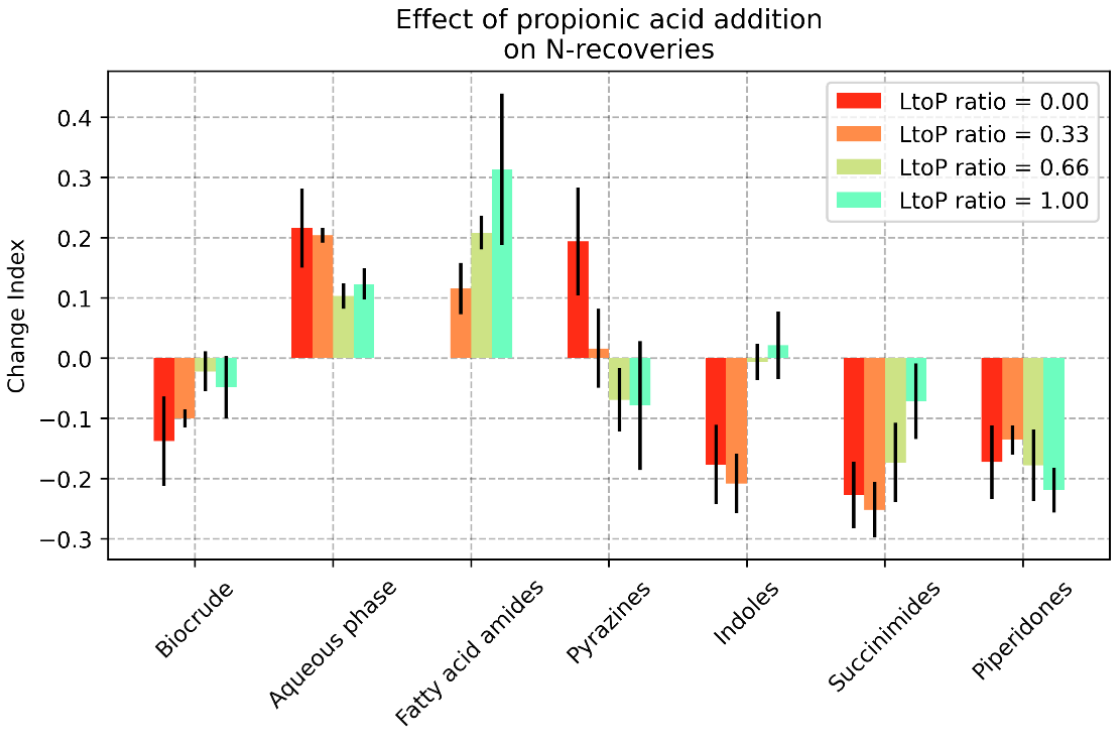

Figure 21. The effect of the addition of propionic acid on the N-recovery into the HTL products biocrude and aqueous phase and specific N-compounds, described by a Change Index

3.3.5 Reaction pathways forming N-heteroatomic compounds

Considering the above observed and described results, a simplified reaction scheme for the formation of the different N-heteroatom species is concluded and is discussed in detail.

The generation of N-heteroatomic compounds includes a variety of different possible reaction pathways. In Figure 22, a scheme is shown derived from hydrothermal degradation of bovine serum albumin (protein), used as protein N-source in this study. This substance first hydroelyss into different peptide oligomers, which are likely to degrade further into small amino compounds [108]. These can be considered intermediates for further consecutive reactions. Amino acids are likely to deaminate, yielding primarily ammonia or primary amines, but by decarboxylation reactions, secondary amines can be formed as well [116,243]. In addition, these amino compounds of appropriate chain length can undergo internal ring closure. The 2-piperidone found in this study, is described as a product of 5-aminovaleric acid [244]. As

presented by the N-recovery of this compound above, it is found that the cellulose and lipid content in the feedstock does not have a significant effect on the formation of this compound. Due to the 5-carbon atoms in the ring structure of 2-piperidone, it is assumed that it can only be formed from the cyclization of specific amino compounds. Otherwise the formation of N-methylsuccinimide, which is assumed to be formed by several reaction mechanisms. On the one hand, amino compounds from peptide degradation can undergo internal ring closure. On the other hand, newly formed amino (amadori intermediates) derivates, consist of a hetero-atomic-5-ring containing four carbon atoms. The formation of succinimide was reported from succinic acid [84]. Succinic acid was found after the hydrothermal degradation of carbohydrates and presents one compound out of a pool of different reactive oxygenated species, such as hydroxymethylfurfural (HMF) or levulinic acid [99,245]. These degradation products contain often a 4-carbon chain between two oxygen functional groups and are assumed to contribute to the formation of such hetero-atomic-5-rings lactams and imides, including these 4 carbons.

The hydrothermal hydrolysis of cellulose into glucose and its subsequent conversion into different products at similar temperatures as applied in this experiment are described extensively in the literature [246,247]. Via amination of these degradation products again various species of these amadori intermediates are formed. Subsequent reactions can then lead to N-heteroaromatics like pyrazines or pyrrols. A pathway for pyrazine formation is proposed by Van Lancker et al. [248]. Dicarbonyls from carbohydrate degradation are aminated to α-aminocarbonyls, which condensate in turn to the corresponding pyrazines. Another proposed reaction mechanism is the formation of diketopiperazine as an intermediate with a subsequent reduction to pyrazine [249]. Other common N-heteroaromatics species are pyrroles and their indole derivates, containing one N, respectively. Pyrroles are likely to be formed from HMF via an aminated intermediate [250,251]. In a subsequent step, these pyrroles can undergo cyclo-addition, forming indole derivates [252].

As demonstrated in the present study, the inclusion of lipids in the reaction mixture impedes the development of N-heteroaromatic compounds and the evaluated heterocyclic N-methylsuccinimide. Previous literature has reported that lipids have the ability to undergo hydrolysis, resulting in the formation of free fatty acids and glycerol [253]. These fatty acids may then react with free ammonia and amines to create stable fatty acid amides with various chain lengths and alkyl substituents, [130]. This reaction pathway is in direct competition with the generation of amino intermediates from the amination of carbohydrate degradation products. Since fatty acid amides are stable and the formation of amino intermediates is suppressed, subsequent cyclization and rearrangement reactions into N-heteroaromatics are not occurring. Addittionaly by substituting cellulose with lipids in the model feedstock mixture, the LtoP-ratio increases, making free amines more likely to react with free fatty acids and form stable amides. Otherwise, the amines would react with an oxy-compound to form an N-heteroaromatic precursor [135]. For example, Inoue et al. identified a wide variety of N-heteroaromatic compounds like indoles and pyridines derivates after hydrothermal conversion of cellulose in an ammonia solution [254]. Their findings let suggest that free amines are highly reactive in a hydrothermal environment and are likely to react into the biocrude phase and form a large quantity and variety of different heterocyclic species [255]. These two reasons, firstly the competing amination and amidation reaction and secondly the addition of lipids reduces the amount of cellulose in the reaction mixture may explain the exponential regression curves observed in the recoveries of nitrogen into designated heteroaromatic species. Adding short-chain carboxylic acids, like propionic acid, can also compete with the formation of amino intermediates, but the resulting propanamide is highly water-soluble and found in the aqueous phase [249].

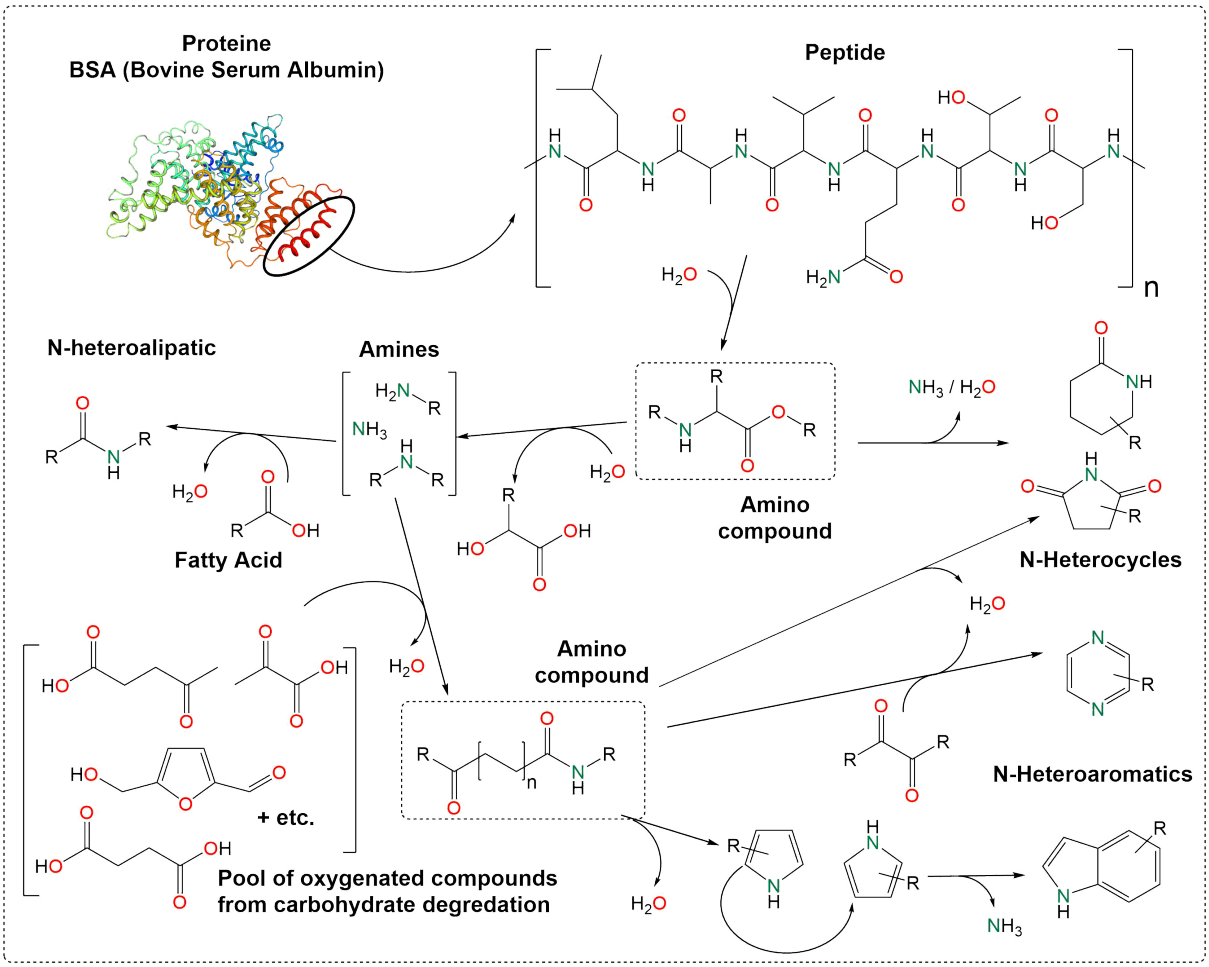

Figure 22. Degradation of Bovine Serum Albumin, the applied nitrogen source in this study and possible formation pathways of different N-hetero compounds

3.4 Conclusion

The hydrothermal conversion of model feedstock composed of cellulose, a lipid and a protein component with different compositions was investigated. The influence of the lipid and cellulose content on the product fractions, as well as the fate of carbon and nitrogen in the product phases, was given. Subsequently, the nitrogen recovery in different, representative heteroatomic species was analysed and discussed, to derive a chemical reaction scheme and to understand the reaction pathways in more detail. The following key findings can be concluded:

(1) That the addition of lipids to the feedstock mixture increases the yield of the biocrude while decreasing the formation of undesired carbonaceous solids.

(2) More carbon is recovered in the biocrude phase at a higher share of lipids in the feedstock. Interestingly this comes along with a lower nitrogen recovery.

(3) Rising the ratio of lipids to protein does increase the formation of fatty acid amides, suggesting that there is a dominant generation of N-heteroaliphatic species, which fate into the biocrude phase. Simultaneously the formation of N-heteroaromatic species is significantly suppressed, that of pyrazines almost interrupted, as fewer of their precursors, the less stable secondary amino compounds are formed.

(4) Free amines are highly reactive species that should be 'trapped' in stable, non-problematic compounds to prevent the amination of carbohydrate degradation products.

(5) Lipids, long-chain as well as short-chain carboxylic acids can act as such amine 'traps', forming N-aliphatic compounds in the biocrude or transferring N into the aqueous product phase.

In further studies, the influence of lipids on the generation of N-heteroaromatic substances should be proven by semi-quantitative high-resolution spectroscopy to identify and record relevant high molecular weight species. Also, the model system should be investigated and validated using real biomass feedstocks like sewage sludge, algae, manure and possible co-liquefaction mixtures. To facilitate beneficial amine trapping, and the use of short-chain carboxylic acids recovered from the by-produced aqueous phase may be investigated.

Chapter 4.

Pre-treatment of sewage sludge to improve biocrude quality

This chapter is based on the publication

Sequential Hydrothermal Processing of Sewage Sludge to Produce Low Nitrogen Biocrude

Joscha Zimmermann[a], *Klaus Raffelt*[a], *Nicolaus Dahmen*[a]

[a] *Institute of Catalysis Research and Technology, Karlsruhe Institute of Technology, 76344 Eggenstein-Leopoldshafen*

Publishing details:

Processes

Volume: 9; Issue: 3

Published on March 9h, 2021

DOI: 10.3390/pr9030491

4.1 Introduction

Sewage sludge is generated from wastewater treatment plants, demand urgent management and proper disposal. More than 10 million tons of sewage sludge were produced in the European Union (EU) in 2010, with a rising amount due to population growth, urbanization and higher regulations on the wastewater effluent [256,257]. Common disposal methods are the use in agriculture, incineration or landfill [60]. However, the sludge management remains a challenging issue for the member states as the European legislations provided with the Directive 2018/851/EC a priority hierarchy in waste management, starting from prevention, to preparing for reuse, to recycling, to energy recovery, and finally to disposal [8]. Besides, the limit levels for pathogens, metal and nutrient application rates to land are set and new issues arise with micro-plastics and pharmaceutical residuals [70,258,259]. The common method to handle excess sewage sludge in Europe is sludge thickening followed by anaerobic digestion (AD) [260]. The AD is not a final solution and is only applied to reduce the amount of sludge for subsequent transportation to the incineration plant [261].

As sewage sludge is a waste product with a relatively high content of organic matter, it has gained interest for thermochemical utilization [219]. For instance, hydrothermal liquefaction (HTL) can convert wet feedstocks, like sewage sludge to renewable fuel [20]. After mechanical dewatering, sewage sludge still contains 80–90% moisture. HTL can skip the energy-intense drying step, as the process takes advantage of the extraordinary properties of hot compressed water at 200–400 °C and 5–35 MPa [20,26,262]. The higher reactivity is caused by a superior ionic product and a low dielectric permittivity, which enhances acid/base and ionic reactions and breaks down cell structures and macromolecules, including carbohydrates, lipids, and proteins [96,224]. The main organic products are the biocrude, char, water-soluble substances and gas. In a lower temperature regime, char production is favored (hydrothermal carbonization), while higher temperature leads to gasification (hydrothermal gasification) [263]. The inorganic components are recovered primarily in a solid phase (above 70 wt. %),

and the rest is mostly solubilized in the water phase and traces can be found in the biocrude [264].

However, there are still some issues to be solved. Biocrude from HTL of sewage sludge suffers from high contents of nitrogen, originating from proteins and differs therefore from fossil crude oils [227,265]. There have been many efforts to refine biocrude into commercial fuels through various extensive methods such as catalytic cracking, hydrotreating, emulsifying and blending [227,266]. Additionally, the role of HTL operating parameters in producing higher biocrude yields and better quality has been elucidated extensively in the past [29]. A new approach to lower nitrogen content and thus to increase biocrude quality is to investigate an upstream hydrothermal pre-treatment, improving the HTL feedstock [267]. A mild hydrothermal treatment is already commonly applied on sewage sludge to improve dewaterability or biodegradability for downstream anaerobic digestion in a wastewater treatment plant [63]. With a focus on the transformation of organic nitrogen during hydrothermal treatment of sewage sludge, Zhuang et al. showed solubilization of nitrogen over a wide temperature range [268]. It was shown that the application of a hydrothermal pre-treatment could reduce the nitrogen content of sewage sludge and led to lower the NO_x emission prior to subsequent combustion [269]. Concerning different biogenic feedstock, Yoshida et al. examined the subcritical water treatment on waste squid and Zhu et al. the decomposing of fish proteins to produce amino acids [270,271]. The combination of a mild hydrothermal pre-treatment with HTL on microalgae lowered successfully the heteroatom content [156]. Jazrawi et al. applied also a two-stage hydrothermal process of algae and added inorganic and organic acids to lower the nitrogen content of the derived biocrude [155]. Furthermore, the pre-treated algae were analysed in deep to gain a better understanding of the process. A different approach was conducted by Guo et al., who tried to pre-treat algae with a pulsed electric field to extract valuable proteins and improve the quality of the subsequently derived biocrude [272].

Nevertheless, most research focus on the relation of yield and the nitrogen content in biocrude when sewage sludge is subjected to a pre-treatment. Preceding research of Fan et al. at IKFT

suggests strong competition of Maillard or amidation reactions of proteins with carbohydrates or fatty acids, respectively [134]. Malliard reactions form N-heterocycles, while amidation of fatty acids leads to long-chain amides. These findings propose a pre-treatment where proteins, carbohydrates and their Maillard products are solubilized in an aqueous supernatant and subsequently removed. We pursue to apply a two-stage hydrothermal process with set reaction conditions, including water and two acid hydrothermal pre-treatments and the subsequent liquefaction. the influence on the interactions of proteins, carbohydrates and fatty acids are addressed the first time on a real biomass. The effect on the yield, carbon and nitrogen distribution and chemical composition of the pre-treated solids and products is therefore discussed in detail.

4.2 Material and methods

4.2.1 Biomass and chemicals

A sample of around 60 kg municipal sewage sludge (MSS), including centrifuged primary and secondary (activated) sludge, was collected at the local wastewater treatment plant (Städtisches Klärwerk, Karlsruhe, Germany) in November 2019. The sample was directly dried at 105 °C for 24 h and collected into two fractions. One fraction was prepared for pre-treatment experiments and sieved to a 5–7 mm grain size by laboratory frame screens. Another fraction was prepared for subsequent HTL experiments and evenly ground with a laboratory rotor mill (Pulverisette, Fritsch, Idar-Oberstein, Germany) with a screen size of 200 µm.

Chemicals used for the experiments were obtained in analytical grade. Citric and sulfuric acid, sodium carbonate, dichloromethane, deuterated chloroform, hexane, hexadecanol, phenol, pentadecane, and FAME mix were obtained from Merck (Darmstadt, Germany). 2-Piperidone and 4-Methyl-indole were purchased from Acros Organics (Acros Organics, Bridgewater, NJ, USA). Hexadecanamide was purchased from Cayman Chemicals (Ann Abor, MI, USA).

4.2.2 Pre-treatment

The pre-treatment of MSS was conducted according to the procedure shown in Figure 23 (A) The used test rig is schematized in the Supporting Information, S 5. It was constructed in-house and consists of a fixed bed reactor (FBR) with reactor volume of 100 mL (diameter = 42 mm, length = 72 mm) and a fritted sinter metal with a pore size of 200 µm to retain the MSS. The reactor was surrounded by an aluminum block heated by cartridges. The leaching agent was pumped into the FBR by an HPLC Pump (PrepStar SD-1, Agilent Technologies, Santa Clara, CA, USA). Subsequently, the leachate was cooled to room temperature with a heat exchanger while the pressure was regulated manually by a backpressure valve.

In one experiment, approximately 30 g of MSS powder was loaded into the reactor. All experiments were performed at 2 MPa reactor pressure to prevent the evaporation of water. After the FBR has been flushed with 75 mL of deionized water with a flow rate of 15 $mL \cdot min^{-1}$ the feed was switched to 5 $mL \cdot min^{-1}$ leaching agent, 0.5 M sulfuric acid (SA), 0.5 M or citric acid (CA), and heated 70 min to 150 °C and kept there for 30 min. The molarity of citric acid and sulfuric acid were assumed to be comparable, as organic acids tend to dissociated incomplete. Then the liquid flow was switched back to de-ionized water and the flow rate was increased to 10 $mL \cdot min^{-1}$ for additional 100 min to wash out residual leaching agent. Similar procedure was conducted with pure de-ionized water (DW) as a blank. During this treatment, every 10 min and between min 50 and 70, every 5 min a sample of 2 mL was taken and filtered with a 0.45 µm Teflon syringe filter to remove high molecular weight impurities, subsequently stored below 5 °C until analysis. The treated MSS was subsequently dried at 105 °C for 24 h and then ground to 200 µm. The experiments were performed in triplicates for every leaching agent. The resulting pre-treated solids were labelled as "DW-Solid," "SA-Solid," and "CA-Solid."

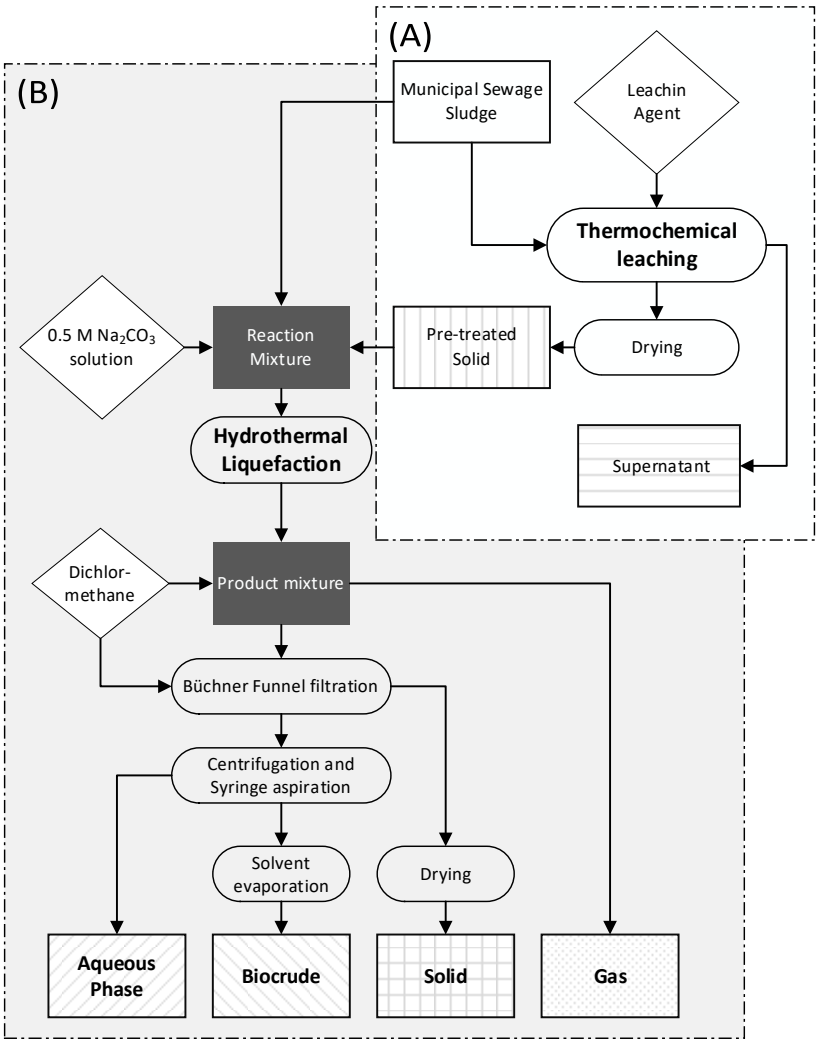

Figure 23. Process procedure: **(A)** pre-treatment and **(B)** hydrothermal liquefaction (HTL) process, including product separation.

4.2.3 Hydrothermal liquefaction

The HTL experiments were conducted according to the procedure schematized in Figure 23 (B) As reaction vessels, in-house build autoclaves (Stainless steel, EN 1.4571) with a capacity of 25 mL were used. To start an experiment, they were filled with a solution containing raw or pre-treated MSS and 0.1 M sodium carbonate (Na_2CO_3) solution occupying 60% of the available volume (solid load of approximately 15 wt. %). The Na_2CO_3 was added to raise the pH into an alkaline reaction environment. The headspace was purged with nitrogen three times and pressurized to 1 MPa, which facilitate the product gas collection after the experiment. The

autoclaves were then sealed with a torque key. In one run, six autoclaves were placed into an isothermal fluidized sand bath (SBL 2, Techne, Stone, UK [214]), set to a temperature of 350 °C, resulting in a reaction pressure of 20 MPa according to the gas saturation pressure of water [22]. The heating rate inside was measured previously as 40 $K \cdot min^{-1}$, resulting in a heating time of 8.75 min. After attaining the reaction temperature, it was held for 20 min. Afterwards, the reactors were rapidly cooled down in a water bath for 10 min. HTL experiments on raw MSS were denoted as "MSS-HTL" and on pre-treated solids "DW-HTL", "SA-HTL", and "CA-HTL" respectively. All experiments were again conducted in triplicates.

After the reaction procedure, the autoclaves were opened in a gas collection system with a known volume and attached manometer (Swagelok, Solon, OH, USA). An aliquot of 100 µL was taken with a gas-tight syringe for further analysis by gas chromatography, equipped with a 2 m Molsieve 5 Å and a 2 m Porapak Q column to flame ionization detector (FID) and thermal conductivity detector (TCD), respectively. The ideal gas law was applied to calculate the total mass of the gas, considering its final pressure after the HTL experiment and its composition.

The residual HTL products in the reactor was mixed with 5 mL dichloromethane (DCM) and separated by a Büchner funnel (47 mm diameter, 0.45 µm pore size, Nylon, Whatman, GE Healthcare, Buckinghamshire, UK). Then, the reactor and filter residue was washed exhaustively with 45 mL DCM. Retained solids including the filter paper were dried overnight at 105 °C. To support the separation of the aqueous phase and the organic phase, the mixture was centrifuged at 7000 rpm (EP 5430, Eppendorf AG, Hamburg, Germany) for 5 min. Subsequently, the aqueous top layer was removed with a syringe and stored below 5 °C for further analysis. DCM in the residual organic phase was removed overnight under a gentle nitrogen stream.

4.2.4 Bulk analysis of feedstock, pre-treated solids and HTL-products

The carbon, hydrogen, nitrogen, and sulfur content of the feedstock, pre-treated solids and biocrude as well as solid products were analysed using a CHNS-Analyser (Vario EL cube, Elementar Analysetechnik GmbH, Hanau, Germany). Further inorganic constituents were analysed by inductively coupled plasma optical emission spectrometry (ICP-OES) (ICP-725; Agilent Technologies, Santa Clara, CA, USA), after microwave-assisted acid digestion in reverse aqua regia (mixture of nitric acid and hydrochloric acid in molar ration of 3:1). Carbon and nitrogen content in aqueous samples were determined by TOC and TNb analyser (DIMATOC 2100 and DIMA-N, Dimatec Analysetechnik GmbH, Essen, Germany).

The storage moisture and ash content of the feedstock were determined by drying the sample at 105 °C and incinerating 500 mg of sample in an automated thermogravimetric analyser (TGA701, Leco, St. Joseph, MI, USA) at 550 °C under air.

The content of crude lipids (saponifiable and unsaponifiable lipids) in the MSS and pre-treated solids was determined by an n-hexane soxhlet extraction [157]. Therefore, 1 g of dried solid sample was put into a cellulose extraction thimble (Whatman, GE Healthcare, Buckinghamshire, UK) and refluxed for 12 h. After extraction, the hexane was removed in a rotary evaporator (40 °C and 50 mbar), weighing the remaining extract to determine the extraction yield. Additionally, 17 amino acids, including alanine (Ala), arginine (Arg), aspartic acid (Asp), cysteine (Cys), glutamic acid (Glu), glycine (Gly), histidine (His), leucine (Leu), lysine (Lys), methionine (Met), phenylalanine (Phe), proline (Pro), serine (Ser), threonine (Thr), tyrosine (Tyr), isoleucine (Ile), and valine (Val) were detected, following hydrolysis the procedure EC-Regulation 152/2009 F [273]. Briefly, proteins were hydrolysed by 6N HCl for 24 h at 110 °C. Subsequently, the amino acids (except tryptophan) were determined via HPLC on a sulfonated polystyrene resin column.

4.2.5 Chemical composition of biocrude

To identify and determine the chemical composition, the biocrude was analysed by a gas chromatograph (GC, Agilent 6890N, Santa Clara, CA, USA) coupled with a mass spectrometric (MS, Agilent 5973N, Santa Clara, CA, USA) and flame ionization detector on an RTX-5MS column (30 m × 0.25 mm × 0.25 mm, Restek Corporation, Bellefonte, PA, USA). All samples were prepared in tetrahydrofuran (THF). 0.5 µL were injected at 280 °C in splitless mode, using helium as carrier gas (1.5 $mL \cdot min^{-1}$). The column oven program started at 70 °C which was held for 2 min and progressing at 8 $K \cdot min^{-1}$ until 180 °C and 4 $K \cdot min^{-1}$ until 280 °C followed by a hold time of 15 min. For identification, the Agilent deconvolution was applied. A Polyarc® micro-reactor (Activated Research Company, Eden Prairie , MN, USA) was installed before the FID detector to enable a direct quantification of identified compounds [274]. For each compound class, a representing compound was chosen: phenol for cyclic-O, valerolactam and skatol for cyclic-N, hexadecanol for aliphatic-O, and hexadecanamide for aliphatic-N was chosen and previously confirmed by the retention time with the pure standard chemical. Pentadecane was applied as a general internal standard.

For quantification, free fatty acids were transesterified to FAME (Fatty Acid Methyl Ester) in order to prevent potential decarboxylation into hydrocarbons during GC-injection. Therefore, a modified method developed by Lepage and Roy [275] was applied. A stock solution containing 500 ppm pentadecane and 50 ppm butylated hydroxytoluene (BHT) was prepared in methanol-hexane (4:1 vol/vol) mixture. Approximately 20 mg of biocrude sample were prepared in a borosilicate glass vial and 500 µL of the stock solution was added. The vials were placed on ice and 100 µL acetyl chloride was added dropwise and then capped under nitrogen. To accelerate the reaction, the vials were placed in an oven for 2 h at 80 °C. After the vials were cooled to room temperature, 1 mL of 0.05 M Na_2CO_3 solution and 500 µL was added, vortexed for 1 min and subsequently centrifuged for 5 min at 7000 rpm. The upper hexane phase (200 µL) was transferred to a GC vial, analysed by GC-MS, and quantified with the previously mentioned Polyarc® micro-reactor. For the integration of peaks and area determination,

Agilent's Mass Hunter internal Chemstation integrator was used (Agilent Technologies, Santa Clara, CA, USA).

Functional groups in the biocrude were semi-quantitatively analysed at room temperature by nuclear magnetic resonance spectroscopy (NMR), recorded on a Bruker 250 MHz NMR (Biospin 250, Bruker, Rheinstetten, Germany). Sample preparation consisted of dissolving 0.1 g of biocrude in 0.7 mL of deuterated chloroform with tetramethylsilane as an internal standard. Before loading the 5 mm NMR-tubes, the solution was filtered through a 0.22 µm syringe filter (Spheros PFTE, LLG Labware, Turnov, Czech Republic), removing suspended particles. ^{1}H spectra were acquired in a 90° pulse angle with a delay of 1 s, 126 scans and a spectral width of 3400 Hz. The resulting signals were processed and integrated with MestReNova 14.1.2 (Mestrelab Research S.L., Santiago de Compostela, Spain). For the integration and functional group assignments, regions for the ^{1}H spectra were given by Mullen et al. [276]. Signals from residual DCM (δ = 5.30 ppm) and a trace of non-deuterated chloroform (δ = 7.26 ppm) and their related areas were excluded by deconvolution [277].

4.2.6 Calculations

The product yields of biocrude, solid and gas phases were calculated by Equation (1).

$$Y_i\ (dry, ash\ free) = \frac{m_i}{m_{sludge\ solid} - m_{ash} - m_{moisture}} \quad (3)$$

where Y is the yield (wt. %), the index *i* is the corresponding phase (biocrude, aqueous phase, gas or solid) and *m* is the mass (g) of the product or feedstock.

The carbon or nitrogen recovery of biocrude, solid, gas, and aqueous phases were calculated by Equation (2).

$$ER_i = \frac{m_i \cdot E_i}{m_{sludge\ solid} \cdot E_{sludge\ solid}} \quad (4)$$

where ER is the element recovery (carbon or nitrogen), the index *i* is the corresponding phase (biocrude, aqueous phase, gas or solid), *m* is the mass (g) and *E* is the element concentration (wt. %). It needs to be noted that the mass of water was defined as constant and formation or consumption of water due to condensation, hydrolysis or water gas shift reactions, were considered as negligible.

A commonly applied expression to characterize the fuel quality of petroleum is the H/C-ratio. For biomass-derived fuels, a modified descriptor (H/C_{eff}), given elsewhere [278], is applied on each sludge solid and biocrude. To get a petroleum-like fuel, the heteroatoms oxygen, nitrogen, and sulfur can be removed as water (H_2O), ammonia (NH_3), and hydrogen sulfide (H_2S), respectively, developing Equation (3).

$$H/C_{eff} = \frac{H - 2O - 3N - 2S}{C} \quad (5)$$

where H/C_{eff} is the effective hydrogen to carbon ratio, where *H*, *O*, *N*, *S*, and *C* represent the element concentrations of hydrogen, oxygen, nitrogen, sulfur, and carbon, respectively.

A change indicator (CI) was calculated to evaluate the effect of pre-treatment on the derived biocrude. CI compares the concentration of specific compounds quantified by GC in the biocrude with and without pre-treatment. A negative CI value indicates a lower, a positive CI value a higher amount of the specific compound. Is the CI value close or equal to zero, there is essentially no effect.

$$CI_i = \frac{C_{i,pre-treatment} - C_{i,no\ pre-treatment}}{C_{i,no\ pre-treatment}} \quad (6)$$

CI is the change indicator; index *i* is the specific compound; $C_{i,pre\text{-}treatment}$ is the concentration of component *i* in the HTL derived biocrude of a pre-treated sludge and $C_{i,no\ pre\text{-}treatment}$ is the concentration of the biocrude from blank sewage sludge.

For all calculations, the propagation of uncertainty is taken into account.

4.3 Results and discussion

4.3.1 Effects of pre-treatment on sewage sludge

Table 8 summarizes the results of the proximate analysis and the elemental, biochemical and ash composition of the MSS and the pre-treated solids. The results show that the MSS has an organic content of 70.0 wt. %, which decreased to 61.9 wt. % by hydrothermal pre-treatment with DW or increased to 75.3 wt. % by treatment with CA, while SA had no notable effect. Due to the different organic content, certain values of the MSS and its derived pre-treated solids are given on a dry ash-free basis for better comparison. It was found that the carbon content of MSS increased due to a hydrothermal treatment from 52.8 wt. % up to 59.4 wt. %, in CA-Solid. On the other hand, the nitrogen content decreased from 7.1 wt. % down to 3.1 wt. %, most effectively by applying SA. Similarly, the oxygen content is reduced, especially after adding acids. It needs to be mentioned that SA treated sludge shows an increased S content of 3.1 wt. %, which can be present as sulphate, but is potentially bound to some organic compounds [155]. The pre-treatment has lowered the N/O ratio and indicates a prioritized extraction of N. In addition, the H/C_{eff} ratio is derived from the elemental composition. Pre-treated solids show a significant higher H/C_{eff}, risen from 0.55 up to 0.67.

Nevertheless, the extraction of N and a potential quality improvement came with a loss of solid organic matter. All pre-treatments indicate a decrease in solid yield. The application of DW and SA shows a solid yield of 54.8 and 52.8 wt. %, while CA has a solid yield of 63.4 wt. %. An increasing temperature led to a higher degree of solubilization of organic material by hydrolysis reactions to form smaller, water-soluble fragments [279]. This can be accelerated by adding an acid [280].

Table 8. Characterization of the feedstock (MSS) and pre-treated solids (DW, SA, CA). The values in brackets indicate the standard deviation.

	MSS	DW-Solid	SA-Solid	CA-Solid
Proximate analysis (dry basis)				
Ash [wt. %]	30.0 (0.1)	38.1 (0.3)	30.5 (0.7)	24.7 (0.1)
Organic [a] [wt. %]	70.0 (0.1)	61.9 (0.3)	69.5 (0.7)	75.3 (0.1)
Elemental analysis (dry, ash-free basis)				
C [wt. %]	52.8 (0.1)	56.3 (0.2)	57.2 (0.5)	59.4 (0.2)
H [wt. %]	7.9 (0.1)	7.7 (0.1)	7.6 (0.1)	7.7 (0.1)
N [wt. %]	7.1 (0.0)	4.7 (0.1)	3.4 (0.1)	3.6 (0.0)
S [wt. %]	0.9 (0.0)	0.9 (0.0)	3.1 (0.2)	0.8 (0.0)
O [a] [wt. %]	31.3 (0.0)	30.4 (0.2)	28.6 (0.8)	28.5 (0.1)
N/O	0.26 (0.00)	0.18 (0.00)	0.14 (0.00)	0.14 (0.0)
H/C_{eff} [b]	0.55 (0.02)	0.59 (0.01)	0.66 (0.03)	0.67 (0.02)
Yield and recovery (dry, ash-free basis)				
Solid yield [wt. %]	-	54.8 (3.3)	52.8 (2.0)	63.4 (2.2)
C-recovery solid phase [wt. %]	-	62.6 (1.7)	56.8 (1.8)	62.7 (2.3)
C-recovery aqueous phase [wt. %]	-	29.0 (1.9)	34.1 (0.9)	31.0 (1.5)
N-recovery solid phase [wt. %]	-	40.3 (2.4)	25.6 (1.2)	28.2 (1.0)
N-recovery aqueous phase [wt. %]	-	50.6 (4.5)	66.7 (0.9)	62.0 (0.7)
Organic composition (dry, ash-free basis)				
Hydrolytic amino acids [wt. %]	21.8	13.5	10.0	9.3
Lipids [c] [wt. %]	21.7 (1.1)	24.4 (1.1)	29.9 (1.4)	28.6 (0.6)
Ash analysis (dry, organic-free basis)				
Al [wt. %]	2.5	2.6	2.3	2.4
Ca [wt. %]	7.6	7.6	5.6	2.8
Fe [wt. %]	18.0	18.1	4.5	5.7
Mg [wt. %]	0.9	0.8	0.3	0.8
P [wt. %]	8.0	8.1	3.4	2.8

[a] Calculated by difference; [b] all H/C_{eff} values were calculated according to Equation (3); [c] saponifiable and un-saponifiable.

Figure 24 shows the extent of C and N recovery in the solid and aqueous phase. For further information, the extraction of C and N into the aqueous phase is depicted in the Supporting Infomation, S 6. The treatment with DW and CA shows very similar carbon recoveries into the solid phase.The maximum recovery of C and N in the aqueous phase is achieved by the SA treatment; up to 34.1 wt. % and 66.7 wt. %, respectively. In summary, more nitrogen than carbon is extracted during the pre-treatment into the aqueous phase, which can be increased by the addition of an acidic agent. The amount of hydrolysable amino acids is lowered due to a pre-treatment with DW from 21.8 wt. % to 13.5 wt. % and the application of an acidic agent halve this amount to 10 wt. % in the SA-Solid and 9.3 wt. % in the CA-Solid, respectively. The

specific amino acid composition is listed in the Supporting Infomation, S 7. All hydrothermal pre-treatments, no matter if DW, SA, or CA is applied, lessen the amount of all amino acids. Similar observations on the amino acid composition were made by Chen et al. [281]. This observed change occurs more or less congruently with the nitrogen extraction and the reduction of the N/O-ratio. It needs to be pointed out that the chosen temperature of 150 °C was indicated as a threshold for protein transfer into the supernatant [151,282]. In addition, the release of NH_4^+ by deamination reactions is often referred [283,284].

Concerning more fundamental studies, proteins are hydrolysed into peptides, which then hydrolyse usually slowly to amino acids [285]. This can be accelerated significantly by applying hydrothermal conditions or even more by adding acids [286]. With increased temperature, amino acids start to decompose under deamination reactions or form together with carbohydrates water-soluble Amadori compounds via Maillard reactions [243,287,288].

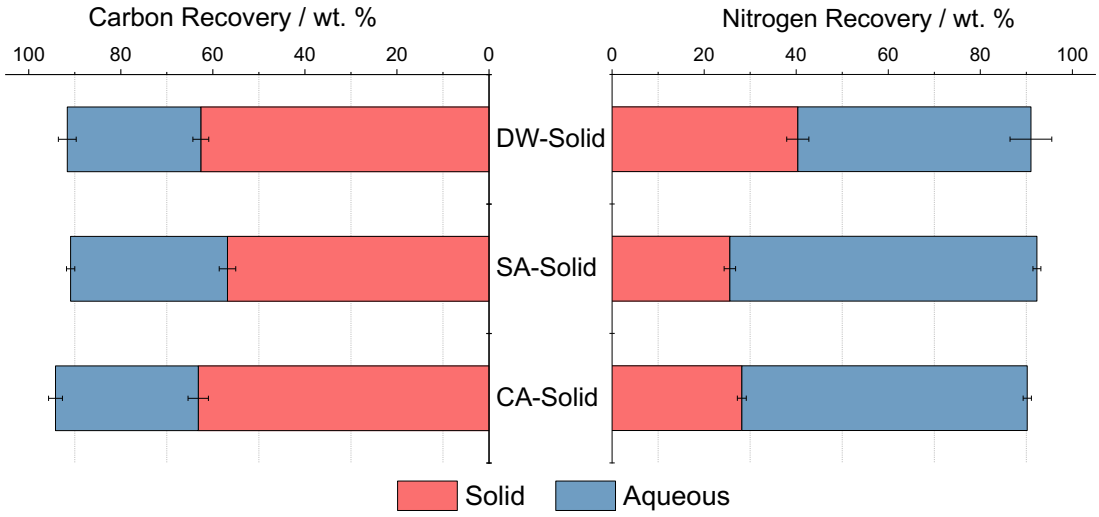

Figure 24. Carbon and nitrogen recovery in the solid phase and aqueous supernatant of hydrothermal pre-treatment.

To visualize the effect of the pre-treatment, Figure 25 shows two Van Krevelen plots. Figure 25 (A) shows the O/C- to H/C-ratio and Figure 25 (B) the N/C- to H/C-ratio of the produced solid materials. Additionally, the directions for removal of water, carbon dioxide, and ammonia, which are typical reactions during the hydrothermal pre-treatment are drawn.

Apparently, in Figure 25 (A) the step from MSS to the solids after pre-treatment is primarily following a dehydration pathway. This phenomenon is typical for lower temperature regimes and can be observed via the formation of hydrochar [289]. The SA-solid shows a slight tendency toward decarboxylation. SA suggests to cause some sort of severity to the reaction, as it is a potential oxidizing inorganic acid. From Figure 25 (B), it can be observed that the step from MSS to the solid pre-treatment products essentially follows the deamination pathway. In summary, acid-treated solids show a higher degree of dehydration and deamination compared to treatment in water only.

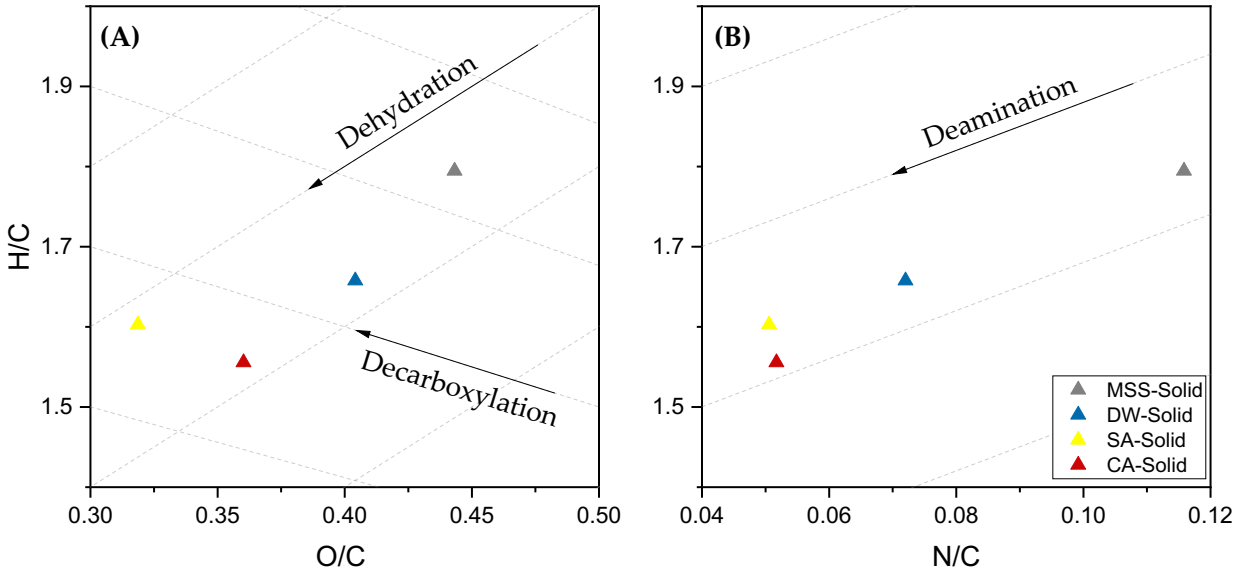

Figure 25. Van Krevelen diagram of MSS and the solids prepared by hydrothermal pre-treatment, **(A)** O/C vs. H/C-ratio and **(B)** N/C vs. H/C-ratio.

As shown in Table 8, the amount of crude lipids is increased from 21.7 wt. % in MSS up to 29 wt. % in SA-solid. Again, both acidic pre-treatments here show the biggest effect. The lipid content increased congruently with the solubilization of organic matter in the aqueous phase. This could be explained by a favored extraction of proteins and carbohydrates. Bougrier et al. and Li et al. reported negligible or even no influence on the solubility of lipids, even with moderately elevated temperatures [151,290]. Furthermore, the significant higher H/C_{eff} value of the pre-treated solids can be referred to its lipid content, as lipids are primarily composed of

fatty acids with long-chain –$(CH_2)_n$– units that contain much fewer heteroatoms than carbohydrates and proteins.

In Table 8 the ash composition of the MSS and the DW, SA and CA solids is given in terms of the main inorganic elements. The pre-treatment with DW shows no effect on the composition, while SA and CA substantially leached calcium (Ca), iron (Fe), magnesium (Mg), and phosphor (P). The Ca amount in the SA solid needs to be mentioned, as it was not as effectively removed as in the CA solid. With regard to the sulfur content from the elemental analysis, this suggests the precipitation with sulphate (SO_4^{2-}), supplied from the SA, to form calcium sulphate ($CaSO_4$). This would explain why the ash is not reduced. Here it needs to be notified, that the subsequent water washing step was not able to remove all acidic residues, especially when using SA [161]. In summary, the pre-treatment with CA removed most of the inorganic constituents, while DW only solubilizes organic matter.

4.3.2 Effect of pre-treatment on the yield and the elemental composition of HTL-products

The obtained solids from the pre-treatment step were again hydrothermally processed at fixed temperature, reaction time and solid load of 350 °C and 30 min and 15 wt. %, respectively. As mentioned above, the solids tend to contain residual acidic compounds, thus Na_2CO_3 is added as an alkaline agent to facilitate the reaction towards the favored biocrude product. First, an acidic reaction condition is reported to increase the repolymerization of intermediates and the formation of undesired solid char [291]. Second, carbonates are believed to lead to a higher degree of deoxygenation and lastly the alkali salts, which may catalyse the fragmentation of macromolecules [292,293]

One important measure of HTL performance is the biocrude yield. As shown in Figure 26, it was found that hydrothermal pre-treatment increases the yield. For DW-HTL derived biocrude the yield is slightly increased to 36.6 wt. %, compared to the one obtained with direct HTL of MSS. It is also shown that an acid pre-treatment results in significantly more HTL biocrude;

39.4 wt. % for SA-HTL and 42.9 wt. % CA-HTL. An explanation for the reduced biocrude yield of MSS- and DW-HTL, could be the reported higher content of metals in the MSS and the DW-Solid. In a study by Chen et al., metals in the are reported to reduce the biocrude yield of HTL of wastewater algae [294]

However, Figure 26 (A) also shows the overall yield related to the MSS feedstock, which is significantly lower when compared to the biocrude yield which results from HTL of pre-treated material. The overall yield does not only depend on the efficiency of converting the pre-treated solids to biocrude but also their production from the original MSS feedstock. Thus, the extraction of organic matter during pre-treatment makes the difference. With regard to the extensive solubilization during the pre-treatment, DW-HTL shows the lowest overall yields with about 20.1 wt. %, while SA-HTL shows a slightly higher value with 21.0 wt. %. The CA-HTL has the highest overall yield over both process steps with 27.2 wt. %. Jazrawi et al. observed a similar trend in two-stage hydrothermal processing on algae [155]. The extraction of organic matter significantly lowered the overall yield. In contrast to the findings here, Jazrawi et al. found a much lower overall yield for the acidic pre-treated solids [155].

With the first view on the yield this process seems disadvantageous, therefore quality evaluation values and chemical composition are presented and discussed in detail below. Furthermore, the aqueous supernatant of the pre-treatment is an untapped issue but could be valorized in anaerobic digestion, as thermal hydrolysis processes are commonly applied in wastewater treatment plants [63,284].

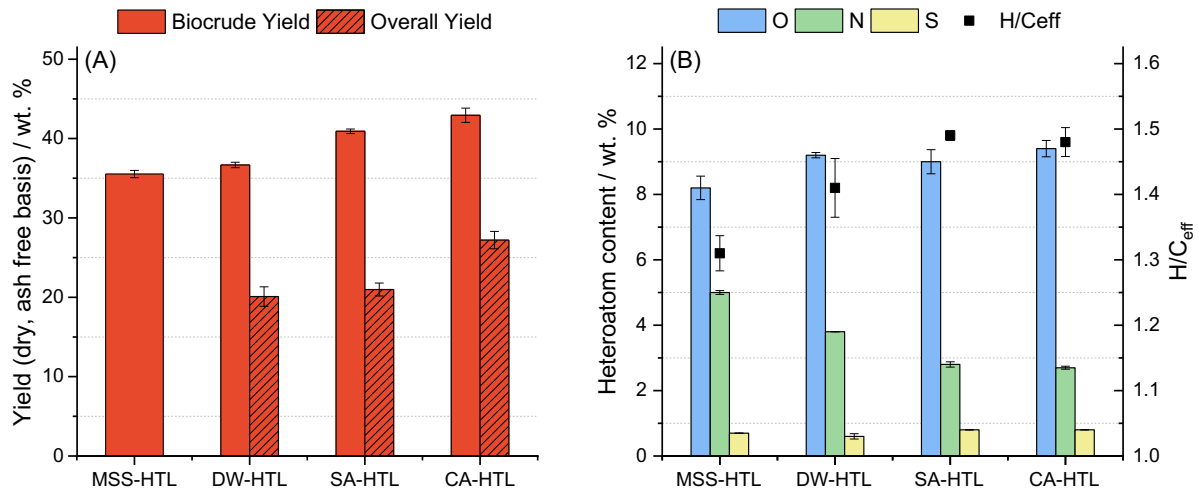

Figure 26. (A) Biocrude yield of hydrothermal liquefaction and the overall yield of the combined process with pre-treatment and **(B)** heteroatom content (O, N, S) and H/Ceff of derived biocrude.

Regarding the elemental analysis of the biocrude products obtained from HTL in Table 9, it was found that the carbon and hydrogen content was greatly increased in comparison to the MSS and the related solids from pre-treatment, while the heteroatoms were removed by HTL. Especially the nitrogen content of the bio-crude from pre-treated solids was reduced. In contrast, the oxygen content is slightly increased, probably due to acid residuals [166]. The effects on the elemental composition have emerged in the H/C_{eff} ratio, which is necessarily increased for the biocrude from the pre-treated feedstock. Elemental composition and derived H/C_{eff} ratio are shown in Figure 26. Generally, the increase of the H/C_{eff} from feedstock to biocrude can be attributed to the reduction of oxygen. The further increase for the pre-treated biocrude is associated with lower nitrogen content. Yoo et al. refer a dependency of the H/C_{eff} value to the biochemical composition of his feedstock algae, in particular a higher lipid content of the feedstock [144]. This suggestion can be applied especially to SA-HTL and CA-HTL It is also noteworthy to mention the absent elevation of sulfur content in the SA-HTL biocrude because the SA-Solid contained more than three times more sulfur, whereas the biocrude of SA-HTL and CA-HTL contain the same proportion of S.

Table 9. Characterization of HTL products. Yield is based on dry, ash free values. The values in brackets indicate the standard deviation.

	MSS-HTL	DW-HTL	SA-HTL	CA-HTL
Biocrude				
Yield [wt. %]	35.5 (0.5)	36.6 (0.2)	39.4 (0.2)	42.9 (0.7)
C [wt. %]	75.6 (0.2)	75.5 (0.2)	76.1 (0.2)	75.9 (0.1)
H [wt. %]	10.4 (0.2)	10.9 (0.2)	11.2 (0.0)	11.2 (0.1)
N [wt. %]	5.0 (0.1)	3.8 (0.0)	2.8 (0.1)	2.7 (0.0)
S [wt. %]	0.7 (0.0)	0.6 (0.1)	0.8 (0.0)	0.8 (0.0)
O [a] [wt. %]	8.2 (0.4)	9.2 (0.1)	9.0 (0.4)	9.4 (0.2)
H/C_{eff} [b]	1.31 (0.03)	1.41 (0.04)	1.49 (0.01)	1.48 (0.02)
C-recovery [wt. %]	50.9 (0.8)	49.3 (0.5)	52.8 (0.5)	54.9 (1.2)
N-recovery [wt. %]	25.1 (0.6)	29.5 (0.3)	32.5 (1.2)	32.7 (0.9)
Aqueous				
C-recovery [wt. %]	19.3 (0.3)	12.4 (2.6)	10.0 (1.6)	13.3 (0.4)
N-recovery [wt. %]	54.3 (3.2)	47.9 (2.7)	45.2 (2.4)	44.7 (1.3)
Solid				
C-recovery [wt. %]	11.0 (1.2)	17.0 (0.2)	19.6 (1.6)	13.3 (1.1)
N-recovery [wt. %]	7.1 (1.0)	16.7 (0.2)	20.8 (0.6)	14.6 (1.2)
Gas				
C-recovery [wt. %]	5.3 (0.5)	6.1 (0.3)	6.0 (0.9)	5.5 (0.5)

[a] Calculated by difference; [b] All H/C_{eff} values were calculated according to Equation (3).

Figure 27 depicts the carbon and nitrogen recovery into the different product phases, namely biocrude, aqueous phase, solid and gas in the HTL step. It can be found that carbon is mainly recovered in the biocrude. MSS-HTL, in comparison to the DW-HTL, shows a small decrease in carbon recovery from 50.9 wt. % to 49.3 wt. %. The acid pre-treatment increases the C-recovery in the biocrude SA-HTL and CA-HTL to 52.8 wt. % and 54.9 wt. %, respectively. The carbon recovery in the aqueous phase is lowered for all pre-treated samples, while it is increased for the solid. Here it needs to be noted, that the aqueous phase of MSS-HTL shows an alkaline pH value of 9.5; however, for DW-, SA- and CA-HTL aqueous phase the pH was almost neutral. As previously mentioned, the SA-solids are believed to contain acidic residues, which aids the formation of a char. Therefore, SA-HTL shows the lowest carbon recovery in the aqueous phase and the highest in the solid. Another explanation for the lower recovery of soluble carbon compounds in the aqueous phase is the upstream removal of carbohydrate and protein oligomeric structures, as their monomers are likely solubilized in the aqueous phase. In terms of gas formation, no significant differences can be observed. For all samples, the C-

recovery could not be closed to 100 wt. % as light volatile compounds are probably lost during the evaporation of DCM. The nitrogen recovery, on the other hand, behaves differently. MSS-HTL shows the lowest nitrogen recovery with 25.1 wt. % and increases with the application of a pre-treatment to 32.5 wt. % for SA-HTL and 32.7 wt. % for CA-HTL biocrude. Recovery of nitrogen in the solid is increased analogously to the carbon recovery in the solid. Again SA-HTL shows here the highest value with 20.8 wt. %. For the aqueous phase, the nitrogen recovery seems to be more or less similar for the two-step HTL, but significantly lower for MSS-HTL. One explanation could be the formation of ammonium carbonate following the reactions (5) and subsequent decomposition (6) [163,295].

$$Na_2CO_3 + 2NH_4^+ \leftrightarrows (NH_4)_2CO_3 + 2Na^+ \quad (7)$$

$$(NH_4)_2CO_3 \rightarrow NH_3 + CO_2 + H_2O \quad (8)$$

Pre-treated samples, on the other hand, likely contain acidic residuals, which instead react with the added Na_2CO_3. Thus, the free ammonium ion can react further into the biocrude fractions to form amines and amides and with a higher proportion of lipids, more fatty acids are formed. These are likely to react with free ammonia further to fatty acid amides [134]. In addition, the overall difference in total nitrogen recovery needs to be mentioned. As the products were separated via vacuum filtration, ammonium was potentially stripped off from the aqueous phase, especially at higher pH values.

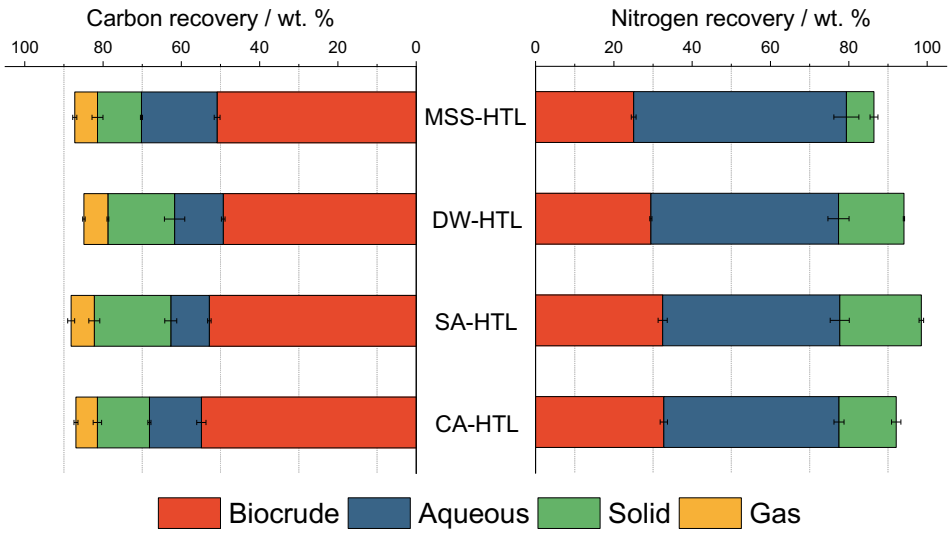

Figure 27. Carbon and nitrogen recovery in the different product phases of HTL.

In Figure 28, two Van Kreveln diagrams are presented. Figure 28 (A) shows the O/C- to H/C-ratio and Figure 28 (B) the N/C- to H/C-ratio. In addition to the MSS and the pre-treated solids, the derived biocrude samples are depicted. To identify the shift in elemental composition during HTL, again the directions for dehydration, decarboxylation, and deamination are drawn. With a look on (A), the HTL of MSS to the corresponding biocrude is following a combination of dehydration and decarboxylation reactions [296]. With the use of a water pre-treated solid DW-HTL, less dehydration takes place. This combination of reactions is mainly shifted to decarboxylation reactions with SA- and CA-HTL. As previously described, during each pre-treatment, the MSS is to a certain extend dehydrated, providing less opportunity for further dehydration reactions during the subsequent HTL. This would refer back to the suggested upstream removal of oligomeric like carbohydrates and proteins. With regard to Figure 28 (B), similarities between dehydration and deamination can be observed. The HTL of MSS to the corresponding biocrude follows mainly the deamination pathway. However, for the DW-HTL the degree of deamination is reduced. The acid pre-treated solids are located perpendicularly on the deamination line to the derived biocrude SA- and CA-HTL. This indicates that deamination occurred in the pre-treatment and not in the HTL-step.

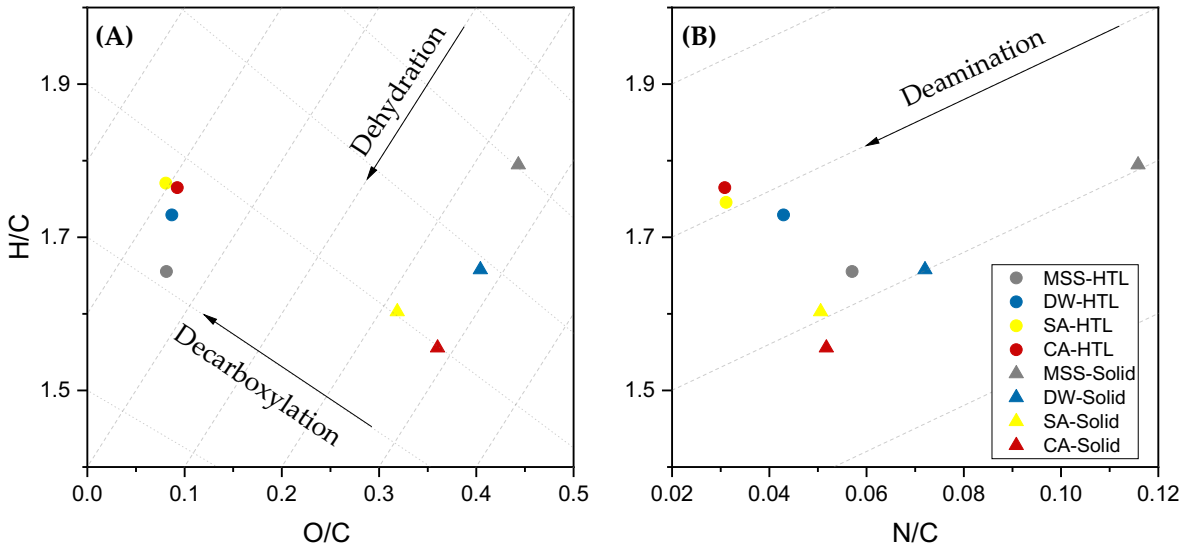

Figure 28. Van Krevelen diagram of MSS, solids from pre-treatment, and HTL derived biocrude, plotted as **(A)** O/C vs. H/C ratio and **(B)** N/C vs. H/C-ratio.

4.3.3 Effect of pre-treatment on the chemical composition of HTL-biocrude

The results of the chemical characterization of HTL biocrude from MSS and the solids from pre-treatment show some markable differences, which are exhibited and discussed in this chapter.

In a qualitative analysis, applying GC–MS, more than 100 compounds were identified via deconvolution for each biocrude sample. The 30 major compounds (quantified by peak area) and their retention time (RT) are listed in Table 10. The total ion current chromatogram (TICC) of each biocrude sample is provided in the Supporting Infomation, S 8. The identified compounds were allocated to eight chemical classes such as aliphatic alcohol, aliphatic alkene, fatty acid, fatty acid amide, ketones, N-heterocycles, phenols and sterols. In general, biocrude contains compounds with high molecular weight and boiling points and therefore only a fraction can be identified by GC–MS. Furthermore, compounds with a low boiling point have probably been lost due to the evaporation of the DCM solvent.

It can be noted that the lower boiling point range (RT < 17 min) of the biocrude consists mainly of cyclic and heteroatomic compounds. Cyclic ketones and phenols are detected in all biocrude

samples and are likely to derive from proteins and carbohydrates [86,292]. The biocrude from direct HTL of MSS shows a major presence of cyclic amides like lactams and cyclic amines like indoles. These N-heterocycles are originated by the degradation of proteins Maillard reactions with sugars [114]. In comparison, the acid pre-treated samples indicate the presence of methoxy phenols, which are referred to as lignin decomposition products [297]. Along with the higher boiling point range (RT > 17 min), pre-treated samples show more long-chain alkenes and alcohols. Latter compounds are decarboxylation and hydrodeoxygenation products of fatty acids, which are highly abundant in all biocrude samples [85,298]. Moreover, the presence of fatty acid amides in all biocrude samples occurs from the reaction of fatty acids and NH_3 and other decarboxylation products of amino acids [299]. Here it needs to be noted that approximately 70–80% of the area is related to the free fatty acids and the resulting derivates (aliphatic alkenes, aliphatic alcohols, fatty acid amide). Compounds at the end of the RT-scale are detected as poly-condensed structures, known as sterols, which are already present in sewage sludge [300]. The qualitative GC-MS results are in agreement with other authors, who reported HTL of sewage sludge [159,213]. Major compounds are oxygenated aromatics along with nitrogen-containing compounds like heterocycles or long-chain amides oils and sterols. When the sludge was rich in lipids, free fatty acids were found.

The effect of the pre-treatment on the HTL of MSS can be further elucidated by the Change Index CI of class representative compounds in the biocrude sample. Five compounds were chosen, namely phenol (phenols), 2-piperidione and 1H-indole, 3-methyl- (N-heterocycles), hexadecanol (aliphatic alcohols), and hexadecanamide (fatty acid amide). Additionally, all fatty acids were quantified via in-situ transesterification to FAME to prevent potential decarboxylation into hydrocarbons during GC-injection. The concentrations are listed in the Supporting Infomation, S 9. With the CI in Figure 29, it can be noted that a pre-treatment with DW and SA reduced the amount of phenol in the derived biocrude by 18.1% and 20.7%, respectively. The concentration of 2-piperidone is significantly reduced by more than 70% in all pre-treated biocrude samples. In the same way, the amount of 1H-indole, 3-methyl is

reduced by approximately 40%. Formation of 2-piperidone was probably following internal condensation reactions of amino acids followed by ring closure [244]. 1H-indole, 3-methyl can be derived from the degradation of tryptophan or other aromatic amino acids via pyrrole formation and subsequent cycloaddition [252,301,302]. Concerning the fatty acids and their alcoholic derivates, a significant increase can be observed.

DW-HTL and derived biocrude show a 25% increased content of free fatty acids, which can be further increased by more than 50% by acid pre-treatment. For hexadecanol, a hydrodeoxygenation product of hexadecanoic acid, the concentration is increased by 20.6% for DW-HTL and by 31.3% for CA-HTL. The highest increase of 52.9% was observed for SA-HTL. The content of hexadecane amide is slightly and non-significantly increased in DW-HTL biocrude. SA-HTL sample shows the highest increase of 17.9% of hexadecanamide. As acidic residuals in the SA-Solid are assumed, the pH is lowered during HTL, close to neutral. Referring to Fu et. al., the formation of amides is decreased under alkaline conditions [241].

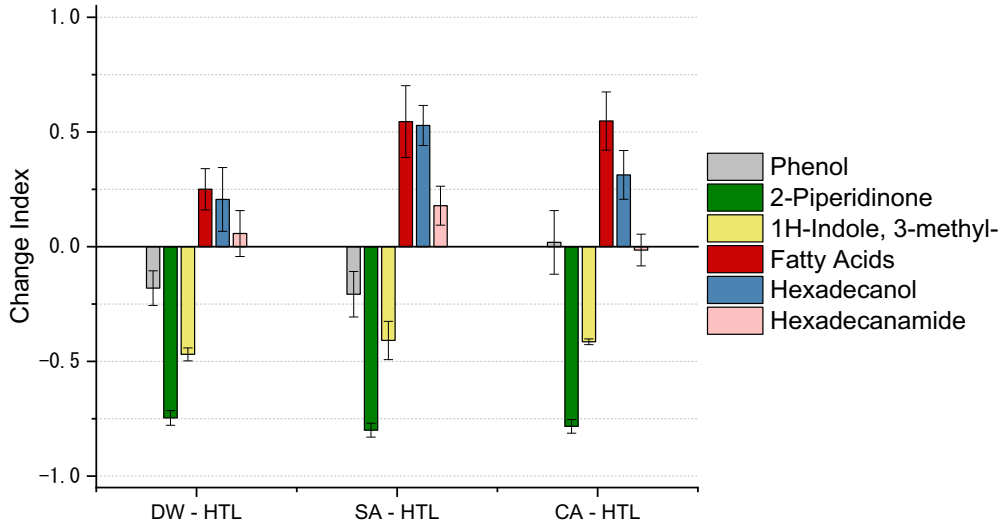

Figure 29. Change indexes (CI) of selected compounds in biocrude derived by hydrothermal liquefaction of pre-treated solids (indexes were calculated based on the comparison to the untreated product).

Table 10. Major compounds of the GC-MS total ion chromatogram areas of biocrude samples from liquefied municipal sewage sludge and pre-treated solids.

RT [min]	Compound Name	MSS-HTL	DE-HTL	SA-HTL	CA-HTL	Class
8.52	Phenol	x	x	x	x	Phenol
9.73	2-Cyclopenten-1-one, 2,3-dimethyl-	x		x	x	Ketone
10.32	2-Pyrrolidinone	x	x			N-heterocycle
10.46	p-Cresol	x	x	x	x	Phenol
10.71	2,5-Pyrrolidinedione, 1-methyl-	x	x			N-heterocycle
10.78	Phenol, 2-methoxy-			x	x	Phenol
10.78	Phenol, 4-methoxy-				x	Phenol
10.78	2-Cyclopenten-1-one, 3,4,5-trimethyl-		x		x	Ketone
11.05	2-Pyrrolidinone, 1-propyl-	x	x			N-heterocycle
12.35	Phenol, 4-ethyl-	x	x	x	x	Phenol
12.65	2-Piperidinone	x				N-heterocycle
12.85	Phenol, 2-methoxy-3-methyl-			x		Phenol
14.91	Indole	x				N-heterocycle
15.78	Piperidine, 1-pentyl-	x	x	x		N-heterocycle
16.29	N-[2-Hydroxyethyl]succinimide	x	x			N-heterocycle
16.66	1H-Indole, 3-methyl-	x	x	x	x	N-heterocycle
17.96	1-Dodecanol			x	x	Aliphatic alcohol
18.25	1-Pentadecene			x	x	Aliphatic alkene
19.53	1-Tetradecanol		x	x	x	Aliphatic alcohol
22.01	1-Heptadecene		x	x	x	Aliphatic alkene
23.73	Tetradecanoic acid	x	x	x	x	Aliphatic alcohol
24.17	1-Hexadecanol	x	x	x	x	Aliphatic alcohol
27.83	Hexadecenoic acid	x	x	x	x	Fatty acid
28.31	Hecadecanoic acid	x	x	x	x	Fatty acid
30.50	Octadecen-1-ol	x	x	x	x	Aliphatic alcohol
26.88	1-Octadecanol	x	x	x	x	Aliphatic alcohol
32.39	Octadecenoic acid	x	x	x	x	Fatty acid
32.82	Octadecanoic acid	x	x	x	x	Fatty acid
28.12	Hexadecanamide	x	x	x	x	Fatty acid amide
28.51	Hexadecanamide, N-methyl	x	x	x	x	Fatty acid amide
29.03	Hexadecanamide, N-ethyl	x	x	x	x	Fatty acid amide
37.11	Octadecenamide	x	x	x	x	Fatty acid amide
37.92	Octadecenamide, N-methyl	x	x	x	x	Fatty acid amide
38.77	Octadecenamide, N-ethyl	x	x	x	x	Fatty acid amide
47.41	Cholest-3-ene, (5.alpha.)-	x	x	x	x	Sterol
48.19	Cholest-2-ene, (5.alpha.)-	x	x	x	x	Sterol
48.64	Cholest-4-ene	x	x	x	x	Sterol
49.05	Cholest-5-ene	x	x	x	x	Sterol

As GC techniques are usually limited by vaporization temperature, ^{1}H NMR was applied to have a better understanding of the complementary functional group distribution in the biocrude. The NMR-spectra and results of the semi-quantitative analysis are summarized in Figure 30. The region in 1.5–0.5 ppm represents aliphatic methyl- and methylene protons. The two most prominent peaks are located at 0.87 ppm (methyl, $-CH_3$) and at 1.25 ppm (methylene $-CH_2-$) protons in alkyl chains [276]. These protons sum up in DW-HTL to 57.2% and in SA- and

CA-HTL samples to 58.6% and 59.7%, respectively. MSS-HTL sample exhibited the lowest alkane functionality with 52.1%. These results were attributed to the high lipid content in the feedstock. Occurring shifts in the region 3.0–1.5 ppm are related to protons in β-position (1.5–1.8 ppm) and α-position (1.9–3.0 ppm) in N- and O-containing functional groups like linear or branched amides and non-aromatic heterocyclic compounds [303]. MSS-HTL shows with 31.4% the highest contribution of protons, which verifies the higher nitrogen content in the biocrude. The results are in good agreement with the GC-MS qualification. The distinguished peak at 3.6 ppm in the region 4.5–3.0 ppm is due to methoxy groups [304]. SA-HTL shows the lowest contribution of protons, which is unexpected as this sample shows plenty of methoxy phenolic compounds by GC-MS. Protons in the hydroxyl group of phenols are represented at 5.4 ppm, together with olefinic bound protons with a triplet at 5.0–4.9 ppm as found in unsaturated fatty acids they are summed up in the region of 6.0–4.5 ppm. No significant differences can be observed among the different biocrude. In the region of 9.0–6.0 ppm, the aromatic and heteroaromatic functionalities were observed in all biocrude samples. This is again in agreement with the by GC-MS detected indoles.

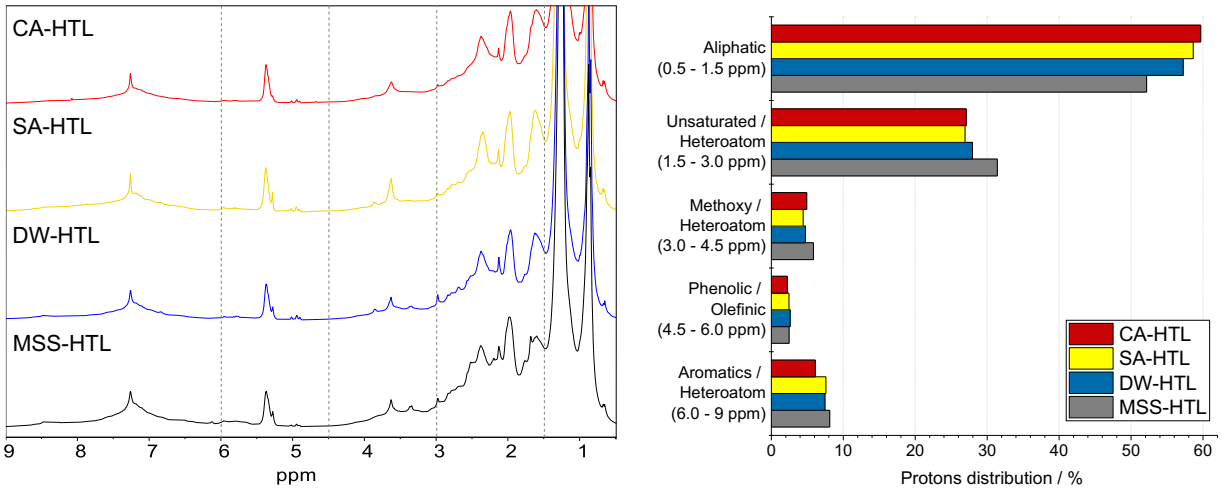

Figure 30. ^{1}H NMR spectra and spectral distribution of functional groups present in biocrude based on integrated peak areas assigned to characteristic spectral regions.

4.4 Conclusions

Municipal sewage sludge, was pre-treated hydrothermally with three different agents namely de-ionized water, sulfuric acid, and citric acid at set reaction conditions. In a subsequent stage, the residual solids were converted to biocrude via HTL and compared to the direct HTL derived product. By applying detailed multi-method characterization of the solids derived from pre-treatment and products from HTL the following conclusions can be drawn:

(1) Bulk analysis of the products from pre-treatment shows a reduction in nitrogen due to solubilization of proteins in the aqueous supernatant, while crude lipids are retained. With the addition of an acidic agent, the solubilization of nitrogen is enhanced.

(2) The yield of hydrothermal liquefaction can be increased due to the hydrothermal acid pre-treatment, under significant concomitant solubilization of organic matter in the pre-treatment. This is reflected in the overall yield after the combined process. An in-depth discussion on potential valorization or recovery of the solubilized organics of the pre-treatment is out of scope of this study, but will be an issue of further studies.

(3) Biocrude quality was increased due to a pre-treatment as the N-heteroatom content is reduced, H/C_{eff} ratio is increased. Furthermore, long-chain aliphatic structures are accumulated and N-heteroatoms are primarily in the form of fatty acid amides. Directly, hydrothermal liquefied sewage sludge suffers from N-heteroatoms bound in a cyclic or even aromatic structure which can affect further upgrading strategies.

This stated process could potentially increase biocrude quality and take usage of existing anaerobic digestion facilities at the wastewater treatment plant.

Chapter 5.

Extraction of nitrogen compounds of sewage sludge biocrude

This chapter is based on the publication

Sequential Extraction and Characterization of Nitrogen Compounds after Hydrothermal Liquefaction of Sewage Sludge

Joscha Zimmermann[a], Stefano Chiaberge[b], Steen B. Iversen[c], Klaus Raffelt[a], Nicolaus Dahmen[a]

[a] Institute of Catalysis Research and Technology, Karlsruhe Institute of Technology, 76344 Eggenstein-Leopoldshafen

[b] Renewable, New Energies and Material Science Research Center Novara, 28100 Novara, Italy

[c] Steeper Energy, Hydrofaction™ Pilot and Test Facility, 9220 Aalborg Øst, Denmark

Publishing details:

Energy and Fuels

Volume: 36; Issue: 23

Published on November 16th, 2022

DOI: 10.1021/ACS.ENERGYFUELS.2C02622

5.1 Introduction

The desired reduction of CO_2 emissions drives society to identify renewable carbon sources for future liquid fuels and chemicals supply. Also, in order to tackle emerging waste management problems, the valorization of the common waste streams has gained global interest [219]. Sewage sludge is a wet waste stream that contains plenty of valuable organics, such as lipids, carbohydrates, proteins, and inorganic material, often precipitated as phosphor salts [159,305]. In northern European countries, sewage sludge is usually incinerated or disposed in landfills [256]. Otherwise sewage sludge is often used in agriculture, but nowadays it is more and more regulated as pharmaceutical and microplastic residues and pathogens are a concern [70,72,80]. The method of thermochemical conversion of sewage sludge into energy, gas, or fuel intermediates includes methods of tackling these issues by pyrolysis, gasification, and combustion. One promising conversion process is the hydrothermal liquefaction (HTL). This process uses the beneficial properties of hot, compressed water at elevated temperatures in the range from 250 to 450 °C and pressures above the saturation pressure of up to 350 bar and can convert moisture-rich wet waste biomass such as sewage sludge to a crude oil-like product, named biocrude [306,307]. During the HTL process, biomass-originated polymers decompose into smaller molecules and even pharmaceutical micropollutants and microplastics are decomposed [308,309].

Due to the often high content of oxygen (18.8–23.5 wt %) and nitrogen (2.5–7.9 wt %) in sewage sludge, the resulting biocrude consists mostly of highly functionalized compounds [66]. Furthermore, the relatively high lipid content (~20 wt %) is suitable for HTL as they are hydrolysed into long-chain fatty acids and other derivates such as fatty alcohols are formed [310,311]. Lignocellulosic material (~15 wt %) results primarily in phenolic compounds, cyclic ketones, and short-chain carbonic acids [312,313]. The high protein content in the sewage sludge (~40 wt %) originates from the microbiological processes during wastewater treatment and leads to the formation of nitrogenated compounds [145,240,314]. Due to the amidation of fatty acids, long-chain amides are formed [130]. Additionally, internal ring closure and

Maillard reactions build up aromatic heterocycles based on pyrrolic or pyridinic ring structures [114].

The direct use of biocrude as a drop-in transportation fuel is limited, as the distillation cut requirements are often not fulfilled due to the high contents of nitrogen and oxygen. Therefore, an extensive upgrading step is required, which would include primarily a catalytic hydrotreating process [315,316]. Because the biocrude contains a large share of nitrogen-functionalized compounds, often bound in an aromatic ring, high hydrogen partial pressure and relatively high reaction temperatures are needed [38]. Double bonds in the aromatic ring need to be saturated and eventually cracked to remove nitrogen, which results in higher hydrogen consumption. Furthermore, it is believed that N-heteroaromatic compounds can form organometallic complexes, likewise as they appear in nature as porphyrin or heme [37,184]. This transfer of inorganic species into the hydrotreating process can lead to irreversible catalyst fouling and plugging [39]. Haider et al. assume that these organometallic compounds led to an increased coke formation [317]. They show often surface-active properties and are assumed to cause the formation of emulsions, which results in difficult product phase separation after the HTL process [173]. Many of the N-compounds derived from the HTL are chemicals of interest to the industry [159]. Numerous research studies have focused on the production of valuable chemical N-compounds derived by the HTL of biomass, agreeing it is a challenge to produce specifically value-added nitrogen-containing compounds, due to the complex composition of the starting biomass [318]. The subsequent separation of N-compounds is therefore of interest, as it happened when the generated biocrude is separated from the aqueous byproducts. Ekpo et al. identified a strong influence of the pH of the aqueous phase on the recovery of nitrogen whereas Chen et al. extracted emulsified N-compound in water [319,320]. Fonts et al. recovered a comparable bio-oil derived by pyrolysis of sewage sludge-added compounds by applying organic and inorganic solvents for fractionation [199]. Nevertheless, to effectively evaluate HTL-biocrude as a potential source of drop-in fuels and to

design an appropriate downstream upgrading process, a full characterization of the biocrude-containing compounds is needed.

For the characterization of biocrude composition, commonly gas chromatography (GC) coupled with mass spectrometry (MS) is used. GC is limited to volatile compounds with lower molecular weight and the conventional MS systems are not able to resolve and identify hundreds of components found in a single analyte as they lack sufficient resolution and mass accuracy [185]. This makes the use of pre-chromatographic separation necessary, reducing the complexity of the product composition. Bio-oils derived from biomass pyrolysis or HTL contain large quantities of polar substances, which would make the results non-comparable. Therefore, specified methods and the use of modified solvent systems are applied [321–323]. Aqueous solutions at different pH values were used in several studies to separate organic compounds by different polarity. Boocock et al. separated oxygen-rich HTL oil derived from aspen wood, whereas Dote et al. and Das et al. applied this acid–base separation method on bio-oil derived from nitrogen-rich biomass feedstocks [197,198,324]. New, advanced analytical systems try to unravel the complexity of the biocrude composition with high mass resolving power and mass accuracy, as provided by Fourier transform ion cyclotron resonance MS (FTICR MS) or other high-resolution MS systems.

This work aims to separate N-compounds from the complex HTL-biocrude matrix, produced from sewage sludge in a state-of-the-art continuous pilot process. In a first step, the biocrude is separated sequentially into four fractions by applying two alkaline and one acidic aqueous solutions. The mass balances and the recovery of carbon and nitrogen are carefully determined. In the following step, the chemical composition of the fractions is analysed by conventional GC–MS and the most abundant N-compounds are identified. With a focus on N-heteroatom classes, their distribution and the double bond equivalent (DBE) were determined by FTICR MS and discussed with preceding results, providing information on functionalization, aromaticity, and structure. That way, the fate of specific N-compounds after treatment with aqueous polar solutions can be determined. Furthermore, a qualitative statement can be given

to plan for further downstream processing and the potential to recover or remove the process valuable and harming organic components, respectively.

5.2 Material and methods

All chemicals used for the experiments were obtained of analytical grade and obtained from Merck (MilliporeSigma).

5.2.1 Biocrude production

The HTL-biocrude sample used in this study was produced at the Pilot and Test Facility in Aalborg, DK. The production campaign in 2019, processed 500 kg of sewage-containing slurry, within the NextGenRoadFuel-Horizon2020 project, which aims to develop an effective technology pathway to valorize the combination of sewage sludge, food waste, and construction wood residues as sustainable drop-in fuels. For this purpose, non-digested sewage sludge in dewatered form (24.9 wt % dry matter) was collected from a wastewater treatment plant located in Farsø, Denmark. A pumpable slurry containing 21 wt % sewage sludge (dry matter), 2.5 wt % sodium hydroxide, and 2.5 wt % potassium carbonate was prepared by mixing the ingredients and diluting them with distilled water to the given concentrations. The slurry was processed at a flow rate of around 30 kg/h and converted at 400 °C and 320 bar above the critical point of water. A mixed emulsion-like liquid product consisting of aqueous, oil, and solid phases was degassed at 60–80 °C and slight overpressure and collected for this study. The collected sample was kept in a 1 L borosilicate bottle and stored in the fridge and subsequent experiments were conducted in early 2020.

5.2.2 Extraction of oil from HTL product

The as-received HTL product must be separated into an organic biocrude, aqueous, and solid phases. Afterward, the proposed sequential extraction methodology could be applied to the

biocrude phase. In a first step, 50 g of HTL product emulsion was separated into aqueous and organic/solid phases by centrifugation at 7000 rpm (Eppendorf EP 5430). The received aqueous supernatant was discharged whereas the precipitate was mixed with 40 mL dichloromethane (DCM), vortexed for 2 min and subsequently centrifuged again with 7000 rpm. The DCM supernatant was filtered through a 0.45 µm nylon filter (GE Whatman) and evaporated overnight under a gentle nitrogen stream.

5.2.3 Sequential extraction

The extraction procedure to separate polar compounds follows a modified procedure, proposed by Boocock et al. [324]. Following a sequential extraction with aqueous solutions of sodium bicarbonate ($NaHCO_3$), sodium hydroxide (NaOH), and hydrochloric acid (HCl). The aqueous extracts were re-extracted with DCM after titration of the aqueous solution to a contrary acidic or alkaline pH. Dissociated organic compounds that are soluble in polar solutions before would be protonated or de-protonated into their non-polar form. An appropriate non-polar solvent could re-extract these compounds. This procedure results in four fractions, fraction F1 and fraction F2 recovered from alkaline agents, fraction F3 recovered from an acidic agent, and the residual fraction F4.

In detail, 5 g of biocrude was mixed in 100 mL DCM and transferred to a separatory funnel filled up with 50 mL of a 0.5 $mol \cdot L^{-1}$ solution of $NaHCO_3$. The mixture was shaken vigorously for 5 min and was allowed 1 h for phase separation. The bottom DCM phase was transferred to a fresh separatory funnel, including the emulsion layer (see Supporting Information, S 11) at the phase boundary. The aqueous supernatant was collected in a beaker and the funnel was washed with 2 mL of DCM, which was added to the second funnel. This procedure was repeated two times with 25 mL of the $NaHCO_3$ solution and two times with 25 mL of deionized water. All aqueous samples were combined in one 400 mL beaker. Next, the DCM phase was extracted by a similar procedure with 0.5 $mol \cdot L^{-1}$ NaOH and with 0.5 $mol \cdot L^{-1}$ HCl, including the same deionized water washing steps. The two collected aqueous alkaline solutions were

titrated with 10 mol·L^{-1} HCl solution to a pH of below 4, and the aqueous acidic solution with 10 mol·L^{-1} NaOH to a pH above 9. Then, each combined solution was transferred from the beaker again to a separatory funnel. Beakers were washed with small amounts of DCM to add precipitated organics to the funnel. The three solutions were re-extracted with the same procedure as described above with 50 mL and two times with 25 mL of DCM. Each extract was filtered through a 0.45 µm nylon filter to remove suspended solids. To yield a solvent-free biocrude, DCM was evaporated under a gentle nitrogen stream overnight.

5.2.4 Characterization of organic fractions

The carbon (C), hydrogen (H), nitrogen (N), and sulfur (S) contents of the biocrude samples, as well as solid products, were analysed using a CHNS analyser (Vario EL cube, Elementar Analysentechnik GmbH, Hanau, Germany). The oxygen (O) content was determined subsequently by difference.

The extracts were analysed by a gas chromatograph (Agilent 6890N, Santa Clara, CA, USA) coupled with a mass spectrometric detector (MSD, Agilent 5973N, Santa Clara, CA, USA) on a Rxi-5MS column with a 30 m × 0.32 mm diameter and a film thickness of 0.25 µm (Restek Corporation, Bellefonte, PA, USA). About 10 mg of samples were prepared in 0.5 mL of chloroform, 0.5 µL of which were injected at 280 °C in 1:20 split mode, using helium as the carrier gas (1.5 mL·min^{-1}). The GC oven program started at 70 °C which was held for 2 min and progressed at 8 °C·min^{-1} to 180 °C and at 4 °C·min^{-1} to 280 °C, followed by a holding time of 15 min. The MSD was operated in 70 eV EI mode with a source temperature of 230 °C and a solvent delay of 4.8 min, followed by scanning from 35 to 500 m/z with a frequency of 3.9 scans per second.

Biocrude and recovered fractions, F1 to F4, were analysed by atmospheric pressure chemical ionization (APCI) in positive ion mode (+) by using a 7 T FTICR (LTQ-FT Ultra Thermo Scientific) MS analyser. These samples were diluted in $CHCl_3$/acetonitrile 1:1 and infused at a

flow rate of 100 μL·min^{-1} by a syringe pump into the APCI ion source. The final concentration of the solution in the APCI ion source was around 0.4–0.6 mg·mL^{-1}; typical APCI (+) conditions were as follows: source heater, 380 °C; source voltage, 5 kV; capillary voltage, 7 V; tube lens voltage, 60 V; capillary temperature at 275 °C; sheath gas, 60 arbitrary units; and auxiliary gas, 10 arbitrary units. The mass spectra were acquired in positive mode with a mass range of m/z 100–1000. The resolution was set to 200,000 (at m/z 400). 360 scans were acquired for each analysis to improve the signal-to-noise ratio using the Booster Elite system (Spectroswiss, Lausanne, Switzerland), which allowed to register directly the transient data. Transients were then processed by Peak-by-Peak-Petroleomic software (Spectroswiss, Lausanne, Switzerland). The 360 transients were first averaged and then FT was applied to obtain a single averaged mass spectrum. The resulting spectrum was further processed to remove the noise (thresholding set to 6 Sigma of the background noise) and internally recalibrated through the unwrapping method [325].

5.2.5 Data analysis and visualization

Data generated by GC–MS were analysed with Agilent's MassHunter quantitative analysis software (unknown analysis) v.10.1 (Agilent, Santa Clara, CA, USA). The compounds were identified by Agilent's deconvolution algorithm and the NIST 2017 library, proposed compounds with a score above 80 were considered as a match. If multiple compounds fulfilled this score, as it often occurred specifically for long-chain aliphatics, the decision was based on chain length, retention time, and alignment with our in-house database. The relative peak area of an identified compound was based on the total-ion-current chromatogram, provided by the software.

The FTICR MS generated data were analysed with Peak-by-Peak-Petroleomic software. Around 6000–8000 different peaks were obtained in each single mass spectrum. The composition constraints used for the composing function were C: 7–80, H: 12–150, N: 0–4; O: 0–4; 13C 0–1. The final attribution of these peaks was obtained using the composing function

of Peak-by-Peak with the error limit of ±2 ppm. The software allows internal recalibration of the mass spectra (using known compounds or internal standards), reducing remarkably the associated errors of less than 1 ppm. The classes were determined through the spectral slice function. An example is attached for the class O1N1 with a wide tolerance of ±500 ppm as shown in Supporting Information, S 16, showing the different slices related to different classes and with the set limit of ±2 ppm used in our approach.

Considering the composition constraints and the statistical distribution of ions in each class (Gaussian-like distributions similar to those found for crude oil samples), the multiple matches for a single ion can occur only at high m/z values (the slice distributions widen over m/z 500). At such high values of m/z, the ion intensities were found to be lower; therefore, we believe that the risk of wrong assignment would not impact the overall characterization of the sample.

The molecular formulas were categorized according to different parameters, such as the number of heteroatoms (N, O, and S) and the degree of saturation expressed as DBE. DBE values were calculated based on the molecular formula $C_cH_hN_nO_oS_s$, according to the following equation:

$$\mathrm{DBE} = c + 1 - \frac{h}{2} + \frac{n}{2} \qquad (9)$$

Specific classes of species were determined according to the heteroatoms present, and their relative abundances were used for deriving class distribution plots. The most abundant classes were then visualized in DBE versus carbon number (Cn) plots according to their carbon number, DBE value, and relative abundance in the mass spectrum using a color code.

The predicted empirical formulas were searched within the ChemSpider database to identify possible structures [326]. The proposed structures from the database were compared with compounds identified by previous GC–MS analysis or checked with the literature on HTL-biocrude analysis.

For data processing and plotting the Python libraries, NumPy, Pandas, and Matplotlib were used. Principal component analysis (PCA) was performed with the scikit-learn package within Python. The sums of relative abundances for each heteroatomic class were scaled and used as input variables for PCA. Chemical structures were drawn with ChemDraw Professional 10.1 (PerkinElmer, MA, USA).

5.3 Results and discussion

5.3.1 Elemental analysis of HTL-biocrude extracts and corresponding yields

The elemental composition of the biocrude and the received extracts, F1, F2, F3, and F4, based on dry basis, as well the H/C- and N/C-ratios and extraction yields is compiled in Table 11. The elemental composition of the biocrude is in agreement with products obtained from continuous HTL of sewage sludge, referred by Jarvis et al. and Haider et al. [45,185]. To compare the samples with petroleum, the average elemental composition provided by Speight is added to the table [187]. It is visible that biocrude and the extracted fractions show a lower C- and H-content, than the referenced petroleum. Furthermore, all fractions show also lower C-contents than the biocrude. This could be related to the precipitation of not-analysed, surface-active carbonaceous material during the extraction procedure, which is shown in Supporting Information, S 11. Petroleum crude is usually characterized by a low heteroatom N- and O-content, which differs largely from the biocrude and extracted samples. The N-content is slightly lower than that in the original fractions 1, 2, and 4, with no significant effect. Otherwise, F3 shows a substantially higher value. Contrary to the N-content, the O-content is lower in F3.

Table 11. Biocrude and extract yields and composition. The number in parenthesis shows the standard deviation of the mean.

	Dimension	Biocrude	Fraction 1	Fraction 2	Fraction 3	Fraction 4	Petroleum [187]
C	wt. %	76.0	74.7 (1.0)	74.0 (0.7)	73.8 (0.4)	75.8 (0.1)	83 – 87
H	wt. %	11.0	11.0 (0.7)	11.4 (0.9)	9.2 (0.2)	11.7 (0.0)	10 – 14
N	wt. %	3.8	3.0 (0.4)	1.9 (0.3)	9.5 (0.5)	3.5 (0.3)	0.1 – 2
S	wt. %	1.0	0.8 (0.1)	0.7 (0.3)	0.7 (0.2)	0.7 (0.0)	0.05 – 6
O [a]	wt. %	8.2	10.4 (1.8)	12.1 (1.2)	6.8 (0.4)	8.4 (0.3)	0.05 – 1.5
H/C	mol H/ mol C	1.74	1.77	1.84	1.49	1.86	1.38 – 2.02
N/C	mol N/ mol C	0.04	0.03	0.02	0.11	0.04	0.00 – 0.02
Extraction yield [b]	wt. %	-	11.0 (0.9)	13.6 (1.3)	5.2 (0.9)	54.3 (3.2)	-

[a] is calculated by difference; [b] based on the biocrude extract

Analysing the H/C-ratios and comparing the original biocrude with its extracts and petroleum, it can be noted that F2 and F4 show increased values close to the higher range petroleum ratios. This is a strong indication of an accumulation of aliphatic structures with O- or N-functionalization. F3 shows a relatively low H/C-ratio, close to a bituminous fraction [187].

Concerning the C- and N-recoveries as shown in Figure 31, an accumulated recovery of 83.2 ± 6.2% of C and 77.7 ± 9.5% of N could be archived. Most C and N are recovered in F4. For the ratio between N- and C-recovery, F3 shows by far the highest value with about 2.56, whereas F1 and F4 do not differ significantly with values of 0.8 and 0.91, respectively, and F2 shows the lowest ratio with 0.51.

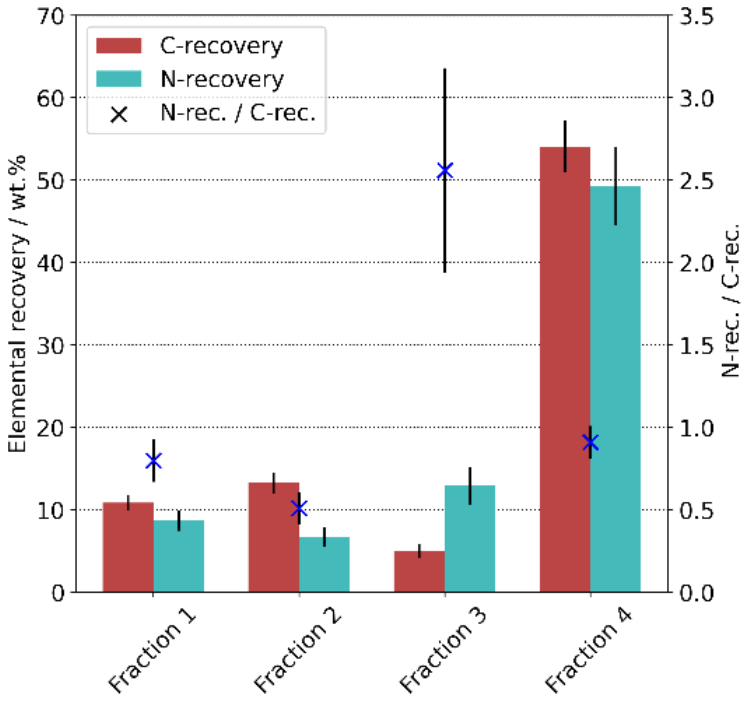

Figure 31. Elemental recovery and ratio of biocrude extracts

5.3.2 Gas chromatography–mass spectrometry

The identification of volatile compounds in the extracted fractions was carried out by GC–MS. The 20 most abundant peaks and their resulting compounds are classified by their functionalization into six groups and the relative peak areas of the total-ion-current chromatogram of each identified compound are summed up. The occurrence of these groups in the biocrude and the different fractions is shown in Figure 32. The related chromatograms of each fraction are shown in Supporting Information, S 12 and the identified compounds are listed in Supporting Information, S 13.

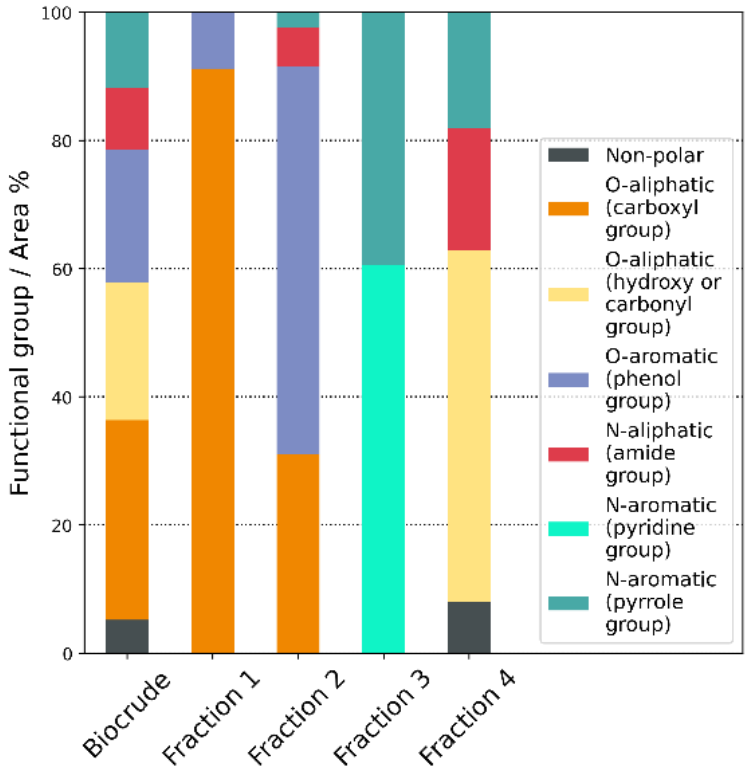

Figure 32. GC-MS results of the most abundant compounds in the extracted fractions (F1 to F4) given in area percentage

Within the biocrude, non-polar compounds with different O- and N- functionalizations are identified, which accumulated in the following extracted fractions F1, F2, F3, and residual F4. The main compounds identified in F1 are O-containing aliphatic structures functionalized by a carboxyl group such as fatty acids. The relative area of this compound group amounts to 91.2% of the identified signals. In addition, a small proportion of 8.8% of the identified compounds are O-containing aromatics such as phenols, possibly branched with methyl groups. Both, carboxyl and phenol groups are found as well in F2 with a relative area of 31 and 60.1%, respectively. A small share of the peaks can be allocated to N-functionalized groups with aliphatic compounds such as amides and with aromatic compounds with a pyrrole group such as indole derivates. All of the identified compounds in F3 contain N-heteroaromatic structures consisting of either pyridine or a pyrrole functional group with a relative peak area share of 60.5, and 39.5%, respectively. It should be noted that the pyrrole functional groups may also contain a pyridine group, for example, in the form of pyridoindoles. Compounds

containing pyridine-functionalized compounds were exclusively found in F3 by GC–MS analysis. The residual fraction F4 shows a large share of 54.8% of the relative peak area of identified compounds which are related to aliphatic compounds with hydroxyl or carbonyl groups. The most dominant compounds here are fatty acid alcohols as well as sterol derivates. An additional 19.2 and 17.9% of the identified compounds account for aliphatic amides (fatty acid amides) and heteroaromatic pyrrole (indoles) groups. Non-polar compounds found in this fraction reach a share of 8.1%.

Although a large variety of compounds were identified by GC–MS, the poor resolution of peaks does not allow the determination of organic compounds present in lower abundances. This does occur especially for N-heteroaromatic compounds, as these are present in a wide variety of different derivates. Additionally, the compounds of higher molecular weight and larger polarity are eluted slowly from the GC column, resulting in an even lower resolution. For this reason, a high-resolution MS technique was applied.

5.3.3 Fourier transform ion cyclotron resonance mass spectrometry

To get an even more detailed characterization of N-containing species in the three fractions obtained from extraction, a Petroleomic approach was employed. Common soft ionization techniques such as APPI, electrospray ionization, and APCI in positive ion mode are especially suitable for proton-accepting functionalized groups such as amines or pyridines. As N-heteroaromatic species also appear in pyrrolic forms (pyrrole, indole, and carbazole derivates), which are not strong proton acceptors, therefore, APCI seems to be the most suitable ionization technique and was applied in this study too [327,328]. Negative ion modes are suitable for hydrogen-donating compounds as they are primarily found in O-heteroatom-containing substances. Phenols are an example of this and are assumed to be largely underestimated with the ion source conditions employed, as they are not effectively ionized [328]. Therefore, in the following section, the discussion on the O-functionalized group is a more qualitative one.

5.3.4 Heteroatom class distribution

The heteroatom class distribution determined from positive APCI mode FTICR MS of the four extracted fractions is shown in Figure 33. The results can be divided into 14 classes, denoted by the number of N- and O-atoms in a given compound (N1, N2, N3, O1, O1N1, O1N2, O1N3, O2, O2N1, O2N2, O3, O3N1, O3N2, and O4). It needs to be noted that the results are given in relative abundances in each class. Thus, no information on absolute content is provided.

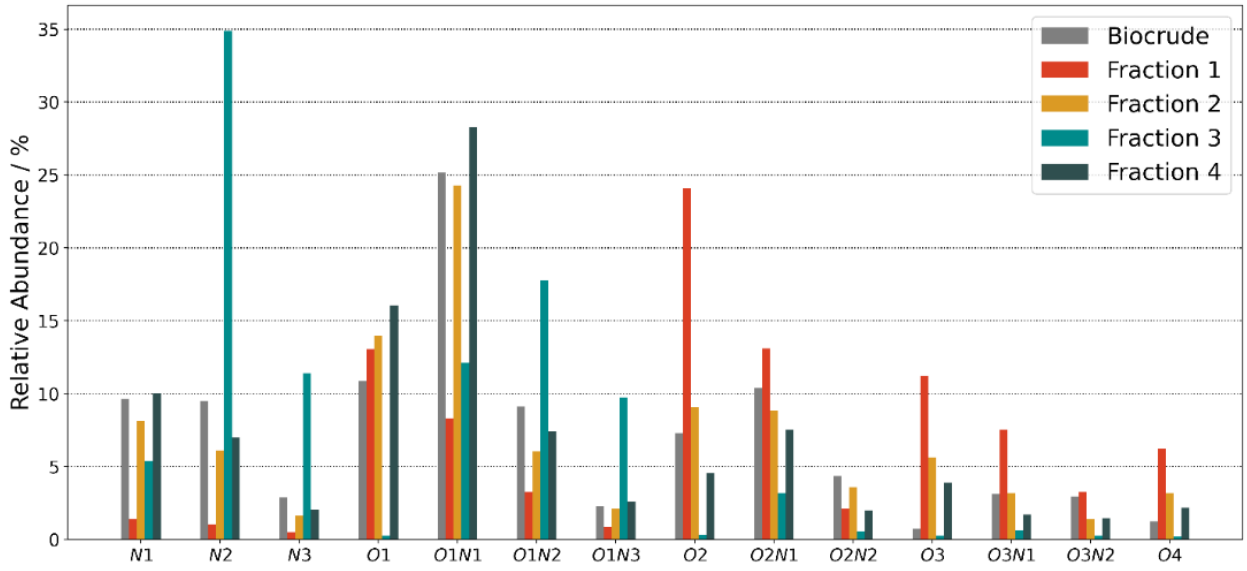

Figure 33. Heteroatom distribution (molar heteroatom content) of selected classes in the biocrude and extracted fractions F1-4

In F1, high abundances of oxygenated species can be identified in graduating order of O2 (24.1%), O2N1 (13.0%), and O1 (13.1%). The three most abundant classes in F2 are oxygenated as well, namely O1N1 (24.3%), O1 (14.0%), and O2 (9.1%). The third fraction F3 shows high abundances for classes containing predominantly multiple nitrogen atoms such as N2 (34.9%), O1N2 (17.8%), and N3 (12.1%). The residual fraction F4 is nearly identical in heteroatom distribution to F2, in the order of the class O1N1 (28.3%), O1 (16.1%), and N1 (10.0%) as the most abundant ones.

To identify relations and differences between the extracted fractions based on the abundance of heteroatomic classes, an explorative PCA was applied. PCA is used for exploratory data analysis, reducing the 14 input variables of the relative abundances for each heteroatomic class into principal components. The two principal components (PC1 and PC2) are able to describe 92.5% of the total explainable variance. The score plot of PC1 versus PC2 is shown in Figure 34 (A). PC1 accounts for a variance of 66.5% and shows large differences between alkaline extracted F1 (PC1 value of –4.2) and the acid extracted F3 (PC1 value of 5.3). F2 has a negative PC1 value of –0.9 and shows proximity to F4 with a value of 0.1. The starting material biocrude shows a PC1 value of –0.2. To identify the orientation of specific classes, the loadings, responsible for PC1 and PC2, are analysed and plotted in Figure 34 (B). PC1 is strongly moved into a negative value by oxygenated classes on the left, namely O2–4, O2N1, and O3N1–2. Multi-nitrogenated classes such as N2–3 and O1N2–3 are orientated on the right and affect PC1 to positive values. This match the presence of O-functionalized groups such as carboxylic acids from previous GC–MS analysis. This suggests that the donation of protons governs the trend of PC1 to the left. Contrary to the acceptance of a proton, the basic character of N in the form of pyridine and amine compounds governs the trend along PC1 to the right. This is again in agreement with the previous GC–MS results of F3. The classes N1, O1N1, O1, and O2N2 are orientated close to the center along PC1 and can be considered to be less affected by acids and bases. Matching compounds to these four classes were again found by GC–MS, predominantly in F2 and F4. Furthermore, these classes are responsible for negative PC2 values, whereas multi-heteroatom classes with a higher degree of functionalization weigh PC2 into positive values. F1 and F3 show positive PC2 values of 2.7 and 1.9, respectively. Biocrude, F2, and F4 have negative values of –1.8, –1.1, and –1.72, respectively. It can be observed that these three fractions are clustering, indicating small differences in terms of their heteroatom class distribution.

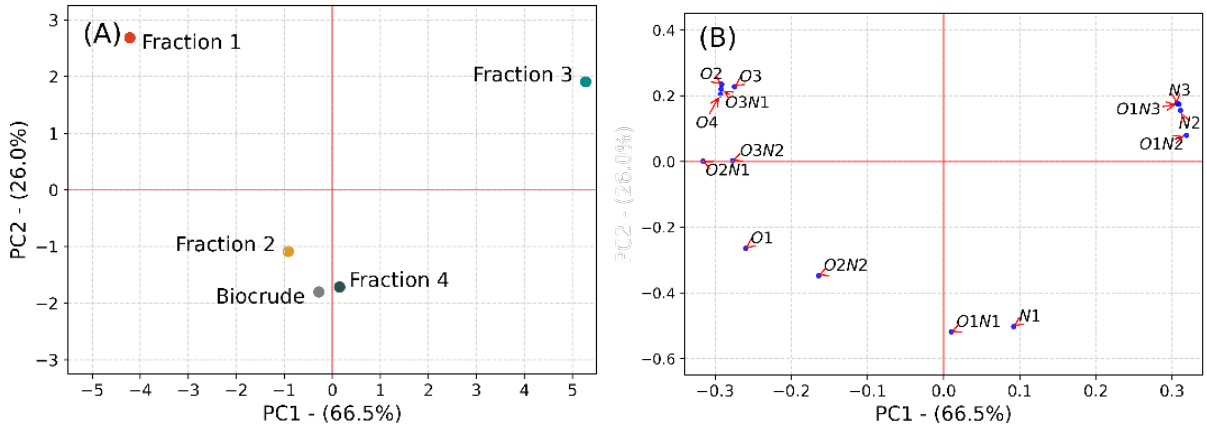

Figure 34. (A) Scoring plot and **(B)** loadings plot from the principal component analysis (PCA) of the relative abundances of heteroatom classes in the biocrude and extracted fractions F1-4.

5.3.5 Compositional space of specific heteroatom classes

The composition of the most abundant N-containing classes found in the extracted fractions is explored in relative intensity scatter plots of Cn versus DBE. These plots are class-specific and give additional information about the primary compounds present in each fraction. With the information of the Cn and DBE values, the base structure of a species can be determined. Lower DBE values between 1 and 3 suggest the presence of aliphatics, whereas higher values above 4, especially with low Cn, are probably related to condensed, aromatic structures. In addition, Cn provides information about the degree of alkylation of a certain species. A higher Cn suggests the alkylation of the base structure with longer or multiple alkyl chains. In addition, the dominant O-containing classes O1 and O2 are shown for qualitative purposes in the Supporting Information S 14. In the following, the DBE versus Cn plots for different classes of substances are presented and discussed.

Nx-Classes

The classes functionalized exclusively with nitrogen, N1 and N2, are shown within their relative intensity scatter plots in Figure 35. The molecular structures of the discussed substances are depicted in Figure 36.

The N1 class in the biocrude shows a relative abundance of 9.6% including 216 species. F1 shows a low relative abundance with 1.4%, including 119 species with the highest intensity are identified with a DBE of 4 and a Cn of 10. Suggested structures are depicted in Figure 36. As a certain acidity is expected from compounds in this fraction, it is suggested, that these species are related to tetrahydro-indole structures instead of pyridines. Similar compounds are found within the species of the N1 class in F2 and F4, but with a much lower intensity. For both these fractions, this class represents 8.0 and 8.4% of all 266 and 297 identified species, respectively. In addition, both fractions show high intensities within an area between a DBE of 6–10 and a Cn of 10–16, suggesting alkylated N-heteroaromatic structures [327]. In F2, the highest intensities are identified at a DBE of 6 and 9 and a Cn of 10–13. Different indole and carbazole derivates were identified by GC–MS and have a corresponding DBE, suggesting the presence of more such compounds in this fraction, with more or higher alkyl chains. In F4, the highest intensities seem to concentrate at a DBE of 7 and 8 and a Cn of 13–14. These values hint at tetrahydro-carbazol and dihydro-carbazole compounds. Due to the overall higher Cn in F3, a higher alkylation than in F2 can be assumed. Long-chain aliphatic species are found with relatively low intensity at a DBE of 2 and a Cn between 16 and 18, in the form of nitriles. These compounds are formed by amidation and subsequent dehydration of fatty acids [128]. Considering the orientation along PC1 in the previous PCA, N1 species in F2 and F4 tend to show light acidic/non-polar characteristics which applies to the before described structures [329]. The relative abundance of the N1 class of F3 is given with 5.4% comprising 105 species and is therefore relatively low considering the fact that this fraction contains the highest N-content of all fractions. The highest intensities within this class are located at a DBE of 5 and 8 and a Cn of 10–12. The orientation of PC1 suggests the appearance of basic N-compounds, which can accept protons. The identified compounds by GC–MS, referring to such DBE values are derivates of tetrahydro-quinoline and phenyl-pyridine. More such compounds are suggested in this fraction with a higher degree of alkylation. The basicity of N in these compounds was analysed and described in comparable extracts with similar species by Zaki et

al. and Cao et al. on N-rich HTL-biocrude from spirulina and pyrolysis oil from sewage sludge [321,330]. As the compositional space of F3 is starting from a DBE value of 4, it is suggested that no alkaline primary or secondary amines are present in sewage sludge biocrude. Within the N1 class, notable differences between the biocrude and F4 within the compositional space are missing. The relative abundance is slightly increasing, and the identified species are more or less in the same range. This is in line with the observations made by PCA, where a clustering of these two fractions is observed. The N2 class within the biocrude is showing a relative abundance of 9.5% over a 290 species. Within F1, an even lower relative abundance of 1.0% over 108 compounds is given. The highest intensities are found at a DBE of 6 and a Cn of 11–13.

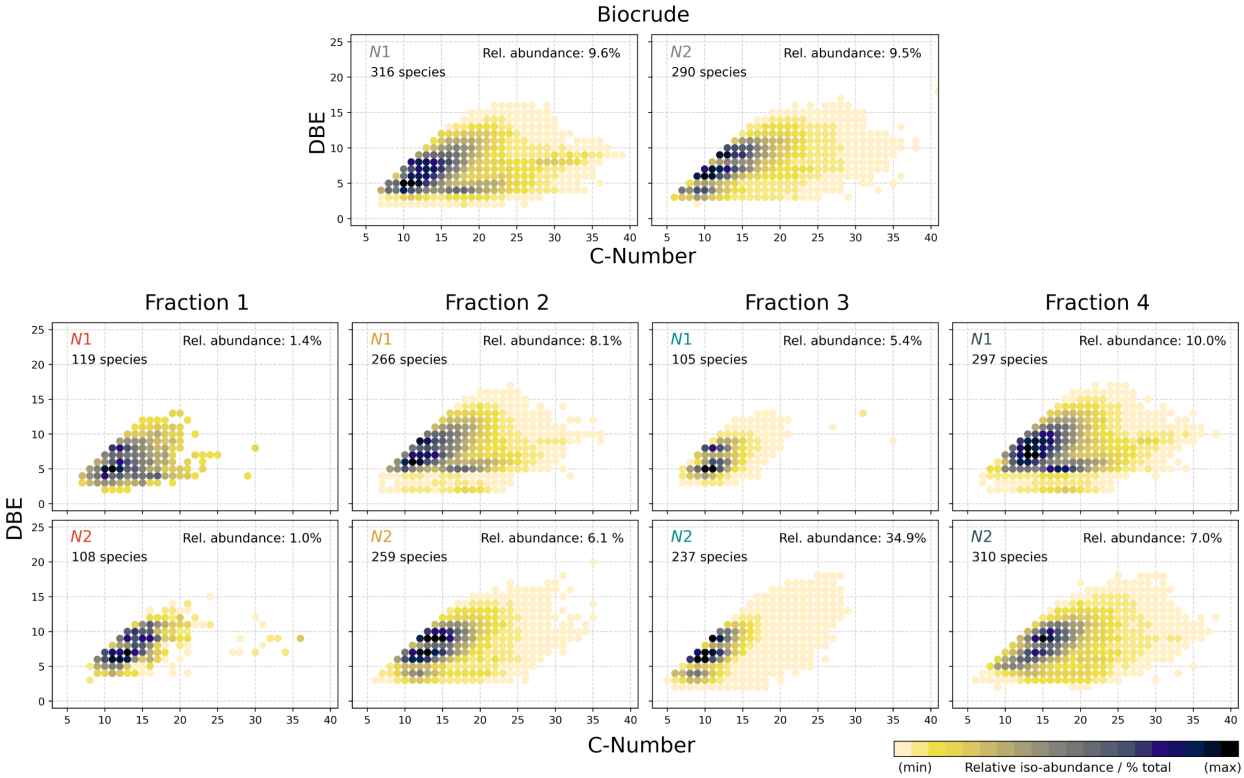

Figure 35. Relative intensity scatter plots of Cn vs DBE distribution of the class N1, N2 of the extracted fractions.

Similar species showed high intensities in F2 and F3. Other than the N1 class, F2 and F3 show comparable compositional spaces within their relative intensity scatter plots. The N2 class shows in F2 a relative abundance of 6.1% over a range of 259 species. In F3, this class shows an

extraordinary high relative abundance of 34.4%, covered by 237 species. In both of these fractions, the highest intensities are located at a DBE of 6, 7, 9, and 10. In F2, the Cn of these species are 11–15, whereas in F3 the Cn is lower with a value between 9 and 11. These species are suggested to refer to benzimidazole or azaindole derivates at a DBE of 6 or also in combination with an added benzene ring, carbazoline derivates at a DBE of 9 are also identified by GC–MS analysis [329]. The appearance of these compounds in F2, F3, and even in small amounts in F1, can be explained by the amphoteric character able to act as weak acids and bases [331]. Furthermore, strong basic species are suggested to be present in F3, such as bipyridines, naphthyridine, and quinazoline, with a degree of aliphatic alkylation and addition of benzene rings. The relative abundance of the N_2 class in F4 with about 7% is spread over a wide range of 311 species, again located in the aromatic area with a DBE of 6–9 and a Cn of 13–16. The extensive variation in Cn for any given DBE value and the high count of detected species with 311, indicates a large degree of alkylation, which is related to the low polarity of this fraction.

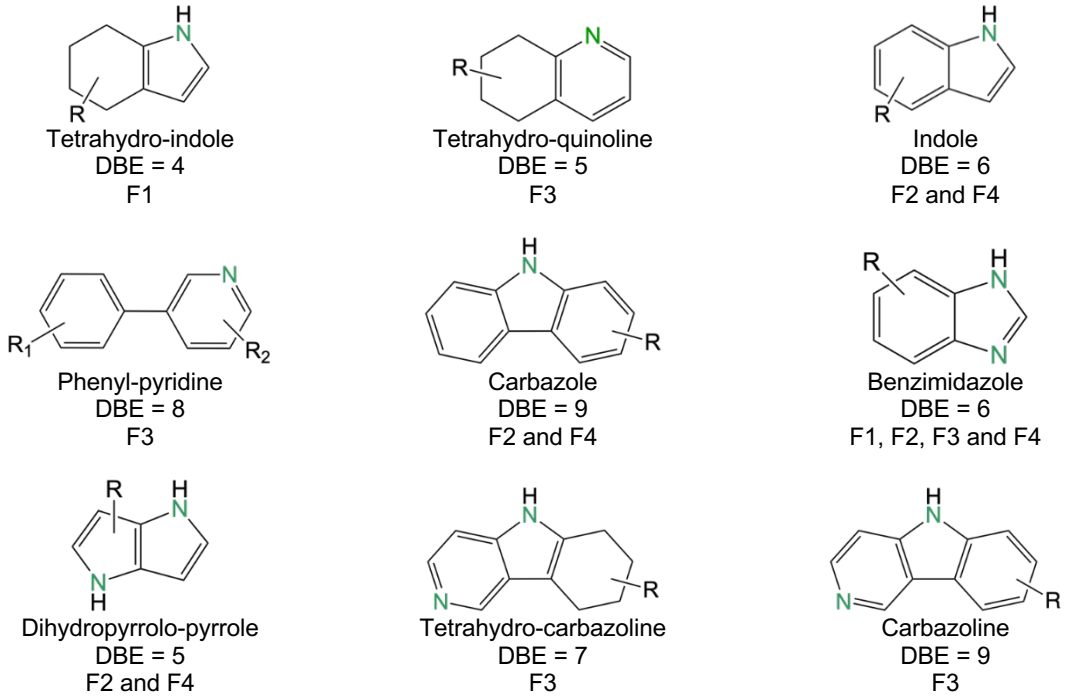

Figure 36. Suggested N1 and N2 species within the extracted fractions.

These compounds can be related to carbazole derivates and species that could be based on the structures of benzopyrazines and dihydropyrrolo-pyrroles, which are common Maillard reaction products or possible melanoid fragments [332,333]. Within the N2 class, the relative abundance is decreasing from the biocrude to F4, which can be referred to the string accumulation of such species in F3. The previously described structures of the N1 and N2 class are schematized in Figure 36. The abbreviation "R" within the chemical structure is representing different alkyl chain residues. In addition, the DBE value and the suggested fraction are highlighted.

O*x*N*x*-Classes

The relative intensity scatter plots of classes functionalized with N and O, namely O1N1, O1N2, and O2N1 are shown in Figure 37. The molecular structures of the discussed substances are depicted in Figure 38.

The O1N1 class shows a relative abundance of F1 of 8.3% with a range of 309 species. The highest intensity is located at a DBE of 2 and a Cn of 16, which can be related to C16 fatty acid amide. Further, the abundances at a DBE of 8 and a Cn of 12 and 13 stand out. These species are suggested to be composed of short-chain aliphatic amides, connected to a naphthalene structure, as latter is able to donate a proton. F2 and F4 show similarities within their compositional space. The relative abundances of this O1N1 class are given in both fractions with high values of 24.3 and 28.3% with a large variety of 350 and 373 species, respectively. The highest intensities are located in the aliphatic area with a DBE of 1 and 2 at Cn values between 16 and 18; they can be related to fatty acid amides which are common amidation products of fatty acids and amines during the HTL process [130]. F3 shows a relative abundance of 12.1% of O1N1 species with a comparatively low number of 151 species. The intensities are highest at a DBE of 6 and a Cn between 10 and 14. These can be associated with basic pyridine structures in addition to a furan ring, namely furopyridines. Similar compounds are assumed to appear in HTL-biocrude from sewage sludge as well as shale oil samples [334,335].

The 216 species within the O1N2 classes in F1 results in a relative abundance of 3.3%. The highest intensities of species are located at a DBE of 4 and a Cn of 10–12, likely to sustain of pyrrole-carboxylic acids, amidated with a short-chain amine. These species are again found in F2, but with a much lower intensity. This fraction shows a relative abundance of 6.0% and covers 329 species. The highest intensities are recognized at a DBE of 7–9 and a Cn from 13 to 16. These species are assumed to be indoles, derivatized amides, or other N-heteroaromatics, such as benzimidazoles with higher DBE substituted with methoxy groups [129]. A similar compositional space is identified in F4, which shows a relative abundance of 7.4% with 358 species. In addition, high intensity can be noted at a DBE of 2 and a Cn of 16, which is likely related to a nitrogenated aliphatic compound, but which has not been reported in hydrothermal conversion products so far. Fraction F3 shows 267 species in the O1N2 class at a significant relative abundance of 17.8%. The related species are again located in the aromatic area, with a broad intensity range between the DBE values of 6–10 and a Cn of 11–18. These species can be accounted for O-substituted pyridine-based structure or other strong basic N-containing compounds, such as aromatic branched amines. The O2N1 class in F1 shows a relative abundance of 13.1% covering a range of 383 species. High intensities are sharply located at a DBE of 2 and a Cn of 16 and 18.

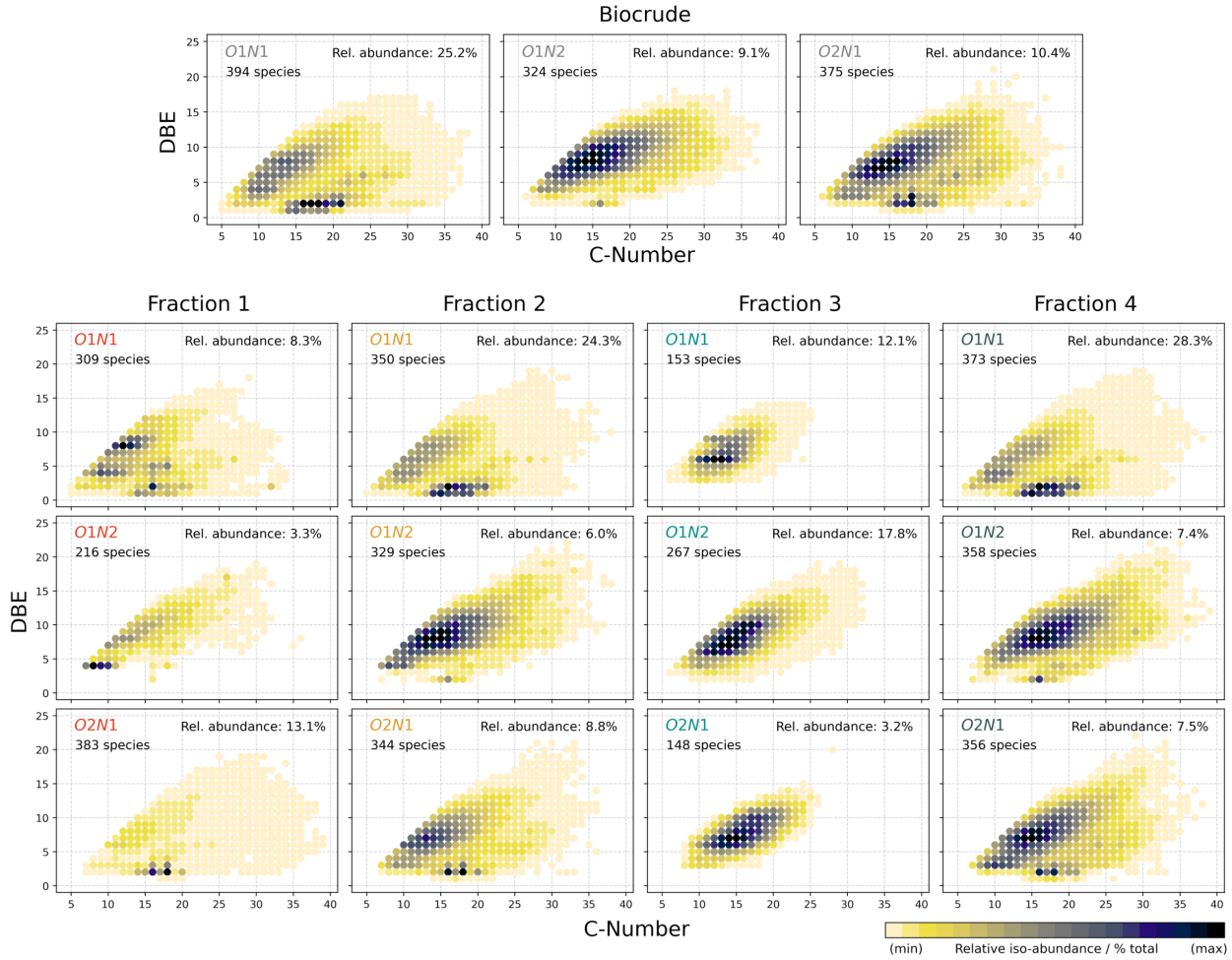

Figure 37. Relative intensity scatter plots of Cn vs DBE distribution of the classes O_xN_x of the extracted fractions.

These species can clearly be defined as long-chain aliphatics that originate from fatty acids, including a combination of carboxylic with amine groups or amide with a hydroxy group or a ketone group. Described species also appear in F2 and F4 with high intensities. These fractions show a relative abundance of 8.8 and 7.5%, including 344 and 356 species, respectively. In addition, increased intensities in F2 are identified in the aromatic region, especially at a DBE of 7 and a Cn of 13, likely including indole and carboxylic groups. In F4, the aromatic region shows increased intensities over a broad range. A maximum is located at a DBE of 3 and a Cn of 10, suggesting the presence of pyrroles, branched with methoxy or hydroxyl groups. Another maximum of intensities with wider distribution is identified at a DBE of 7 and 8, from a DBE of 14 to 16, allocating species including N-heteroaromatics identified in N1 class in

combination with hydroxy, methoxy, carbonyl, or carboxyl branches. On the contrary, F3 does not show any aliphatic species within the detected 148 species of the O2N1 class. The plot represents a relative abundance of 3.2% with the highest intensity identified at a DBE of 7 and a Cn between 15 and 17. These species are assumed to consist of furopyridines and methoxy or hydroxyl substitutions or alkylated amines with benzene or a hydroxyl group branched. Comparing the relative abundances and compositional space of the O*x*N*x* classes of the biocrude and F4, only minor effects can be observed. For the O1N1 and O2N1 class, the space abundances are slightly increased, whereas the identified species are decreased.

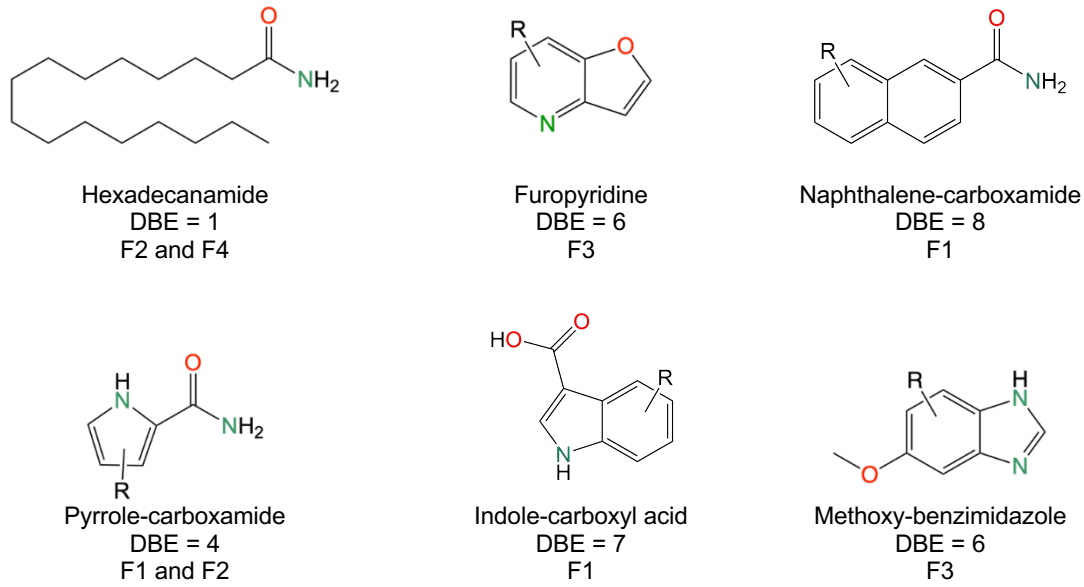

Figure 38. Suggested O_xN_x species within the extracted fractions.

Otherwise, in the O1N2 class the relative abundance is decreased, as again a majority of these compounds accumulate in F3. The described structures of the O1N1, O1N2, and O2N1 classes are schematized in Figure 37.

O*x*-Classes

Qualitatively, the O-containing O1 and O2 classes are discussed briefly. Their relative intensity scatter plots are shown in Supporting Information, S 14. As only low relative abundances of the O*x* species are found in fraction F3, only for F1, F2, and F4 plots are shown. Within the compositional space of the graphs, high intensities with a DBE of 0–3 and a Cn of 16–18 are

identified, suggesting the presence of saturated and unsaturated fatty acids, as well as their decarboxylation and dehydration products such as fatty acid alcohols and ketones. In F4, increased intensities are noted in an area of higher DBE and low Cn space, which is likely to be identified as (poly)aromatics, branched by an aliphatic hydroxyl or a carbonyl group. Additionally, at a DBE of 5 and a Cn of 26, increased intensities are related to sterol derivatives. Phenols that are identified in F1 and F2 from GC–MS measurements are assumed to not be effectively ionized by APCI in the positive ion mode [328].

5.3.6 Aromaticity of N-containing classes

The DBE to C (DBE/C) ratio was calculated to derive information about the corresponding aromaticity distribution of the 10 N-containing classes (N1, N2, N3, O1N1, O1N2, O1N3, O2N1, O2N2, O3N1, and O3N2) within the biocrude and extracted fractions F1 to F4. Previous studies on HTL biocrude fractions and pyrolysis oil samples demonstrated the usefulness of this method [336,337]. Ratios above a value of >0.7 can be assumed as aromatic species, whereas species above a value of >0.9 are poly-aromatic [338]. The ratios are displayed by violin plots in Figure 39. The kernel density plots are generated, by estimating and smoothing the frequency distribution of the DBE/C ratio. The inner boxplots identify the median value (white dot) and quartiles (black bar) and upper and lower whiskers (black line). The median is the value that lies exactly in the middle of data distribution. With the quartiles, the lowest and highest 25% frequencies are labeled. The whiskers define the minimum and maximum values, showing possible outliers of the frequency distribution. In addition, the mean and the arithmetic average values are given.

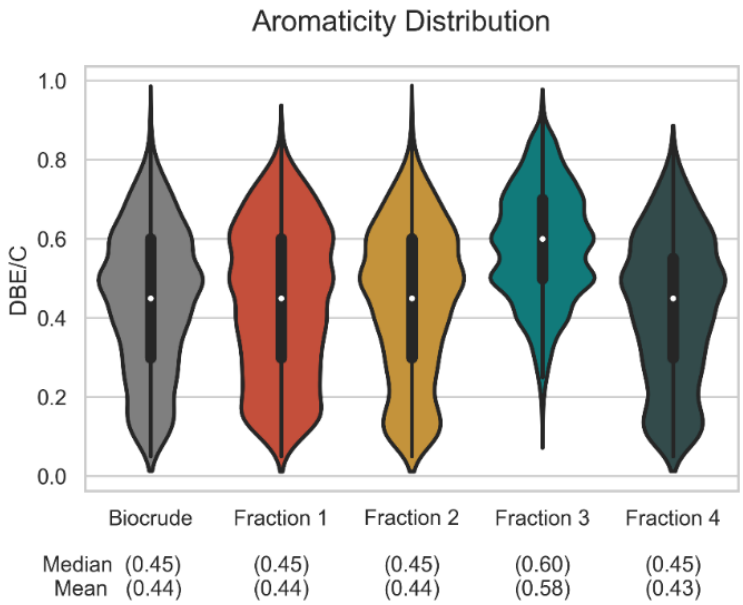

Figure 39. Violin plots of the aromatic distribution of N-containing compounds within the biocrude and the different fractions F1 – F4. The distribution of the aromaticity (DBE/C) is represented as kernel-density plots including box plots. In addition, the median and mean values of the distribution are given.

Figure 9. Violin plots of the aromatic distribution of N-containing compounds within the biocrude and the different fractions F1–F4. The distribution of the aromaticity (DBE/C) is represented as kernel density plots including boxplots. In addition, the median and mean values of the distribution are given.

The biocrude shows a kernel density curve with a peak at a value of 0.5 and median and mean values of 0.45 and 0.44, respectively. F1 shows an aromatic distribution up to a DBE/C value of 0.9 with a median at 0.45 and a mean at 0.44. The quartile bar ranges from 0.3 to 0.6 and the kernel density curve has a slight peak at a value of 0.6. In F2, the DBE/C distribution was found to show identical median and mean values, as well as that of the quartile bar. Peaks on the kernel density can be identified at DBE/C values of 0.1 and 0.5. Fraction F3 shows a divergent distribution pattern, with a peak around 0.5 and 0.6. The median and mean values in this fraction show the highest values of all fractions with 0.60 and 0.58, respectively. Furthermore, the quartile bar is assumed to be relatively narrow, reaching from 0.5 to 0.7. The kernel distribution plot of F4 shows almost the identical pattern as found for F2, with the same median value as for F1 and F2, but with a lower mean value at 0.43. In addition, fraction F4 shows the

lowest upper quartile at 0.55, and with a lower quartile at 0.3, a narrow density distribution. The wide, uniform spread of species functionalized with an N-group in F1, can be related to the general low abundances within this fraction. F2 and F4 show local maxima in a lower range of DBE/C, according to the presence of aliphatic amide structures. Additionally, higher DBE/C ratios are related to the abundance of N-heteroaromatics such as previously identified pyrrole-based species (alkylated indole or carbazole derivates) which become more acidic with a higher degree of aromatization [339]. F3 shows a high aromatization degree with a relatively high mean value of the distribution. It is assumed that no nitrogenated aliphatic compounds are present in this fraction, only as a short side chain of aromatic species. The increased DBE/C values in this fraction can be referred to as multiple nitrogenated structures such as alkylated benzimidazoles or carbazolines.

5.4 Conclusion

The sequential extraction with two alkaline and one acidic aqueous solution could enrich complex and organic N-containing acids or bases in different extracts. Non-polar N-compounds remain within the residual fraction and are not able to be extracted by polar aqueous solutions. The mass balance and determination of the element content show significantly higher N- than C-recovery in the acid extracted fraction (F3). Nevertheless, the composition of the residual fraction (F4) remains quite complex, as a large share (50 wt % of N) of the N-compounds seems not to be extracted by aqueous basic or acidic solutions. In addition, the subsequent characterization of N-compounds of the biocrude at the molecular level was improved by the following. GC–MS resolution could be drastically increased, which led to improved identification of basic N-compounds and an association with FTICR MS to determine the structures of detected N-species. The results confirmed the presence of N-compounds in the acidic fraction (F3), as every identified compound is functionalized with N. The combination of the polar extraction methodology and the combination of GC–MS and FTICR MS analysis suggests that the basic N-functionalizations such as pyridinic-N are almost exclusively found

in the acid extracted fraction (F3). Otherwise, a minor share of pyrrole and amide N-compounds is found in alkaline extracted fractions (F1 and F2). Most of the N-compounds found here are combined with a carboxylic acid group. Overall, these fractions resemble the residual F4, where N-compounds are found to be based on pyrrole and a large share consisting of amides. This is again reflected in the distribution of aromaticity of N-compounds over the fractions. Otherwise, the acidic extracted fraction shows a strong indication of the presence of N-heteroaromatics and no long-chain aliphatic structures.

Finally, with the gained knowledge a qualitative statement on the polarity behaviour of N-compounds in HTL-biocrude from sewage sludge can be given. This is extremely important for the development of further downstream processes to a valuable fuel. The results suggest that N-heteroaromatics are strongly affected by the presence of polar groups. Eventually, the overall content of both heteroatoms and aromatic molecules must be reduced with a combination of suitable extraction, adsorption, or hydrotreating processes.

Chapter 6. Final conclusion and outlook

The "Hydrothermal Fractionation of Sewage Sludge" was presented as a series of processes designed to enhance the efficiency of the hydrothermal liquefaction (HTL) process, which converts biogenic waste into a drop-in fuel. The objective of this work was to reduce the nitrogen and heteroatom content in the HTL biocrude prior to further hydrotreatment. The study comprised four chapters, addressing the four research questions derived from the knowledge gaps identified from the literature review on the state-of-the-art.

The effect of the wastewater treatment process:

To date, the impact of the source of municipal sewage sludge on the yield and quality of HTL-derived biocrude has not been systematically investigated in the literature. Through the collection and comprehensive characterization of various, representative sewage sludge samples, a significant impact of the preceding wastewater composition and the subsequent treatment process on the overall composition was observed. In particular, the elemental and organic composition mainly consisting of large molecules (lipids, proteins, carbohydrates) was found to vary strongly, which, in turn, affects the HTL process and the resultant biocrude yield and quality. My contribution to the state of knowledge shows that the crude fat (lipids) content in the sewage sample is the most influential factor on the biocrude yield and quality. Results showed that a high crude fat content led to a higher biocrude yield and increased production of aliphatic biocrude. Consequently the nitrogen content was found to be low in biocrude derived from sludge samples with a high crude lipid content. Interestingly the recovery of nitrogen from the feedstock to the final biocrude was increased in such cases.

Lipids and carbohydrates and their competition for amines:

It has been noted from the literature review that the impact of varying ratios of biogenic large molecules in the composition of HTL-feedstocks on the recovery of nitrogen and the formation of undesired nitrogen-heteroaromatic compounds remains an under-explored topic. Therefore, in this study the hydrothermal conversion of a model feedstock composed of cellulose, lipid, and protein components with varying composition was investigated. It was demonstrated that

the incorporation of lipids into the feedstock mixture increases the yield of biocrude while suppressing the formation of unwanted carbonaceous solids. Notably here, this was accompanied by a minor decrease of nitrogen recovery into the biocrude. So far, this systematic investigation confirms already know findings. Moreover, increasing the ratio of lipids to protein results in an enhancement of fatty acid amide formation. This suggests that there is a dominant generation of nitrogen-containing heteroaliphatic species that are incorporated into the biocrude phase. At the same time, the formation of nitrogen-heteroaromatic species is significantly reduced, and that of pyrazines is almost eliminated. It is assumed that fewer precursors (less stable secondary amino compounds) are produced. Therefore, both long-chain fatty acids and short-chain carboxylic acids (volatile fatty acids) can effectively scavenge highly reactive amines, resulting in the formation of nitrogen-aliphatic compounds within the biocrude or even transferring nitrogen into the aqueous product phase.

Upstream improvement of the sewage sludge HTL-feedstock:

The influence of pretreatment on the composition of biogenic feedstocks from municipal sewage sludge and subsequent HTL was investigated. A pre-treatment process including de-ionized water, sulphuric acid, or citric acid agents under mild hydrothermal conditions was evaluated. This was then followed by the HTL of residual solids to produce biocrude. Analysis of pre-treated samples revealed a solubilisation of unwanted proteins into the aqueous phase. With acidic agents, this nitrogen solubilization was further increased. Additionally, lipid retention was observed, which increased again the subsequent yield of biocrude of the HTL conversion. However, with the simultaneous dissolution of the organic matter in the pre-treatment agent and the subsequent hydrothermal conversion, the total yield of biocrude is significantly reduced. It should be noted that a preceding reduction of nitrogen is accompanied by a loss of potentially valuable carbonaceous material. The results also showed that the recovery of nitrogen in the biocrude after the HTL-conversion step was increased in lipid-rich, pre-treated samples. In terms of biocrude quality, the pre-treatment resulted in an increase in the H/C_{eff} ratio due to the accumulation of highly saturated long-chain aliphatic structures and

the presence of nitrogen-heteroatoms primarily in the form of fatty acid amides. In contrast, direct HTL of sewage sludge resulted in the formation of nitrogen-containing heteroaromatic structures, which would increase the hydrogen demand in further upgrading processes.

Extraction of unwanted nitrogen post-HTL:

The phase separation downstream HTL is still an unsolved issue and a strong quality determining factor. The results of this study highlight this importance in the development of an extraction methodology. The sequential extraction of the biocrude using a combination of alkaline and acidic aqueous solutions showed that the nitrogen-containing compounds can be enriched in different extracts. The results indicated that the presence of polar groups influences the behaviour of nitrogen-heteroaromatics in the biocrude. This information is crucial for the development of further downstream processes towards the production of a valuable fuel. The molecular characterization confirmed the presence of nitrogen-functionalized compounds in the acidic extracted fraction, while pyrrole and amide compounds were found in the alkaline extracted fractions. The results suggest that a combination of suitable extraction, adsorption, or hydrotreating processes will be necessary to reduce the overall content of both heteroatoms and aromatic molecules in the biocrude.

Where to go from here?

In conclusion, the transfer of nitrogen into the biocrude phase during the Hydrothermal Liquefaction (HTL) of municipal sewage sludge and proteinaceous biomass cannot be prevented, but decreased. The optimal case would be a hydrothermal liquefaction of a sewage sludge rich in lipids and poor in hydrocarbons, in combination with a mild hydrothermal pre-treatment, should result in a biocrude with a low nitrogen content. At the same time, the chemical composition should consist of more fatty acid amides and fewer N-heteroaromatic compounds. In addition, the pre-treatment should have a minor effect on the loss of potentially valuable carbonaceous material.

Furthermore, the biochemical composition of the feedstock, composed of lipids, carbohydrates, and proteins, provides valuable insight into the nitrogen recovery and the nature of formed species. A comprehensive evaluation of the entire valorisation process, from feedstock to drop-in fuel, can identify potential strategies to effectively reduce the nitrogen content and minimize the formation of unwanted heteroaromatics. This may involve the optimization of the sewage sludge feedstock, pre-treatment or co-liquefaction with suitable large molecules, and the integration of phase separation and recovery methods to produce high-quality biocrude.

The treatment of wastewater and sewage sludge is already a complex process that should continue to ensure the safe discharge of wastewater into surface waters. However, this waste stream contains valuable organic carbon that should be utilized. The objective of this work was to theoretically investigate current wastewater treatment processes and, if necessary and possible, improve them with a novel hydrothermal sludge valorization process. This approach would include the extended inclusion in the concept of the water-energy nexus and the recycling of waste streams from the hydrothermal processes studied here. One example of such a process is thermal hydrolysis, which is already applied in some wastewater treatment plants but primarily for reducing sewage sludge generation. By utilizing existing anaerobic digestion facilities within the plant, the thermal hydrolysis process could potentially increase the quality of biocrude. Additionally, research into integrating anaerobic digestion, with a focus on ammonia-rich hydrolysis supernatants, should be conducted to enable the recovery of these effluents.

The gained knowledge about the behaviour of duifferent nitrogen-containing compounds can then be applied to design an extraction process for unwanted nitrogen compounds, which can be integrated into future advanced phase separation processes.

References

[1] The European Commision, The European Green Deal, Brussel, 2019. https://www.taylorfrancis.com/books/9781136392412/chapters/10.4324/9780080495781-12.

[2] BMWK - Durchbruch für ambitionierten Ausbau erneuerbarer Energien bis 2030: neue EU-Richtlinie für erneuerbare Energien beschlossen, (n.d.). https://www.bmwk.de/Redaktion/DE/Pressemitteilungen/2023/03/20230330-durchbruch-fur-ambitionierten-ausbau-erneuerbarer-energien-bis-2030.html (accessed May 10, 2023).

[3] C. Panoutsou, S. Germer, P. Karka, S. Papadokostantakis, Y. Kroyan, M. Wojcieszyk, K. Maniatis, P. Marchand, I. Landalv, Advanced biofuels to decarbonise European transport by 2030: Markets, challenges, and policies that impact their successful market uptake, Energy Strategy Reviews 34 (2021) 100633. https://doi.org/10.1016/j.esr.2021.100633.

[4] The European Commision, Directive 2018/2001, Official Journal of the European Union 2018 (2018).

[5] J. Tomei, R. Helliwell, Food versus fuel? Going beyond biofuels, Land Use Policy 56 (2016) 320–326. https://doi.org/10.1016/j.landusepol.2015.11.015.

[6] European Climate Foundation, Roadmap 2050: A practical guide to a prosperous, low-carbon europe, 2016. https://doi.org/10.4324/9781315690995.

[7] The European Commision, Directive 2008/98/EC, Official Journal of the European Union (2008). http://www.bloomsburycollections.com/book/fundamental-texts-on-european-private-law-1/directive-2008-122-ec-of-the-european-parliament-and-of-the-council.

[8] The European Commision, Directive 2018/851, Official Journal of the European Union

(2018).

[9] The European Commision, Environmental, economic and social impacts of the use of sewage sludge on land, Final Report Part I: Overview Report, 2008. https://ec.europa.eu/environment/archives/waste/sludge/pdf/part_i_report.pdf.

[10] A. Gianico, C.M. Braguglia, A. Gallipoli, D. Montecchio, G. Mininni, Land application of biosolids in europe: Possibilities, con-straints and future perspectives, Water 13 (2021). https://doi.org/10.3390/w13010103.

[11] A. Abuşoğlu, E. Özahi, A. İhsan Kutlar, H. Al-jaf, Life cycle assessment (LCA) of digested sewage sludge incineration for heat and power production, Journal of Cleaner Production 142 (2017) 1684–1692. https://doi.org/10.1016/j.jclepro.2016.11.121.

[12] P. Zhao, Y. Shen, S. Ge, Z. Chen, K. Yoshikawa, Clean solid biofuel production from high moisture content waste biomass employing hydrothermal treatment, Applied Energy 131 (2014) 345–367. https://doi.org/10.1016/j.apenergy.2014.06.038.

[13] J. Peccia, P. Westerhoff, We Should Expect More out of Our Sewage Sludge, (2015). https://doi.org/10.1021/acs.est.5b01931.

[14] A. Banerjee, A. Banerjee, T. Bhaskar, T. Bhaskar, D. Ghosh, D. Ghosh, A biorefinery approach for sewage sludge, Waste Biorefinery: Integrating Biorefineries for Waste Valorisation (2020) 393–421. https://doi.org/10.1016/B978-0-12-818228-4.00015-0.

[15] B. Behera, S. Mari Selvam, P. Balasubramanian, Hydrothermal processing of microalgal biomass: Circular bio-economy perspectives for addressing food-water-energy nexus, Bioresource Technology 359 (2022) 127443. https://doi.org/10.1016/J.BIORTECH.2022.127443.

[16] P. Foladori, G. Andreottola, G. Ziglio, Sludge Reduction Technologies in Wastewater Treatment Plants, IWA Publishing, London, 2010. https://doi.org/10.2166/9781780401706.

[17] O. Suárez-Iglesias, J.L. Urrea, P. Oulego, S. Collado, M. Díaz, Valuable compounds from sewage sludge by thermal hydrolysis and wet oxidation. A review, Science of The Total Environment 584–585 (2017) 921–934. https://doi.org/10.1016/j.scitotenv.2017.01.140.

[18] C. Falco, N. Baccile, M.-M. Titirici, Morphological and structural differences between glucose, cellulose and lignocellulosic biomass derived hydrothermal carbons, Green Chemistry 13 (2011) 3273. https://doi.org/10.1039/c1gc15742f.

[19] A. Kruse, A. Funke, M.-M. Titirici, Hydrothermal conversion of biomass to fuels and energetic materials, Current Opinion in Chemical Biology 17 (2013) 515–521. https://doi.org/10.1016/j.cbpa.2013.05.004.

[20] A. Dimitriadis, S. Bezergianni, Hydrothermal liquefaction of various biomass and waste feedstocks for biocrude production: A state of the art review, Renewable and Sustainable Energy Reviews 68 (2017) 113–125. https://doi.org/10.1016/j.rser.2016.09.120.

[21] C.U. Jensen, J.K. Rodriguez Guerrero, S. Karatzos, G. Olofsson, S.B. Iversen, Fundamentals of Hydrofaction™: Renewable crude oil from woody biomass, Biomass Conversion and Biorefinery 7 (2017) 495–509. https://doi.org/10.1007/S13399-017-0248-8/FIGURES/12.

[22] VDI ev., VDI Heat Atlas, Springer Berlin Heidelberg, Berlin, Heidelberg, 2010. https://doi.org/10.1007/978-3-540-77877-6.

[23] W. Wagner, A. Pruß, The IAPWS Formulation 1995 for the Thermodynamic Properties of Ordinary Water Substance for General and Scientific Use, Journal of Physical and Chemical Reference Data 31 (2002) 387–535. https://doi.org/10.1063/1.1461829.

[24] M. Uematsu, E.U. Frank, Static Dielectric Constant of Water and Steam, Journal of Physical and Chemical Reference Data 9 (1980) 1291–1306. https://doi.org/10.1063/1.555632.

[25] A. V. Bandura, S.N. Lvov, The ionization constant of water over wide ranges of temperature and density, Journal of Physical and Chemical Reference Data 35 (2006) 15–30. https://doi.org/10.1063/1.1928231.

[26] A. Kruse, N. Dahmen, Water – A magic solvent for biomass conversion, The Journal of Supercritical Fluids 96 (2015) 36–45. https://doi.org/10.1016/j.supflu.2014.09.038.

[27] G. Akerlof, Dielectric Constants of some organic Solvent-Water Mixtures at various Temperatures, Journal of the American Chemical Society 54 (1932) 4125–4139. https://doi.org/10.1021/ja01350a001.

[28] A. Kruse, E. Dinjus, Hot compressed water as reaction medium and reactant, The Journal of Supercritical Fluids 39 (2007) 362–380. https://doi.org/10.1016/j.supflu.2006.03.016.

[29] J. Akhtar, N.A.S. Amin, A review on process conditions for optimum bio-oil yield in hydrothermal liquefaction of biomass, Renewable and Sustainable Energy Reviews 15 (2011) 1615–1624. https://doi.org/10.1016/j.rser.2010.11.054.

[30] J.A. Ramirez, R.J. Brown, T.J. Rainey, A review of hydrothermal liquefaction bio-crude properties and prospects for upgrading to transportation fuels, Energies 8 (2015) 6765–6794. https://doi.org/10.3390/en8076765.

[31] M.J. Montgomery, Dissertation: Analyzing the Effect of Fuel Nitrogen on Soot Formation, Yale, 2021.

[32] A.H. Zacher, M. V. Olarte, D.M. Santosa, D.C. Elliott, S.B. Jones, A review and perspective of recent bio-oil hydrotreating research, Green Chem. 16 (2014) 491–515. https://doi.org/10.1039/C3GC41382A.

[33] M.C. Loeffler, N.C. Li, Role of nitrogen- and sulphur-containing compounds in the ageing of liquid fuels, Fuel 64 (1985) 1047–1053. https://doi.org/10.1016/0016-2361(85)90104-8.

[34] M.N. Siddiquee, A. de Klerk, Heterocyclic Addition Reactions during Low Temperature Autoxidation, Energy & Fuels 29 (2015) 4236–4244. https://doi.org/10.1021/acs.energyfuels.5b00767.

[35] P. Dufresne, A. Quesada, S. Mignard, Influence of Nitrogen Feed Content On The Performances of A Zeolite Hydrocracking Catalyst, in: Stud. Surf. Sci. Catal., 1989: pp. 301–315. https://doi.org/10.1016/S0167-2991(08)61073-3.

[36] Z. Li, G. Wang, Q. Shi, C. Xu, J. Gao, Retardation Effect of Basic Nitrogen Compounds on Hydrocarbons Catalytic Cracking in Coker Gas Oil and Their Structural Identification, Industrial & Engineering Chemistry Research 50 (2011) 4123–4132. https://doi.org/10.1021/ie102117x.

[37] G.H.C. Prado, A. de Klerk, Metals Removal from Metal-Bridged Molecules by Acid Treatment of Oilsands Bitumen and Subfractions, Energy & Fuels 30 (2016) 20–30. https://doi.org/10.1021/acs.energyfuels.5b01482.

[38] E. Furimsky, F.E. Massoth, Hydrodenitrogenation of Petroleum, Catalysis Reviews 47 (2005) 297–489. https://doi.org/10.1081/CR-200057492.

[39] E. Furimsky, F.E. Massoth, Deactivation of hydroprocessing catalysts, Catalysis Today 52 (1999) 381–495. https://doi.org/10.1016/S0920-5861(99)00096-6.

[40] D.C. Elliott, Historical developments in hydroprocessing bio-oils, Energy & Fuels 21 (2007) 1792–1815. https://doi.org/10.1021/ef070044u.

[41] T.C. Ho, Hydrodenitrogenation Catalysis, Catalysis Reviews 30 (1988) 117–160. https://doi.org/10.1080/01614948808078617.

[42] R. Prins, Catalytic hydrodenitrogenation, in: Adv. Catal., 2001: pp. 399–464. https://doi.org/10.1016/S0360-0564(02)46025-7.

[43] G.H.C. Prado, Y. Rao, A. de Klerk, Nitrogen Removal from Oil: A Review, Energy & Fuels 31 (2017) 14–36. https://doi.org/10.1021/acs.energyfuels.6b02779.

[44] R. Kumar, V. Strezov, Thermochemical production of bio-oil: A review of downstream processing technologies for bio-oil upgrading, production of hydrogen and high value-added products, Renewable and Sustainable Energy Reviews 135 (2021) 110152. https://doi.org/10.1016/j.rser.2020.110152.

[45] M.S. Haider, D. Castello, L.A. Rosendahl, Two-stage catalytic hydrotreatment of highly nitrogenous biocrude from continuous hydrothermal liquefaction: A rational design of the stabilization stage, Biomass and Bioenergy 139 (2020) 105658. https://doi.org/10.1016/j.biombioe.2020.105658.

[46] J.L. Wagner, E. Jones, A. Sartbaeva, S.A. Davis, L. Torrente-Murciano, C.J. Chuck, V.P. Ting, Zeolite Y supported nickel phosphide catalysts for the hydrodenitrogenation of quinoline as a proxy for crude bio-oils from hydrothermal liquefaction of microalgae, Dalton Transactions 47 (2018) 1189–1201. https://doi.org/10.1039/C7DT03318D.

[47] P. Cantinho, M. Matos, M.A. Trancoso, M.M.C. dos Santos, Behaviour and fate of metals in urban wastewater treatment plants: a review, International Journal of Environmental Science and Technology 13 (2016) 359–386. https://doi.org/10.1007/s13762-015-0887-x.

[48] B. Wiechmann, C. Dienemann, C. Kabbe, S. Brandt, I. Vogel, A. Roskosch, Sewage sludge management in Germany, 2013.

[49] Metcalf & Eddy, Wastewater Engineering: Treatment and Reuse, 4th ed., McGraw-Hill, 2002.

[50] S. Yeoman, T. Stephenson, J.N. Lester, R. Perry, The removal of phosphorus during wastewater treatment: A review, Environmental Pollution 49 (1988) 183–233. https://doi.org/10.1016/0269-7491(88)90209-6.

[51] W.A. Shewa, T. Dong, W. Mu, K. Murray, M. Dagnew, The impact of chemically enhanced primary treatment on the downstream liquid and solid train processes, Water Environment Research 92 (2020) 359–368. https://doi.org/10.1002/WER.1170.

[52] L.M.M. de Bruin, M.K. de Kreuk, H.F.R. van der Roest, C. Uijterlinde, M.C.M. van Loosdrecht, Aerobic granular sludge technology: An alternative to activated sludge?, Water Science and Technology 49 (2004) 1–7. https://doi.org/10.2166/wst.2004.0790.

[53] S.Y. Gebremariam, M.W. Beutel, D. Christian, T.F. Hess, Research Advances and Challenges in the Microbiology of Enhanced Biological Phosphorus Removal—A Critical Review, Water Environment Research 83 (2011) 195–219. https://doi.org/10.2175/106143010X12780288628534.

[54] Y. Cao, M.C.M. van Loosdrecht, G.T. Daigger, Mainstream partial nitritation–anammox in municipal wastewater treatment: status, bottlenecks, and further studies, Applied Microbiology and Biotechnology 101 (2017) 1365–1383. https://doi.org/10.1007/S00253-016-8058-7/TABLES/2.

[55] G.K. Morse, S.W. Brett, J.A. Guy, J.N. Lester, Review: Phosphorus removal and recovery technologies, Science of the Total Environment 212 (1998) 69–81. https://doi.org/10.1016/S0048-9697(97)00332-X.

[56] O.A.H. Jones, N. Voulvoulis, J.N. Lester, Human Pharmaceuticals in Wastewater Treatment Processes, Critical Reviews in Environmental Science and Technology 35 (2005) 401–427. https://doi.org/10.1080/10643380590956966.

[57] L. Zhang, C. Xu, P. Champagne, W. Mabee, Overview of current biological and thermo-chemical treatment technologies for sustainable sludge management, Waste Management and Research 32 (2014) 586–600. https://doi.org/10.1177/0734242X14538303/FORMAT/EPUB.

[58] M.K. De Kreuk, J.J. Heijnen, M.C.M. Van Loosdrecht, Simultaneous COD, nitrogen, and phosphate removal by aerobic granular sludge, Biotechnology and Bioengineering 90 (2005) 761–769. https://doi.org/10.1002/BIT.20470.

[59] H. Yoshida, T.H. Christensen, C. Scheutz, Life cycle assessment of sewage sludge management: A review, Waste Management and Research 31 (2013) 1083–1101. https://doi.org/10.1177/0734242X13504446/FORMAT/EPUB.

[60] A. Kelessidis, A.S. Stasinakis, Comparative study of the methods used for treatment and final disposal of sewage sludge in European countries, Waste Management 32 (2012) 1186–1195. https://doi.org/10.1016/j.wasman.2012.01.012.

[61] E. Neyens, J. Baeyens, R. Dewil, B. De Heyder, Advanced sludge treatment affects extracellular polymeric substances to improve activated sludge dewatering, Journal of Hazardous Materials 106 (2004) 83–92. https://doi.org/10.1016/J.JHAZMAT.2003.11.014.

[62] U. Kepp, I. Machenbach, N. Weisz, O.E. Solheim, Enhanced stabilisation of sewage sludge through thermal hydrolysis - three years of experience with full scale plant, Water Science and Technology 42 (2000) 89–96. https://doi.org/10.2166/WST.2000.0178.

[63] W.P.F. Barber, Thermal hydrolysis for sewage treatment: A critical review, Water Research 104 (2016) 53–71. https://doi.org/10.1016/j.watres.2016.07.069.

[64] B. Cieślik, P. Konieczka, A review of phosphorus recovery methods at various steps of wastewater treatment and sewage sludge management. The concept of “no solid waste generation” and analytical methods, Journal of Cleaner Production 142 (2017) 1728–1740. https://doi.org/10.1016/J.JCLEPRO.2016.11.116.

[65] EurEau, Europe’s Water in Figures, Brussels, 2021. www.eureau.org (accessed November 22, 2022).

[66] I. Fonts, G. Gea, M. Azuara, J. Ábrego, J. Arauzo, Sewage sludge pyrolysis for liquid production: A review, Renewable and Sustainable Energy Reviews 16 (2012) 2781–2805. https://doi.org/10.1016/j.rser.2012.02.070.

[67] M. Li, B. Xiao, X. Wang, J. Liu, Consequences of sludge composition on combustion performance derived from thermogravimetry analysis, Waste Management 35 (2015) 141–147. https://doi.org/10.1016/j.wasman.2014.10.004.

[68] M. Ischia, C. Perazzolli, R. Dal Maschio, R. Campostrini, Pyrolysis study of sewage sludge by TG-MS and TG-GC-MS coupled analyses, Journal of Thermal Analysis and Calorimetry 87 (2007) 567–574. https://doi.org/10.1007/s10973-006-7690-3.

[69] A. Magdziarz, M. Wilk, Thermal characteristics of the combustion process of biomass and sewage sludge, Journal of Thermal Analysis and Calorimetry 114 (2013) 519–529. https://doi.org/10.1007/s10973-012-2933-y.

[70] P. Verlicchi, E. Zambello, Pharmaceuticals and personal care products in untreated and treated sewage sludge: Occurrence and environmental risk in the case of application on soil — A critical review, Science of The Total Environment 538 (2015) 750–767. https://doi.org/10.1016/j.scitotenv.2015.08.108.

[71] M.C. Monea, D.K. Löhr, C. Meyer, V. Preyl, J. Xiao, H. Steinmetz, H. Schönberger, A. Drenkova-Tuhtan, Comparing the leaching behavior of phosphorus, aluminum and iron from post-precipitated tertiary sludge and anaerobically digested sewage sludge aiming at phosphorus recovery, Journal of Cleaner Production 247 (2020) 119129. https://doi.org/10.1016/J.JCLEPRO.2019.119129.

[72] S.S.A. Syed-Hassan, Y. Wang, S. Hu, S. Su, J. Xiang, Thermochemical processing of sewage sludge to energy and fuel: Fundamentals, challenges and considerations, Renewable and Sustainable Energy Reviews 80 (2017) 888–913. https://doi.org/10.1016/j.rser.2017.05.262.

[73] European Commission, Disposal and recycling routes for sewage sludge: Part 3 - Scientific and technical report, Luxembourg, 2001. http://europa.eu.int/comm/environment/pubs/home.htm (accessed November 23, 2022).

[74] I. Fonts, M. Azuara, G. Gea, M.B. Murillo, Study of the pyrolysis liquids obtained from different sewage sludge, Journal of Analytical and Applied Pyrolysis 85 (2009) 184–191. https://doi.org/10.1016/J.JAAP.2008.11.003.

[75] M.C. Chrispim, M. Scholz, M.A. Nolasco, Phosphorus recovery from municipal wastewater treatment: Critical review of challenges and opportunities for developing countries, Journal of Environmental Management 248 (2019) 109268. https://doi.org/10.1016/J.JENVMAN.2019.109268.

[76] M. Schnell, T. Horst, P. Quicker, Thermal treatment of sewage sludge in Germany: A review, Journal of Environmental Management 263 (2020) 110367. https://doi.org/10.1016/j.jenvman.2020.110367.

[77] G.C. Becker, D. Wüst, H. Köhler, A. Lautenbach, A. Kruse, Novel approach of phosphate-reclamation as struvite from sewage sludge by utilising hydrothermal carbonization, Journal of Environmental Management 238 (2019) 119–125. https://doi.org/10.1016/j.jenvman.2019.02.121.

[78] E. Ovsyannikova, P.J. Arauzo, G.C. Becker, A. Kruse, Experimental and thermodynamic studies of phosphate behavior during the hydrothermal carbonization of sewage sludge, 692 (2019) 147–156. https://doi.org/10.1016/j.scitotenv.2019.07.217.

[79] W. Rulkens, Sewage sludge as a biomass resource for the production of energy: Overview and assessment of the various options, Energy & Fuels 22 (2008) 9–15. https://doi.org/10.1021/ef700267m.

[80] M.D. Hatinoğlu, F.D. Sanin, Sewage sludge as a source of microplastics in the environment: A review of occurrence and fate during sludge treatment, Journal of Environmental Management 295 (2021) 113028. https://doi.org/10.1016/j.jenvman.2021.113028.

[81] P. Khuwijitjaru, S. Adachi, R. Matsuno, Solubility of Saturated Fatty Acids in Water at Elevated Temperatures, Bioscience, Biotechnology, and Biochemistry 66 (2002) 1723–1726. https://doi.org/10.1271/bbb.66.1723.

[82] M. Ravber, Hydrothermal Degradation of Fats, Carbohydrates and Proteins in Sunflower Seeds after Treatment with Subcritical Water, Chemical and Biochemical Engineering Quarterly 29 (2015) 351–355. https://doi.org/10.15255/CABEQ.2015.2193.

[83] W.W. Nawar, Thermal degradation of lipids. A review, Journal of Agricultural and Food Chemistry 17 (1969) 18–21. https://doi.org/10.1021/JF60161A012/ASSET/JF60161A012.FP.PNG_V03.

[84] M. Déniel, G. Haarlemmer, A. Roubaud, E. Weiss-Hortala, J. Fages, Hydrothermal liquefaction of blackcurrant pomace and model molecules: Understanding of reaction mechanisms, Sustainable Energy and Fuels 1 (2017) 555–582. https://doi.org/10.1039/c6se00065g.

[85] M. Watanabe, T. Iida, H. Inomata, Decomposition of a long chain saturated fatty acid with some additives in hot compressed water, Energy Conversion and Management 47 (2006) 3344–3350. https://doi.org/10.1016/j.enconman.2006.01.009.

[86] P. Biller, A.B. Ross, Potential yields and properties of oil from the hydrothermal liquefaction of microalgae with different biochemical content, Bioresource Technology 102 (2011) 215–225. https://doi.org/10.1016/j.biortech.2010.06.028.

[87] S. Changi, A.J. Matzger, P.E. Savage, Kinetics and pathways for an algal phospholipid (1,2-dioleoyl-sn-glycero-3-phosphocholine) in high-temperature (175–350 °C) water, Green Chemistry 14 (2012) 2856. https://doi.org/10.1039/c2gc35639b.

[88] E. Jardé, L. Mansuy, P. Faure, Organic markers in the lipidic fraction of sewage sludges, Water Research 39 (2005) 1215–1232. https://doi.org/10.1016/J.WATRES.2004.12.024.

[89] A. Shanableh, Production of useful organic matter from sludge using hydrothermal treatment, Water Research 34 (2000) 945–951. https://doi.org/10.1016/S0043-1354(99)00222-5.

[90] A.I. Rushdi, K.F. Al-Mutlaq, S.K. Sasmal, B.R.T. Simoneit, Alteration of sewage sludge biomass into oil-like products by hydrous pyrolysis methods, Fuel 103 (2013) 970–979. https://doi.org/10.1016/J.FUEL.2012.07.065.

[91] R. Obeid, N. Smith, D.M. Lewis, T. Hall, P. van Eyk, A kinetic model for the hydrothermal liquefaction of microalgae, sewage sludge and pine wood with product characterisation of renewable crude, Chemical Engineering Journal 428 (2022) 131228. https://doi.org/10.1016/J.CEJ.2021.131228.

[92] D.C. Hietala, P.E. Savage, Reaction pathways and kinetics of cholesterol in high-temperature water, Chemical Engineering Journal 265 (2015) 129–137. https://doi.org/10.1016/J.CEJ.2014.12.020.

[93] W. Bühler, E. Dinjus, H.J. Ederer, A. Kruse, C. Mas, Ionic reactions and pyrolysis of glycerol as competing reaction pathways in near- and supercritical water, The Journal of Supercritical Fluids 22 (2002) 37–53. https://doi.org/10.1016/S0896-8446(01)00105-X.

[94] O. Bobleter, Hydrothermal degradation of polymers derived from plants, Progress in Polymer Science 19 (1994) 797–841. https://doi.org/10.1016/0079-6700(94)90033-7.

[95] F. Behrendt, Y. Neubauer, M. Oevermann, B. Wilmes, N. Zobel, Direct liquefaction of biomass, Chemical Engineering and Technology 31 (2008) 667–677. https://doi.org/10.1002/ceat.200800077.

[96] S.S. Toor, L. Rosendahl, A. Rudolf, Hydrothermal liquefaction of biomass: A review of subcritical water technologies, Energy 36 (2011) 2328–2342. https://doi.org/10.1016/j.energy.2011.03.013.

[97] S.M. Changi, J.L. Faeth, N. Mo, P.E. Savage, Hydrothermal Reactions of Biomolecules Relevant for Microalgae Liquefaction, Industrial & Engineering Chemistry Research 54 (2015) 11733–11758. https://doi.org/10.1021/acs.iecr.5b02771.

[98] I.A. Basar, H. Liu, H. Carrere, E. Trably, C. Eskicioglu, A review on key design and operational parameters to optimize and develop hydrothermal liquefaction of biomass for biorefinery applications, Green Chemistry 23 (2021) 1404–1446. https://doi.org/10.1039/D0GC04092D.

[99] A. Kruse, A. Gawlik, Biomass Conversion in Water at 330–410 °C and 30–50 MPa. Identification of Key Compounds for Indicating Different Chemical Reaction Pathways, Industrial & Engineering Chemistry Research 42 (2003) 267–279. https://doi.org/10.1021/ie0202773.

[100] T.M. Aida, N. Shiraishi, M. Kubo, M. Watanabe, R.L. Smith, Reaction kinetics of d-xylose in sub- and supercritical water, The Journal of Supercritical Fluids 55 (2010) 208–216. https://doi.org/10.1016/j.supflu.2010.08.013.

[101] J.C. Speck, The Lobry De Bruyn-Alberda Van Ekenstein Transformation, Advances in Carbohydrate Chemistry 13 (1958) 63–103. https://doi.org/10.1016/S0096-5332(08)60352-5.

[102] B.M. Kabyemela, T. Adschiri, R.M. Malaluan, K. Arai, Kinetics of Glucose Epimerization and Decomposition in Subcritical and Supercritical Water, Industrial and Engineering Chemistry Research 36 (1997) 1552–1558. https://doi.org/10.1021/ie960250h.

[103] M.J. Antal, W.S.L. Mok, G.N. Richards, Mechanism of formation of 5-(hydroxymethyl)-2-furaldehyde from d-fructose and sucrose, Carbohydrate Research 199 (1990) 91–109. https://doi.org/10.1016/0008-6215(90)84096-D.

[104] Z. Srokol, A.-G. Bouche, A. van Estrik, R.C.. Strik, T. Maschmeyer, J.A. Peters, Hydrothermal upgrading of biomass to biofuel; studies on some monosaccharide model compounds, Carbohydrate Research 339 (2004) 1717–1726. https://doi.org/10.1016/j.carres.2004.04.018.

[105] G.C.A. Luijkx, F. van Rantwijk, H. van Bekkum, Hydrothermal formation of 1,2,4-benzenetriol from 5-hydroxymethyl-2-furaldehyde and d-fructose, Carbohydrate Research 242 (1993) 131–139. https://doi.org/10.1016/0008-6215(93)80027-C.

[106] A. Kruse, P. Maniam, F. Spieler, Influence of Proteins on the Hydrothermal Gasification and Liquefaction of Biomass. 2. Model Compounds, Industrial & Engineering Chemistry Research 46 (2007) 87–96. https://doi.org/10.1021/ie061047h.

[107] P. Körner, Hydrothermal Degradation of Amino Acids, ChemSusChem 14 (2021) 4947–4957. https://doi.org/10.1002/cssc.202101487.

[108] T. Rogalinski, S. Herrmann, G. Brunner, Production of amino acids from bovine serum albumin by continuous sub-critical water hydrolysis, The Journal of Supercritical Fluids 36 (2005) 49–58. https://doi.org/10.1016/j.supflu.2005.03.001.

[109] T.M. Aida, M. Oshima, R.L. Smith, Controlled Conversion of Proteins into High-Molecular-Weight Peptides without Additives with High-Temperature Water and Fast Heating Rates, ACS Sustainable Chemistry & Engineering 5 (2017) 7709–7715. https://doi.org/10.1021/acssuschemeng.7b01146.

[110] F. Pietrucci, J.C. Aponte, R. Starr, A. Pérez-Villa, J.E. Elsila, J.P. Dworkin, A.M. Saitta, Hydrothermal Decomposition of Amino Acids and Origins of Prebiotic Meteoritic Organic Compounds, ACS Earth and Space Chemistry 2 (2018) 588–598. https://doi.org/10.1021/acsearthspacechem.8b00025.

[111] A.T. Quitain, H. Daimon, K. Fujie, S. Katoh, T. Moriyoshi, Microwave-Assisted Hydrothermal Degradation of Silk Protein to Amino Acids, (2006). https://doi.org/10.1021/ie0580699.

[112] J. Li, T.B. Brill, Spectroscopy of Hydrothermal Reactions 25: Kinetics of the Decarboxylation of Protein Amino Acids and the Effect of Side Chains on Hydrothermal Stability, The Journal of Physical Chemistry A 107 (2003) 5987–5992. https://doi.org/10.1021/jp0224766.

[113] Y. Dote, S. Inoue, T. Ogi, S.Y. Yokoyama, Studies on the direct liquefaction of protein-contained biomass: The distribution of nitrogen in the products, Biomass and Bioenergy 11 (1996) 491–498. https://doi.org/10.1016/S0961-9534(96)00045-1.

[114] Y. Fan, U. Hornung, N. Dahmen, A. Kruse, Hydrothermal liquefaction of protein-containing biomass: study of model compounds for Maillard reactions, Biomass Conversion and Biorefinery 8 (2018) 909–923. https://doi.org/10.1007/s13399-018-0340-8.

[115] Y. Fan, A. Hoffmann, U. Hornung, K. Raffelt, T.A. Zevaco, N. Dahmen, Hydrothermal, catalyst-free production of a cyclic dipeptide from lysine, Journal of Analytical and Applied Pyrolysis 168 (2022) 105792. https://doi.org/10.1016/j.jaap.2022.105792.

[116] J.D. Sheehan, P.E. Savage, Molecular and Lumped Products from Hydrothermal Liquefaction of Bovine Serum Albumin, ACS Sustainable Chemistry & Engineering 5 (2017) 10967–10975. https://doi.org/10.1021/acssuschemeng.7b02854.

[117] J.D. Sheehan, P.E. Savage, Reaction pathways and kinetics of tryptophan in hot, compressed water, Chemical Engineering Journal 390 (2020) 124600. https://doi.org/10.1016/j.cej.2020.124600.

[118] S.I.D.F.S. Martins, Unravelling the Maillard reaction network by multiresponse kinetic modelling, Wageningen Universiteit, 2003. https://edepot.wur.nl/121418%0A%0A (accessed December 6, 2022).

[119] T. Minowa, S. Inoue, T. Hanaoka, Y. Matsumura, Hydrothermal Reaction of Glucose and Glycine as Model Compounds of Biomass, Journal of the Japan Institute of Energy 83 (2004) 794–798. https://doi.org/10.3775/jie.83.794.

[120] A.A. Peterson, R.P. Lachance, J.W. Tester, Kinetic evidence of the maillard reaction in hydrothermal biomass processing: Glucose-glycine interactions in high-temperature, high-pressure water, Industrial and Engineering Chemistry Research 49 (2010) 2107–2117. https://doi.org/10.1021/ie9014809.

[121] A. Adams, R.C. Borrelli, V. Fogliano, N. De Kimpe, Thermal degradation studies of food melanoidins, Journal of Agricultural and Food Chemistry 53 (2005) 4136–4142. https://doi.org/10.1021/jf047903m.

[122] A. Kruse, A. Krupka, V. Schwarzkopf, C. Gamard, T. Henningsen, Influence of Proteins on the Hydrothermal Gasification and Liquefaction of Biomass. 1. Comparison of Different Feedstocks, Industrial & Engineering Chemistry Research 44 (2005) 3013–3020. https://doi.org/10.1021/ie049129y.

[123] G.P. Rizzi, Free Radicals in the Maillard Reaction, Food Reviews International 19 (2003) 375–395. https://doi.org/10.1081/FRI-120025481.

[124] B.L. Milić, M. V. Piletić, The mechanism of pyrrole, pyrazine and pyridine formation in non-enzymic browning reaction, Food Chemistry 13 (1984) 165–180. https://doi.org/10.1016/0308-8146(84)90071-2.

[125] G. Teri, L. Luo, P.E. Savage, Hydrothermal Treatment of Protein, Polysaccharide, and Lipids Alone and in Mixtures, Energy & Fuels 28 (2014) 7501–7509. https://doi.org/10.1021/ef501760d.

[126] R. Posmanik, D.A. Cantero, A. Malkani, D.L. Sills, J.W. Tester, Biomass conversion to bio-oil using sub-critical water: Study of model compounds for food processing waste, The Journal of Supercritical Fluids 119 (2017) 26–35. https://doi.org/10.1016/j.supflu.2016.09.004.

[127] A. Croce, E. Battistel, S. Chiaberge, S. Spera, F. De Angelis, S. Reale, A Model Study to Unravel the Complexity of Bio-Oil from Organic Wastes, ChemSusChem 10 (2017) 171–181. https://doi.org/10.1002/cssc.201601258.

[128] B.R.T. Simoneit, A.I. Rushdi, M.R.B. Abas, B.M. Didyk, Alkyl amides and nitriles as novel tracers for biomass burning, Environmental Science and Technology 37 (2003) 16–21. https://doi.org/10.1021/es020811y.

[129] C. Torri, L. Garcia Alba, C. Samorì, D. Fabbri, D.W.F. Brilman, Hydrothermal treatment (HTT) of microalgae: Detailed molecular characterization of HTT oil in view of HTT mechanism elucidation, Energy & Fuels 26 (2012) 658–671. https://doi.org/10.1021/ef201417e.

[130] S. Chiaberge, I. Leonardis, T. Fiorani, G. Bianchi, P. Cesti, A. Bosetti, M. Crucianelli, S. Reale, F. De Angelis, Amides in bio-oil by hydrothermal liquefaction of organic wastes: A mass spectrometric study of the thermochemical reaction products of binary mixtures of amino acids and fatty acids, Energy & Fuels 27 (2013) 5287–5297. https://doi.org/10.1021/ef4009983.

[131] A. Matayeva, D. Bianchi, S. Chiaberge, F. Cavani, F. Basile, Elucidation of reaction pathways of nitrogenous species by hydrothermal liquefaction process of model compounds, Fuel 240 (2019) 169–178. https://doi.org/10.1016/j.fuel.2018.11.136.

[132] S. Changi, M. Zhu, P.E. Savage, Hydrothermal reaction kinetics and pathways of phenylalanine alone and in binary mixtures, ChemSusChem 5 (2012) 1743–1757. https://doi.org/10.1002/cssc.201200146.

[133] M. Déniel, G. Haarlemmer, A. Roubaud, E. Weiss-Hortala, J. Fages, Energy valorisation of food processing residues and model compounds by hydrothermal liquefaction, Renewable and Sustainable Energy Reviews 54 (2016) 1632–1652. https://doi.org/10.1016/j.rser.2015.10.017.

[134] Y. Fan, U. Hornung, K. Raffelt, N. Dahmen, The influence of lipids on the fate of nitrogen during hydrothermal liquefaction of protein-containing biomass, Journal of Analytical and Applied Pyrolysis 147 (2020) 104798. https://doi.org/10.1016/j.jaap.2020.104798.

[135] H.O. LeClerc, R. Atwi, S.F. Niles, A.M. McKenna, M.T. Timko, R.H. West, A.R. Teixeira, Elucidating the role of reactive nitrogen intermediates in hetero-cyclization during hydrothermal liquefaction of food waste, Green Chemistry (2022). https://doi.org/10.1039/D2GC01135B.

[136] J. Yang, Q. (Sophia) He, H. Niu, A. Dalai, K. Corscadden, N. Zhou, Microwave-assisted hydrothermal liquefaction of biomass model components and comparison with conventional heating, Fuel 277 (2020) 118202. https://doi.org/10.1016/j.fuel.2020.118202.

[137] European Commission, Scenarios for integration of bio-liquids in existing REFINERY processes | 4REFINERY Project | Fact Sheet | H2020 | CORDIS, (n.d.). https://doi.org/10.3030/727531.

[138] European Commission, Biorefinery combining HTL and FT to convert wet and solid organic, industrial wastes into 2nd generation biofuels with highest efficiency | Heat-To-Fuel Project | Fact Sheet | H2020 | CORDIS, (n.d.). https://doi.org/10.3030/764675.

[139] European Commission, Hydrothermal liquefaction: Enhanced performance and feedstock flexibility for efficient biofuel production | HyFlexFuel Project | Fact Sheet | H2020 | CORDIS, (n.d.). https://doi.org/10.3030/764734.

[140] European Commission, Biofuels from WASTE TO ROAD transport | WASTE2ROAD Project | Fact Sheet | H2020 | CORDIS, (n.d.). https://doi.org/10.3030/818120.

[141] European Commission, Sustainable Drop-In Transport fuels from Hydrothermal Liquefaction of Low Value Urban Feedstocks | NextGenRoadFuels Project | Fact Sheet | H2020 | CORDIS, (n.d.). https://doi.org/10.3030/818413.

[142] European Commission, Black Liquor to Fuel by Efficient HydroThermal Application integrated to Pulp Mill | BL2F Project | Fact Sheet | H2020 | CORDIS, (n.d.). https://doi.org/10.3030/884111.

[143] Ak. Suzuki, T. Nakamura, S.-Y. Yokoyama, T. Ogi, K. Koguchi, Conversion of sewage sludge to heavy oil by direct thermochemical liquefaction., JOURNAL OF CHEMICAL ENGINEERING OF JAPAN 21 (1988) 288–293. https://doi.org/10.1252/jcej.21.288.

[144] G. Yoo, M.S. Park, J.-W. Yang, M. Choi, Lipid content in microalgae determines the quality of biocrude and Energy Return On Investment of hydrothermal liquefaction, Applied Energy 156 (2015) 354–361. https://doi.org/10.1016/j.apenergy.2015.07.020.

[145] F. Cheng, Z. Cui, L. Chen, J. Jarvis, N. Paz, T. Schaub, N. Nirmalakhandan, C.E. Brewer, Hydrothermal liquefaction of high- and low-lipid algae: Bio-crude oil chemistry, Applied Energy 206 (2017) 278–292. https://doi.org/10.1016/j.apenergy.2017.08.105.

[146] M. Ellersdorfer, Hydrothermal co-liquefaction of chlorella vulgaris with food processing residues, green waste and sewage sludge, Biomass and Bioenergy 142 (2020) 105796. https://doi.org/10.1016/j.biombioe.2020.105796.

[147] L. Leng, J. Li, X. Yuan, J. Li, P. Han, Y. Hong, F. Wei, W. Zhou, Beneficial synergistic effect on bio-oil production from co-liquefaction of sewage sludge and lignocellulosic biomass, Bioresource Technology 251 (2018) 49–56. https://doi.org/10.1016/j.biortech.2017.12.018.

[148] O.M. Adedeji, J.S. Russack, L.A. Molnar, S.K. Bauer, Co-Hydrothermal Liquefaction of Sewage Sludge and Beverage Waste for High-Quality Bio-energy Production, Fuel 324 (2022) 124757. https://doi.org/10.1016/J.FUEL.2022.124757.

[149] R. Liu, W. Tian, S. Kong, Y. Meng, H. Wang, J. Zhang, Effects of inorganic and organic acid pretreatments on the hydrothermal liquefaction of municipal secondary sludge, Energy Conversion and Management 174 (2018) 661–667. https://doi.org/10.1016/j.enconman.2018.08.058.

[150] S. Pilli, S. Yan, R.D. Tyagi, R.Y. Surampalli, Thermal Pretreatment of Sewage Sludge to Enhance Anaerobic Digestion: A Review, Critical Reviews in Environmental Science and Technology 45 (2015) 669–702. https://doi.org/10.1080/10643389.2013.876527.

[151] C. Bougrier, J.P. Delgenès, H. Carrère, Effects of thermal treatments on five different waste activated sludge samples solubilisation, physical properties and anaerobic digestion, Chemical Engineering Journal 139 (2008) 236–244. https://doi.org/10.1016/j.cej.2007.07.099.

[152] J. Dwyer, D. Starrenburg, S. Tait, K. Barr, D.J. Batstone, P. Lant, Decreasing activated sludge thermal hydrolysis temperature reduces product colour, without decreasing degradability, Water Research 42 (2008) 4699–4709. https://doi.org/10.1016/J.WATRES.2008.08.019.

[153] G. Chen, M. Hu, G. Du, S. Tian, Z. He, B. Liu, W. Ma, Hydrothermal Liquefaction of Sewage Sludge by Microwave Pretreatment, Energy & Fuels 34 (2020) 1145–1152. https://doi.org/10.1021/acs.energyfuels.9b02155.

[154] W. Costanzo, U. Jena, R. Hilten, K.C. Das, J.R. Kastner, Low temperature hydrothermal pretreatment of algae to reduce nitrogen heteroatoms and generate nutrient recycle streams, Algal Research 12 (2015) 377–387. https://doi.org/10.1016/j.algal.2015.09.019.

[155] C. Jazrawi, P. Biller, Y. He, A. Montoya, A.B. Ross, T. Maschmeyer, B.S. Haynes, Two-stage hydrothermal liquefaction of a high-protein microalga, Algal Research 8 (2015) 15–22. https://doi.org/10.1016/j.algal.2014.12.010.

[156] Z. Huang, A. Wufuer, Y. Wang, L. Dai, Hydrothermal liquefaction of pretreated low-lipid microalgae for the production of bio-oil with low heteroatom content, Process Biochemistry 69 (2018) 136–143. https://doi.org/10.1016/j.procbio.2018.03.018.

[157] M. Olkiewicz, M.P. Caporgno, A. Fortuny, F. Stüber, A. Fabregat, J. Font, C. Bengoa, Direct liquid–liquid extraction of lipid from municipal sewage sludge for biodiesel production, Fuel Processing Technology 128 (2014) 331–338. https://doi.org/10.1016/j.fuproc.2014.07.041.

[158] C. Kech, A. Galloy, C. Frippiat, A. Piel, D. Garot, Optimization of direct liquid-liquid extraction of lipids from wet urban sewage sludge for biodiesel production, Fuel 212 (2018) 132–139. https://doi.org/10.1016/j.fuel.2017.10.010.

[159] Y. Fan, F.G. Fonseca, M. Gong, A. Hoffmann, U. Hornung, N. Dahmen, Energy valorization of integrating lipid extraction and hydrothermal liquefaction of lipid-extracted sewage sludge, Journal of Cleaner Production 285 (2021) 124895. https://doi.org/10.1016/j.jclepro.2020.124895.

[160] K. Kapusta, Effect of ultrasound pretreatment of municipal sewage sludge on characteristics of bio-oil from hydrothermal liquefaction process, Waste Management 78 (2018) 183–190. https://doi.org/10.1016/J.WASMAN.2018.05.043.

[161] Z. Zhu, S.S. Toor, L. Rosendahl, D. Yu, G. Chen, Influence of alkali catalyst on product yield and properties via hydrothermal liquefaction of barley straw, Energy 80 (2015) 284–292. https://doi.org/10.1016/j.energy.2014.11.071.

[162] S. ya Yokoyama, A. Suzuki, M. Murakami, T. Ogi, K. Koguchi, E. Nakamura, Liquid fuel production from sewage sludge by catalytic conversion using sodium carbonate, Fuel 66 (1987) 1150–1155. https://doi.org/10.1016/0016-2361(87)90315-2.

[163] A.A. Shah, S.S. Toor, F. Conti, A.H. Nielsen, L.A. Rosendahl, Hydrothermal liquefaction of high ash containing sewage sludge at sub and supercritical conditions, Biomass and Bioenergy 135 (2020) 105504. https://doi.org/10.1016/j.biombioe.2020.105504.

[164] L. Qian, S. Wang, P.E. Savage, Hydrothermal liquefaction of sewage sludge under isothermal and fast conditions, Bioresource Technology 232 (2017) 27–34. https://doi.org/10.1016/J.BIORTECH.2017.02.017.

[165] C. Prestigiacomo, J. Zimmermann, U. Hornung, K. Raffelt, N. Dahmen, O. Scialdone, A. Galia, Effect of transition metals and homogeneous hydrogen producers in the hydrothermal liquefaction of sewage sludge, Fuel Processing Technology 237 (2022) 107452. https://doi.org/10.1016/J.FUPROC.2022.107452.

[166] A.B. Ross, P. Biller, M.L. Kubacki, H. Li, A. Lea-Langton, J.M. Jones, Hydrothermal processing of microalgae using alkali and organic acids, Fuel 89 (2010) 2234–2243. https://doi.org/10.1016/j.fuel.2010.01.025.

[167] A.A. Shah, S.S. Toor, T.H. Seehar, R.S. Nielsen, A. H. Nielsen, T.H. Pedersen, L.A. Rosendahl, Bio-Crude Production through Aqueous Phase Recycling of Hydrothermal Liquefaction of Sewage Sludge, Energies 13 (2020) 493. https://doi.org/10.3390/en13020493.

[168] K. Kohansal, S. Toor, K. Sharma, R. Chand, L. Rosendahl, T.H. Pedersen, Hydrothermal liquefaction of pre-treated municipal solid waste (biopulp) with recirculation of concentrated aqueous phase, Biomass and Bioenergy 148 (2021) 106032. https://doi.org/10.1016/j.biombioe.2021.106032.

[169] T. Rahman, H. Jahromi, P. Roy, S. Adhikari, E. Hassani, T.S. Oh, Hydrothermal liquefaction of municipal sewage sludge: Effect of red mud catalyst in ethylene and inert ambiences, Energy Conversion and Management 245 (2021) 114615. https://doi.org/10.1016/j.enconman.2021.114615.

[170] C. Prestigiacomo, P. Costa, F. Pinto, B. Schiavo, A. Siragusa, O. Scialdone, A. Galia, Sewage sludge as cheap alternative to microalgae as feedstock of catalytic hydrothermal liquefaction processes, The Journal of Supercritical Fluids 143 (2019) 251–258. https://doi.org/10.1016/j.supflu.2018.08.019.

[171] Y. Zhai, H. Chen, B.B. Xu, B. Xiang, Z. Chen, C. Li, G. Zeng, Influence of sewage sludge-based activated carbon and temperature on the liquefaction of sewage sludge: Yield and composition of bio-oil, immobilization and risk assessment of heavy metals, Bioresource Technology 159 (2014) 72–79. https://doi.org/10.1016/J.BIORTECH.2014.02.049.

[172] A. Sayegh, S. Merkert, J. Zimmermann, H. Horn, F. Saravia, Treatment of Hydrothermal-Liquefaction Wastewater with Crossflow UF for Oil and Particle Removal, Membranes 12 (2022) 255. https://doi.org/10.3390/membranes12030255.

[173] H. Li, Z. Zhu, J. Lu, J. Watson, D. Kong, K. Wang, Y. Zhang, Z. Liu, Establishment and performance of a plug-flow continuous hydrothermal reactor for biocrude oil production, Fuel 280 (2020) 118605. https://doi.org/10.1016/j.fuel.2020.118605.

[174] P.A. Marrone, D.C. Elliott, J.M. Billing, R.T. Hallen, T.R. Hart, P. Kadota, J.C. Moeller, M.A. Randel, A.J. Schmidt, Bench-Scale Evaluation of Hydrothermal Processing Technology for Conversion of Wastewater Solids to Fuels, Water Environment Research 90 (2018) 329–342. https://doi.org/10.2175/106143017X15131012152861.

[175] Y. Mathieu, L. Sauvanaud, L. Humphreys, W. Rowlands, T. Maschmeyer, A. Corma, Opportunities in upgrading biomass crudes, Faraday Discussions 197 (2017) 389–401. https://doi.org/10.1039/C6FD00208K.

[176] J. Lu, Z. Liu, Y. Zhang, P.E. Savage, 110th Anniversary: Influence of Solvents on Biocrude from Hydrothermal Liquefaction of Soybean Oil, Soy Protein, Cellulose, Xylose, and Lignin, and Their Quinary Mixture , Industrial & Engineering Chemistry Research 58 (2019) 13971–13976. https://doi.org/10.1021/acs.iecr.9b02442.

[177] S.B. Iversen, C.U. Jensen, G. Olofsson, J.K.R. Guerrero, A. Ironside, S. Karatzos, L. Li, WO2018177877 - Seperation Method for high pressure processing System, WO/2018/177877, 2018.

[178] H. Jahromi, T. Rahman, P. Roy, S. Adhikari, Hydrotreatment of solvent-extracted biocrude from hydrothermal liquefaction of municipal sewage sludge, Energy Conversion and Management 263 (2022) 115719. https://doi.org/10.1016/J.ENCONMAN.2022.115719.

[179] M.S. Vlaskin, A. V. Grigorenko, Y.I. Kostyukevich, E.N. Nikolaev, G.N. Vladimirov, N.I. Chernova, S. V. Kiseleva, O.S. Popel, A.Z. Zhuk, Influence of solvent on the yield and chemical composition of liquid products of hydrothermal liquefaction of Arthrospira platensis as revealed by Fourier transform ion cyclotron resonance mass spectrometry, European Journal of Mass Spectrometry 24 (2018) 363–374. https://doi.org/10.1177/1469066718771209.

[180] J. Yang, Q. (Sophia) He, K. Corscadden, H. Niu, The impact of downstream processing methods on the yield and physiochemical properties of hydrothermal liquefaction bio-oil, Fuel Processing Technology 178 (2018) 353–361. https://doi.org/10.1016/j.fuproc.2018.07.006.

[181] J. Watson, J. Lu, R. de Souza, B. Si, Y. Zhang, Z. Liu, Effects of the extraction solvents in hydrothermal liquefaction processes: Biocrude oil quality and energy conversion efficiency, Energy 167 (2019) 189–197. https://doi.org/10.1016/j.energy.2018.11.003.

[182] C. Reichardt, T. Welton, Solvents and Solvent Effects in Organic Chemistry, Wiley-VCH Verlag GmbH & Co. KGaA, Weinheim, Germany, 2010. https://doi.org/10.1002/9783527632220.

[183] K.O. Albrecht, Y. Zhu, A.J. Schmidt, J.M. Billing, T.R. Hart, S.B. Jones, G. Maupin, R. Hallen, T. Ahrens, D. Anderson, Impact of heterotrophically stressed algae for biofuel production via hydrothermal liquefaction and catalytic hydrotreating in continuous-flow reactors, Algal Research 14 (2016) 17–27. https://doi.org/10.1016/j.algal.2015.12.008.

[184] J.M. Jarvis, N.M. Sudasinghe, K.O. Albrecht, A.J. Schmidt, R.T. Hallen, D.B. Anderson, J.M. Billing, T.M. Schaub, Impact of iron porphyrin complexes when hydroprocessing algal HTL biocrude, Fuel 182 (2016) 411–418. https://doi.org/10.1016/j.fuel.2016.05.107.

[185] J.M. Jarvis, K.O. Albrecht, J.M. Billing, A.J. Schmidt, R.T. Hallen, T.M. Schaub, Assessment of Hydrotreatment for Hydrothermal Liquefaction Biocrudes from Sewage Sludge, Microalgae, and Pine Feedstocks, Energy & Fuels 32 (2018) 8483–8493. https://doi.org/10.1021/acs.energyfuels.8b01445.

[186] M.S. Haider, S. Chiaberge, A. Siviero, M.A. Isik, D. Castello, T.H. Pedersen, L.A. Rosendahl, Understanding the demetallization of nitrogen-rich hydrothermal liquefaction biocrudes by FTICR mass spectrometry: Recalcitrant effect of metalloporphyrins and basic nitrogenates, Fuel 334 (2023) 126755. https://doi.org/10.1016/j.fuel.2022.126755.

[187] J.G. Speight, The Chemistry and Technology of Petroleum, 5th ed., CRC Press, Boca Raton, 2014. https://doi.org/10.1201/b16559.

[188] M.F. Ali, S. Abbas, A review of methods for the demetallization of residual fuel oils, Fuel Processing Technology 87 (2006) 573–584. https://doi.org/10.1016/J.FUPROC.2006.03.001.

[189] C.U. Jensen, Dissertation: PIUS -H ydrofaction(TM) Platform with Integrated Upgrading Step, Aalborg Universitet, 2018.

[190] M.S. Haider, M.A. Isik, D. Castello, T.H. Pedersen, L.A. Rosendahl, Demineralization of Miscanthus Biocrude Obtained from Catalytic Hydrothermal Liquefaction: Conditioning through Acid Washing, Processes 9 (2021) 1035. https://doi.org/10.3390/pr9061035.

[191] J. Jiang, Dissertation: Demetallation of Biocrude from Hydrothermal Liquefaction of Microalgae, Pennsylvania State University, 2019.

[192] G. Caumette, C.P. Lienemann, I. Merdrignac, B. Bouyssiere, R. Lobinski, Element speciation analysis of petroleum and related materials, Journal of Analytical Atomic Spectrometry 24 (2009) 263–276. https://doi.org/10.1039/b817888g.

[193] A.M. Madgavkar, D.M. Washecheck, US4790930A - Two-step heterocyclic nitrogen extraction from petroleum oils, 1987.

[194] J. Qi, Y. Yan, Y. Su, F. Qu, Y. Dai, Extraction of Nitrogen Compounds from Catalytically Cracked Diesel Oil with a Volatile Carboxylic Acid Based on Reversible Chemical Complexation, Energy & Fuels 12 (1998) 788–791. https://doi.org/10.1021/ef980003l.

[195] Y. Feng, A study on the process conditions of removing basic nitrogen compounds from gasoline, Petroleum Science and Technology 22 (2004) 1517–1525. https://doi.org/10.1081/LFT-200027848.

[196] D.Y. Han, G.X. Li, Z.B. Cao, X.Y. Zhai, M.M. Yuan, A study on the denitrogenation of fushun shale oil, Energy Sources, Part A: Recovery, Utilization and Environmental Effects 35 (2013) 622–628. https://doi.org/10.1080/15567036.2010.509085.

[197] Y. Dote, T. Ogi, S. Yokoyama, T. Minowa, S. Sawayama, T. Hayashi, A. Suzuki, Analysis of Oil Derived from Liquefaction of Sewage Sludge, in: Bridg. A.V. Adv. Thermochem. Biomass Convers., Springer, Dordrecht, 1993: pp. 1378–1384. https://doi.org/10.1007/978-94-011-1336-6_108.

[198] D.D. Das, M.I. Schnitzer, C.M. Monreal, P. Mayer, Chemical composition of acid–base fractions separated from biooil derived by fast pyrolysis of chicken manure, Bioresource Technology 100 (2009) 6524–6532. https://doi.org/10.1016/j.biortech.2009.06.104.

[199] I. Fonts, A. Navarro-Puyuelo, N. Ruiz-Gómez, M. Atienza-Martínez, A. Wisniewski, G. Gea, Assessment of the Production of Value-Added Chemical Compounds from Sewage Sludge Pyrolysis Liquids, Energy Technology 5 (2017) 151–171. https://doi.org/10.1002/ente.201600183.

[200] H. Ben Salah, P. Nancarrow, A. Al-Othman, Ionic liquid-assisted refinery processes – A review and industrial perspective, Fuel 302 (2021) 121195. https://doi.org/10.1016/J.FUEL.2021.121195.

[201] H.F. Hizaddin, M.K. Hadj-Kali, A. Ramalingam, M. Ali Hashim, Extractive denitrogenation of diesel fuel using ammonium- and phosphonium-based deep eutectic solvents, The Journal of Chemical Thermodynamics 95 (2016) 164–173. https://doi.org/10.1016/J.JCT.2015.12.009.

[202] G.C. Laredo, N. V. Likhanova, I. V. Lijanova, B. Rodriguez-Heredia, J.J. Castillo, P. Perez-Romo, Synthesis of ionic liquids and their use for extracting nitrogen compounds from gas oil feeds towards diesel fuel production, Fuel Processing Technology 130 (2015) 38–45. https://doi.org/10.1016/J.FUPROC.2014.08.025.

[203] M.C. Ali, Q. Yang, A.A. Fine, W. Jin, Z. Zhang, H. Xing, Q. Ren, Efficient removal of both basic and non-basic nitrogen compounds from fuels by deep eutectic solvents, Green Chemistry 18 (2015) 157–164. https://doi.org/10.1039/C5GC01823D.

[204] G.C. Laredo, P.M. Vega-Merino, F. Trejo-Zárraga, J. Castillo, Denitrogenation of middle distillates using adsorbent materials towards ULSD production: A review, Fuel Processing Technology 106 (2013) 21–32. https://doi.org/10.1016/j.fuproc.2012.09.057.

[205] B.M. Cieślik, J. Namieśnik, P. Konieczka, Review of sewage sludge management: standards, regulations and analytical methods, Journal of Cleaner Production 90 (2015) 1–15. https://doi.org/10.1016/j.jclepro.2014.11.031.

[206] L. Qian, S. Wang, D. Xu, Y. Guo, X. Tang, L. Wang, Treatment of municipal sewage sludge in supercritical water: A review, Water Research 89 (2016) 118–131. https://doi.org/10.1016/J.WATRES.2015.11.047.

[207] Umweltbundesamt, KLÄRSCHLAMM- ENTSORGUNG in der Bundesrepublik Deutschland, (n.d.). www.umweltbundesamt.de (accessed November 22, 2022).

[208] Verordnung über die Verwertung von Klärschlamm,Klärschlammgemisch und Klärschlammkompost(Klärschlammverordnung - AbfKlärV), 2017. www.gesetze-im-internet.de (accessed November 24, 2022).

[209] A. Bauen, N. Bitossi, L. German, A. Harris, K. Leow, Sustainable Aviation Fuels, Johnson Matthey Technology Review 64 (2020) 234–235. https://doi.org/10.1595/205651320X15816756012040.

[210] T.H. Pedersen, C.U. Jensen, L. Sandström, L.A. Rosendahl, Full characterization of compounds obtained from fractional distillation and upgrading of a HTL biocrude, Applied Energy 202 (2017) 408–419. https://doi.org/10.1016/j.apenergy.2017.05.167.

[211] E. Ovsyannikova, A. Kruse, G.C. Becker, Feedstock-Dependent Phosphate Recovery in a Pilot-Scale Hydrothermal Liquefaction Bio-Crude Production, Energies 13 (2020) 379. https://doi.org/10.3390/en13020379.

[212] R.B. Madsen, M. Glasius, How Do Hydrothermal Liquefaction Conditions and Feedstock Type Influence Product Distribution and Elemental Composition?, Industrial & Engineering Chemistry Research 58 (2019) 17583–17600. https://doi.org/10.1021/acs.iecr.9b02337.

[213] D.R. Vardon, B.K. Sharma, J. Scott, G. Yu, Z. Wang, L. Schideman, Y. Zhang, T.J. Strathmann, Chemical properties of biocrude oil from the hydrothermal liquefaction of Spirulina algae, swine manure, and digested anaerobic sludge, Bioresource Technology 102 (2011) 8295–8303. https://doi.org/10.1016/j.biortech.2011.06.041.

[214] Techne, SBL-1, SBL-2, SBL-2D Fluidised Baths; Operator's Manual, (2003). http://www.techne-calibration.com/adminimages/Techne_SBL1_2_2D.pdf (accessed August 8, 2020).

[215] VDLUFA Methodenbuch, Band III, Verband Deutscher Landwirtschaftlicher Untersuchungs- und Forschungsanstalten, 1976.

[216] W.H.J. Hattingh, P.G. Thiel, M.L. Siebert, Determination of protein content of anaerobic digesting sludge, Water Research 1 (1967) 185–189. https://doi.org/10.1016/0043-1354(67)90008-5.

[217] F. Mariotti, D. Tomé, P.P. Mirand, Converting Nitrogen into Protein—Beyond 6.25 and Jones' Factors, Critical Reviews in Food Science and Nutrition 48 (2008) 177–184. https://doi.org/10.1080/10408390701279749.

[218] S.A. Channiwala, P.P. Parikh, A unified correlation for estimating HHV of solid, liquid and gaseous fuels, Fuel 81 (2002) 1051–1063. https://doi.org/10.1016/S0016-2361(01)00131-4.

[219] P. Manara, A. Zabaniotou, Towards sewage sludge based biofuels via thermochemical conversion – A review, Renewable and Sustainable Energy Reviews 16 (2012) 2566–2582. https://doi.org/10.1016/j.rser.2012.01.074.

[220] H.-C. Flemming, Sorption sites in biofilms, Water Science and Technology 32 (1995) 27–33. https://doi.org/10.2166/wst.1995.0256.

[221] L. Karygianni, Z. Ren, H. Koo, T. Thurnheer, Biofilm Matrixome: Extracellular Components in Structured Microbial Communities, Trends in Microbiology 28 (2020) 668–681. https://doi.org/10.1016/j.tim.2020.03.016.

[222] Z. Wu, R.P. Rodgers, A.G. Marshall, Two- and Three-Dimensional van Krevelen Diagrams: A Graphical Analysis Complementary to the Kendrick Mass Plot for Sorting Elemental Compositions of Complex Organic Mixtures Based on Ultrahigh-Resolution Broadband Fourier Transform Ion Cyclotron Resonance, Analytical Chemistry 76 (2004) 2511–2516. https://doi.org/10.1021/ac0355449.

[223] H. Chowdhury, B. Loganathan, Third-generation biofuels from microalgae: a review, Current Opinion in Green and Sustainable Chemistry 20 (2019) 39–44. https://doi.org/10.1016/j.cogsc.2019.09.003.

[224] A. Kruse, E. Dinjus, Hot compressed water as reaction medium and reactant, The Journal of Supercritical Fluids 39 (2007) 362–380. https://doi.org/10.1016/j.supflu.2006.03.016.

[225] P. Biller, A.B. Ross, Production of biofuels via hydrothermal conversion, Elsevier Ltd, 2016. https://doi.org/10.1016/B978-0-08-100455-5.00017-5.

[226] P. SundarRajan, K.P. Gopinath, J. Arun, K. GracePavithra, A. Adithya Joseph, S. Manasa, Insights into valuing the aqueous phase derived from hydrothermal liquefaction, Renewable and Sustainable Energy Reviews 144 (2021) 111019. https://doi.org/10.1016/j.rser.2021.111019.

[227] L. Leng, W. Zhang, H. Peng, H. Li, S. Jiang, H. Huang, Nitrogen in bio-oil produced from hydrothermal liquefaction of biomass: A review, Chemical Engineering Journal 401 (2020) 126030. https://doi.org/10.1016/j.cej.2020.126030.

[228] M.S. Haider, D. Castello, K.M. Michalski, T.H. Pedersen, L.A. Rosendahl, Catalytic hydrotreatment of microalgae biocrude from continuous hydrothermal liquefaction: Heteroatom removal and their distribution in distillation cuts, Energies 11 (2018). https://doi.org/10.3390/en11123360.

[229] E. Furimsky, Catalytic hydrodeoxygenation, Applied Catalysis A: General 199 (2000) 147–190. https://doi.org/10.1016/S0926-860X(99)00555-4.

[230] D. Leckel, Catalytic hydroprocessing of coal-derived gasification residues to fuel blending stocks: Effect of reaction variables and catalyst on hydrodeoxygenation (HDO), hydrodenitrogenation (HDN), and hydrodesulfurization (HDS), Energy & Fuels 20 (2006) 1761–1766. https://doi.org/10.1021/ef060034d.

[231] T. V. Choudhary, S. Parrott, B. Johnson, Understanding the hydrodenitrogenation chemistry of heavy oils, Catalysis Communications 9 (2008) 1853–1857. https://doi.org/10.1016/j.catcom.2008.03.002.

[232] K. Kohansal, K. Sharma, M.S. Haider, S.S. Toor, D. Castello, L.A. Rosendahl, J. Zimmermann, T.H. Pedersen, Hydrotreating of bio-crude obtained from hydrothermal liquefaction of biopulp: effects of aqueous phase recirculation on the hydrotreated oil, Sustainable Energy & Fuels 6 (2022) 2805–2822. https://doi.org/10.1039/D2SE00399F.

[233] J. Zimmermann, K. Raffelt, N. Dahmen, Sequential Hydrothermal Processing of Sewage Sludge to Produce Low Nitrogen Biocrude, Processes 9 (2021) 491. https://doi.org/:

[234] Swiss-Model, Crystaline Structure of Bovine Serum albumin - Bos taurus, (2022). https://swissmodel.expasy.org/repository/uniprot/P02769?template=3v03.

[235] D. Jung, M. Zimmermann, A. Kruse, Hydrothermal Carbonization of Fructose: Growth Mechanism and Kinetic Model, ACS Sustainable Chemistry & Engineering (2018) acssuschemeng.8b02118. http://pubs.acs.org/doi/10.1021/acssuschemeng.8b02118 (accessed October 14, 2018).

[236] X. Chen, X. Peng, X. Ma, J. Wang, Investigation of Mannich reaction during co-liquefaction of microalgae and sweet potato waste, Bioresource Technology 284 (2019) 286–292. https://doi.org/10.1016/j.biortech.2019.03.136.

[237] M. Alhnidi, J.W. Straten, S.A. Nicolae, V. Hoffmann, M. Titirici, A. Kruse, Thermal treatment versus hydrothermal carbonization: How to synthesize <scp>nitrogen-enriched</scp> carbon materials for energy storage applications?, International Journal of Energy Research 46 (2022) 1622–1636. https://doi.org/10.1002/er.7275.

[238] A. Gollakota, P.E. Savage, Hydrothermal Liquefaction of Model Food Waste Biomolecules and Ternary Mixtures under Isothermal and Fast Conditions, ACS Sustainable Chemistry and Engineering 6 (2018) 9018–9027. https://doi.org/10.1021/acssuschemeng.8b01368.

[239] A. Kruse, N. Dahmen, Hydrothermal biomass conversion: Quo vadis?, Journal of Supercritical Fluids 134 (2017) 114–123. https://doi.org/10.1016/j.supflu.2017.12.035.

[240] J. Zimmermann, S. Chiaberge, S.B. Iversen, K. Raffelt, N. Dahmen, Sequential Extraction and Characterization of Nitrogen Compounds after Hydrothermal Liquefaction of Sewage Sludge, Energy & Fuels 36 (2022) 14292–14303. https://doi.org/10.1021/acs.energyfuels.2c02622.

[241] X. Fu, Y. Liao, C.R. Glein, M. Jamison, K. Hayes, J. Zaporski, Z. Yang, Direct Synthesis of Amides from Amines and Carboxylic Acids under Hydrothermal Conditions, ACS Earth and Space Chemistry 4 (2020) 722–729. https://doi.org/10.1021/acsearthspacechem.0c00009.

[242] N. Kitadai, Thermodynamic Prediction of Glycine Polymerization as a Function of Temperature and pH Consistent with Experimentally Obtained Results, Journal of Molecular Evolution 78 (2014) 171–187. https://doi.org/10.1007/s00239-014-9616-1.

[243] W. Abdelmoez, H. Yoshida, T. Nakahasi, Pathways of Amino Acid Transformation and Decomposition in Saturated Subcritical Water Conditions, International Journal of Chemical Reactor Engineering 8 (2010). https://doi.org/10.2202/1542-6580.1903.

[244] M.N. Islam, T. Kaneko, K. Kobayashi, Reaction of Amino Acids in a Supercritical Water-Flow Reactor Simulating Submarine Hydrothermal Systems, Bulletin of the Chemical Society of Japan 76 (2003) 1171–1178. https://doi.org/10.1246/bcsj.76.1171.

[245] R. Weingarten, W.C. Conner, G.W. Huber, Production of levulinic acid from cellulose by hydrothermal decomposition combined with aqueous phase dehydration with a solid acid catalyst, Energy and Environmental Science 5 (2012) 7559–7574. https://doi.org/10.1039/c2ee21593d.

[246] A. Sinag, A. Kruse, V. Schwarzkopf, Key compounds of the hydropyrolysis of glucose in supercritical water in the presence of K2CO3, Industrial and Engineering Chemistry Research 42 (2003) 3516–3521. https://doi.org/10.1021/ie030079r.

[247] J. Remón, M. Laseca, L. García, J. Arauzo, Hydrogen production from cheese whey by catalytic steam reforming: Preliminary study using lactose as a model compound, Energy Conversion and Management 114 (2016) 122–141. https://doi.org/10.1016/j.enconman.2016.02.009.

[248] F. Van Lancker, A. Adams, N. De Kimpe, Formation of Pyrazines in Maillard Model Systems of Lysine-Containing Dipeptides, Journal of Agricultural and Food Chemistry 58 (2010) 2470–2478. https://doi.org/10.1021/jf903898t.

[249] R.B. Madsen, P. Biller, M.M. Jensen, J. Becker, B.B. Iversen, M. Glasius, Predicting the Chemical Composition of Aqueous Phase from Hydrothermal Liquefaction of Model Compounds and Biomasses, Energy & Fuels 30 (2016) 10470–10483. https://doi.org/10.1021/acs.energyfuels.6b02007.

[250] F.W. Lichtenthaler, Unsaturated O - and N -Heterocycles from Carbohydrate Feedstocks, Accounts of Chemical Research 35 (2002) 728–737. https://doi.org/10.1021/ar010071i.

[251] B. Wozniak, S. Tin, J.G. de Vries, Bio-based building blocks from 5-hydroxymethylfurfural via 1-hydroxyhexane-2,5-dione as intermediate, Chemical Science 10 (2019) 6024–6034. https://doi.org/10.1039/C9SC01309A.

[252] A.R. Katritzky, F.J. Luxem, R. Murugan, J. V. Greenhill, M. Siskin, Aqueous high-temperature chemistry of carbo- and heterocycles. 19. Pyrroles and indoles, Energy & Fuels 6 (1992) 450–455. https://doi.org/10.1021/ef00034a014.

[253] Y. Fan, U. Hornung, N. Dahmen, Hydrothermal liquefaction of sewage sludge for biofuel application: A review on fundamentals, current challenges and strategies, Biomass and Bioenergy 165 (2022) 106570. https://doi.org/10.1016/j.biombioe.2022.106570.

[254] S. Inoue, K. Okigawa, T. Minowa, T. Ogi, Liquefaction of ammonia and cellulose: effect of nitrogen/carbon ratio in the feedstock, Biomass and Bioenergy 16 (1999) 377–383. https://doi.org/10.1016/S0961-9534(99)00003-3.

[255] C.U. Jensen, L.A. Rosendahl, G. Olofsson, Impact of nitrogenous alkaline agent on continuous HTL of lignocellulosic biomass and biocrude upgrading, Fuel Processing Technology 159 (2017) 376–385. https://doi.org/10.1016/j.fuproc.2016.12.022.

[256] Eurostat, Sewage sludge production and disposal in the EU, (2020). http://appsso.eurostat.ec.europa.eu/nui/submitViewTableAction.do (accessed August 8, 2020).

[257] M.C. Collivignarelli, A. Abbà, M.C. Miino, V. Torretta, What advanced treatments can be used to minimize the production of sewage sludge in WWTPs?, Applied Sciences 9 (2019) 1–24. https://doi.org/10.3390/app9132650.

[258] M. Collivignarelli, A. Abbà, A. Frattarola, M. Carnevale Miino, S. Padovani, I. Katsoyiannis, V. Torretta, Legislation for the Reuse of Biosolids on Agricultural Land in Europe: Overview, Sustainability 11 (2019) 6015. https://doi.org/10.3390/su11216015.

[259] A.M. Mahon, B. O'Connell, M.G. Healy, I. O'Connor, R. Officer, R. Nash, L. Morrison, Microplastics in Sewage Sludge: Effects of Treatment, Environmental Science & Technology 51 (2017) 810–818. https://doi.org/10.1021/acs.est.6b04048.

[260] M. Thomsen, M. Seghetta, M.H. Mikkelsen, S. Gyldenkærne, T. Becker, D. Caro, P. Frederiksen, Comparative life cycle assessment of biowaste to resource management systems – A Danish case study, Journal of Cleaner Production 142 (2017) 4050–4058. https://doi.org/10.1016/j.jclepro.2016.10.034.

[261] X. Hao, Q. Chen, M.C.M. van Loosdrecht, J. Li, H. Jiang, Sustainable disposal of excess sludge: Incineration without anaerobic digestion, Water Research 170 (2020). https://doi.org/10.1016/j.watres.2019.115298.

[262] X. Yin, P. Han, X. Lu, Y. Wang, A review on the dewaterability of bio-sludge and ultrasound pretreatment, Ultrasonics Sonochemistry 11 (2004) 337–348. https://doi.org/10.1016/j.ultsonch.2004.02.005.

[263] M.T. Munir, S.S. Mansouri, I.A. Udugama, S. Baroutian, K. V. Gernaey, B.R. Young, Resource recovery from organic solid waste using hydrothermal processing: Opportunities and challenges, Renewable and Sustainable Energy Reviews 96 (2018) 64–75. https://doi.org/10.1016/j.rser.2018.07.039.

[264] F. Conti, S.S. Toor, T.H. Pedersen, T.H. Seehar, A.H. Nielsen, L.A. Rosendahl, Valorization of animal and human wastes through hydrothermal liquefaction for biocrude production and simultaneous recovery of nutrients, Energy Conversion and Management 216 (2020) 112925. https://doi.org/10.1016/j.enconman.2020.112925.

[265] J.G. Speight, Handbook of Petroleum Product Analysis, John Wiley & Sons, Inc, Hoboken, NJ, 2014. https://doi.org/10.1002/9781118986370.

[266] F. Obeid, T. Chu Van, R. Brown, T. Rainey, Nitrogen and sulphur in algal biocrude: A review of the HTL process, upgrading, engine performance and emissions, Energy Conversion and Management 181 (2019) 105–119. https://doi.org/10.1016/j.enconman.2018.11.054.

[267] X. Gu, L. Yu, N. Pang, J.S. Martinez-Fernandez, X. Fu, S. Chen, Comparative techno-economic analysis of algal biofuel production via hydrothermal liquefaction: One stage versus two stages, Applied Energy 259 (2020) 114115. https://doi.org/10.1016/j.apenergy.2019.114115.

[268] X. Zhuang, Y. Huang, Y. Song, H. Zhan, X. Yin, C. Wu, The transformation pathways of nitrogen in sewage sludge during hydrothermal treatment, Bioresource Technology 245 (2017) 463–470. https://doi.org/10.1016/j.biortech.2017.08.195.

[269] P. Zhao, H. Chen, S. Ge, K. Yoshikawa, Effect of the hydrothermal pretreatment for the reduction of NO emission from sewage sludge combustion, Applied Energy 111 (2013) 199–205. https://doi.org/10.1016/j.apenergy.2013.05.029.

[270] H. Yoshida, O. Tavakoli, Sub-critical Water Hydrolysis Treatment for Waste Squid Entrails and Production of Amino Acids, Organic Acids, and Fatty Acids, JOURNAL OF CHEMICAL ENGINEERING OF JAPAN 37 (2004) 253–260. https://doi.org/10.1252/jcej.37.253.

[271] X. Zhu, C. Zhu, L. Zhao, H. Cheng, Amino Acids Production from Fish Proteins Hydrolysis in Subcritical Water, Chinese Journal of Chemical Engineering 16 (2008) 456–460. https://doi.org/10.1016/S1004-9541(08)60105-6.

[272] B. Guo, B. Yang, A. Silve, S. Akaberi, D. Scherer, I. Papachristou, W. Frey, U. Hornung, N. Dahmen, Hydrothermal liquefaction of residual microalgae biomass after pulsed electric field-assisted valuables extraction, Algal Research 43 (2019) 101650. https://doi.org/10.1016/j.algal.2019.101650.

[273] E. Commission, Commission regulation (EC) No 152/2009 of 27 January 2009 laying down the methods of sampling and analysis for the official control of feed, Official Journal of the European Union (2009) 1–130.

[274] L. Bai, D.D. Carlton, K.A. Schug, Complex mixture quantification without calibration using gas chromatography and a comprehensive carbon reactor in conjunction with flame ionization detection, Journal of Separation Science 41 (2018) 4031–4037. https://doi.org/10.1002/jssc.201800383.

[275] G. Lepage, C.C. Roy, Direct transesterification of all classes of lipids in a one-step reaction., Journal of Lipid Research 27 (1986) 114–120. https://doi.org/10.1016/S0022-2275(20)38861-1.

[276] C.A. Mullen, G.D. Strahan, A.A. Boateng, Characterization of Various Fast-Pyrolysis Bio-Oils by NMR Spectroscopy †, Energy & Fuels 23 (2009) 2707–2718. https://doi.org/10.1021/ef801048b.

[277] G.R. Fulmer, A.J.M. Miller, N.H. Sherden, H.E. Gottlieb, A. Nudelman, B.M. Stoltz, J.E. Bercaw, K.I. Goldberg, NMR Chemical Shifts of Trace Impurities: Common Laboratory Solvents, Organics, and Gases in Deuterated Solvents Relevant to the Organometallic Chemist, Organometallics 29 (2010) 2176–2179. https://doi.org/10.1021/om100106e.

[278] G.W. Huber, A. Corma, Synergies between Bio- and Oil Refineries for the Production of Fuels from Biomass, Angewandte Chemie International Edition 46 (2007) 7184–7201. https://doi.org/10.1002/anie.200604504.

[279] M. Park, N. Kim, S. Lee, S. Yeon, J.H. Seo, D. Park, A study of solubilization of sewage sludge by hydrothermal treatment, Journal of Environmental Management 250 (2019) 109490. https://doi.org/10.1016/j.jenvman.2019.109490.

[280] E. Neyens, J. Baeyens, M. Weemaes, B. De Heyder, Hot acid hydrolysis as a potential treatment of thickened sewage sludge, Journal of Hazardous Materials 98 (2003) 275–293. https://doi.org/10.1016/S0304-3894(03)00002-5.

[281] S. Chen, B. Dong, X. Dai, H. Wang, N. Li, D. Yang, Effects of thermal hydrolysis on the metabolism of amino acids in sewage sludge in anaerobic digestion, Waste Management 88 (2019) 309–318. https://doi.org/10.1016/j.wasman.2019.03.060.

[282] C.A. Wilson, J.T. Novak, Hydrolysis of macromolecular components of primary and secondary wastewater sludge by thermal hydrolytic pretreatment, Water Research 43 (2009) 4489–4498. https://doi.org/10.1016/j.watres.2009.07.022.

[283] Y. Xue, H. Liu, S. Chen, N. Dichtl, X. Dai, N. Li, Effects of thermal hydrolysis on organic matter solubilization and anaerobic digestion of high solid sludge, Chemical Engineering Journal 264 (2015) 174–180. https://doi.org/10.1016/j.cej.2014.11.005.

[284] T. Yuan, Y. Cheng, Z. Zhang, Z. Lei, K. Shimizu, Comparative study on hydrothermal treatment as pre- and post-treatment of anaerobic digestion of primary sludge: Focus on energy balance, resources transformation and sludge dewaterability, Applied Energy 239 (2019) 171–180. https://doi.org/10.1016/j.apenergy.2019.01.206.

[285] H.-D. Belitz, W. Grosch, P. Schieberle, Amino Acids, Peptides, Proteins, in: Food Chem., Springer Berlin Heidelberg, Berlin, Heidelberg, 2008: pp. 8–92. https://doi.org/10.1007/978-3-540-69934-7_2.

[286] G. Brunner, Processing of Biomass with Hydrothermal and Supercritical Water, in: Hydrothermal Supercrit. Water Process., Elsevier, 2014: pp. 395–509. https://doi.org/10.1016/B978-0-444-59413-6.00008-X.

[287] E. Andersson, N.G. Holm, The stability of some selected amino acids under attempted redox constrained hydrothermal conditions, Origins of Life and Evolution of the Biosphere 30 (2000) 9–23. https://doi.org/10.1023/a:1006668322298.

[288] S.I.F.S. Martins, M.A.J.S. Van Boekel, A kinetic model for the glucose/glycine Maillard reaction pathways, Food Chemistry 90 (2005) 257–269. https://doi.org/10.1016/j.foodchem.2004.04.006.

[289] V. Hoffmann, D. Jung, J. Zimmermann, C.R. Correa, A. Elleuch, K. Halouani, A. Kruse, Conductive carbon materials from the hydrothermal carbonization of vineyard residues for the application in electrochemical double-layer capacitors (EDLCs) and direct carbon fuel cells (DCFCs), Materials 12 (2019). https://doi.org/10.3390/MA12101703.

[290] Y.-. Y. Li, T. Noike, Upgrading of Anaerobic Digestion of Waste Activated Sludge by Thermal Pretreatment, Water Science and Technology 26 (1992) 857–866. https://doi.org/10.2166/wst.1992.0466.

[291] S. Yin, Z. Tan, Hydrothermal liquefaction of cellulose to bio-oil under acidic, neutral and alkaline conditions, Applied Energy 92 (2012) 234–239. https://doi.org/10.1016/j.apenergy.2011.10.041.

[292] A. Demirbaş, Mechanisms of liquefaction and pyrolysis reactions of biomass, Energy Conversion and Management 41 (2000) 633–646. https://doi.org/10.1016/S0196-8904(99)00130-2.

[293] E. Chornet, R.P. Overend, Biomass Liquefaction: An Overview, in: Fundam. Thermochem. Biomass Convers., Springer Netherlands, Dordrecht, 1985: pp. 967–1002. https://doi.org/10.1007/978-94-009-4932-4_54.

[294] W. Chen, W. Qian, Y. Zhang, Z. Mazur, C. Kuo, K. Scheppe, L.C. Schideman, B.K. Sharma, Effect of ash on hydrothermal liquefaction of high-ash content algal biomass, Algal Research 25 (2017) 297–306. https://doi.org/10.1016/j.algal.2017.05.010.

[295] K.H. Zapp, K.H. Wostbrock, M. Schäfer, S. Kimihiko, H. Seiter, W. Zwick, R. Creutziger, H. Leiter, Ammonium Compounds, (2012). https://doi.org/10.1002/14356007.a02.

[296] L. Qian, S. Wang, P.E. Savage, Fast and isothermal hydrothermal liquefaction of sludge at different severities: Reaction products, pathways, and kinetics, Applied Energy 260 (2020) 114312. https://doi.org/10.1016/j.apenergy.2019.114312.

[297] H. Pińkowska, P. Wolak, A. Złocińska, Hydrothermal decomposition of alkali lignin in sub- and supercritical water, Chemical Engineering Journal 187 (2012) 410–414. https://doi.org/10.1016/j.cej.2012.01.092.

[298] X. Liu, M. Yang, Z. Deng, A. Dasgupta, Y. Guo, Hydrothermal hydrodeoxygenation of palmitic acid over Pt/C catalyst: Mechanism and kinetic modeling, Chemical Engineering Journal 407 (2021) 126332. https://doi.org/10.1016/j.cej.2020.126332.

[299] L. Garcia Alba, C. Torri, C. Samorì, J. van der Spek, D. Fabbri, S.R.A. Kersten, D.W.F. (Wim) Brilman, Hydrothermal Treatment (HTT) of Microalgae: Evaluation of the Process As Conversion Method in an Algae Biorefinery Concept, Energy & Fuels 26 (2012) 642–657. https://doi.org/10.1021/ef201415s.

[300] D. V. McCalley, M. Cooke, G. Nickless, Effect of sewage treatment on faecal sterols, Water Research 15 (1981) 1019–1025. https://doi.org/10.1016/0043-1354(81)90211-6.

[301] S.C. Moldoveanu, Analytical pyrolysis of other natural organic polymers, in: Anal. Pyrolysis Nat. Org. Polym., 1st ed., Elsevier, 2021: pp. 427–429. https://doi.org/10.1016/B978-0-12-818571-1.00012-1.

[302] C. He, K. Wang, Y. Yang, P.N. Amaniampong, J.-Y. Wang, Effective Nitrogen Removal and Recovery from Dewatered Sewage Sludge Using a Novel Integrated System of Accelerated Hydrothermal Deamination and Air Stripping, Environmental Science & Technology 49 (2015) 6872–6880. https://doi.org/10.1021/acs.est.5b00652.

[303] C. Gai, Y. Zhang, W.-T. Chen, P. Zhang, Y. Dong, Energy and nutrient recovery efficiencies in biocrude oil produced via hydrothermal liquefaction of Chlorella pyrenoidosa, RSC Advances 4 (2014) 16958. https://doi.org/10.1039/c3ra46607h.

[304] L. Ingram, D. Mohan, M. Bricka, P. Steele, D. Strobel, D. Crocker, B. Mitchell, J. Mohammad, K. Cantrell, C.U. Pittman, Pyrolysis of Wood and Bark in an Auger Reactor: Physical Properties and Chemical Analysis of the Produced Bio-oils, Energy & Fuels 22 (2008) 614–625. https://doi.org/10.1021/ef700335k.

[305] L. Korving, M. Van Loosdrecht, P. Wilfert, Effect of Iron on Phosphate Recovery from Sewage Sludge, in: Phosphorus Recover. Recycl., Springer Singapore, Singapore, 2019: pp. 303–326. https://doi.org/10.1007/978-981-10-8031-9_21.

[306] D. Castello, T.H. Pedersen, L.A. Rosendahl, Continuous Hydrothermal Liquefaction of Biomass: A Critical Review, Energies 11 (2018) 3165. https://doi.org/10.3390/en11113165.

[307] A.R.K. Gollakota, N. Kishore, S. Gu, A review on hydrothermal liquefaction of biomass, Renewable and Sustainable Energy Reviews 81 (2018) 1378–1392. https://doi.org/10.1016/j.rser.2017.05.178.

[308] L.B. Silva Thomsen, P.N. Carvalho, J.S. dos Passos, K. Anastasakis, K. Bester, P. Biller, Hydrothermal liquefaction of sewage sludge; energy considerations and fate of micropollutants during pilot scale processing, Water Research 183 (2020) 116101. https://doi.org/10.1016/j.watres.2020.116101.

[309] R. Chand, K.K. Sadetmahaleh, T.H. Pedersen, S. Toor, J. Vollertsen, The fate of microplastics when making sludge into crude oil–the impact of a hydrothermal liquefaction process on microplastics in wastewater treatment plant sludge., Micro2020: Fate and Impacts of Microplastics: Knowledge and Responsibilities (2020).

[310] A. Chacón-Parra, D. Lewis, P. van Eyk, The effect of ethanol as a homogeneous catalyst on the reaction kinetics of hydrothermal liquefaction of lipids, Chemical Engineering Journal 414 (2021) 128832. https://doi.org/10.1016/j.cej.2021.128832.

[311] R.B. Madsen, H. Zhang, P. Biller, A.H. Goldstein, M. Glasius, Characterizing Semivolatile Organic Compounds of Biocrude from Hydrothermal Liquefaction of Biomass, Energy & Fuels 31 (2017) 4122–4134. https://doi.org/10.1021/acs.energyfuels.7b00160.

[312] T.H. Pedersen, L.A. Rosendahl, Production of fuel range oxygenates by supercritical hydrothermal liquefaction of lignocellulosic model systems, Biomass and Bioenergy 83 (2015) 206–215. https://doi.org/10.1016/j.biombioe.2015.09.014.

[313] E. Panisko, T. Wietsma, T. Lemmon, K. Albrecht, D. Howe, Characterization of the aqueous fractions from hydrotreatment and hydrothermal liquefaction of lignocellulosic feedstocks, Biomass and Bioenergy 74 (2015) 162–171. https://doi.org/10.1016/j.biombioe.2015.01.011.

[314] F. Zhu, L. Zhao, H. Jiang, Z. Zhang, Y. Xiong, J. Qi, J. Wang, Comparison of the Lipid Content and Biodiesel Production from Municipal Sludge Using Three Extraction Methods, Energy & Fuels 28 (2014) 5277–5283. https://doi.org/10.1021/ef500730c.

[315] D.C. Elliott, T.R. Hart, G.G. Neuenschwander, L.J. Rotness, G. Roesijadi, A.H. Zacher, J.K. Magnuson, Hydrothermal Processing of Macroalgal Feedstocks in Continuous-Flow Reactors, (2013). https://doi.org/10.1021/sc400251p.

[316] D. Castello, M.S. Haider, L.A. Rosendahl, Catalytic upgrading of hydrothermal liquefaction biocrudes: Different challenges for different feedstocks, Renewable Energy 141 (2019) 420–430. https://doi.org/10.1016/j.renene.2019.04.003.

[317] M.S. Haider, D. Castello, L.A. Rosendahl, The Art of Smooth Continuous Hydroprocessing of Biocrudes Obtained from Hydrothermal Liquefaction: Hydrodemetallization and Propensity for Coke Formation, Energy & Fuels 35 (2021) 10611–10622. https://doi.org/10.1021/acs.energyfuels.1c01228.

[318] H. Wu, H. Li, Z. Fang, Hydrothermal amination of biomass to nitrogenous chemicals, Green Chemistry 23 (2021) 6675–6697. https://doi.org/10.1039/d1gc02505h.

[319] U. Ekpo, A.B. Ross, M.A. Camargo-Valero, L.A. Fletcher, Influence of pH on hydrothermal treatment of swine manure: Impact on extraction of nitrogen and phosphorus in process water, Bioresource Technology 214 (2016) 637–644. https://doi.org/10.1016/j.biortech.2016.05.012.

[320] W.T. Chen, L. Tang, W. Qian, K. Scheppe, K. Nair, Z. Wu, C. Gai, P. Zhang, Y. Zhang, Extract Nitrogen-Containing Compounds in Biocrude Oil Converted from Wet Biowaste via Hydrothermal Liquefaction, ACS Sustainable Chemistry and Engineering 4 (2016) 2182–2190. https://doi.org/10.1021/acssuschemeng.5b01645.

[321] Z.H. Kazi, M.I. Schnitzer, C.M. Monreal, P. Mayer, Separation and identification of heterocyclic nitrogen compounds in biooil derived by fast pyrolysis of chicken manure, Journal of Environmental Science and Health, Part B 46 (2010) 51–61. https://doi.org/10.1080/03601234.2010.515506.

[322] L. Garcia Alba, C. Torri, C. Samorì, J. van der Spek, D. Fabbri, S.R.A. Kersten, D.W.F. (Wim) Brilman, Hydrothermal Treatment (HTT) of Microalgae: Evaluation of the Process As Conversion Method in an Algae Biorefinery Concept, Energy & Fuels 26 (2012) 642–657. https://doi.org/10.1021/ef201415s.

[323] J. Han, X. Li, S. Kong, G. Xian, H. Li, X. Li, J. Li, J. Zhang, H. Meng, H. Wang, H. Du, F. Zeng, Characterization of column chromatography separated bio-oil obtained from hydrothermal liquefaction of Spirulina, Fuel 297 (2021) 120695. https://doi.org/10.1016/j.fuel.2021.120695.

[324] D.G.B. Boocock, R.K.M.R. Kallury, T.T. Tidwell, Analysis of Oil Fractions Derived from Hydrogenation of Aspen Wood, Analytical Chemistry 55 (1983) 1689–1694. https://doi.org/10.1021/ac00261a012.

[325] A.N. Kozhinov, K.O. Zhurov, Y.O. Tsybin, Iterative method for mass spectra recalibration via empirical estimation of the mass calibration function for fourier transform mass spectrometry-based petroleomics, Analytical Chemistry 85 (2013) 6437–6445. https://doi.org/10.1021/ac400972y.

[326] ChemSpider Database, Royal Society of Chemistry (2021). http://www.chemspider.com/ (accessed November 25, 2021).

[327] S. Chiaberge, A. Siviero, C. Passerini, S. Pavoni, D. Bianchi, M.S. Haider, D. Castello, Co-processing of Hydrothermal Liquefaction Sewage Sludge Biocrude with a Fossil Crude Oil by Codistillation: A Detailed Characterization Study by FTICR Mass Spectrometry, Energy & Fuels 35 (2021) 13830–13839. https://doi.org/10.1021/acs.energyfuels.1c01673.

[328] A.K. Huba, K. Huba, P.R. Gardinali, Understanding the atmospheric pressure ionization of petroleum components: The effects of size, structure, and presence of heteroatoms, Science of the Total Environment 568 (2016) 1018–1025. https://doi.org/10.1016/j.scitotenv.2016.06.044.

[329] J.M. Jarvis, J.M. Billing, R.T. Hallen, A.J. Schmidt, T.M. Schaub, Hydrothermal Liquefaction Biocrude Compositions Compared to Petroleum Crude and Shale Oil, Energy & Fuels 31 (2017) 2896–2906. https://doi.org/10.1021/acs.energyfuels.6b03022.

[330] J.P. Cao, X.Y. Zhao, K. Morishita, X.Y. Wei, T. Takarada, Fractionation and identification of organic nitrogen species from bio-oil produced by fast pyrolysis of sewage sludge, Bioresource Technology 101 (2010) 7648–7652. https://doi.org/10.1016/j.biortech.2010.04.073.

[331] H. Walba, R. Ruiz-Velasco, LFER [Linear Free Energy Relations] for amphoteric 5- (or 6-)substituted benzimidazoles, The Journal of Organic Chemistry 34 (1969) 3315–3320. https://doi.org/10.1021/jo01263a020.

[332] N. Sudasinghe, B. Dungan, P. Lammers, K. Albrecht, D. Elliott, R. Hallen, T. Schaub, High resolution FT-ICR mass spectral analysis of bio-oil and residual water soluble organics produced by hydrothermal liquefaction of the marine microalga Nannochloropsis salina, Fuel 119 (2014) 47–56. https://doi.org/10.1016/j.fuel.2013.11.019.

[333] M. Murata, Browning and pigmentation in food through the Maillard reaction, Glycoconjugate Journal 38 (2021) 283–292. https://doi.org/10.1007/s10719-020-09943-x.

[334] J.M. Jarvis, J.M. Billing, R.T. Hallen, A.J. Schmidt, T.M. Schaub, Hydrothermal Liquefaction Biocrude Compositions Compared to Petroleum Crude and Shale Oil, Energy & Fuels 31 (2017) 2896–2906. https://doi.org/10.1021/acs.energyfuels.6b03022.

[335] L. He, Y. Ma, C. Yue, J. Wu, S. Li, Q. Wang, B. Wang, Transformation mechanisms of organic S/N/O compounds during microwave pyrolysis of oil shale: A comparative research with conventional pyrolysis, Fuel Processing Technology 212 (2021). https://doi.org/10.1016/j.fuproc.2020.106605.

[336] A. Gaspar, E. Zellermann, S. Lababidi, J. Reece, W. Schrader, Characterization of Saturates, Aromatics, Resins, and Asphaltenes Heavy Crude Oil Fractions by Atmospheric Pressure Laser Ionization Fourier Transform Ion Cyclotron Resonance Mass Spectrometry, Energy & Fuels 26 (2012) 3481–3487. https://doi.org/10.1021/ef3001407.

[337] Y. Xu, W. Schrader, Studying the Complexity of Biomass Derived Biofuels, Energies 14 (2021) 2032. https://doi.org/10.3390/en14082032.

[338] J.M. Santos, A. Vetere, A. Wisniewski, M.N. Eberlin, W. Schrader, Modified SARA Method to Unravel the Complexity of Resin Fraction(s) in Crude Oil, Energy & Fuels 34 (2020) 16006–16013. https://doi.org/10.1021/acs.energyfuels.0c02833.

[339] F.G. Bordwell, G.E. Drucker, H.E. Fried, Acidities of carbon and nitrogen acids: the aromaticity of the cyclopentadienyl anion, The Journal of Organic Chemistry 46 (1981) 632–635. https://doi.org/10.1021/jo00316a032.

Supporting Information

Supporting Information - Chapter 3

S 1. ANOVAs of applied correlations over LtoP ratio

ANOVA – Yield Biocrude

Source	Sum of Squares	df	Mean Square	Value	Prob > F	
Model	2908.39	1	2908.39	376.05	< 0.0001	highly significant
A-L/P-Ratio	*2908.39*	*1*	*2908.39*	*376.05*	*< 0.0001*	highly significant
Residual	100.54	13	7.73			
Lack of Fit	*46.41*	*5*	*9.28*	*1.37*		*not significant*
Pure Error	*54.13*	*8*	*6.77*			
Cor Total	*3008.93*	*14*				

ANOVA – Yield Solid Residue

Source	Sum of Squares	df	Mean Square	Value	Prob > F	
Model	14.45	1	14.45	164.20	< 0.0001	highly significant
A-L/P-Ratio	*14.45*	*1*	*14.45*	*164.20*	*< 0.0001*	highly significant
Residual	1.14	13	0.088			
Lack of Fit	*0.32*	*5*	*0.063*	*0.61*	*0.6950*	*not significant*
Pure Error	*0.83*	*8*	*0.10*			
Cor Total	15.60	14				

ANOVA – N-recovery of Fatty Acid Amides

Source	Sum of Squares	df	Mean Square	Value	Prob > F	
Model	12.27	1	12.27	1221.69	< 0.0001	highly significant
A-L/P-Ratio	*12.27*	*1*	*12.27*	*1221.69*	*< 0.0001*	highly significant
Residual	0.13	13	0.010			
Lack of Fit	*0.078*	*5*	*0.016*	*2.36*	*0.1340*	*not significant*
Pure Error	*0.053*	*8*	*6.592E-003*			
Cor Total	12.41	14				

ANOVA – N-recovery of Indoles

Source	Sum of Squares	df	Mean Square	Value	Prob > F	
Model	20.51	1	20.51	516.98	< 0.0001	highly significant
A-L/P-Ratio	*20.51*	*1*	*20.51*	*516.98*	*< 0.0001*	highly significant
Residual	0.52	13	0.040			
Lack of Fit	*0.35*	*5*	*0.071*	*3.51*	*0.0565*	*not significant*
Pure Error	*0.16*	*8*	*0.020*			
Cor Total	21.03	14				

ANOVA – N-recovery of Pyrazines

Source	Sum of Squares	df	Mean Square	Value	Prob > F	
Model	18.38	1	18.38	44.98	< 0.0001	highly significant
A-L/P-Ratio	*18.38*	*1*	*18.38*	*44.98*	*< 0.0001*	highly significant
Residual	3.68	9	0.41			
Lack of Fit	*3.43*	*4*	*0.86*	*17.42*	*0.0039*	*significant*
Pure Error	*0.25*	*5*	*0.049*			
Cor Total	22.06	10				

ANOVA – N-recovery of Succinimides

Source	Sum of Squares	df	Mean Square	Value	Prob > F	
Model	10.45	1	10.45	128.74	< 0.0001	highly significant
A-L/P-Ratio	*10.45*	*1*	*10.45*	*128.74*	*< 0.0001*	highly significant
Residual	1.06	13	0.081			
Lack of Fit	*0.72*	*5*	*0.14*	*3.47*	*0.0579*	*not significant*
Pure Error	*0.33*	*8*	*0.042*			
Cor Total	11.50	14				

ANOVA – N-recovery of Piperidones

Source	Sum of Squares	df	Mean Square	Value	Prob > F

Model	0.23	1	0.23	0.73	0.4069	not significant
A-L/P-Ratio	*0.23*	*1*	*0.23*	*0.73*	*0.4069*	not significant
Residual	4.09	13	0.31			
Lack of Fit	*1.05*	*5*	*0.21*	*0.55*	*0.7329*	*not significant*
Pure Error	*3.03*	*8*	*0.38*			
Cor Total	4.32	14				

S 2. Quantification, qualification ions and calibration curves of reference substances

Substance	Quantifier	Qualifier	Equation	R^2
Pyrazine, 2-Methyl	94	67	y = 111810.408737 · x + 8723.663908	0.9926
Pyrazine, 2,6-Dimethyl	108	42	y = 131397.019796 · x - 15011.578582	0.9953
Succinimide, N-methyl	113	56	y = 80030.210913 · x - 25355.006611	0.9916
2-Piperidone	99	43	y = 54915.918536 · x - 42922.174011	0.9790
Quinoline	129	102	y = 249191.378272 · x - 40282.965438	0.9961
Indole	117	89	y = 229969.550835 · x - 34371.143086	0.9942
Quinoline, 2-Methyl	143	128	y = 242942.434271 · x + 4106.703238	0.9953
Indole, 2-Methyl	130	131	y = 285012.596634 · x + 2933.644306	0.9948
Quinoline, 2,6-Dimethyl	157	156	y = 250759.389066 · x - 2943.446771	0.9956
Indole, 2,3-Dimethyl	144	130	y = 196498.788156 · x - 21416.102674	0.9940
Hexadecanamide	59	72	y = 7205.220520 · x - 5422.749899	0.9954
Hexadecanamide, N-methyl	73	86	Hexadecanamide as calibration reference	
Hexadecanamide, N-ethyl	87	100	Hexadecanamide as calibration reference	
Octadecanamide	59	72	y = 6410.254439 · x - 4973.639275	0.9961
Octadecanamide, N-methyl	73	86	Octadecanamide as calibration reference	
Octadecanamide, N-ethyl	87	100	Octadecanamide as calibration reference	

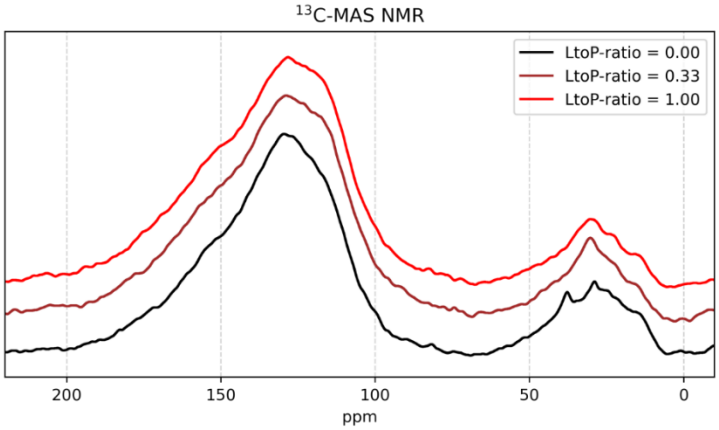

S 3. 13C-MAS NMR results of solid samples from a model feedstock with a LtoP ratio of 0.00, 0.33 and 1.00

RT	Compound	Quality	Area	Area %
6,78	2-Cyclopenten-1-one, 3-methyl-	98	959288	0,82
6,92	Phenol	97,8	2575648	2,21
7,58	2,3,4-Trimethylpyrrole	87	531088	0,46
7,99	2-Pyrrolidinone, 1-methyl-	90,6	1474077	1,26
8,00	2-Cyclopenten-1-one, 2,3-dimethyl-	90,6	1270545	1,09
8,19	Phenol, 2-methyl-	84,6	850553	0,73
8,45	**2-Pyrrolidinone**	**95,1**	**3001960**	**2,58**
8,55	p-Cresol	98,5	5722127	4,91
8,59	Furan, 2-propyl-	86,7	648767	0,56
8,78	**N-methylsuccinimide**	**93,9**	**1034746**	**0,89**
8,84	2-Cyclopenten-1-one, 2,3,4-trimethyl-	82,5	641049	0,55
8,92	1H-Pyrrole, 2-ethyl-3,5-dimethyl-	82,6	501792	0,43
9,08	1-Ethyl-2-pyrrolidinone	89,3	1916251	1,64
9,39	1H-Pyrrole, 2,3,4,5-tetramethyl-	88,8	871113	0,75
9,49	2,5-Pyrrolidinedione, 1-ethyl-	89,4	783955	0,67
9,82	1H-Pyrrole, 3-ethyl-2,4,5-trimethyl-	81,2	814050	0,70
9,90	2(1H)-Pyridinone, 5-methyl-	76,8	1909058	1,64
9,97	Phenol, 4-ethyl-	89	2373089	2,04
10,11	1H-Pyrrole, 3,4-diethyl-2-methyl-	86,6	685937	0,59
10,11	1H-Pyrrole, 3-ethyl-2,4,5-trimethyl-	87,1	661751	0,57
10,15	Octanoic acid	77,8	3145170	2,70
11,10	Phenol, 4-(methylamino)-	75	623918	0,54
11,45	Caprolactam	88,6	1424746	1,22
11,60	N-[2-Hydroxyethyl]succinimide	87,4	654526	0,56
12,74	Piperidine, 1-pentyl-	77,9	3537239	3,03
13,12	N-[2-Hydroxyethyl]succinimide	80,8	1654249	1,42
13,32	**1H-Indole, 2-methyl-**	**77,3**	**1689989**	**1,45**
14,71	Indolizine, 2,8-dimethyl-	79,2	1162582	1,00
14,80	**1H-Indole, 2,3-dimethyl-**	**90,4**	**948951**	**0,81**
15,04	***Butylated Hydroxytoluene***	***97***	***THF additive***	
15,59	2-Naphthalenamine	88,5	613480	0,53
15,79	Indolizine, 2-methyl-6-ethyl-	79,1	1142646	0,98
16,25	1H-Indole, 2,3,5-trimethyl-	89,7	836618	0,72
17,07	1-Naphthalenamine, N,N-dimethyl-	88,4	974131	0,84
17,30	1,7-Trimethylene-2,3-dimethylindole	76,4	1332700	1,14
17,84	7-Isopropyl-4-morpholinomethyl-2-azulenamine	76,5	677833	0,58
22,42	Pyrrolo[1,2-a]pyrazine-1,4-dione, hexahydro-3-(2-methylpropyl)-	76,5	4243931	3,64
26,05	**Hexadecanamide**	**95,2**	**12526944**	**10,75**
26,50	N-Methyldodecanamide	81,5	4819778	4,13
26,96	2,5-Piperazinedione, 3-benzyl-6-isopropyl-	88,1	1261373	1,08
27,15	Arachidamide, N-ethyl-	86,1	4345638	3,73
27,48	2,5-Piperazinedione, 3-benzyl-6-isopropyl-	80,9	877274	0,75
28,73	Pyrrolo[1,2-a]pyrazine-1,4-dione, hexahydro-3-(phenylmethyl)-	92,6	1836682	1,58
28,86	9-Octadecenamide, (Z)-	76	7186195	6,16

29,22	**Octadecanamide**	**89,9**	**2926833**	**2,51**
29,40	Pyrrolo[1,2-a]pyrazine-1,4-dione, hexahydro-3-(phenylmethyl)-	89	1145318	0,98
29,74	Arachidamide, N-methyl-	81,3	1281120	1,10
30,08	9-Octadecenamide, N,N-dimethyl-	77,6	3986349	3,42
30,37	Arachidamide, N-ethyl-	77,5	961928	0,83
31,03	Arachidamide, N-3-methylbutyl-	78,2	2970893	2,55
32,23	Pyrrolidine, 1-(1-oxooctadecyl)-	75,8	2526090	2,17
32,50	Octadecanamide, N-(2-methylpropyl)-	75,9	1139720	0,98
34,13	Stearamide, N-(3-methylbutyl)-	84,2	717034	0,62
35,12	13-Cyclopentyltridecanoic acid, pyrrolidide	75,6	1853459	1,59
35,23	Pyrrolidine, 1-(1-oxo-9-octadecenyl)-, (E)-	82,8	6002180	5,15
35,24	Pyrrolidine, 1-(1-oxo-9-octadecenyl)-	86,1	4312745	3,70

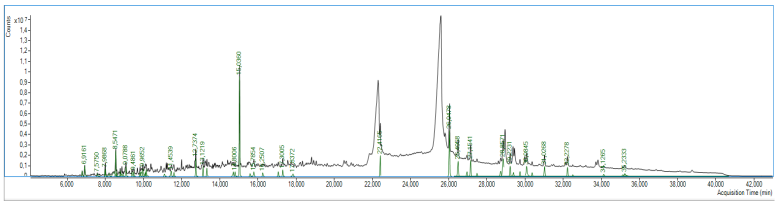

S 4. TIC Scan of model sample with a LtoP-ratio of 0.33. Resulting compounds and chromatogram

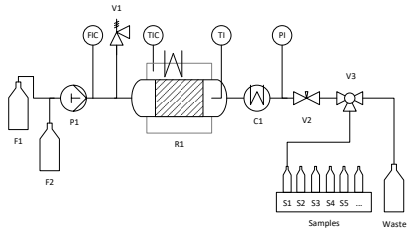

S 5. PID of test rig. F1: De-ionized water, F2: Leaching agent, P1: HPLC-pump, V1: safety valve, R1: Fixed Bed Reactor with heating block, C1: cooler, V2: Backpressure valve, V3: three-way valve

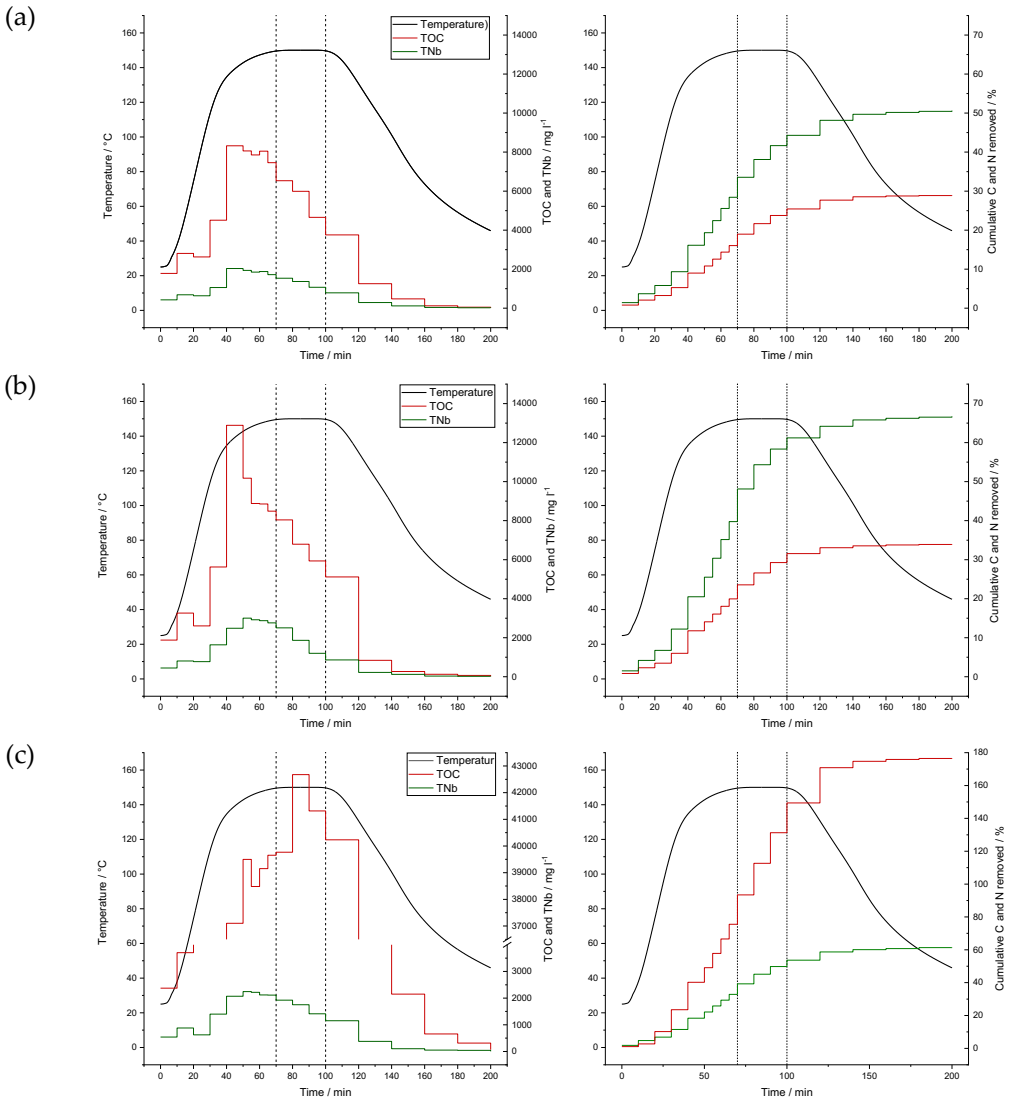

S 6. TOC and TNb concentration and cumulative C and N removal from MSS with (a) DW, (b) SA and (c) CA, as leaching agent. For CA-treatment the TOC-value of the 0.5M CA was subtracted to receive the real and final cumulative C- removed from the solid.

S 7. Content of amino acids in sewage sludge (MSS) and pre-treated solids (DE, SA, CA)

Amino acid (dry ash free) [wt. %]	MSS	DW	SA	CA
Alanine (Ala)	2.4	1.2	0.9	0.8
Arginine (Arg)	0.8	0.6	0.4	0.4
Aspartic acid (Asp)	2.2	1.6	1.0	0.7
Cysteine(Cys)	0.3	0.0	0.0	0.0
Glutamic acid (Glu)	2.8	2.4	1.6	1.5
Glycine (Gly)	1.8	0.7	0.6	0.4
Histidine (His)	0.3	0.2	0.1	0.2
Isoleucine (Iso)	1.2	0.7	0.6	0.6
Leucine (Leu)	1.8	1.2	1.1	1.1
Lysine (Lys)	1.2	0.3	0.4	0.2
Methionine (Met)	0.5	0.2	0.2	0.2
Phenylalanine (Phe)	1.1	0.8	0.7	0.7
Proline (Pro)	1.1	0.8	0.4	0.5
Serine (Ser)	0.9	0.7	0.5	0.5
Threonine (Thr)	1.3	0.7	0.5	0.4
Tyrosine (Tyr)	0.7	0.4	0.4	0.3
Valine (Val)	1.7	1.0	0.8	0.8
Sum of amino acids	**21.8**	**13.5**	**10.0**	**9.3**

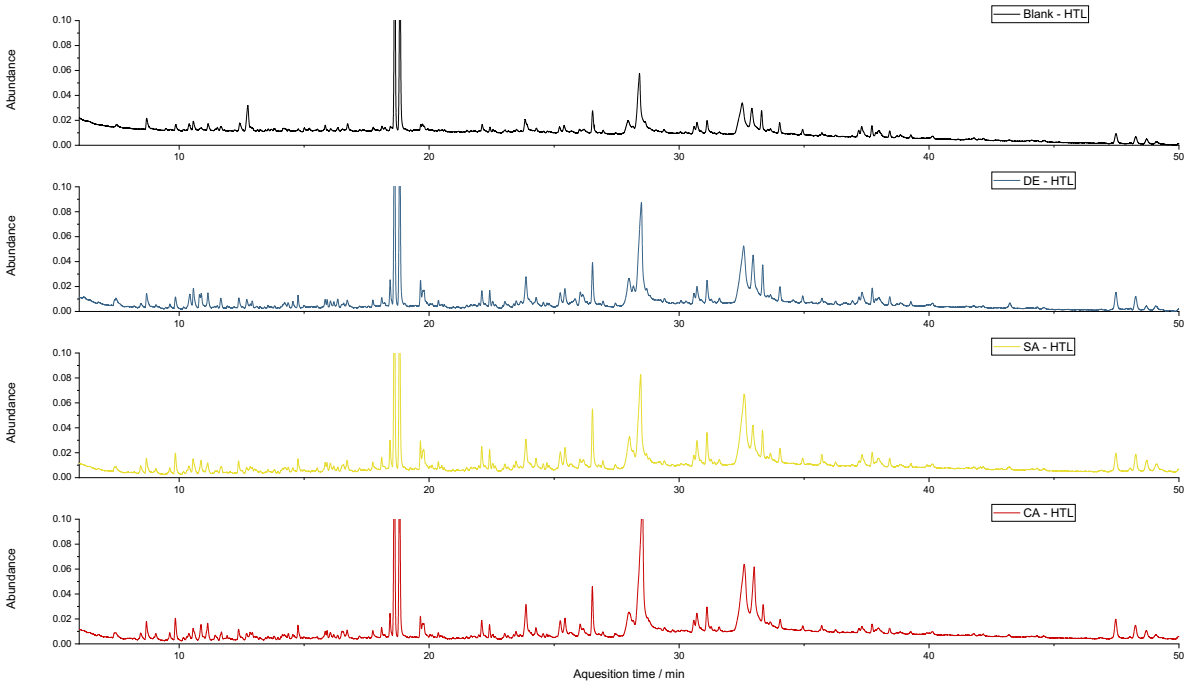

S 8. GC-TIC Chromatogram of MSS-HTL, DW-HTL, SA-HTL and CA-HTL derived biocrude

S 9. Concentration of fatty acids in biocrude samples.

Feedstock	MSS-HTL	DE-HTL	SA-HTL	CA-HTL
C12:0 [wt. %]	0.1 (0.0)	0.2 (0.0)	0.2 (0.0)	0.2 (0.0)
C14:0 [wt. %]	0.4 (0.0)	0.5 (0.0)	0.6 (0.1)	0.6 (0.0)
C15:0 [wt. %]	0.1 (0.0)	0.2 (0.0)	0.2 (0.1)	0.3 (0.0)
C16:0 [wt. %]	1.0 (0.1)	1.3 (0.1)	1.7 (0.1)	1.5 (0.0)
C16:1[a] [wt. %]	3.2 (0.3)	4.6 (0.2)	6.0 (0.7)	5.7 (0.3)
C18:0 [wt. %]	5.8 (0.3)	6.1 (0.6)	8.1 (0.4)	7.7 (0.2)
C18:1[b] [wt. %]	2.4 (0.2)	3.4 (0.2)	3.4 (1.4)	4.3 (0.3)
Sum	13.1 (0.5)	16.4 (0.7)	20.2 (1.6)	20.3 (0.5)

[a] Containing all hexadecenoic acid isomers
[b] Containing all octadecenoic acid isomers

S 10. Concentration of representative compounds in biocrude samples. The values in brackets indicate the standard deviation

	MSS-HTL	DE-HTL	SA-HTL	CA-HTL
Phenol [wt. %]	0.20 (0.01)	0.16 (0.01)	0.16 (0.02)	0.20 (0.03)
2-Piperidinone [wt. %]	0.35 (0.04)	0.09 (0.05)	0.07 (0.01)	0.08 (0.01)
1H-Indole, 3-methyl [wt. %]	0.49 (0.01)	0.26 (0.01)	0.29 (0.04)	0.29 (0.01)
Fatty acids[a] [wt. %]	13.09 (0.50)	16.37 (0.69)	20.24 (1.61)	20.27 (0.52)
Hexadecanol [wt. %]	2.62 (0.15)	3.16 (0.32)	4.01 (0.00)	3.44 (0.20)
Hexadecanamide [wt. %]	3.01 (0.21)	3.18 (0.20)	3.55 (0.06)	2.97 (0.02)

[a] Sum of all fatty acids detected

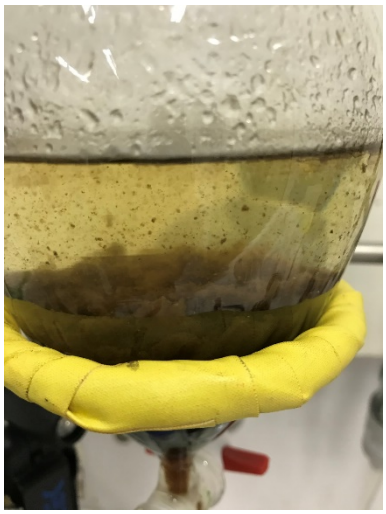

S 11. Precipitate and emulsion formation during the extraction procedure.

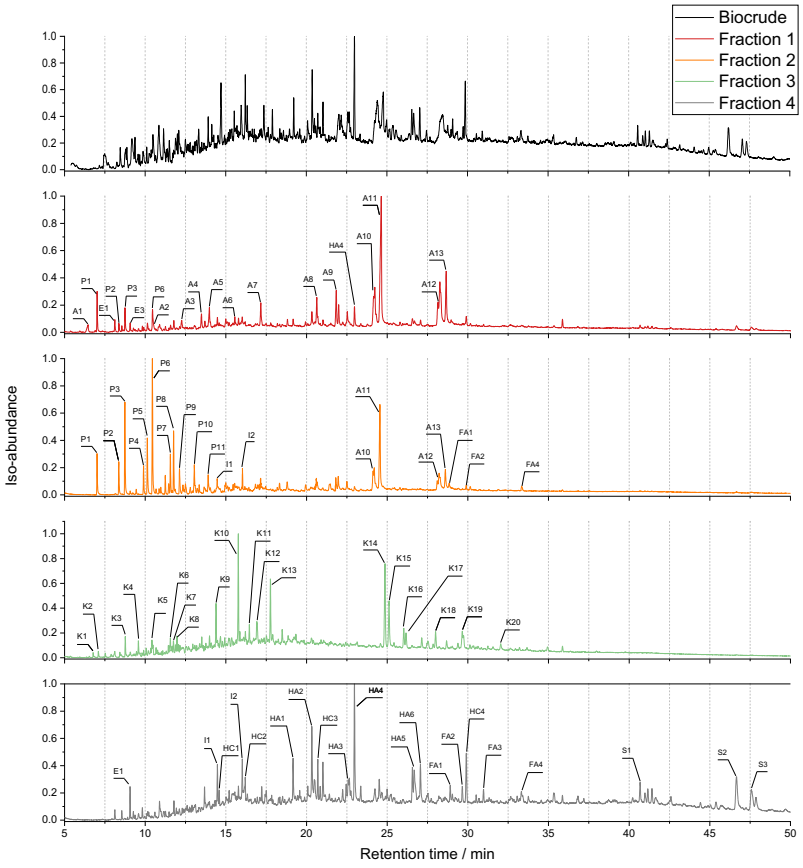

S 12. Total-ion-current-chromatogram of GC-MS analysis of extracted Fraction F1 to F4

S 13. Most prominent compounds identified by GC-MS in the extracted fraction F1 to F4. The identification code (ID) for S§ and the retention time (RT) is given. N-containing compounds are bold

ID	RT [min]	Compound name	F1	F2	F3	F4
A1	6.5	Pentanoic acid, 4-methyl-	X			
A2	10.5	Octanoic acid	X			
A3	12.3	Nonanoic acid	X			
A4	13.5	Hydrocinnamic acid	X			
A5	14.0	Decanoic acid	X			
A6	15.6	Undecanoic acid	X			
A7	17.1	Dodecanoic Acid	X			
A8	20.6	Tetradecanoic Acid	X			
A9	21.8	Pentadacanoic acid	X			
A10	24.2	Hexadecenoic acid	X	X		
A11	24.6	Hexadecanoic acid	X	X		
A12	28.2	Octadecenoic acid	X	X		
A13	28.6	Octadecanoic acid	X	X		
FA1	**28.9**	**Hexadecanamide**		X		X
FA2	**29.6**	**Hexadecanamide, N-methyl**		X		X
FA3	**30.5**	**Hexadecanamide, N-ethyl**				X
FA4	**33.1**	**Octadecanamide**		X		X
E1	8.1	2-Cyclopenten-1-one 2,3-diemethyl-				X
E2	8.5	2-Cyclopenten-1-one, 2,3,4-trimethyl-				X
E3	9.0	2-Cyclopenten-1-one, 3,5,5-trimethyl-				X
I1	**14.5**	**1H-Indole, 3-methyl-**		X		X
I2	**16.0**	**1H-Indole, 2,3- dimethyl-**		X		X
P1	7.0	Phenol	X	X		
P2	8.3	o-Cresol	X	X		
P3	8.7	p-Cresol	X	X		
P4	9.9	Phenol, 4-ethyl-		X		
P5	10.1	Phenol, 3-ethyl-		X		
P6	10.4	Phenol 3,4-dimethyl-	X	X		
P7	11.5	Phenol, 3-ethyl-5-methyl-		X		
P8	11.7	Phenol, 4-ethyl-2-methyl-		X		
P9	12.1	Phenol, 4-propyl-		X		
P10	13.0	Phenol, 3,5-diethyl-		X		
P11	13.9	Phenol, 4-butyl-		X		

ID	RT [min]	Compound name	F1	F2	F3	F4
K1	**6.8**	**Pyridine, 3-ethyl-**			X	
K2	**7.0**	**Pyridine, 2,5-dimethyl-**			X	
K3	**8.8**	**Pyrideine, 3-ethyl-4-methyl-**			X	
K4	**9.6**	**5H-1-Pyridine, 6,7-dihydro-**			X	
K5	**10.**	**Pyridine, 3-ethyl-2,6-dimethyl-**			X	
K6	**11.6**	**Pyridine, 4-pentyl-**			X	
K7	**11.8**	**Quinoline, 1,2,3,4-tetrahydro-**			X	
K8	**12.0**	**Quinoline**			X	
K9	**14.4**	**Quinoline, 4-methyl-**			X	
K10	**15.8**	**Pyridine, 3-phenyl-**			X	
K11	**16.4**	**2p-Tolylpyridine**			X	
K12	**16.9**	**Quinoline, 2,7-dimeethyl-**			X	
K13	**17.7**	**Pyridine, 2-methyl, 5-phenyl-**			X	
K14	**24.8**	**8-Methyl-5H-pyrido[4,3-b]indole**			X	
K15	**25.1**	**9H-Pyrido[3,4-b]indole**			X	
K16	**26.1**	**5,7-Dimethylpyrimido-[3,4-a]-indole**			X	
K17	**26.2**	**5-Ethylpyrimido-[3,4-a]-indole**	**%**		X	
K18	**28.0**	**Phenanthrolin**			X	
K19	**29.6**	**5-Methyl-1,10-phenanthroline**			X	
K20	**32.0**	**Neocuproine**			X	
HC1	14.6	Tetradecane				X
HC2	16.2	Pentadecane				X
HC3	20.7	1-Hexadecanone				X
HC4	29.9	Retene				X
HA1	19.2	Tetradecan-1-ol				X
HA2	20.3	Pentadecan-1-ol				X
HA3	22.6	9-Hexadecen-1-ol	X			X
HA4	23.0	Hexadecan-1-ol	X			X
HA5	26.6	9-Octadecen-1-ol				X
HA6	27.0	Octadecen-1-ol				X
S1	40.6	Sterol derivat				X
S2	46.7	Sterol derivat				X
S3	47.6	Sterol derivat				X

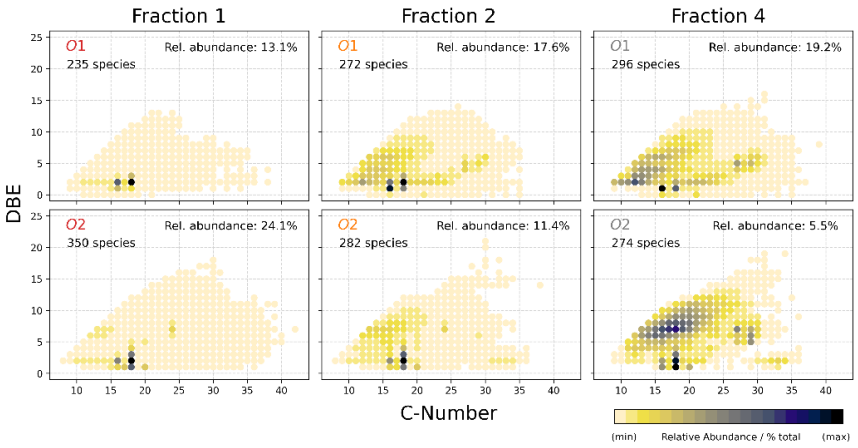

S 14. Relative intensity plots of Cn vs DBE distribution of the class O1-2 of the extracted fractions

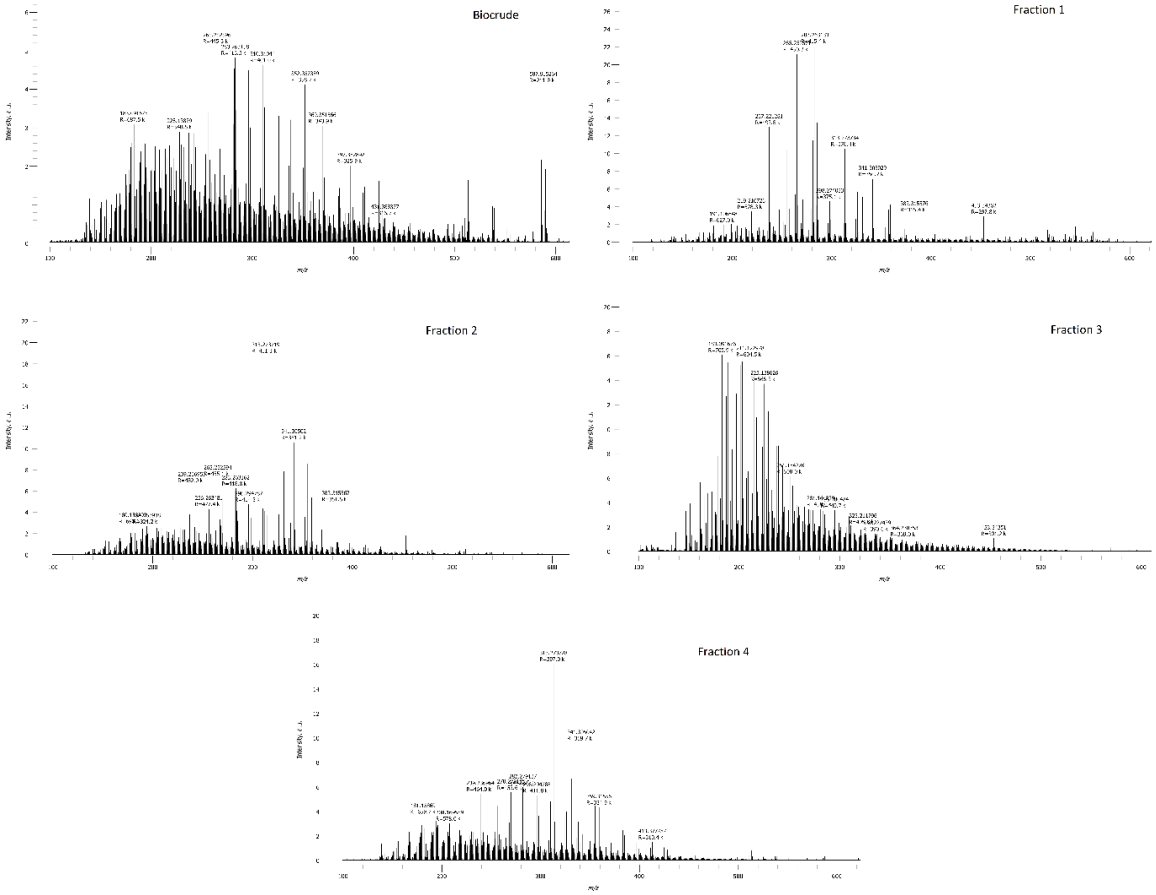

S 15. FT-ICR MS spectra of biocrude and extracted fractions F1-4

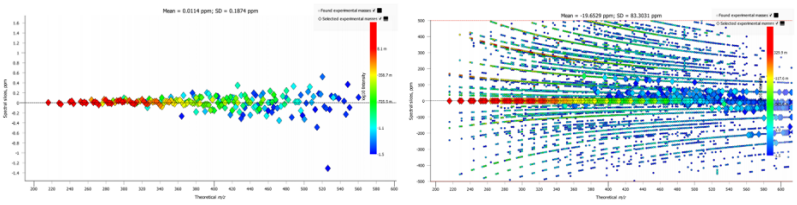

S 16. Example spectral slices for O1N1 clas

List of Figures

List of Tables

List of Figures and Tables in Supporting Infomation